VŠB – Technical University of Ostrava
Faculty of Electrical Engineering and Computer Science

# Enhancing the Physical Layer Security of Wireless Communication Networks with Wireless Power Transfer

Ph.D. THESIS

2021 Hung Duy Ha

VSB TECHNICAL UNIVERSITY OF OSTRAVA | FACULTY OF ELECTRICAL ENGINEERING AND COMPUTER SCIENCE

Department of Telecommunications
17. listopadu 2172/15, 708 00 Ostrava, Czech Republic

Ph.D. Thesis

# ENHANCING THE PHYSICAL LAYER SECURITY OF WIRELESS COMMUNICATION NETWORKS WITH WIRELESS POWER TRANSFER

Delivered in April 2021

Doctoral Study Program:
P1807 Computer Science, Communication Technology and Applied Mathematics

Doctoral Study Branch:
2601V018 Communication Technology

PhD. Student: Hung Duy Ha
Student ID: HAD0045
Email: duy.hung.ha.st@vsb.cz

Supervisor: prof. Ing. Miroslav Vozňák, Ph.D.
Email: miroslav.voznak@vsb.cz

# Declaration

I declare that this thesis was written on the basis of original research conducted by me under the guidance of my supervisor at the Faculty of Electrical Engineering and Computer Science at VŠB - Technical University of Ostrava as a candidate for the Doctor of Communication Technology.

My work included below was conducted under the supervision of **prof. Miroslav Vozňák**. This thesis has never been submitted for any other degree or award at any other universities or educational institution.

This is a true copy of the thesis, including required final revisions, as accepted by my examiners. I understand that my thesis may be made electronically available to the public.

Ostrava, April, 2021

# Acknowledgement

This thesis marks the end of my journey in obtaining my Ph.D. It has been a period of intense learning, not only in the scientific arena but also on a personal level. Writing this dissertation has had a great personal impact and I would like to reflect on the people who have supported and helped me so much throughout this period.

First and foremost, I would like to express my deepest appreciation to my supervisor **prof. Miroslav Vozňák** for his careful guidance and providing me with the best possible work environment. He helped me tremendously in acquiring knowledge on many topics, both related and unrelated to this thesis. He continually and convincingly conveyed a spirit of adventure in regard to research and new challenges. Without his guidance and persistent help, this dissertation would not have been possible.

Special thanks to **Dr. Ha Dac Binh** for providing insight into some of the problems encountered along the way. He helped me understand new topics quickly and guided me through effective research methods. Under his guidance, I successfully overcame many difficulties and learned much. I remember with delight the moments when he offered me valuable suggestions and corrections and reviewed my progress in the thesis.

I am also extremely indebted to **Dr. Tran Thanh Phuong, Dr. Tran Trung Duy and Dr. Nguyen Nhat Tan** for providing the for their valuable advice, constructive criticism and extensive discussions concerning my work.

Finally, I wish to thank members of my family for their support and encouragement throughout my studies.

**Abstrakt**

V posledních letech se pozornost v bezdrátových sítích přesunula z témat limitů spektrální účinnosti a kvality služeb (QoS) na energetickou účinnost a zelenou komunikaci, zejména v sítích páté generace (5G) a šesté generace (6G), jakož i v sítích IoT, aby se snížila spotřeba energie mobilních zařízení a senzorů. Na druhé straně se v současné komunikaci klade stále větší důraz na bezpečnost, přičemž zabezpečení fyzické vrstvy se stává účinnou a perspektivní metodou, a to kromě kryptografických technik, které se používají ve vyšších vrstvách.

Motivován výše uvedeným se v této disertační práci snažím navrhnout strategie pro integraci technologie získávání energie a zabezpečení fyzické vrstvy v kontextu bezdrátových přenosových sítí. Konkrétně se zaměřuji na studium výkonnostních parametrů z pohledu bezpečnosti a spolehlivosti komunikace v relay sítích umožňujících získávání energie za přítomnosti odposlechů nebo odposlechových kanálů. Zkoumám efektivitu různých strategií nebo protokolů pro získávání energie a různých bezpečnostních technik na fyzické vrstvě, jako je kooperativní rušení či výběr relay uzlu, abych doporučil konkrétní modely, které mohou zlepšit celkovou výkonnost komunikačních systémů. Pro analýzu výkonnosti se berou v úvahu následující faktory: pravděpodobnost výpadku (OP), pravděpodobnost zachycení, kapacita utajení, pravděpodobnost výpadku utajení (SOP). Výrazy uzavřených forem těchto faktorů jsou v této dizertaci odvozeny pro každé nově navržené schéma.

Na druhé straně je také zkoumán vliv různých nežádoucích podmínek, jako je odhad chyb v kanále a vliv hardwaru na výkonnost navrhovaných schémat získávání energie a bezpečnostních strategií na fyzické vrstvě pro bezdrátové přenosové sítě. Dále jsou použity pokročilé komunikační techniky, včetně víceskokové komunikace, plně duplexní komunikace, komunikace MIMO s diverzitními technikami a neortogonálním vícenásobným přístupem NOMA. Za účelem ověření platnosti odvozených matematických vztahů je pro každý získaný výsledek nastavena a spuštěna nezávislá simulace metodou Monte Carlo.

**Klíčová slova**: Zabezpečení fyzické vrstvy, získávání energie, výkon utajení, pravděpodobnost výpadku, propustnost, NOMA.

**Abstract**

In recent years, the main focus for wireless networks has been shifted from spectral efficiency and quality of service (QoS) constraints to energy efficiency and green communication, especially in the fifth generation (5G) and sixth generation (6G) networks as well as IoT networks, to reduce the power consumption of mobile devices and sensor. On the other hand, security has become more and more important in contemporary communication and physical layer security has been considered as an effective and a perspective method to enhance the information security beside the cryptography techniques that are used in upper layers.

Motivated by the above issue, in this dissertation I aim to propose strategies to integrate energy harvesting technology and physical layer security in the context of wireless relay networks. Specifically, I focus on studying the security and reliability performance of energy harvesting enabled relaying networks in the presence of eavesdroppers or wiretap channels. I investigate the efficiency of different energy harvesting strategies or protocols and various security techniques at physical layer, such as cooperative jamming or relay selection to recommend specific models that can improve the overall performance of the communications systems. For performance analysis, the following factors are considered: outage probability (OP), intercept probability, secrecy capacity, secrecy outage probability (SOP). The closed-forms expressions of these factors are derived for each newly-proposed scheme in this dissertation.

On the other hand, the effect of different undesired condition, such as channel estimation error and hardware impairment, on the performance of the proposed energy harvesting schemes and security strategies at physical layer for wireless relay networks is also investigated. Furthermore, advanced communication techniques, including multi-hop communication, full-duplex communications, multiple-input multiple output (MIMO) communications with diversity techniques, and non-orthogonal multiple-access (NOMA), are also applied to enhance the system performance. In order to verify a validity of the derived mathematical expressions, an independent Monte Carlo simulation is set up and run for each achieved result.

**Keywords**: Physical Layer Security, Energy Harvesting, Secrecy Performance, Outage Probability, Throughput, NOMA.

# Contents

## List of symbols and abbreviations

| | |
|---|---|
| 5G | Fifth Generation |
| 6G | Sixth Generation |
| AF | Amplify-and-Forward |
| AN | Artificial-Noise |
| ASC | Average Secrecy Capacity |
| ASR | Average Secrecy Rate |
| AT | Achievable Throughput |
| AWGN | Additive White Gaussian Noise |
| BCP | BroadCast Phase |
| BER | Bit Error Rate |
| BFSK | Binary Frequency-Shift Keying |
| BPSK | Binary Phase-Shift Keying |
| CCI | Co-Channel Interference |
| CDF | Cumulative Density Function |
| CHs | Cluster Heads |
| CJ | Cooperative Jamming |
| CPC | Circuit Power Consumption |
| CSI | Channel Sate Information |
| DAS | Distributed Antenna System |
| DF | Decode-and-Forward |
| E2E | End-to-End |
| EC | Ergodic Capacity |
| EE | Energy Efficiency |
| EH | Energy Harvesting |
| FD | Full-Duplex |
| H2J | Harvest-to-Jam |
| HD | Half-duplex |
| HI | Hardware Impairment |
| HTC | Harvest-Then-Cooperate |
| INID | Independent and not Necessarily Identically Distributed |
| IoT | Internet of Things |
| IT | Information Transmission |
| M-LEACH | Multi-hop Low-Energy Adaptive Clustering Hierarchy |
| MAP | Multiple-Access Phase |
| MAX-EH | MAXimum Energy Harvested |
| MAX-IP | MAXimum Interference Power |

| | |
|---|---|
| MIMO | Multiple-Input Multiple-Output |
| MRC | Maximal-Ratio Combining |
| NF | Noise Forwarding |
| NOMA | Non-Orthogonal Multiple Access |
| OFDMA | Orthogonal Frequency Division Multiple Access |
| OP | Outage Probability |
| OWFD | One-Way Full-Duplex |
| OWHD | One-Way Half-Duplex |
| PB | Power Beacon |
| PDF | Probability Density Function |
| PLS | Physical-Layer Security |
| PRS | Partial Relay Selection |
| PS | Power Splitting |
| PSR | Power Splitting Relaying |
| QoS | Quality of Service |
| QPSK | Quadrature Phase Shift Keying |
| RAND | RANDom jammer selection |
| RF | Radio Frequency |
| RV | Random Variable |
| SEP | Symbol Error Probability |
| SNR | Signal-to-Noise Ratio |
| SOP | Secrecy Outage Probability |
| SWIPT | Rate of Simultaneous Wireless Information and Power Transfer |
| TPSR | Time-Switching and Power Splitting |
| TS | Time Switching |
| TSR | Time Switching Relaying |
| TWFD | Two-Way Full-Duplex |
| TWHD | Two-Way Half-Duplex |
| TWRC | Two-Way Relay Channel |
| WET | Wireless Energy Transfer |
| WPCN | Wireless Powered Communication Networks |
| WPT | Wireless Power Transfer |

# 1 Introduction

## 1.1 Motivation and goals

Today, wireless devices such as mobile phones, smartphones, iPads, laptops, etc. have become no stranger to the everyday lives of humans. Information security for these devices is thus an important issue in communications, especially in government, military, finance, and banking services. So far, data encryption and decryption algorithms such as AES or Blowfish have been employed to ensure information security. These algorithms are commonly applied at the application layer with the assumption that the link between the transmitter and receiver (physical layer) has been set and is error-free. However, in wireless communication systems, especially in distributed networks such as wireless sensor networks and ad hoc wireless networks, the distributed nature of the channel makes it vulnerable to attack or eavesdropping. The current solution for wireless communication is to apply complex data encryption and decryption techniques (at the application layer). However, this is inefficient in a fast-fading radio environment. More importantly, large-scale networks such as encryption protection are unfeasible. Recently, physical layer security, which achieves secure transmissions by exploiting the dynamics in the physical layer, has drawn much attention [1], [2]. Coupled with the rapid development of wireless devices is the need for energy for these devices. The applications on wireless devices, in addition to the ever-increasing demand for monitors, increase power dissipation. One of the solutions to meet this need is to make batteries that can store large amounts of energy. In addition, fast and convenient charging is another direction many research staff and manufacturers are pursuing today. There are many ways to recharge, but wireless charging is still the most convenient and easy method. Some examples of wireless charging are solar, heat energy, and radio frequency (RF). In particular, RF technology is the emerging method for charging. A typical radio power station consists of an uninterruptible access point that broadcasts radio signals that carry both information and energy to the terminals. At these terminals, some activity occurs as the information receiver (IR) decodes the received signal, while another receiver (ER) receives energy by drawing energy from electromagnetic waves. To overcome the extremely large attenuation due to propagation through the wireless environment, energy loading devices must be deployed near the access point. Naturally, the new concept of physical layer security can be applied to wireless networks with RF power transfer in order to achieve robust secure transmission. Physical layer security (PLS) has been studied in various scenarios, but a paucity of research contributions on investigating the security issues of RF power transfer networks still persists, which is the motivation for this dissertation. Note that the employment of RF power transfer in wireless networks results in dynamic power at the receivers, which makes the analysis of the PLS of RF power transfer networks different from that of wireless networks without RF power transfer.

## 1.2 Purpose of the Research

- Dissertation for new RF energy harvesting wireless communication network models.
- Suggestions for new protocols to enhance the physical layer security for wireless networks.
- Analyses of the secrecy performance of these proposed systems through expressions of the probability of existence of security capacity and the secrecy outage probability (SOP) derived from the use of the statistical characteristics of dynamic channels.
- Simulation and evaluation of the security performance of these systems.

## 1.3 Dissertation Thesis Structure

This dissertation is organized as follows: Section 2 presents the background of the dissertation, Section 3 determines the aims of the proposed research, and Section 4 shows the State-of-the-Art. Section 5 introduces Performance Analysis of RF EH protocols, especially the hybrid TPSR, for various network models under different channel and transceiver conditions. Section 6 is design secrecy protocols at the physical layer and propose methods of calculating and analyzing secrecy performance of wireless networks. Section 7 integrate energy harvesting together with other advanced techniques to further strengthen network security and reliability. Last but not least, section 8 contains a conclusion and future work plans. The references and candidate's published research papers are at the end of the thesis.

# 2 Background

## 2.1 5G-6G network development trend

Commercial approvals have been officially declared for the deployment of fifth generation (5G) wireless systems in numerous countries, with 5G enabled smart phones and infrastructures already appearing in the market [3]. Prior to recently emerging commercial applications of 5G, research exploring future wireless systems has already extended to the concept of beyond 5G (B5G). Furthermore, since 2018, scholars have begun to focus on the concept of 6G and its applications [4]. The architecture in Fig. 2.1 presents a bridge from the 5G networks towards beyond 5G/6G networks. The architecture also defines the applications and services that will be offered by the 6G network [5]. In [3], the authors have identified five 6G core services and

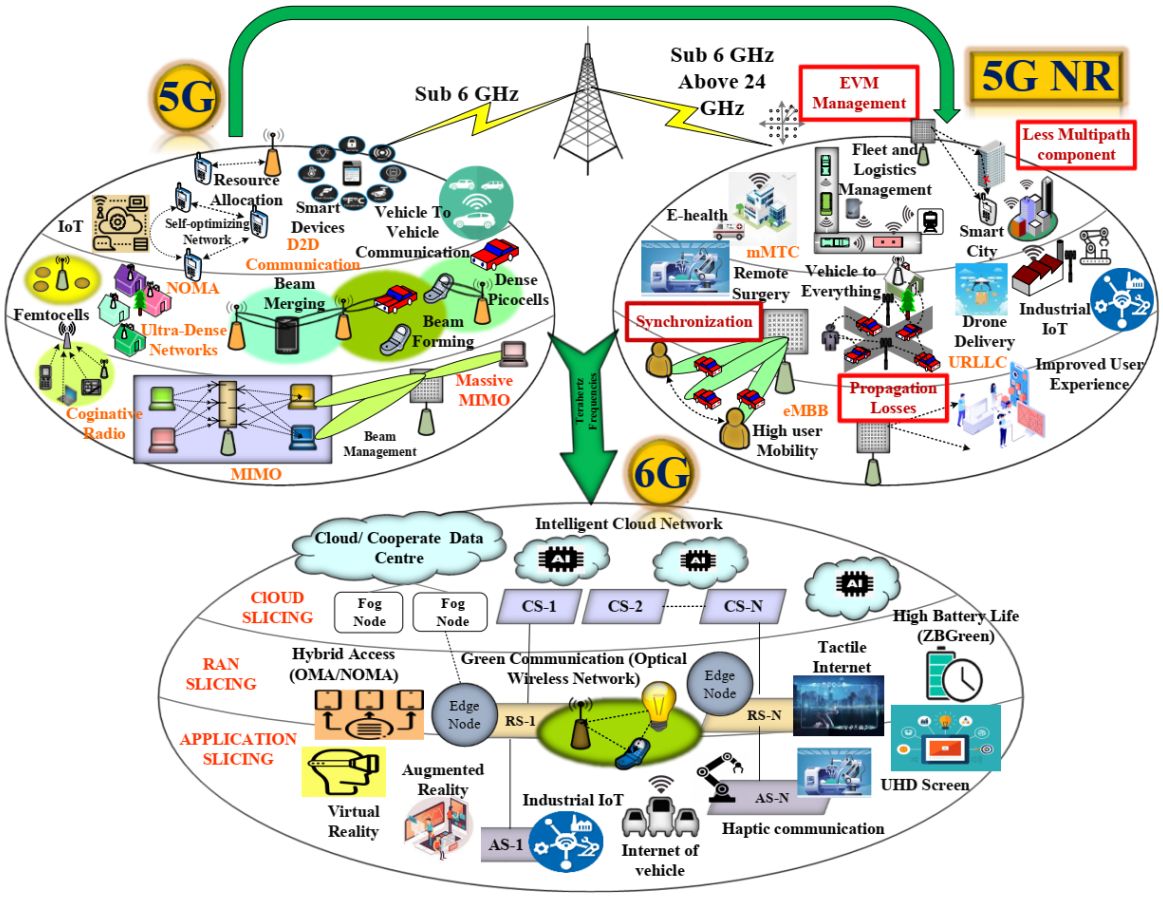


Figure 2.1: A recommended architecture for next-generation wireless communication [5].

enlisted two centricities and eight key performance indices (KPIs) to describe these services, as well as enabling technologies to fulfill these KPIs. According to this paper, one of the 6G core service is focused on providing secure wireless computing in the digital world, contrasting

with the scenario centric services based on 5G and B5G evolutions. Cyber and physical layer security issues within wireless networks are widespread in daily life. Security should therefore be considered as a basic performance requirement of wireless computing in 6G. In [5], the authors discussed six challenges for 6G networks, including trustworthiness (i.e. 6G should provide the proper tools to enable protection of end-users). The authors also recommended seven 6G technology components, including higher frequencies, distributed coherent massive MIMO, integrated connectivity and sensing, integrated AI for automation, serviced-based networks, flexible topologies and deployments, and zero-energy devices.

It is readable from the above mentioned technology trend prediction that integration of technologies and security are two important issues in the development of next generation wireless networks. These issues are also my main interest of research for my PhD studying. In my dissertation, I focus on the integration of RF EH techniques (as one of the seven technology components mentioned above) and physical layer security in different advanced schemes of wireless networks. This integration also includes other candidate techniques for 5G, B5G, and 6G networks, such as MIMO, NOMA, FD, cognitive radio networks, etc. The next two subsections present some background knowledge on RF EH and physical layer security.

## 2.2 RF Energy Harvesting (EH)

The proliferation of wireless devices and the spread of wireless communication networks render the task of energy supply an ever-growing challenge. Reliable and sustainable energy sources should be deployed to guarantee effective performance of wireless networks. In recent years, EH technologies are emerging as a promising method to power the nodes of a wireless communication network [6], [7]. EH communication devices are able to harvest ambient energy from their surrounding environment, and are therefore less dependent to nonrenewable energy sources and can enjoy a prolonged lifetime. The idea of using renewable ambient energy sources rises the possibility of having green communication networks.

The concept of wireless power transfer (WPT) was first proposed by Nikola Tesla in 1899, which focused on high-power-consumption applications. This area emerged again with recent advances in silicon technology and multiple-antenna technology. It is expected that innovative WPT networks are the key enabler of the IoT to connect all devices together via wireless powered sensors for the development of smart cities [8].

The existing WPT technologies can be categorized into three classes: inductive coupling, magnetic resonant coupling, and RF-based WPT. In contrast to the first two technologies, RF-based wireless information and power transfer (WIPT) exploits the far-field properties of EM waves, which enable concurrent wireless charging and data communication over long distances. In addition, RF-based WIPT utilizes the RF spectrum and the radiation is regulated by the government to ensure safety. More importantly, RF signals can serve as a dual-purpose carriers for conveying both information and power simultaneously [9].

### 2.2.1 Receiver Structure for WIPT

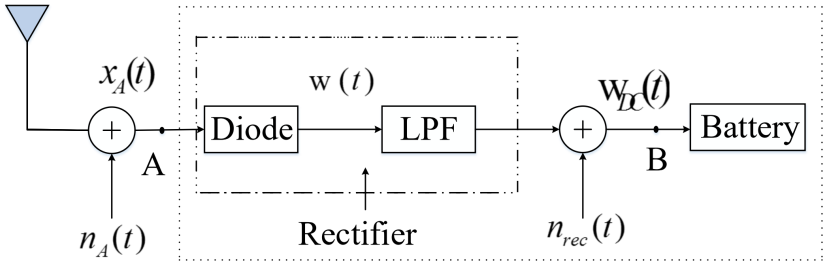


Figure 2.2: A typical architecture for RF-based EH receiver circuit.

Figure 2.2 illustrates the typical architecture of a RF-based EH receiver, which contains a rectifying circuit, consisting of a diode and a passive low-pass filter (LPF). This circuit converts received RF signals to DC signals to charge the built-in battery, which stores the energy. According to the energy conservation law, the harvested energy can be expressed as

$$E_h = \frac{\eta P_t G T}{d^\theta}, \tag{2.1}$$

where $\eta \in (0, 1)$ denotes the overall energy conversion efficiency at the receiver, $P_t$ is the transmit power, $d$ is the distance between the energy transmitter and its receiver, $\theta$ denotes the path loss factor, $T$ denotes the block time, and $G$ represents the combined gain of the transmit and receive antennas as well as the channel. RF-based EH technology can be classified into simultaneous WIPT (SWIPT), wireless-powered communication (WPC), and wireless-powered backscatter communication (WPBC), e.g., [10], [11]. Specifically, in SWIPT networks, cf. Figure 2.3a, a transmitter broadcasts an information-carrying signal to provide information and energy delivery service simultaneously. In wireless-powered communication networks (WPCNs) as in Fig. 2.3b, wireless-powered devices first harvest energy, from dedicated energy transmitters (ET) or from ambient RF sources, such as hybrid access points (H-APs), and then exploit the harvested energy to transmit information signals. Hybrid access points (H-APs) are deployed which are capable of sending wireless power to users via WET in the downlink (DL) as well as coordinating wireless information transfer (WIT) to/ from users in the DL/ uplink (UL), respectively. In WPBC, cf. Figure 2.3c, energy is transferred in the downlink and information is transferred in the uplink, where backscatter modulation at a tag is used to reflect and modulate the incoming RF signal for communication with a reader (e.g., access point). Since no oscillators are needed at the tags to generate carrier signals, backscatter communications generally entail orders-of-magnitude lower power consumption than conventional radio communications.

The first and ideal receiver design for WIPT was introduced in the seminal paper of Varshney [12], where the information and the power can be extracted from the same received signal receiver. It was pointed out later that [13] such an assumption cannot be realized in practical

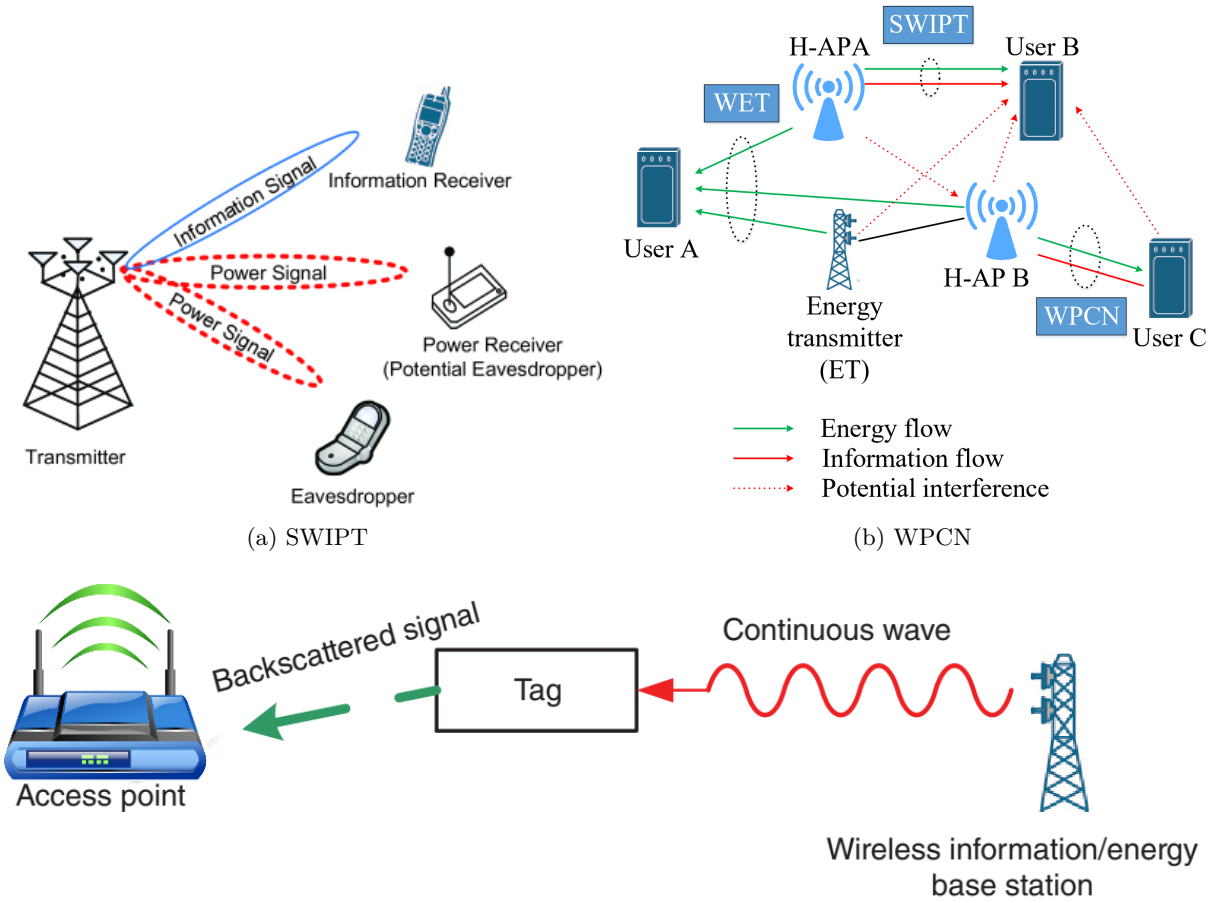


(a) SWIPT

(b) WPCN

(c) WPBC

Figure 2.3: Different forms of WIPT.

systems because EH circuits harvest the energy of the received signal directly in the RF domain, which destroys the modulated information (e.g., phase-embedded information) in the signal. In addition, conventional information decoding is performed in the digital baseband and the frequency down-converted signals cannot be used for EH [8]. Zhang and Ho in [13] proposed to split the received RF power into two distinct parts, one for EH and the other one for information decoding. This lead to two practical receiver architectures for WIPT, namely, time-switching receiver (TSR) and power splitting receiver (PSR), as illustrated in Fig. 2.4.

For the TSR, at any time the received signal is only connected either to the information receiver or to the energy receiver. The receiver switches between the co-located EH circuit and information decoding circuit for harvesting energy and decoding information in successive time slots. This receiver is considered to be easy to implement but with the reduction in throughput.

For the PSR, the received signal is split into two streams by a power divider with a fixed power ratio, which are used for EH and ID, respectively. This receiver incurs a higher receiver complexity compared to the TS process, but it enables the possibility of SWIPT and is more

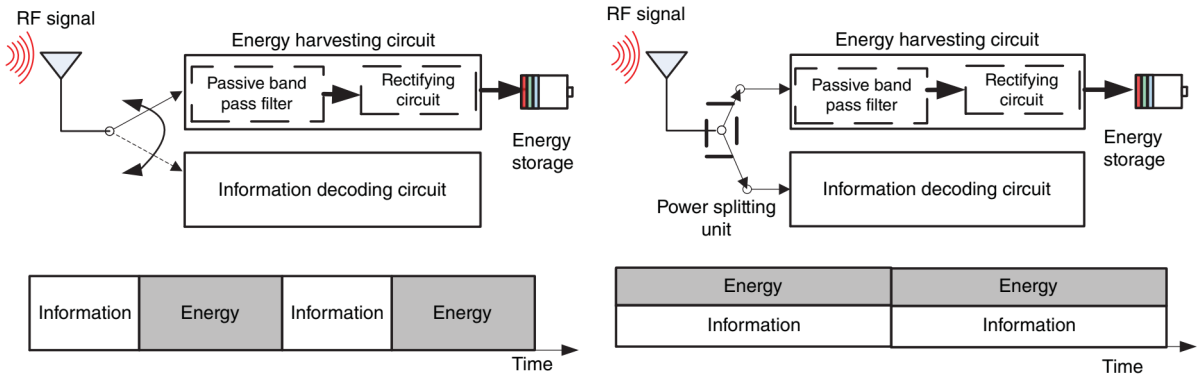


(a) Time-switching receiver

(b) Power splitting receiver

Figure 2.4: Practical receiver structures for WIPT.

suitable for applications with critical information/energy or delay constraints than the TSR [8].

### 2.2.2 WIPT in Cooperative Networks

#### 2.2.2.1 EH model in half-duplex relay networks

A typical EH-based HD relay network over a specific fading channel (maybe Rayleigh, Rician or Nakagami-m fading) is illustrated in Fig. 2.5, in which the source (S) and destination (D) can exchange their signal with the help of a relay (R).

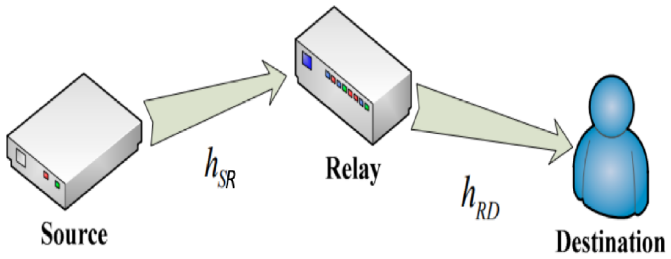


Figure 2.5: A simple HD relay network.

As mentioned above, two traditional EH schemes are usually considered, namely TSR protocol and PSR protocol [14]. For TSR protocol, as presented in Fig. 2.6a, the total symbol duration T is divided into two intervals with lengths $\alpha$ and $1-\alpha$, respectively, where $0 \leq \alpha \leq 1$. The first interval corresponds to the EH phase, and the second interval corresponds to the information transmission phase (which in turn can be divided into two sub-phases: from S to R and R to D, respectively).

During the first interval (EH phase), the RF signal received by R can be formulated as

$$y_r = h x_s + n_r, \tag{2.2}$$

where $x_s$ is the energy-transmitted signal with $E\left\{|x_s|^2\right\} = P_s$, $n_r$ is the zero-mean additive white Gaussian noise (AWGN) with variance $N_0$. Here $E(\cdot)$ denotes the expectation operation.

Then, the total harvested energy of $R$ during EH time $\alpha T$ is given by

$$E_R = \eta P_S |h_{SR}|^2 \alpha T, \tag{2.3}$$

where $0 < \eta < 1$ is the energy conversion efficiency which depends on the rectification process and the EH circuitry [15] and $P_S$ denotes the transmission power of the source S.

During the third interval (information forwarding phase), the relay uses this amount of energy to forward the source message to the destination. By the law of energy conservation, the average transmit power of $R$ can be found by

$$P_R^{(TSR-HD)} = \frac{E_R}{(1-\alpha)T/2} = \frac{2\eta\alpha P_S |h_{SR}|^2}{(1-\alpha)} = \kappa P_S |h_{SR}|^2, \tag{2.4}$$

where we define $\kappa \triangleq \frac{2\eta\alpha}{1-\alpha}$.

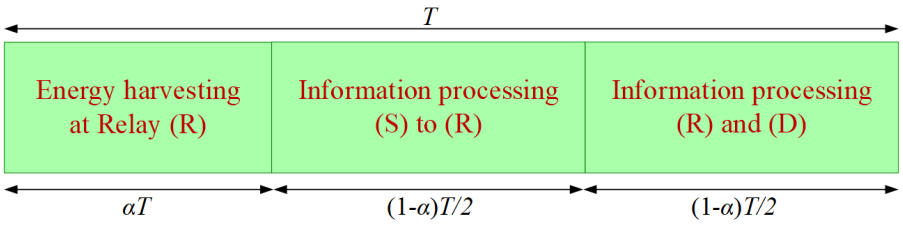


(a) TSR EH protocol

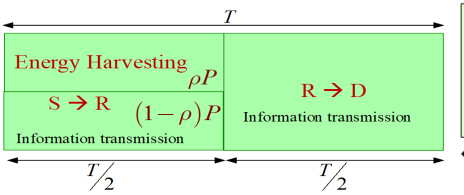


(b) PSR EH protocol

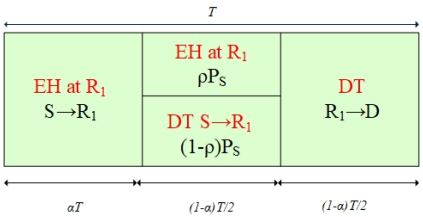


(c) TPSR EH protocol

Figure 2.6: EH protocols for HD relay networks.

For the PSR protocol, presented in Fig. 2.6b, the total symbol duration $T$ is divided into two intervals with lengths $T/2$ and $T/2$, respectively. The first $T/2$ interval is used for the source to relay information transmission, and the remaining half, $T/2$ is used for the relay to destination information transmission. During the first half of the block time, the fraction of the received

signal power, $(1-\rho)P$ ($P$ is the transmit power of source) is used for EH, and the remaining received power, $\rho T$ is used by the source to relay the information message, where $0 \leq \rho \leq 1$.

The received RF signal at the input of the EH unit can be calculated as

$$y_{h,r} = \sqrt{\rho} y_r = \sqrt{\rho} h x_s + \sqrt{\rho} n_r \tag{2.5}$$

From Equation (2.5), the harvested energy at R in the first interval $T/2$ can be formulated as the following

$$E_R = \eta \rho P |h_{SR}|^2 \frac{T}{2}. \tag{2.6}$$

R uses this amount of energy to forward the information signal in the second phase. By the law of energy conservation, the transmit power at R in the second phase can be calculated as

$$P_R^{(PSR-HD)} = \frac{E_h}{T/2} = \frac{\eta \rho P |h_{SR}|^2 (T/2)}{T/2} = \eta \rho P |h_{SR}|^2 \tag{2.7}$$

Besides the two protocols mentioned above, I also study a new protocol that was recently introduced, called the hybrid time-switching and power-splitting (TPSR) protocol [16]. Fig. 2.6c shows the time allocation in each transmission block. In the first interval of length $\alpha T$, where $0 \leq \alpha < 1$, S transfers energy by RF signal to the relay $R_1$. In the next $(1-\alpha)T/2$ interval, the power of the signal sent by S is split into two components: the first component with a power of $\rho P_s, (0 \leq \rho \leq 1)$ is used to harvest energy, while the second component with a power of $(1-\rho)P_s$ is used to decode the information at $R_1$. In the final interval with length $(1-\alpha)T/2$, $R_1$ transfers information to D using the harvested energy from previous intervals [17], [18].

By the similar analysis as above, we can get the formula for the total harvested energy by the relay R as

$$E_{R_1} = \eta P_S |h_{SR_1}|^2 \left[ \alpha T + \rho \frac{(1-\alpha)T}{2} \right]. \tag{2.8}$$

and the average transmit power of the relay during the information forwarding phase can be found as

$$P_{R_1}^{(TPSR-HD)} = \frac{E_{R_1}}{(1-\alpha)T/2} = \frac{\eta P_S |h_{SR_1}|^2 [2\alpha + \rho(1-\alpha)]}{(1-\alpha)} \tag{2.9}$$

#### 2.2.2.2 EH model in full-duplex relay networks

Fig. 2.7 plots the system model of a FD relay network with one source (S), one relay (R) and one destination (D). In our model, every terminal operates in a FD mode, where the relay is equipped with two antennas, one for transmitting and the other for receiving. In this system

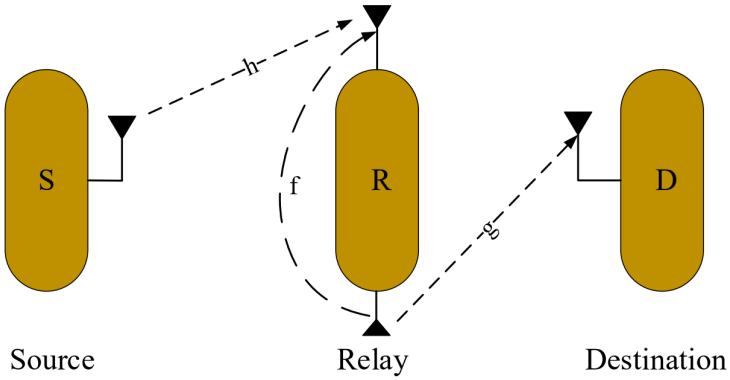


Figure 2.7: A simple EH-based FD relay network

model, we denote the channel gain between node S and the relay R is $h_{SR}$, between the relay $R$ and the destinations, $D$ is $h_{RD}$, the self-interference channel gain at $R$ is $h_{RR}$. Furthermore, the relay has only the energy to serve their purpose, so it needs to harvest the energy from the node before forwarding the information messages to the destination. The three EH protocols are summarized in Fig. 2.8. The EH model for FD networks only differs from the HD networks

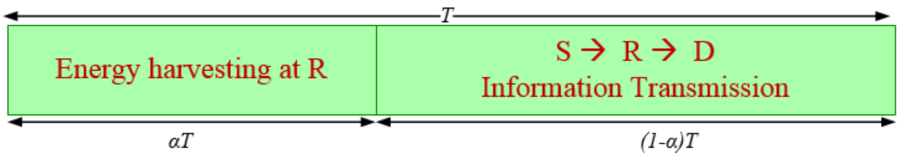


(a) TSR EH protocol

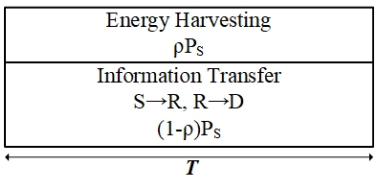


(b) PSR EH protocol

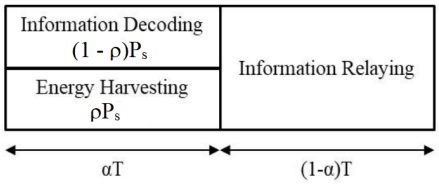


(c) TPSR EH protocol

Figure 2.8: EH protocols for FD relay networks.

by the information forwarding time. So, we can easily get the formulas of the average transmit power by the relay for three above protocols respectively as

$$P_R^{(TSR-FD)} = \frac{E_R}{(1-\alpha)T} = \frac{\eta\alpha T P_S |h_{SR}|^2}{(1-\alpha)T} = \frac{\kappa P_S |h_{SR}|^2}{2} \tag{2.10}$$

$$P_R^{(PSR-FD)} = \frac{E_R}{T} = \frac{\eta\rho P_S|h_{SR}|^2 T}{T} = \eta\rho P_S|h_{SR}|^2 \tag{2.11}$$

$$P_R^{(TPSR-FD)} = \frac{E_R}{(1-\alpha)T} = \frac{\eta P_S|h_{SR}|^2\alpha\rho}{(1-\alpha)} = \frac{\kappa\rho P_S|h_{SR}|^2}{2} \tag{2.12}$$

where $\kappa \triangleq \frac{2\eta\alpha}{1-\alpha}$.

## 2.3 Physical Layer Security in Wireless Communication Networks

### 2.3.1 Introduction

Today, wireless communications are increasingly used for a very wide range of applications, including banking and other financial transactions, social networking, environmental monitoring, and many others. Therefore, the security of wireless communication networks is of critical societal interest. Wireless security has traditionally been implemented at the higher layers rather than physical layer of wireless communication networks model. Data confidentiality, encryption are the primary methods of ensuring information security and its work well in most current situations. However, in some emerging networking technologies, issues of key management or computational complexity make the use of data encryption difficult. For examples, in wireless ad-hoc networks, the messages may pass through many intermediate terminals on the way from source to destination. Sensor or radio-frequency identification (RFID) networks might arise in the envisioned IoT, in which the end devices are of very lack of energy and computational capability. For the above reasons, PLS in wireless cooperative networks has become a major research topic in recent years, and considerable progress has been made in understanding the fundamental ability of the physical layer to support secure communications and in determining the consequent limits of this ability [19]. In particular, there are two principal properties of radio transmission namely diffusion and superposition can be exploited to provide data confidentiality through several mechanisms that degrade the ability of potential eavesdroppers to gain information about confidential messages. These mechanisms include the exploitation of fading, interference or artificial noise, path diversity and spectrum sharing, all of which also lead to potential techniques for implementation in practical wireless communication systems.

### 2.3.2 Information Theoretic Perspective

The problem of secure communication from an information theoretic perspective was first studied by Shannon. This work focused on symmetric key encryption systems, perhaps a more relevant development in this area was Aaron Wyner's work on the wiretap channel, which introduced the idea that secrecy can be imparted by the communication channel itself without resorting to the use of shared secret keys [20].

As show in Fig. 2.9, Alice wants to transmit a confidential message M to Bob while keeping it secret from Eve. Accordingly, Alice must encode the message M into a codeword $X^n$, Bob

will receive $Y^n$ and recover the original message. Note that a codeword of length n makes use of the channel n times; i.e.,$X^n = (X^l, ..., X^n)$, where $X^i$ is sent in the $i^{th}$ channel use. Similarly, $Y^n = (Y^l, ..., Y^n)$ and $Z^n = (Z^l, ..., Z^n)$ describe corresponding channel outputs at the legitimate receiver and eavesdropper, respectively.

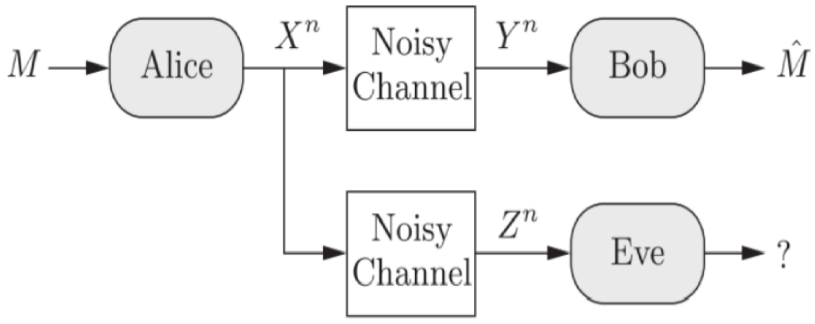


Figure 2.9: Wyner's wiretap channel.

The secrecy is defined in terms of equivocation, or conditional entropy. Specially, it required that the conditional entropy $\frac{1}{n}H(M|Z^n) \approx \frac{1}{n}H(M)$ so that the knowledge of the channel output $Z^n$ does not decrease the uncertainty rate about the message M; in other words, it does not provide any information about M. This criterion is known as weak secrecy and is often equivalently written in terms of mutual information as

$$\frac{1}{n}I(M; Z^n) \xrightarrow[n\to\infty]{} 0. \tag{2.13}$$

This quantity describes the information leaked about M to Eve in terms of a rate due to the normalization by the block length n. This definition of secrecy has its vulnerabilities as in [21] and can be strengthened by dropping the division by n to

$$I(M; Z^n) \xrightarrow[n\to\infty]{} 0. \tag{2.14}$$

This condition is termed strong secrecy and the intuition is to have the total amount of information leaked to Eve disappear as $n \to \infty$. Strong secrecy for the wiretap channel was first considered in [1]. Recently, different approaches to achieve strong secrecy were presented in [22], [23]. This demonstrates the usefulness of the strong secrecy criterion and establishes a desirable and practically relevant operational meaning.

$$C_s = \max_{V-X-(Y,Z)} (I(V;Y) - I(V;Z)), \tag{2.15}$$

where the maximization is over all random variables V and X such that the Markov chain relationship $X - Y - (Y, Z)$ is satisfied.

Obviously, the mutual information term $I(V;Y)$ represents the channel quality of the legitimate link and describes the rate at which Alice can reliably transmit to Bob. Accordingly, the term $I(V;Z)$ represents the channel quality of the eavesdropper link and the maximum transmission rate is penalized exactly by this quantity. Another important observation is that to have a positive secrecy capacity, the channel to Bob must have have an advantage over Eve.

### 2.3.3 Physical Layer Security over Fading Channel

The information theoretic approaches to security discussed above for discrete memoryless channels are extended to models for physical wireless channels. As a result, PLS mechanism will be established by exploiting the fading channel of wireless communications. Recall the Gaussian wiretap channel, one of the most basic model for wireless channels, having linear time-invariant multiplicative links corrupted by AWGN [24]. When Alice transmits a signal $X_i$, the received signals $Y_{B,i}$ at Bob and $Y_{E,i}$ at Eve at channel use i can then be expressed as

$$\begin{aligned} Y_{B,i} &= h_B X_i + N_{B,i}, \\ Y_{E,i} &= h_E X_i + N_{E,i}. \end{aligned} \tag{2.16}$$

where $h_B$ and $h_E$ are the channel gains between Alice and Bob and between Alice and Eve, respectively, and $N_{B,i}$ and $N_{E,i}$ are AWGNs, independent of the transmitted signals, with zero means and variances $\sigma_B^2$ and $\sigma_E^2$, respectively. Here, white noise refers to a random process that is independent from channel use to channel use. Considering an average transmit power constraint of P, the secrecy capacity of the Gaussian wiretap channel is given by

$$C_s = \frac{1}{2}\log\left(1+\frac{P|h_B|^2}{\sigma_B^2}\right) - \frac{1}{2}\log\left(1+\frac{P|h_E|^2}{\sigma_E^2}\right). \tag{2.17}$$

where all $h_{B,i}$, $h_{E,i}$, $N_{B,i}$, and are mutually independent. Here, $h_{B,i}$ and $h_{E,i}$ are fading coefficients that characterize the communication conditions at channel use i. The input signal is subject to an average power $\frac{1}{n}\sum_{i=1}^{n} E\left[X_i^2\right] \leq P$ constraint and the noise processes, which are independent from channel use to channel use, are Gaussian with zero means and variance $\sigma_B^2$ and $\sigma_E^2$ respectively, as before.

For ergodic fading channels, the fading coefficients are independent and identically distributed and are allowed to change from channel use to channel use. Hence, Alice, Bob, and Eve might experience a different fading state for each channel use. Assuming that all terminals have perfect channel state information (CSI) about the current fading state, so-called instantaneous CSI, the ergodic secrecy capacity has been proposed in [25] and is given as

$$C_s = \max_{E_A|\gamma|\leq P} \left[\frac{1}{2}\log\left(1+\frac{P|h_B|^2}{\sigma_B^2}\right) - \frac{1}{2}\log\left(1+\frac{P|h_E|^2}{\sigma_E^2}\right)\right]. \tag{2.18}$$

where $\gamma$ is the power allocation and $A = \left\{(h_B, h_E) : \frac{|h_B|^2}{\sigma_B^2} > \frac{|h_E|^2}{\sigma_E^2}\right\}$, so that the expectation is taken over all fading realizations in which Bob experiences a better channel in terms of signal to-noise ratio than Eve; i.e., $E_A[.]$ denotes the expectation over all $(h_A, h_E) \in A$.

### 2.3.4 Physical Layer Security in Cognitive Radio Networks

#### 2.3.4.1 Cognitive Radio Networks

Cognitive radio is a technology that can solve the scarcity of RF spectrum by allowing secondary users to opportunistically access the licensed channels without causing interference to the communications of the primary users [26]. Cognitive radio can change its transmitter parameters based on interaction with the environment in which it operates. There are two main characteristics of the cognitive radios. The first is cognitive capability, which refers to the ability of the radio technology to sense the information from its radio environment. Through this capability, the spectrum resources that are not used by primary users can be detected. Consequently, the best spectrum allocation schemes and transmission parameters can be selected. The second is re-configurability which enables a user to change the transmitting channel quickly and adaptively according to the radio environment. The components of a cognitive radio network show in Fig. 2.10 and can be classified as: the primary networks and the cognitive networks. The primary network (or licensed network) is referred to as an existing network, where the primary users have a license to operate in a certain spectrum band. If primary networks have an infrastructure, primary user activities are controlled through primary base stations. Due to their priority in spectrum access, the operations of primary users should not be affected by unlicensed users. The cognitive radio network (also called secondary network, or unlicensed network) does not have a license to operate in a desired band. Thus, additional functionality is required for cognitive radio users to share the licensed spectrum band.

#### 2.3.4.2 Physical Layer Security in CRNs

However, characteristics of cognitive radio technology have introduced new types of security threats and challenges in this environment [27]. First, there are both primary users and secondary users in the network and the secondary users should have the ability to tell the difference between primary users and malicious nodes. Second, the accuracy of sensing information gathered by secondary users is important but the malicious users may collect the same things to attack or interfere legitimate users. Owing to this fact, PLS has attracted significant attention in research community as an efficient approach to guaranteeing secrecy in cognitive radio networks. There have been studies that focused on PLS, from various perspectives and configurations, and under the context of cooperative communications [28] and cognitive radio [29].

The theoretical basis of PHY security for MIMO systems was investigated in [30] under the assumption that the perfect CSI of the eavesdropper channel is available. PHY security has also been investigated in relay networks. In [23], the authors proposed cooperative relaying

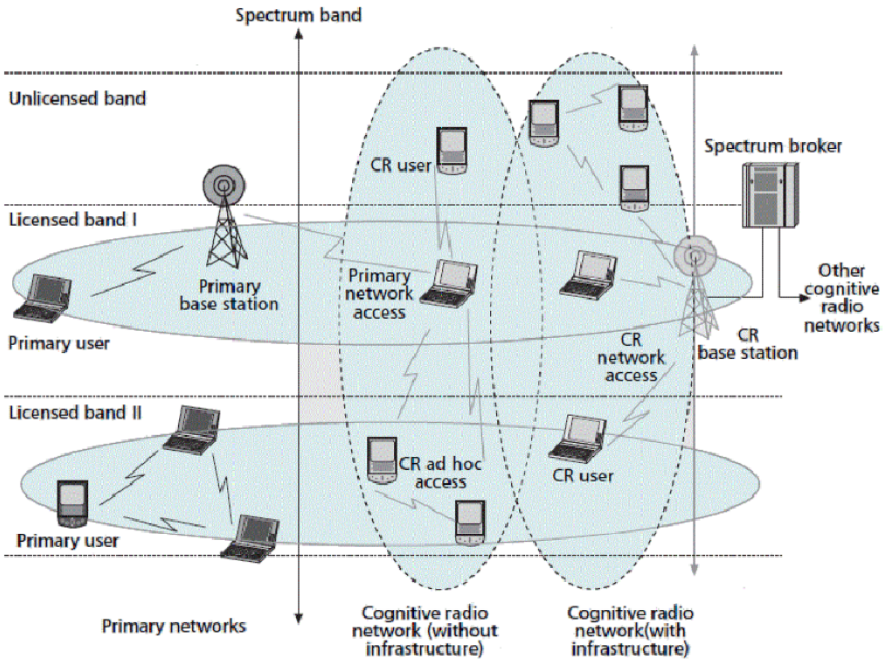


Figure 2.10: Cognitive Radio Network Architecture [23]

.

protocols to increase the secrecy rate. In [27], cooperative beamforming and user selection techniques were exploited to enhance the secrecy rate and SOP. Furthermore, the work in [31] introduced a secure switch-and-stay combining protocol to deal with the high relay switching rate issue of the CSI-based relay selection schemes.

The authors in [25], investigated PHY security through the use of beamforming (BF) combined with the injection of artificial noise. In [32], cooperative jamming was considered to enhance PHY security. Recently, a novel mode in which a relay, called jammer, transmits jamming signals to cause adding interference at the eavesdropper was proposed [20]. In that paper, the authors suggested several relay and jammer selection schemes to enhance the information security. Another related paper is [31], where the authors aimed to maximize the secrecy rate of secondary networks in an underlay cognitive radio MIMO broadcast channel.

Recently, security issues in cognitive radio networks have gained a great attention from the research community. In [33], to improve the PHY security for CRN, algorithms for selecting which secondary users (SU) share the licence spectrum were proposed. These solutions based on the fact that interference from secondary users affects not only on primary users but also on eavesdropper. While in [19], secondary transmitter (ST) was selected such that maximizes the secrecy capacity of the secondary link. Another solution was introduced in [1], where an jamming signal was sent along with information from ST to secondary receiver (SR). Particularly, in that work authors applied optimal theory to design the ST's transmit signal to maximize the secrecy performance of the the secondary network.

# 3 State-of-the-art

The concept of "Information security at the physical layer" was first introduced in 1949 by Prof. Shannon in his pioneering paper titled "Communication Theory of Secrecy Systems" [22]. However, not until recent years, thanks to the rapid development of radio communications, did this new concept attract interest from the academia and signal its widespread adoption in the study of information security for radio communication systems. Researchers have recently focused on information security issues at the physical layer in three main approaches: key-based secrecy, keyless security, and the evaluation of whether a system is capable of ensuring security at the physical layer.

The first approach looks for a security key based on the characteristics of the transmission environment. This is entirely feasible due to the complexity of the transmission environment of wireless communications. For example, different users will have different noisy versions of the transmitted signal, which allows encryption of the security key and ensures security between legitimate users. In 2003, Maurer et al. proposed several key agreement security protocols which can be implemented in a two-way public channel observed in the presence of passive eavesdropping equipment [34]. Ahlswede and Csiszar studied the increase of capacity in security keys with the aid of relevant information and obtained single-letter of the secrecy capacity with many arbitrary endpoints [35]. Chen and Jensen later developed protocols to generate security keys for MIMO systems with a channel correlation coefficient of time and space [36].

The second approach focuses on building a random encryption mechanism which seeks to hide the flow of information in the community to weaken interference eavesdropping devices by mapping each message to many code words according to an appropriate probability distribution. In this way, maximum ambiguity is created at eavesdropping devices, which indicates that communication can be safe without using a security key. Poor and Debbah demonstrated through their research groups that the above approach can be done via cooperative communications [37], by applying antenna selection techniques [1], or by solving the optimization problem using game theory [17]. Another method is the use of artificial noise to improve the security performance in wireless systems, which was proposed by Krikidis [38].

The third approach is to find a method of evaluation of whether the system is capable of ensuring information security. A system is considered capable of ensuring information security if channel legitimate capacity is greater than or at least equal to the eavesdropper channel capacity. The difference between channel legitimate capacity and eavesdropper channel capacity is called secrecy capacity, which is an important index to evaluate the security performance of the system. Performance evaluation of information security protocols at the physical layer for different types of channels was proposed by Sarkar [39]. In 2012, Pinto [40] studied the maximum secrecy capacity of the system and information-sharing capabilities of bugged machines (joint decoding). In another direction, Han's group investigated algorithms, such as matching theory [41] and coalitional games [42], to evaluate information security protocols at the physical layer

of the relay network.

RF has attracted the attention of the scientific community as a separate issue with the transmission of radio information. People have often used navigation antennae or large aperture antennae to overcome the high attenuation of radio energy transmission. With the development of RF energy circuits over the past few decades, low power transmissions for mobile devices in wireless systems have drawn increasing attention [2], [43]. The authors in [2] proposed a structure of wireless networks for RF charging stations overlapping cellular networks.

In [43], the authors proposed a harvest-then-transmit protocol for wireless networks coupled with energy transmission. In addition, many new navigation techniques are under current development to improve the efficiency of wireless energy transfer for mobile applications [43], [44]. The use of RF signals for two purposes of energy transfer and information transmission has been widely accepted until today [12], [45]. Simultaneous wireless information and power transfer (SWIPT) [13] has been proposed for the transmission of RF energy, often in low power areas, such as wireless sensor networks. SWIPT provides an advantage in terms of control to ensure low energy and information transfer requirements without sacrificing much of the transmitter hardware. However, the latest research results suggest that the optimal transfer of information and radio energy must pay for the design of the radio system. [12], [46]. The cause is that the RF signal determines the quality of the information, whereas the mean square value of the RF signal is the transmitted energy. As a result, the amount of information transmitted and transmitted energy cannot simultaneously reach the maximum. This led to the need to redesign the existing wireless network.

Security issues in wireless radio transmission networks with SWIPT appear when the transmitter can amplify information transmission power to facilitate the reception of energy at the receiver, easing the leak of information. One measure to reduce the potential for eavesdropping on unfriendly devices is the antenna orientation, which enhances the security of wireless networks. Much of the current research focuses on the use of artificial noise and interference signals to enhance energy transfer and improve system security. This idea is to attenuate the reception signal at the eavesdropping device by adding an artificial noise signal to the transmission channel.

Regarding the research in Vietnam and the Czech Republic on the topic of this thesis, to the best of my knowledge, some works focused on information security at the physical layer in RF energy transmission networks. Specifically, Bao et al. studied the possibility of using forwarding node selection to increase information security at the physical layer and simultaneously compared the information security capacity of three switch node types. They also studied the possibility of using multi-channel communications to improve the security capacity of radio systems [47]. In addition, other studies investigated and evaluated the security performance of cognitive radio networks [48], PLS performance in dissimilar channel networks with legitimate channel fading different from illegal channel's [49], or PLS of the UWB broadband and multi-legged systems with multiple eavesdropping devices. Recently, the Wireless Communications Research Group

(WiCOM) at Ton Duc Thang University (TDTU) has also published several interesting results on the performance analysis of EH in an advanced communication system such as FD [50], MIMO [51], and NOMA [52] systems. Novel and effective EH protocols [53] and performance analysis of diversity techniques in EH-based wireless relay networks [51] were also investigated, but PLS was not mentioned in these works.

In the Czech Republic, perhaps the most contributions to performance analysis of EH and physical layer security have been from the research lab led by Voznak. In 2019, Huynh [54] delivered a PhD dissertation in which he investigated the performance of EH protocols for two-way relay networks which applied NOMA for enhancing transmission reliability. He also introduced the idea of combining NOMA with PLS to get the best improvement. However, his work was limited to two-way dual-hop single-antenna relay networks with a simple PLS model (only one single-antenna eavesdropper). It should be noted that perfect channel state information and perfect hardware were assumed in that dissertation. However, more advanced PLS schemes were presented in Phu's dissertation [55]. The main goal of Phu's dissertation was to find effective schemes of PLS to enhance the security of cooperative relaying networks, especially in the presence of hardware impairment. This dissertation focused on underlay cognitive radio networks with dual-hop or multi-hop relays, in which a secondary user wants to transmit data to another secondary user without being intercepted by a nearby eavesdropper or interfering with the communication of primary users. The author mainly investigated the security performance of the network in two cases: dual-hop and multi-hop relaying, and the proposed schemes were developed on the relaying selection mechanism. EH was not the main focus in that dissertation. The author only introduced the EH method to supply power for the jammers and degrade the decoding performance of the eavesdropper. Only TSR protocol was considered, and only a direct link between source and destination was applied (without any relay). It is clear that the physical layer information in the radio energy transmission network has not been investigated much and that many challenges still need to be addressed.

# 4 Aims

This section lists the specific goals and a rough plan for each part of the proposed research. Before looking at detailed goals, I would like to present the scope of my dissertation, which is limited to the following. First, my dissertation thesis focuses on different techniques applied to the physical layer. Regarding the wireless channel models, I consider three models, including Rayleigh, Rician, and Nakagami-m channels. The secrecy performance metrics include secrecy capacity, probability of non-zero secrecy capacity, security outage probability, and intercept probability. Channel estimation errors and hardware impairment levels, if they exist, will be modeled as Gaussian random variables throughout the dissertation. For EH purposes, I focus on harvesting from RF signals, either from the communication nodes or the power beacons.

## 4.1 Aim 1: Extend the research on RF energy harvesting protocols, especially the hybrid TSR and PSR protocol, for a broader range of wireless relaying network models under different channel and transceiver conditions.

Energy harvesting from the RF signal sources to prolong the lifetime of energy-constrained wireless networks such as cellular networks or wireless sensor networks has been investigated for at least a decade. To contribute to the continuous development of EH, I study novel wireless network models that take into account the radio energy transfer. Specifically, advanced techniques that have been the candidates for 5G and 6G mobile communications, such as full-duplex (FD) communication [56], non-orthogonal multiple-access (NOMA) [57], etc., should be studied together with RF energy harvesting protocols to ascertain novel communication schemes that could enhance the overall system performance. My first goal is to derive the closed-form expressions of the OP and the average throughput of these systems as the key performance metrics. The validity of the derived expressions are checked with independent simulations. From these results, the impact of EH parameters, such as the TS factor and PS factor, and other transceiver and channel parameters, such as source transmission rate and transmitting-power-to-noise ratio, the channel average gain on system performance can be revealed. For certain scenarios, either the optimal TS or PS ratio is determined to maximize the information throughput from the sources to the destinations.

## 4.2 Aim 2: Proposal of a new secrecy protocol at the physical layer and a comparison the secrecy performance with existing protocols to validate that my protocol achieves better results.

Besides the conventional cryptographic techniques employed to improve security, the pioneering work by Wyner [58] on wiretap channels and subsequent [59], [60] work showed that secrecy can also be guaranteed along with reliability by introducing randomness in coding or signaling to

confuse the eavesdropper at the physical layer. This is known as physical layer security (PLS). During the last decade, PLS has experienced a resurgence of interest from a host of scientists [61] due to its potential to enhance the quality of communication to satisfy the vast demand of mobile users.

Hence, I focus on some novel secrecy protocols at the physical layer for wireless relay networks. In this part of my dissertation, I provide a security analysis for some advanced PLS protocols for wireless relay networks, where the users communicate with the aid of intermediate relay nodes but suffer eavesdropping from unfriendly users. In this context, both the reliability and security aspect should be taken into consideration. In particular, I analyze and present performance evaluation expressions regarding the PLS of the system, such as the amount of security, the probability of the existence of security capacity, and the probability of the security stop. From the analyses, as the second aim, I propose new advanced protocols which can enhance the security of wireless sensor relay networks (WSRN). Again, the effect of the various channel and transceiver parameters on the reliability and security performance of the networks mentioned above is investigated carefully through analysis and simulation.

## 4.3 Aim 3: Integrate EH and PLS together with other advanced techniques (such as MIMO beamforming, multi-hop communications, jamming, etc.) to further strengthen the capacity to ensure better network security and reliability than the used approaches nowadays.

To the best of our knowledge, the study of PLS in RF EH-based networks has not been investigated much in the literature. One of the most recent results of PLS in EH-based networks [62], which was published in early 2020, only considered a simple relay network with a single relay. Motivated by these above facts, I provide a thorough analysis in this dissertation of the reliability and security performance of various models of wireless relay networks which employ EH protocols in the presence of eavesdroppers.

I derive the closed-form expression of key performance factors for my proposed models, including the OP of legitimate communications, the intercept probability of the eavesdropper (IP), the SOP of the system, and the average secrecy capacity (ASC). In fact, this is a challenging problem since the probability analysis involves many random variables, which complicates derivation. It is worth noting that optimal values of the EH parameters, such as the time-switching factor and PS factor for each relay and jammer configuration, should be available. These are determined in this dissertation.

Furthermore, advanced techniques to further enhance the information security capabilities of the network are integrated into my new system model, including MIMO beamforming or diversity, multi-hop relaying, and friendly jamming. The general method for achieving this goal is an assessment of the results acquired alongside the constraints to propose better solutions and compare the obtained results with previous studies under the same conditions.

# 5 Performance Analysis of RF EH protocols, especially the hybrid TPSR, for various network models under different channel and transceiver conditions

For achieving the first goal of my dissertation, I apply all available RF EH protocols, including TSR, PSR, and hybrid TPSR protocols, to different configurations of wireless cooperative networks and provide the thorough performance analysis of these systems.

## 5.1 RF Energy Harvesting in Full-Duplex Relaying Networks

FD transmission is a promising technique to enhance the capacity of communication systems. In this section, we propose and investigate the system performance of the EH-based two-way FD relaying network over Rician fading environment. I introduce two models that apply RF energy harvesting, including two-way relaying model and multi-source relaying model. [HDH04], [HDH06], [HDH10], [HDH11], [HDH14], [HDH15], [HDH16] [HDH17].

### 5.1.1 Energy harvesting based two-way full-duplex relaying network over a Rician fading environment

#### 5.1.1.1 Introduction

In the 5G era, wireless networks should offer up to tens of Gbps data rate to support a variety of emerging services, which stimulates researchers to continually explore innovative techniques with higher spectrum efficiency. The concept of FD technique, which allows the communication node to transmit and receive signals over the same frequency band at the same time slot, has been proposed and discussed [63], [64]. In comparison with the HD mode, FD mode can double the spectral efficiency, because it exploits the resources more efficiently.

Two-way relaying, where two users exchange information with each other via a single or multiple relays, provides improved spectral efficiency compared to conventional one-way relaying by using either superposition coding or physical layer network coding at relays. Relaying and FD schemes are combined to achieve higher data rates [65], [66]. In [65], the authors investigate one-way FD (OWFD) relaying and two-way HD (TWHD) relaying to minimize/recover the spectral efficiency loss associated with one-way HD (OWHD) relaying which requires additional resources (e.g., time slots or frequencies) to transmit data. In [66] and [67], the authors present OWFD relaying with multiple antennas to provide a solution to overcome the spectral efficiency loss in OWHD relaying. In [68], the authors investigate OWFD relaying with opportunistic relay selection to enhance the performance of OWHD relaying. It can be seen that most previous works are focused on OWFD relaying, and there have been few works on two-way FD (TWFD) relaying.

In this section, the system performance of the time-switching EH-based TWFD relay network over Rician fading environment is proposed and investigated. Firstly, we analyze and demon-

strate the analytical expressions of the AT, OP, the optimal TS factor, and SER of the proposed system. In the second step, the effect of various system parameters on the system performance is presented and investigated. In the final step, the analytical results are also demonstrated by Monte-Carlo simulation.

#### 5.1.1.2 System Model

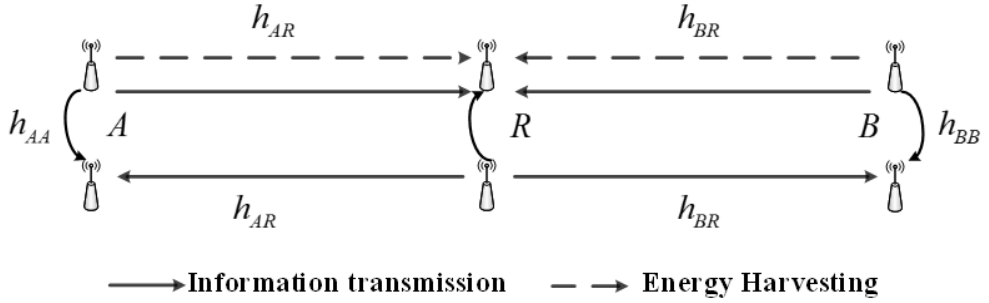


Figure 5.1: System model.

In this part, I investigate the performance of EH methods applied for a TWFD relaying network over Rician fading environment, which is illustrated in Fig. 5.1. The information transmission and energy transfer between the nodes A, B via the helping relay R. Each node has two antennas, which are responsible for signal transmission and reception, respectively. EH and information processing at the relay follow the TSR protocol similar to Fig. 2.8a. The information transfer process should consist of two phases: (i) multiple-access phase: two sources A and B send their message to the relay; and (ii) broadcast phase: relay R amplifies the sum of two received signals from A and B, then broadcasts it to A and B again. At each node A and B, its own message is subtracted from the received signal, and the remaining signal is decoded to see the original message from the other source. [HDH10].

Using (2.10) for each source and then combining them together, we get the average transmission power of $R$ as

$$P_R = \frac{E_R}{(1-\alpha)T} = \frac{\eta\alpha T P_{AB}}{(1-\alpha)T}\left(|h_{AR}|^2 + |h_{BR}|^2\right) = \frac{\kappa}{2}P_{AB}\left(|h_{AR}|^2 + |h_{BR}|^2\right), \tag{5.1}$$

where $\kappa \triangleq \frac{2\eta\alpha}{1-\alpha}$.

For FD system, the multiple-access phase (MAP) and the broadcast phase (BCP) can occur at the same time. Therefore, the received signal at the relay can be expressed as

$$y_R = h_{AR}x_A + h_{BR}x_B + h_{RR}x_R + n_R, \tag{5.2}$$

where $x_A$, $x_B$ are the transmission signal from A and B, respectively, $h_{RR}$ denotes the residual self-interference channel at R and $n_R$ the zero-mean additive white Gaussian noise (AWGN) with variance $N_0$, $E\{|x_A|^2\} = E\{|x_B|^2\} = P_{AB}$; $E\{|x_R|^2\} = P_R$. Here $E\{\cdot\}$ denotes the expectation operation, $h_{AR}$, $h_{BR}$ are the Rician channel gains.

In this model, the amplify-and-forward (AF) relaying strategy is used. Hence, the received signal at relay R is amplified by a factor $\beta$ which is given by

$$\beta = \frac{x_R}{y_R} = \sqrt{\frac{P_R}{P_{AB}|h_{AR}|^2 + P_{AB}|h_{BR}|^2 + P_R|h_{RR}|^2 + N_0}}. \tag{5.3}$$

Then the received signal at the node A can be express as

$$y_A = h_{AR}x_R + h_{AA}x_A + n_A, \tag{5.4}$$

where $x_R$ are the transmission signal from $R$, $h_{AA}$ denotes the residual self-interference channel at node $A$ and $n_A$ is the zero-mean AWGN with variance $N_0$. Combining (5.2) and (5.3), (5.4) can be rewritten as

$$y_A = \beta h_{AR}^2 x_A + \beta h_{AR}h_{BR}x_B + \beta h_{AR}h_{RR}x_R + \beta h_{AR}n_R + h_{AA}x_A + n_A. \tag{5.5}$$

In (5.5), the first term of equation ($\beta h_{AR}^2 x_A$) can be removed due to network coding as presented in [69]. By substituting (5.1), (5.3) into (5.5) and doing some algebras, the received signal-to-interference-plus-noise ratio (SINR) at node A can be obtained as

$$\gamma_A = \frac{\kappa\psi^2|h_{AR}|^2|h_{BR}|^2\left(|h_{AR}|^2 + |h_{BR}|^2\right)}{\left[\left(|h_{AR}|^2 + |h_{BR}|^2\right)\psi\left(\kappa|h_{AR}|^2N_0 + 2N_0\right)\right] + 2}, \tag{5.6}$$

where we denote $\psi = \frac{P_{AB}}{\Omega_{RR}+1} = \frac{P_{AB}}{\Omega_{AA}+1}$.

At high SINR regime, (5.6) can be approximated as

$$\gamma_A \approx \frac{\kappa\psi XY}{\kappa XN_0 + 2N_0} = \frac{\kappa\varphi\omega_1\omega_2}{\kappa\omega_1 + 2}, \tag{5.7}$$

where $\varphi = \frac{\psi}{N_0}, \omega_1 = |h_{AR}|^2, \omega_2 = |h_{BR}|^2$.

In this analysis, please note that for convenience, the residual self-interference (RSI) at the three nodes is modeled as i.i.d. AWGN with zero mean and variance of $\Omega_{RR}$, $\Omega_{AA}$, $\Omega_{BB}$, respectively [70]. In addition, please note that if we set $\Omega = \Omega_{RR} = \Omega_{AA} = \Omega_{BB} = 0$ and replace $\kappa$ by $2\kappa$, $\gamma_A$ turns into SINR of HD AF relay system. For similarity, we can obtain SINR at node B as $\gamma_B = \frac{\kappa\varphi\omega_1\omega_2}{\kappa\omega_2+1}$.

#### 5.1.1.3 System Performance

In this work, we consider the delay limited transmission mode, where the average throughput

can be computed from the OP. Due to symmetry of the problem, I only provide the results for node A.

**Theorem 5.1** *The OP at the source node A can compute by*

$$P_{out,A} = 1 - 2a_1a_2e^{-\frac{b_2\gamma_{th}}{\varphi}} \sum_{l=0}^{\infty}\sum_{k=0}^{\infty}\sum_{m=0}^{l}\sum_{n=0}^{m} \frac{K^{l+k}b_1^{\frac{k+n-1}{2}}b_2^{\frac{2m+k-n-1}{2}}}{l!n!(m-n)!(k!)^2\kappa^{\frac{k+n+1}{2}}} \left(\frac{\gamma_{th}}{\varphi}\right)^{m+\frac{k-n+1}{2}} K_{k-n+1}\left(2\sqrt{\frac{b_1b_2\gamma_{th}}{\kappa\varphi}}\right), \tag{5.8}$$

*where $K_v(\cdot)$ is the modified Bessel function of the second kind and $v^{th}$ order.*

**Proof** From [71] the probability density function (PDF) of the random variable (RV) $\omega_i$, where $i \in \{1, 2\}$, can be formulated by

$$f_{\omega_i}(x) = \frac{(K+1)e^{-K}}{\lambda_i} e^{-\frac{(K+1)x}{\lambda_i}} I_0\left(2\sqrt{\frac{K(K+1)x}{\lambda_i}}\right), \tag{5.9}$$

where $\lambda_i$ is the mean value of RV $\omega_i$, K is the Rician K-factor defined as the ratio of the power of the line-of-sight (LOS) component to the scattered components and $I_0(\cdot)$ is the zero-th order modified Bessel function of the first kind. Now, by using $a_i = \frac{(K+1)e^{-K}}{\lambda_i}, b_i = \frac{K+1}{\lambda_i}$ and $I_0(x) = \sum_{l=0}^{\infty} \frac{x^{2l}}{2^{2l}(l!)^2}$ [72], the equation (5.9) can be rewritten as

$$f_{\omega_i}(x) = a_i \sum_{l=0}^{\infty} \frac{(b_iK)^l}{(l!)^2} x^l e^{-b_ix}. \tag{5.10}$$

The cumulative density function (CDF) of $\omega_i$ can be obtained like in [73], [74]. We have:

$$F_{\omega_i}(\varsigma) = \int_0^{\varsigma} f_{\omega_i}(x)dx = 1 - \frac{a_i}{b_i}\sum_{l=0}^{\infty}\sum_{m=0}^{l} \frac{K^l {b_i}^m}{l!m!}\varsigma^m e^{-b_i\varsigma}. \tag{5.11}$$

Then the OP at the node A can calculate as

$$P_{out,A} = F_{\gamma_A}(\gamma_{th}) = \Pr(\gamma_A < \gamma_{th}) = \Pr\left(\frac{\kappa\varphi\omega_1\omega_2}{\kappa\omega_1 + 2} < \gamma_{th}\right). \tag{5.12}$$

where $\gamma_{th} = 2^{2R} - 1$. Now (5.12) can reformulate as

$$P_{out,A} = \int_0^{\infty} \Pr\left\{\omega_2 < \frac{\gamma_{th}\kappa\omega_1 + 2\gamma_{th}}{\kappa\varphi\omega_1}|\omega_1\right\} f_{\omega_1}(\omega_1)d\omega_1 = \int_0^{\infty} F_{\omega_2}\left(\frac{\gamma_{th}\kappa\omega_1 + 2\gamma_{th}}{\kappa\varphi\omega_1}\right) f_{\omega_1}(\omega_1)d\omega_1. \tag{5.13}$$

Combining (5.13) with (5.9), (5.10) we have:

$$P_{out,A} = 1 - \int_0^{\infty} \frac{a_2}{b_2} \sum_{l=0}^{\infty} \sum_{m=0}^{l} \frac{K^l {b_2}^m}{l!m!} \left[\frac{\kappa\omega_1\gamma_{th} + 2\gamma_{th}}{\kappa\varphi\omega_1}\right]^m e^{-b_2\left[\frac{\kappa\omega_1\gamma_{th}+2\gamma_{th}}{\kappa\varphi\omega_1}\right]} a_1 \sum_{l=0}^{\infty} \frac{(b_1 K)^l}{(l!)^2} \omega_1^l e^{-b_1\omega_1} d\omega_1$$
$$= 1 - \int_0^{\infty} a_1 a_2 \sum_{l=0}^{\infty} \sum_{k=0}^{\infty} \sum_{m=0}^{l} \frac{K^{l+k} b_2^{m-1} b_1^k}{l!m!(k!)^2} \left(\frac{\gamma_{th}}{\varphi}\right)^m \left[1 + \frac{2}{\kappa\omega_1}\right]^m e^{-\frac{b_2\gamma_{th}}{\varphi}} e^{\frac{-2b_2\gamma_{th}}{\kappa\varphi\omega_1}} \omega_1^k e^{-b_1\omega_1} d\omega_1. \tag{5.14}$$

By applying the equation $(x+y)^m = \sum_{n=0}^{m} \binom{m}{n} x^{m-n} y^n$ to (5.14), the OP can demonstrate as

$$P_{out,A} = 1 - \int_0^{\infty} a_1 a_2 \sum_{l=0}^{\infty} \sum_{k=0}^{\infty} \sum_{m=0}^{l} \frac{K^{l+k} b_1^k b_2^{m-1}}{l!m!(k!)^2} \left(\frac{\gamma_{th}}{\varphi}\right)^m \sum_{n=0}^{m} \binom{m}{n} \left[\frac{2}{\kappa\omega_1}\right]^n e^{\frac{-b_2\gamma_{th}}{\varphi}} e^{\frac{-2b_2\gamma_{th}}{\kappa\varphi\omega_1}} \omega_1^k e^{-b_1\omega_1} d\omega_1$$
$$= 1 - a_1 a_2 e^{\frac{-b_2\gamma_{th}}{\varphi}} \sum_{l=0}^{\infty} \sum_{k=0}^{\infty} \sum_{m=0}^{l} \sum_{n=0}^{m} 2^n \frac{K^{l+k} b_1^k b_2^{m-1}}{l!n!(m-n)!(k!)^2 \kappa^n} \left(\frac{\gamma_{th}}{\varphi}\right)^m \int_0^{\infty} \omega_1^{k-n} e^{\frac{-2b_2\gamma_{th}}{\kappa\varphi\omega_1}} e^{-b_1\omega_1} d\omega_1. \tag{5.15}$$

Using [72, pp. 3.471, 9], the (5.15) can reformulate as

$$\begin{aligned} P_{out,A} &= 1 - 2a_1 a_2 e^{-\frac{b_2\gamma_{th}}{\varphi}} \\ &\times \sum_{l=0}^{\infty} \sum_{k=0}^{\infty} \sum_{m=0}^{l} \sum_{n=0}^{m} \frac{2^n K^{l+k} b_1^k b_2^{m-1}}{l!n!(m-n)!(k!)^2 \kappa^n} \left(\frac{\gamma_{th}}{\varphi}\right)^m \left(\frac{2b_2\gamma_{th}}{b_1\kappa\varphi}\right)^{\frac{k-n+1}{2}} K_{k-n+1}\left(2\sqrt{\frac{2b_2 b_1\gamma_{th}}{\kappa\varphi}}\right) \\ &= 1 - 2a_1 a_2 e^{-\frac{b_2\gamma_{th}}{\varphi}} \\ &\times \sum_{l=0}^{\infty} \sum_{k=0}^{\infty} \sum_{m=0}^{l} \sum_{n=0}^{m} \frac{2^{\frac{n+k+1}{2}} K^{l+k} b_1^{\frac{k+n-1}{2}} b_2^{\frac{2m+k-n-1}{2}}}{l!n!(m-n)!(k!)^2 \kappa^{\frac{k+n+1}{2}}} \left(\frac{\gamma_{th}}{\varphi}\right)^{m+\frac{k-n+1}{2}} K_{k-n+1}\left(2\sqrt{\frac{2b_1 b_2\gamma_{th}}{\kappa\varphi}}\right). \end{aligned} \tag{5.16}$$

■

As a result of Theorem 5.1, the **achievable throughput** at the source nodes A and B can be computed by

$$\tau_j = (1 - P_{out\_j})(1-\alpha)R, \tag{5.17}$$

where $j \in \{A, B\}$.

Next, the expressions for the symbol error rate (SER) at nodes A and B of the proposed system are derived. Thus, we have SER equations as

$$SER_j = E\left[\varpi Q(\sqrt{2\theta\gamma_j})\right] = \frac{\varpi\sqrt{\theta}}{2\sqrt{\pi}} \int_0^{\infty} \frac{e^{-\theta x}}{\sqrt{x}} F_{\gamma_j}(x) dx, \tag{5.18}$$

where $j \in \{A, B\}$ and $Q(t) = \frac{1}{\sqrt{2\pi}} \int_t^\infty e^{-x^2/2} dx$ is the Gaussian Q-function, $\varpi$ and $\theta$ are constants which depend on modulation type. For example, $(\varpi, \theta) = (1, 1)$ for binary phase-shift keying (BPSK), $(\varpi, \theta) = (1, 2)$ for quadrature phase shift keying (QPSK).

**Theorem 5.2** *The SER at the node A of the proposed system is given as*

$$SER_A = \frac{\varpi}{2} - \frac{a_1 a_2 \varpi \sqrt{\theta}}{\sqrt{\pi}} \sum_{l=0}^{\infty} \sum_{k=0}^{\infty} \sum_{m=0}^{l} \sum_{n=0}^{m} \frac{K^{l+k} 2 b_1^{\frac{k+n-2}{2}} b_2^{\frac{2m+k-n-2}{2}}}{l! n! (m-n)! (k!)^2 \kappa^{\frac{k+n}{2}} \varphi^{m+\frac{k-n}{2}}} \left[\frac{b_2}{\varphi} + \theta\right]^{-\left(\frac{2m-n+k+1}{2}\right)}$$
$$\times \Gamma\left(m + \frac{1}{2}\right) \Gamma\left(m - n + k + \frac{3}{2}\right) \exp\left[\frac{b_1 b_2}{\kappa b_2 + \kappa\theta\varphi}\right] W_{-\frac{2m-n+k+1}{2}, \frac{k-n+1}{2}}\left[\frac{2 b_1 b_2}{\kappa\{b_2 + \theta\varphi\}}\right], \quad (5.19)$$

**Proof** From (5.18), we have:

$$SER_A = \frac{\varpi\sqrt{\theta}}{2\sqrt{\pi}} \int_0^\infty \frac{e^{-\theta x}}{\sqrt{x}} dx - \frac{a_1 a_2 \varpi \sqrt{\theta}}{\sqrt{\pi}}$$
$$\times \int_0^\infty \frac{e^{-\theta x}}{\sqrt{x}} e^{\frac{-b_2 x}{\varphi}} \sum_{l=0}^{\infty} \sum_{k=0}^{\infty} \sum_{m=0}^{l} \sum_{n=0}^{m} \frac{2^{\frac{k+n+1}{2}} K^{l+k} b_1^{\frac{k+n-1}{2}} b_2^{\frac{2m+k-n-1}{2}}}{l! n! (m-n)! (k!)^2 \kappa^{\frac{k+n+1}{2}}} \left(\frac{x}{\varphi}\right)^{m+\frac{k-n+1}{2}} K_{k-n+1}\left(\sqrt{\frac{8 b_1 b_2 x}{\kappa\varphi}}\right) dx$$
$$= \frac{\varpi\sqrt{\theta}}{2\sqrt{\pi}} \int_0^\infty \frac{e^{-\theta x}}{\sqrt{x}} dx - \frac{a_1 a_2 \varpi \sqrt{\theta}}{\sqrt{\pi}}$$
$$\times \sum_{l=0}^{\infty} \sum_{k=0}^{\infty} \sum_{m=0}^{l} \sum_{n=0}^{m} \frac{2^{\frac{k+n+1}{2}} K^{l+k} b_1^{\frac{k+n-1}{2}} b_2^{\frac{2m+k-n-1}{2}}}{l! n! (m-n)! (k!)^2 \kappa^{\frac{k+n+1}{2}} \varphi^{m+\frac{k-n+1}{2}}} \int_0^\infty x^{\frac{2m-n+k}{2}} e^{-x\left(\frac{b_2}{\varphi}+\theta\right)} K_{k-n+1}\left(\sqrt{\frac{8 b_1 b_2 x}{\kappa\varphi}}\right) dx. \quad (5.20)$$

Let $J_2 = \int_0^\infty x^{\frac{2m-n+k}{2}} e^{-x\left[\frac{b}{\varphi}+\theta\right]} K_{k-n+1}\left(2b\sqrt{\frac{x}{\kappa\varphi}}\right) dx$. By using [72, pp. 3.361, 1], we have:

$$\frac{\varpi\sqrt{\theta}}{2\sqrt{\pi}} \int_0^\infty \frac{e^{-\theta x}}{\sqrt{x}} dx = \frac{\varpi\sqrt{\theta}}{2\sqrt{\pi}} \frac{\sqrt{\pi}}{\sqrt{\theta}} = \frac{\varpi}{2} \quad (5.21)$$

By using [72, p. 6.643.3], we have:

$$\int_0^\infty t^{\mu-\frac{1}{2}} e^{-\alpha t} K_{2v}(2\beta\sqrt{t}) dt = \frac{\alpha^{-\mu}}{2\beta} \Gamma\left(\mu - v + \frac{1}{2}\right) \Gamma\left(\mu + v + \frac{1}{2}\right) \exp\left(\frac{\beta^2}{2\alpha}\right) W_{-\mu,v}\left(\frac{\beta^2}{\alpha}\right), \quad (5.22)$$

Table 5.1: Simulation parameters.

| Symbol | Name | Value |
|---|---|---|
| $\eta$ | Energy harvesting efficiency | 0.7 |
| $\lambda_1$ | Mean of $\|h_{AR}\|^2$ | 0.5 |
| $\lambda_2$ | Mean of $\|h_{BR}\|^2$ | 0.5 |
| $K$ | Rician K-factor | 3 |
| $\gamma_{th}$ | SNR threshold | 7 |
| $\mathrm{P}_{AB}/\mathrm{N}_0$ | Source power to noise ratio | 0-30dB |
| $\Omega_{AA} = \Omega_{BB} = \Omega_{RR} = \Omega$ | Residual self-interference | 0-15dB |
| $R$ | Source rate | 1.5 bit/s/Hz |

where $\Gamma(\cdot)$ is the gamma function and $W(\cdot)$ is the Whittaker function. Then we get:

$$J_2 = \left[\frac{b}{\varphi} + \theta\right]^{-\frac{2m-n+k+1}{2}} \frac{\sqrt{\kappa\varphi}}{2b\sqrt{(2)}} \Gamma\left(m + \frac{1}{2}\right) \Gamma\left(m - n + k + \frac{3}{2}\right) \exp\left(\frac{b^2}{\kappa b + \kappa\theta\varphi}\right) \times W_{-\frac{2m-n+k+1}{2}, \frac{k-n+1}{2}}\left[\frac{2b^2}{\kappa\{b + \theta\varphi\}}\right] \tag{5.23}$$

and

$$SER_A = \frac{\varpi}{2} - \frac{a^2\varpi\sqrt{\theta}}{\sqrt{\pi}} \sum_{l=0}^{\infty}\sum_{k=0}^{\infty}\sum_{m=0}^{l}\sum_{n=0}^{m} \frac{2^{\frac{k+n+1}{2}} K^{l+k} b^{m+k-1}}{l!n!(m-n)!(k!)^2 \kappa^{\frac{k+n+1}{2}} \varphi^{m+\frac{k-n+1}{2}}} \left[\frac{b}{\varphi} + \theta\right]^{-\frac{2m-n+k+1}{2}} \frac{\sqrt{\kappa\varphi}}{2b\sqrt{2}} \times \Gamma\left(m + \frac{1}{2}\right) \Gamma\left(m - n + k + \frac{3}{2}\right) \exp\left[\frac{b^2}{\kappa b + \kappa\theta\varphi}\right] W_{-\frac{2m-n+k+1}{2}, \frac{k-n+1}{2}}\left[\frac{2b^2}{\kappa\{b + \theta\varphi\}}\right]. \tag{5.24}$$

From (5.23) we can have (5.19). ∎

#### 5.1.1.4 Optimal time-switching factor

The optimal value $\alpha^*$ can be obtained by solving the equation $\frac{d\tau_j(\alpha)}{d\alpha} = 0$. Given the AT expression in (5.8) and (5.17), this optimization problem does not admit a closed-form solution. However, the optimal $\alpha^*$ is efficiently solved via numerical calculation, as illustrated below. Here, we can use Golden section search algorithm to find the optimal factor $\alpha^*$. This algorithm has been used in many global optimization problems in communications, for example, in [75]. The detailed algorithm, as well as the related theory, is described in [76], [77].

#### 5.1.1.5 Numerical Results and Discussion

In this part, we investigate the system performance of the EH based TWFD relaying network over Rician fading environment by using the Monte Carlo simulation [77], [78]. The simulation parameters are listed in Table 5.1.

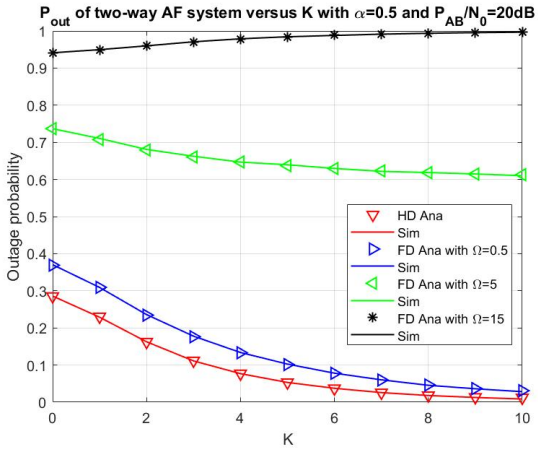


(a) Outage probability

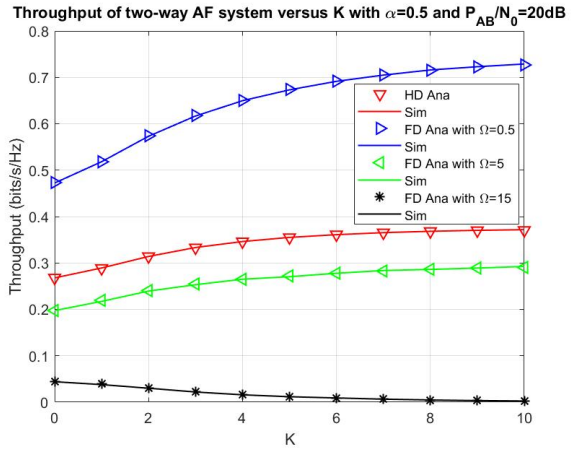


(b) Achievable throughput

Figure 5.2: OP and achievable throughput of the EH-based TWFD relay network versus the Rician K-factor $K$

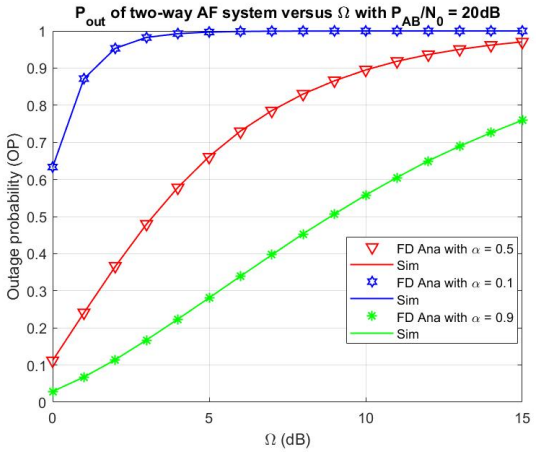


(a) Outage probability

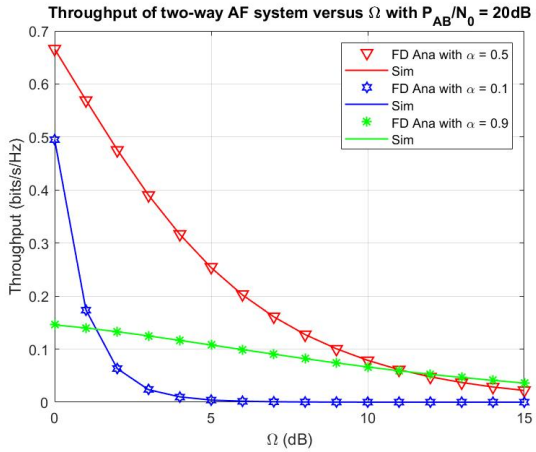


(b) Achievable throughput

Figure 5.3: OP and achievable throughput of the EH-based TWFD relay network versus RSI power $\Omega$

The influence of the Rician K-factor K on the OP and throughput of the model system is shown in Fig. 5.2a and Fig. 5.2b, respectively. In this simulation process, the main parameters of the proposed system are set as the following: $\alpha = 0.5$, $\mathrm{P}_{AB}/\mathrm{N}_0 = 20$ dB, $\Omega = \{0; 0.5; 5; 15\}$. Fig. 5.2a and 5.2b shows that the OP decreased and the throughput increased crucially while K varied from 0 to 10.

The influence of RSI $\Omega$ on the OP and the AT of the model system is illustrated in Fig. 5.3a and Fig. 5.3b. Here, $\alpha$ is set at 0.5, 0.1, 0.9 and the ratio $\mathrm{P}_{AB}/\mathrm{N}_0$ at 20 dB. From the simulation, it is clear that the AT increases and the OP decrease significantly while $\Omega$ varies from 0 to 15.

Moreover, Fig. 5.4a and Fig. 5.4b present the effect of the ratio $\mathrm{P}_{AB}/\mathrm{N}_0$ on the OP and the

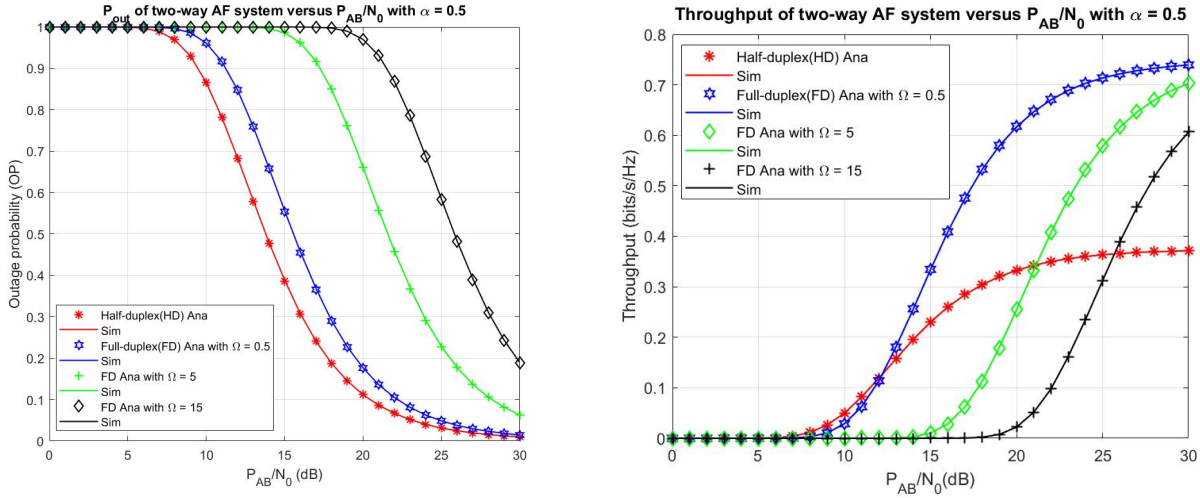


(a) Outage probability (b) Achievable throughput

Figure 5.4: OP and achievable throughput of the EH-based TWFD relay network versus the ratio $P_{AB}/N_0$.

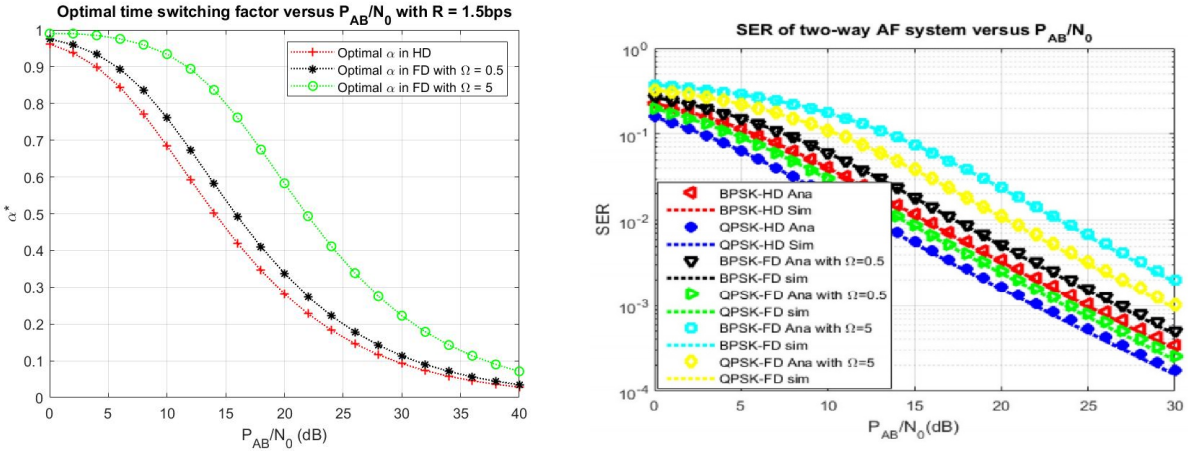


(a) Optimal TS factor (b) SER

Figure 5.5: Optimal TS factor and SER of the EH-based TWFD relay network versus the ratio $P_{AB}/N_0$.

AT with $\Omega = \{0; 0.5; 5; 15\}$ and $\alpha = 0.5$ for the proposed system. From the results, it is showed that the AT increases and the OP decreased significantly when the ratio $P_{AB}/N_0$ increased from 0 to 30 dB.

Finally, the optimal TS factor versus the ratio $P_{AB}/N_0$ is proposed in Fig. 5.5a and Fig. 5.5b shows SER of the proposed system versus $P_{AB}/N_0$. In all above figures, the simulation results match tightly with analytical expressions in part 5.1.1.3.

### 5.1.2 Multi-source DF FD Cooperative Networks with PSR-protocol-based EH over Rayleigh Fading Channel

Another work of mine on FD relaying network is to investigate the case of multiple sources in decode-and-forward (DF) cooperative networks with PSR-based EH FD over a Rayleigh fading channel, as presented below. [HDH04], [HDH06], [HDH08], [HDH17].

#### 5.1.2.1 Introduction

RF EH for wireless communication systems presents a new paradigm that allows wireless nodes to recharge their batteries from the RF signals instead of fixed power grids and the traditional energy sources [64], [79], [80]. Since RF signal can carry energy and information simultaneously, EH and SWIPT are becoming a more and more promising research direction [6], [73], [81]. The author in [82] investigated the incorporation of cooperative MIMO two-way relay systems, where a FD AF relay is equipped with multiple antennas. The work in [83] was extended in [84], where the achievable sum rate of a cooperative system with FD MIMO AF relaying was maximized. The cooperative relay networks were studied in [85]. Here, a relay harvests energy from the RF signals broadcasted by a source and then utilizes it to assist in the information transfer from the source to its final destination.

In our current work, we investigate the multi-source DF FD relaying network cooperative networks with PSR-based EH over Rayleigh fading channel. In this model, the sources and the destination communicate with each other by both direct link and intermediate helping relay. First, we investigate source selection for the best system performance. Then, the closed-form expression of the OP and the SER are derived. Finally, the Monte Carlo simulation is used for validating the analytical expressions in connection with all main possible system parameters.

#### 5.1.2.2 System Model

Fig. 5.6 plot the system model with multiple sources (Sn), one relay (R) and one destination (D). The transmission model follows the principles of analog network coding, and this concept is the extension of linear network coding to multi-hop wireless networks. In our model, every terminal operates in FD mode and relay works in DF mode. The multiple sources and destination nodes communicate by two links: direct link and the link via the intermediate relay. In this system model, we denote the channel gain between node Sn and the relay R is $h_{R_nD}$, between the relay $R$ and the destinations, $D$ is $h_{RD}$, and the direct link between multi-source and D is $h_{S_nD}$. Moreover, the self-interference channel at $R$ is $h_{RR}$. All the channels are assumed to Rayleigh fading channels. Furthermore, the relay has only the energy to serve their purpose, so it needs to harvest the energy from the node before forwarding the information messages to the destination. The EH and information processing for this proposed model system are presents in Fig. 5.7. In this protocol, the transmission is divided into blocks of length $T$. Each transmission block consists of two time slots. In the first-half time slot $T/2$, the selected source $S_n$ transfers the information to the destination by the direct link between the source and destination. In the

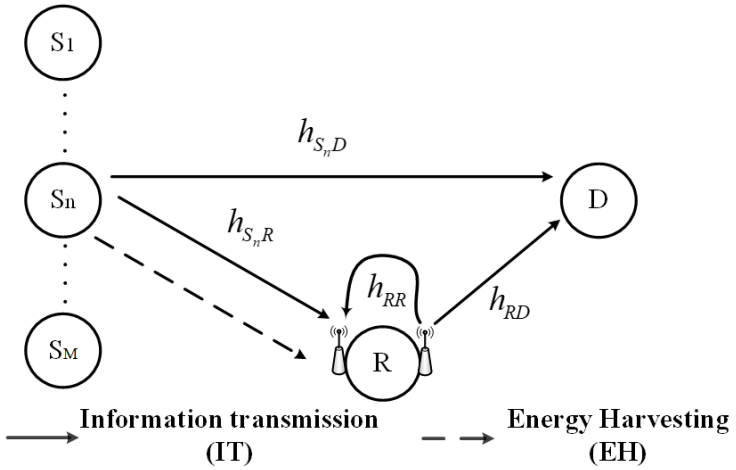


Figure 5.6: System model.

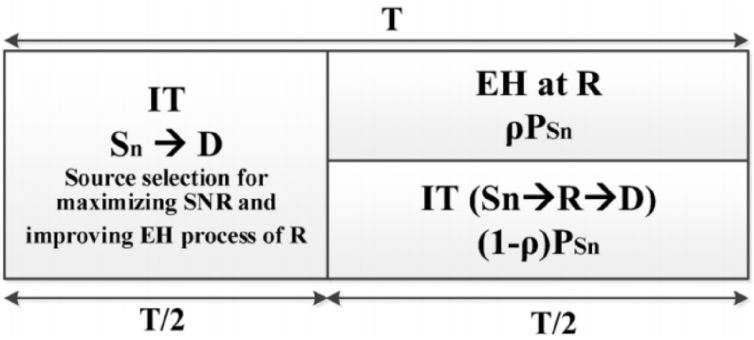


Figure 5.7: EH and information processing by the adaptive relaying protocol.

remaining half-interval time slot $T/2$, the selected source transfer information to the destination with helping of the relay $R$. In this remaining interval time, the EH from the multi-source at the relay node $R$ is $\rho P_{S_n}$, and the information signal is transferred to relay with the power $(1-\rho)P_s$. Finally, the information transformation from the multi-source to the destination is accomplished by both direct link and via helping relay R. [HDH08].

#### 5.1.2.3 System Performance

Supposing the source $S_n$ is chosen to send its information and energy. During the second time slot, $S_n$ sends the signal $x_{S_n}$ to R and D with transmit power $P_{S_n}$. In the second time slot, the received signals at relay R and destination D are, respectively, given by

$$y_r = \sqrt{1-\rho} h_{S_nR} x_{S_n} + h_{RR} x_r + n_r, \tag{5.25}$$

and

$$y_d^1 = h_{RD}x_r + n_d^1, \tag{5.26}$$

where $E\left\{|x_s|^2\right\} = P_{s_n}$, $E\left\{|x_r|^2\right\} = P_r$, $n \in (1, 2, ..., M)$, $h_{RR}$ is loopback interference channel, $n_r$ and $n_d^1$ are i.i.d. AWGN with variance $N_0$, $h_{RD}$ is the relay to destination channel gain. In the first time slot, $S_n$ will transmit the data to the destination directly, the received signal at destination can be given as

$$y_d^2 = h_{S_nD}x_{S_n} + n_d^2, \tag{5.27}$$

where $h_{S_nD}$ is the source $S_n$ to destination channel gain, $n_d^2$ is the AWGN with variance $N_0$.

In the second interval, the average transmitted power at the relay can be calculated as

$$P_r = \eta\rho P_{S_n}|h_{S_nR}|^2, \tag{5.28}$$

where $P_{S_n}$ is the transmitted power at source $S_n$, $h_{S_nR}$ is the source $S_n$ to relay channel gain.

From (5.25) and (5.28), the SNR at the relay can be calculated as

$$\gamma_1 = \frac{(1-\rho)|h_{S_nR}|^2 P_{S_n}}{|h_{RR}|^2 P_r + N_0} = \frac{(1-\rho)|h_{S_nR}|^2 P_{S_n}}{\eta\rho P_{s_n}|h_{S_nR}|^2|h_{RR}|^2 + N_0} \approx \frac{(1-\rho)}{\eta\rho|h_{RR}|^2}. \tag{5.29}$$

From (5.26) and (5.28), the SNR at the destination can be calculated as

$$\gamma_2 = \frac{P_r|h_{RD}|^2}{N_0} = \frac{\eta\rho P_{S_n}|h_{S_nR}|^2|h_{RD}|^2}{N_0}. \tag{5.30}$$

From (5.27), the SNR at the destination in the first time slot can be obtained as

$$\gamma_3 = \frac{P_{s_n}|h_{S_nD}|^2}{N_0}. \tag{5.31}$$

After using selection combining (SC) at receiver, the received SNR at D with DF relaying is given by

$$\gamma_{e2e} = \max\left[\min\left(\gamma_1, \gamma_2\right), \gamma_3\right]. \tag{5.32}$$

#### 5.1.2.4 Source selection

From (5.32), the best source $S_{n^*}$ would be selected to maximize the received SNR at the destination to optimize the transmission performance as the following

$$n^* = \arg \max_{1 \le n \le M} \max\left[\min\left(\gamma_1, \gamma_2\right), \gamma_3\right]. \tag{5.33}$$

We propose the optimal source selection protocol in which the best selection source is selected as follows

$$\omega_1 = \max_{n=1,2,\ldots,M} (|h_{S_nR}|^2), \tag{5.34}$$

$$\omega_3 = \max_{n=1,2,\ldots,M} (|h_{S_nD}|^2). \tag{5.35}$$

As in [86], the CDF of $\omega_i$ can be given by

$$F_{\omega_i}(y) = \sum_{p=0}^{M} (-1)^p C_M^p e^{-py/\lambda_i}, \tag{5.36}$$

where $\lambda_i$ is the mean of RV $\omega_i$, $i \in \{1, 3\}$ and $C_M^p = \frac{M!}{p!(M-p)!}$. Then, the corresponding PDF can be obtained by

$$f_{\omega_i}(y) = \frac{1}{\lambda_i} \sum_{p=0}^{M-1} (-1)^p C_{M-1}^p M e^{-(p+1)y/\lambda_i}. \tag{5.37}$$

From (5.32), the OP of DF system can be expressed as

$$\begin{aligned} OP &= \Pr(\gamma_{e2e} < \gamma_{th}) = \Pr[\max\{\min(\gamma_1, \gamma_2), \gamma_3\} < \gamma_{th}] \\ &= \Pr\left[\min\left(\frac{(1-\rho)}{\eta\rho|h_{RR}|^2}, \frac{\eta\rho P_{s_n}|h_{RD}|^2 \max\limits_{1\le n\le M}|h_{S_nR}|^2}{N_0}\right) < \gamma_{th}\right] \Pr\left(\frac{P_{s_n}\max\limits_{1\le n\le M}|h_{S_nD}|^2}{N_0} < \gamma_{th}\right) \\ &= \Pr\left[\min\left(\frac{(1-\rho)}{\eta\rho\omega}, \eta\rho\gamma_0\omega_1\omega_2\right) < \gamma_{th}\right] . \Pr\left(\frac{P_{s_n}\omega_3}{N_0} < \gamma_{th}\right), \end{aligned} \tag{5.38}$$

where we denote $\omega = |h_{RR}|^2$, $\omega_1 = \max\limits_{1\le n\le M}|h_{S_nR}|^2$, $\omega_2 = |h_{RD}|^2$, $\omega_3 = \max\limits_{1\le n\le M}|h_{S_nD}|^2$, $\gamma_0 = \frac{P_{s_n}}{N_0}$, $\gamma_{th} = 2^{2R} - 1$ is a threshold of the proposed system, R is the source rate. Now, we have:

$$P_1 = \Pr\left[\min\left(\frac{(1-\rho)}{\eta\rho\omega}, \eta\rho\gamma_0\omega_1\omega_2\right) < \gamma_{th}\right] = 1 - \Pr\left[\frac{(1-\rho)}{\eta\rho\omega} \ge \gamma_{th}\right] \Pr(\eta\rho\gamma_0\omega_1\omega_2 \ge \gamma_{th}). \tag{5.39}$$

Let us denote that

$$P_{11} = \Pr\left[\frac{(1-\rho)}{\eta\rho\omega} \ge \gamma_{th}\right] = \Pr\left[\omega \le \frac{(1-\rho)}{\eta\rho\gamma_{th}}\right] = 1 - e^{-\frac{(1-\rho)}{\eta\rho\gamma_{th}\lambda}}, \tag{5.40}$$

where $\lambda$ is the mean of RV $\omega$.

$$P_{12} = \Pr\left(\eta\rho\gamma_0\omega_1\omega_2 \geq \gamma_{th}\right) = 1 - \Pr\left(\omega_2 < \frac{\gamma_{th}}{\eta\rho\gamma_0\omega_1}\right) = 1 - \int_0^{\infty} F_{\omega_2}\left(\frac{\gamma_{th}}{\eta\rho\gamma_0\omega_1}|\omega_1\right) f_{\omega_1}(\omega_1) d\omega_1. \tag{5.41}$$

By using (5.36), equation (5.41) can be reformulated as

$$\begin{aligned} P_{12} &= \frac{1}{\lambda_1}\int_0^{\infty}\sum_{p=0}^{M-1}(-1)^p C_{M-1}^p M e^{-\frac{\gamma_{th}}{\eta\rho\gamma_0\omega_1\lambda_2}} e^{-\frac{(p+1)\omega_1}{\lambda_1}} d\omega_1 \\ &= \sum_{p=0}^{M-1}\frac{(-1)^p C_{M-1}^p M}{\lambda_1}\int_0^{\infty} e^{-\frac{\gamma_{th}}{\kappa\gamma_0\omega_1\lambda_2}} e^{-\frac{(p+1)\omega_1}{\lambda_1}} d\omega_1, \end{aligned} \tag{5.42}$$

where $\lambda_2$ is the mean of RV $\omega_2$.

By applying [72, p. 3.324.1], (5.42) can be rewritten as

$$P_{12} = 2\sum_{p=0}^{M-1}(-1)^p C_{M-1}^p M\sqrt{\frac{\gamma_{th}}{\kappa\gamma_0\lambda_1\lambda_2}} K_1\left(2\sqrt{\frac{(p+1)\gamma_{th}}{\kappa\gamma_0\lambda_1\lambda_2}}\right), \tag{5.43}$$

where $K_v(\cdot)$ is the modified Bessel function of the second kind and $v^{th}$ order. Next, by using (5.36) we have:

$$P_2 = \Pr\left(\frac{P_{s_n}\omega_3}{N_0} < \gamma_{th}\right) = F_{\omega_3}\left(\frac{\gamma_{th}}{\gamma_0}\right) = \sum_{p=0}^{M}(-1)^p C_M^p e^{-\frac{p\gamma_{th}}{\gamma_0\lambda_3}}. \tag{5.44}$$

Finally, by substituting (5.41),(5.43), (5.44) into (5.38) and letting $K = M-1$, we get the OP expression as

$$\begin{aligned} OP = &\left[1 - 2\left(1 - e^{\frac{-(1-\rho)}{\eta\rho\gamma_{th}\lambda}}\right)\sum_{p=0}^{M-1}(-1)^p\binom{M-1}{p} M\sqrt{\frac{\gamma_{th}}{\eta\rho\gamma_0\lambda_1\lambda_2}} K_1\left(2\sqrt{\frac{(p+1)\gamma_{th}}{\eta\rho\gamma_0\lambda_1\lambda_2}}\right)\right] \\ &\times\sum_{p=0}^{M}(-1)^p\binom{M}{p} e^{\frac{-p\gamma_{th}}{\gamma_0\lambda_3}} \\ &= \sum_{p=0}^{M}(-1)^p C_M^p e^{-\frac{p\gamma_{th}}{\gamma_0\lambda_3}} - 2\sum_{p=0}^{M}\sum_{l=0}^{K}(-1)^{p+l} C_M^p C_K^l (K+1) e^{-\frac{p\gamma_{th}}{\gamma_0\lambda_3}}\sqrt{\frac{\gamma_{th}}{\eta\rho\gamma_0\lambda_1\lambda_2}} K_1\left(2\sqrt{\frac{(l+1)\gamma_{th}}{\eta\rho\gamma_0\lambda_1\lambda_2}}\right) \\ &+ 2\sum_{p=0}^{M}\sum_{l=0}^{K}(-1)^{p+l} C_M^p C_K^l (K+1) e^{-\frac{p\gamma_{th}}{\gamma_0\lambda_3}} e^{-\frac{(1-\rho)}{\eta\rho\gamma_{th}\lambda}}\sqrt{\frac{\gamma_{th}}{\eta\rho\gamma_0\lambda_1\lambda_2}} K_1\left(2\sqrt{\frac{(l+1)\gamma_{th}}{\eta\rho\gamma_0\lambda_1\lambda_2}}\right). \end{aligned} \tag{5.45}$$

Then the throughput of this system is derived as

$$\tau = (1 - OP)\frac{R(T/2)}{T} = (1 - OP)\frac{R}{2}. \tag{5.46}$$

In next part, we obtain the expression for SER at the destination, which is defined as (5.18) in Section 5.1. By substituting (5.45) into (5.18) and replace $\gamma_{th} = x$, we have

$$\begin{aligned}
SER = & \frac{\varpi\sqrt{\theta}}{2\sqrt{\pi}} \int_0^\infty \frac{e^{-\theta x}}{\sqrt{x}} \sum_{p=0}^{M} (-1)^p C_M^p e^{-\frac{p\gamma_{th}}{\gamma_0\lambda_3}} dx \\
& - \frac{2\varpi\sqrt{\theta}}{2\sqrt{\pi}} \int_0^\infty \frac{e^{-\theta x}}{\sqrt{x}} \sum_{p=0}^{M}\sum_{l=0}^{K} (-1)^{p+l} C_M^p C_K^l (K+1) e^{-\frac{p\gamma_{th}}{\gamma_0\lambda_3}} \sqrt{\frac{\gamma_{th}}{\eta\rho\gamma_0\lambda_1\lambda_2}} K_1\left(2\sqrt{\frac{(l+1)\gamma_{th}}{\eta\rho\gamma_0\lambda_1\lambda_2}}\right) dx \\
& + \frac{2\varpi\sqrt{\theta}}{2\sqrt{\pi}} \int_0^\infty \frac{e^{-\theta x}}{\sqrt{x}} \sum_{p=0}^{M}\sum_{l=0}^{K} (-1)^{p+l} C_M^p C_K^l (K+1) e^{-\frac{p\gamma_{th}}{\gamma_0\lambda_3}} e^{-\frac{(1-\rho)}{\eta\rho\gamma_{th}\lambda}} \sqrt{\frac{\gamma_{th}}{\eta\rho\gamma_0\lambda_1\lambda_2}} K_1\left(2\sqrt{\frac{(l+1)\gamma_{th}}{\eta\rho\gamma_0\lambda_1\lambda_2}}\right) dx \\
= & \frac{\varpi\sqrt{\theta}}{2\sqrt{\pi}} \sum_{p=0}^{M} (-1)^p C_M^p \int_0^\infty \frac{e^{-x\left(\theta+\frac{p}{\gamma_0\lambda_3}\right)}}{\sqrt{x}} dx \\
& - \frac{\varpi\sqrt{\theta}}{\sqrt{\pi}} \sum_{p=0}^{M}\sum_{l=0}^{K} (-1)^{p+l} C_M^p C_K^l (K+1) \sqrt{\frac{1}{\eta\rho\gamma_0\lambda_1\lambda_2}} \int_0^\infty e^{-x\left(\theta+\frac{p}{\gamma_0\lambda_3}\right)} K_1\left(2\sqrt{\frac{(l+1)x}{\eta\rho\gamma_0\lambda_1\lambda_2}}\right) dx \\
& + \frac{\varpi\sqrt{\theta}}{\sqrt{\pi}} \sum_{p=0}^{M}\sum_{l=0}^{K} (-1)^{p+l} C_M^p C_K^l (K+1) \sqrt{\frac{1}{\eta\rho\gamma_0\lambda_1\lambda_2}} \int_0^\infty e^{-x\left(\theta+\frac{p}{\gamma_0\lambda_3}\right)} e^{-\frac{(1-\rho)}{\eta\rho x\lambda}} K_1\left(2\sqrt{\frac{(l+1)x}{\eta\rho\gamma_0\lambda_1\lambda_2}}\right) dx.
\end{aligned} \tag{5.47}$$

By applying in [72, p. 3.361.2], we can write the first term of (5.47) as

$$J_1 = \varpi\sqrt{\theta} \sum_{p=0}^{M} \frac{(-1)^p C_M^p}{\left(\theta + \frac{p}{\gamma_0\lambda_3}\right)}. \tag{5.48}$$

By applying [72, p. 6.614.5], the second term of (5.47) can be reformulated as

$$\begin{aligned}
J_2 = & \frac{\varpi\sqrt{\theta}}{4} \sum_{p=0}^{M}\sum_{l=0}^{K} (-1)^{p+l} C_M^p C_K^l \frac{1}{\left(\theta + \frac{p}{\gamma_0\lambda_3}\right)^3} \frac{\sqrt{(l+1)}}{\eta\rho\gamma_0\lambda_1\lambda_2} e^{\frac{(l+1)\lambda_3}{2\eta\rho\lambda_1\lambda_2(\theta\gamma_0\lambda_3+p)}} \\
& \times \left[K_1\left(\frac{(l+1)\lambda_3}{2\eta\rho\lambda_1\lambda_2(\theta\gamma_0\lambda_3+p)}\right) - K_0\left(\frac{(l+1)\lambda_3}{2\eta\rho\lambda_1\lambda_2(\theta\gamma_0\lambda_3+p)}\right)\right].
\end{aligned} \tag{5.49}$$

By applying Taylor's series expansion as the followings

$$e^{-x\left(\theta+\frac{p}{\gamma_0\lambda_3}\right)} = \sum_{v=0}^{\infty} \frac{\left[-x\left(\theta+\frac{p}{\gamma_0\lambda_3}\right)\right]^v}{v!} = \sum_{v=0}^{\infty} (-1)^v \left[\left(\theta+\frac{p}{\gamma_0\lambda_3}\right)\right]^v \frac{x^v}{v!}, \tag{5.50}$$

$$e^{-\frac{(1-\rho)}{\eta\rho x\lambda}} = \sum_{t=0}^{\infty} \frac{\left[-\frac{(1-\rho)}{\eta\rho x\lambda}\right]^t}{t!} = \sum_{t=0}^{\infty} (-1)^t \left[\left(\frac{(1-\rho)}{\eta\rho\lambda}\right)\right]^t \frac{1}{t!x^t}, \tag{5.51}$$

the third term of (5.47) can be rewritten as

$$J_3 = \frac{\varpi\sqrt{\theta}}{\sqrt{\pi}} \sum_{p=0}^{M}\sum_{l=0}^{K}\sum_{v=0}^{\infty}\sum_{t=0}^{\infty} \frac{(-1)^{p+l+v+t}}{v!t!} \left[\left(\theta + \frac{p}{\gamma_0\lambda_3}\right)\right]^{v} \left[\left(\frac{(1-\rho)}{\eta\rho\lambda}\right)\right]^{t} C_M^p C_K^l (K+1) \sqrt{\frac{1}{\eta\rho\gamma_0\lambda_1\lambda_2}} \times \int_0^{\infty} x^{v-t} \times K_1\left(2\sqrt{\frac{(l+1)x}{\eta\rho\gamma_0\lambda_1\lambda_2}}\right) dx. \tag{5.52}$$

Here we employ the formula (6.561.16) in [72]:

$$\int_0^{\infty} x^{\mu} K_n(ax)\, dx = 2^{\mu-1} a^{-\mu-1} \Gamma\left(\frac{1+\mu+n}{2}\right) \Gamma\left(\frac{1+\mu-n}{2}\right)$$

$$\overset{x=\sqrt{y}}{\Rightarrow} \int_0^{\infty} y^{\frac{\mu-1}{2}} K_n(a\sqrt{y})\, dy = 2^{\mu} a^{-\mu-1} \Gamma\left(\frac{1+\mu+n}{2}\right) \Gamma\left(\frac{1+\mu-n}{2}\right). \tag{5.53}$$

where $\Gamma(\cdot)$ is the gamma function.

By applying (5.53) with n = 1, we can get

$$\begin{aligned} J_3 &= \frac{\varpi\sqrt{\theta}}{\sqrt{\pi}} \sum_{p=0}^{M}\sum_{l=0}^{K}\sum_{v=0}^{\infty}\sum_{t=0}^{\infty} \frac{(-1)^{p+l+v+t}}{v!t!} \left[\left(\theta + \frac{p}{\gamma_0\lambda_3}\right)\right]^{v} \left[\left(\frac{(1-\rho)}{\eta\rho\lambda}\right)\right]^{t} C_M^p C_K^l (K+1) \sqrt{\frac{1}{\eta\rho\gamma_0\lambda_1\lambda_2}} \\ &\times 2^{2v-2t+1} \times \left[2\sqrt{\frac{(l+1)}{\eta\rho\gamma_0\lambda_1\lambda_2}}\right]^{-2v+2t-2} \Gamma\left(v-t+\frac{3}{2}\right) \Gamma\left(v-t+\frac{1}{2}\right) \\ &= \frac{\varpi\sqrt{\theta}}{2\sqrt{\pi}} \sum_{p=0}^{M}\sum_{l=0}^{K}\sum_{v=0}^{\infty}\sum_{t=0}^{\infty} \frac{(-1)^{p+l+v+t}}{v!t!} \left[\left(\theta + \frac{p}{\gamma_0\lambda_3}\right)\right]^{v} \left[\left(\frac{(1-\rho)}{\lambda}\right)\right]^{t} C_M^p C_K^l (K+1) \\ &\times \frac{(l+1)^{t-v-1}}{(\eta\rho)^{2t-v-1/2} (\gamma_0\lambda_1\lambda_2)^{t-v-1/2}} \Gamma\left(v-t+\frac{3}{2}\right) \Gamma\left(v-t+\frac{1}{2}\right). \end{aligned} \tag{5.54}$$

Finally, SER of the proposed system can be calculated by

$$\begin{aligned} SER &= \varpi\sqrt{\theta} \sum_{p=0}^{M} \frac{(-1)^p C_M^p}{\left(\theta + \frac{p}{\gamma_0\lambda_3}\right)} - \frac{\varpi\sqrt{\theta}}{4} \sum_{p=0}^{M}\sum_{l=0}^{K} (-1)^{p+l} C_M^p C_K^l \frac{1}{\left(\theta + \frac{p}{\gamma_0\lambda_3}\right)^3} \times \frac{\sqrt{(l+1)}}{\eta\rho\gamma_0\lambda_1\lambda_2} \\ &\times e^{\frac{(l+1)\lambda_3}{2\eta\rho\lambda_1\lambda_2(\theta\gamma_0\lambda_3+p)}} \left[K_1\left(\frac{(l+1)\lambda_3}{2\eta\rho\lambda_1\lambda_2(\theta\gamma_0\lambda_3+p)}\right) - K_0\left(\frac{(l+1)\lambda_3}{2\eta\rho\lambda_1\lambda_2(\theta\gamma_0\lambda_3+p)}\right)\right] \\ &+ \frac{\varpi\sqrt{\theta}}{2\sqrt{\pi}} \sum_{p=0}^{M}\sum_{l=0}^{K}\sum_{v=0}^{\infty}\sum_{t=0}^{\infty} \frac{(-1)^{p+l+v+t}}{v!t!} \left[\left(\theta + \frac{p}{\gamma_0\lambda_3}\right)\right]^{v} \left[\left(\frac{(1-\rho)}{\lambda}\right)\right]^{t} C_M^p C_K^l (K+1) \\ &\times \frac{(l+1)^{t-v-1}}{(\eta\rho)^{2t-v-1/2} (\gamma_0\lambda_1\lambda_2)^{t-v-1/2}} \Gamma\left(v-t+\frac{3}{2}\right) \Gamma\left(v-t+\frac{1}{2}\right). \end{aligned} \tag{5.55}$$

#### 5.1.2.5 Numerical Results and Discussion

In this part, we investigate the performance of the proposed system by Monte Carlo simulation.

Table 5.2: Simulation parameters.

| Symbol | Name | Value |
|---|---|---|
| $\eta$ | EH efficiency | 0.8 |
| $\lambda_1$ | Mean of $\|h_{SR}\|^2$ | 0.5 |
| $\lambda_2$ | Mean of $\|h_{RD}\|^2$ | 0.5 |
| $\lambda_3$ | Mean of $\|h_{SD}\|^2$ | 0.5 |
| $\lambda$ | Mean of $\|h_{RR}\|^2$ | 0.5 |
| $\gamma_{th}$ | SNR threshold | 1 |
| $P_S/N_0$ | Source power to noise ratio | -5 $\rightarrow$ 10dB |
| $R$ | Source rate | 0.5 bit/s/Hz |

The simulation parameters are listed in Table 5.2.

The influence of the PS factor $\rho$ on the OP and throughput of the proposed system is shown

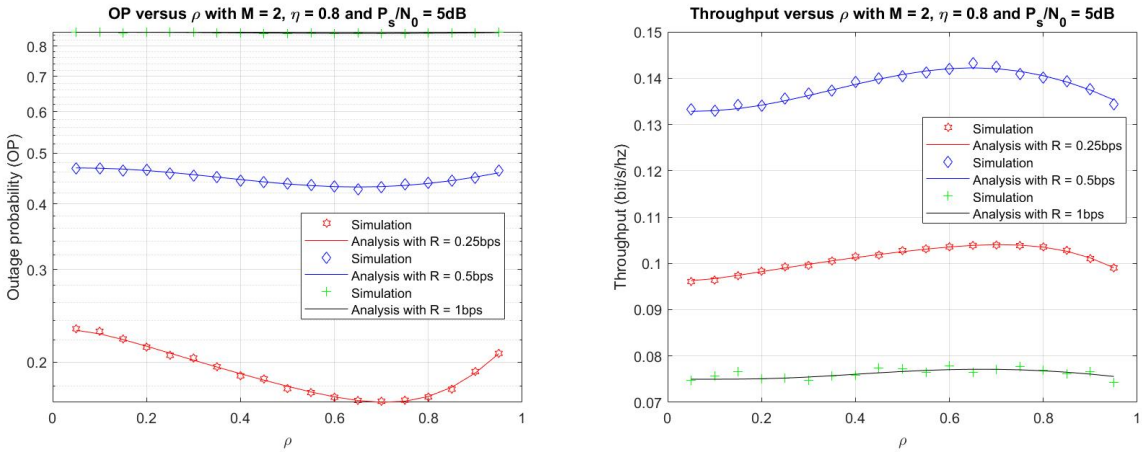


(a) Outage probability

(b) Achievable throughput

Figure 5.8: OP and achievable throughput of the multi-source PSR-based EH FD-DF relay network versus the power splitting factor $\rho$.

in Fig. 5.8a and Fig. 5.8b, respectively. In this simulation, the main parameters of the proposed system are set as the following: M = 2, $P_S/N_0$ = 5 dB, $R \in \{0.25; 0.5; 1\}$. It is showed that there exists an optimal $\rho$ to minimize OP and maximize the throughput.

Moreover, Fig. 5.9a and Fig. 5.9b present the effect of M on the OP and the AT with $P_S/N_0$ = {1, 3, 5} dB, R = 0.5 bps, $\rho = 0.35$ and $\eta = 0.8$ for the proposed system. From the results, it is showed that the AT increases and the OP decreased significantly when M increased from 1 to 10.

In the same way, the influence of the source power to noise ratio $P_S/N_0$ on the OP and the AT of the system model with $M = \{1, 3, 5\}$, R = 0.5 bps, $\rho = 0.5$ and $\eta = 0.8$ are illustrated in the Fig. 5.10a and 5.10b, respectively. As shown, the OP decreases and the system throughput increases significantly when $P_S/N_0$ increases from –5 to 10 dB.

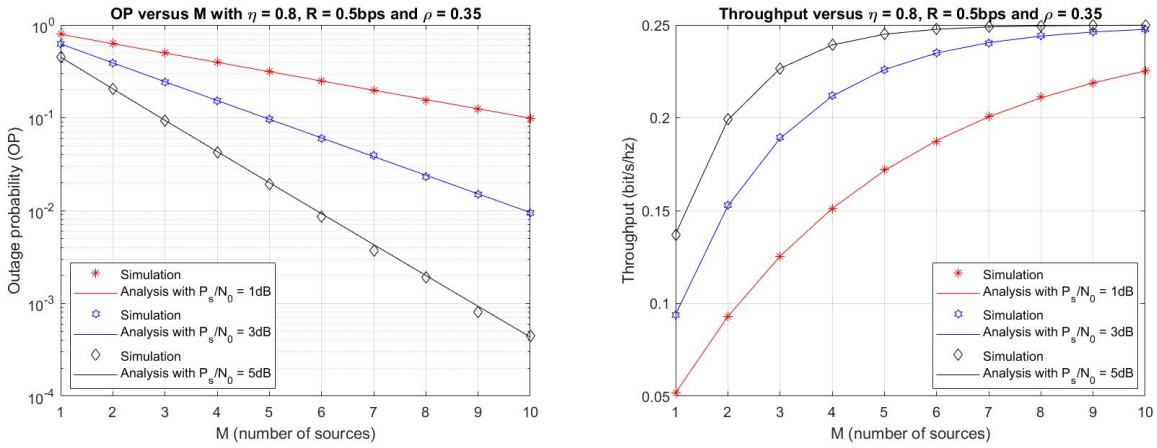


(a) Outage probability (b) Achievable throughput

Figure 5.9: OP and achievable throughput of the multi-source PSR-based EH FD-DF relay network versus number of sources M.

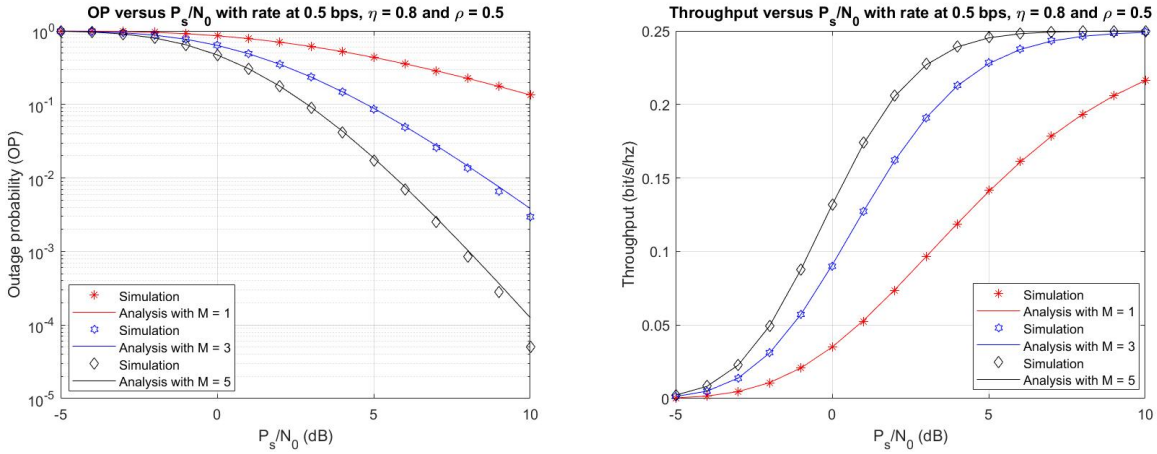


(a) Outage probability (b) Achievable throughput

Figure 5.10: OP and achievable throughput of the multi-source PSR-based EH FD-DF relay network versus the source power to noise ratio $P_s/N_0$.

Finally, SER of the proposed system versus M and the ratio $P_S/N_0$ are presented in Fig. 5.11a and 5.11b, respectively. In all above figures, the simulation results match tightly with analytical expressions in part 5.1.2.4.

### 5.1.3 Summary

As the first solution for Aim 1, I propose two EH-based communication schemes for FD relaying networks. In the first one, TSR protocol is applied for TWFD relay networks over Rician channel, while in the second one a multi-source PSR-based EH-FD-DF relay network over Rayleigh fading

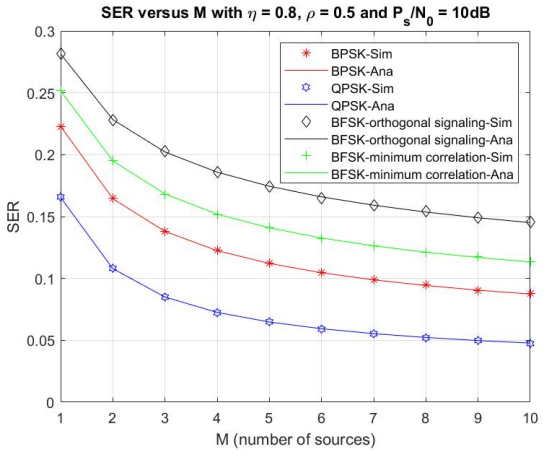


(a) With respect to number of sources M

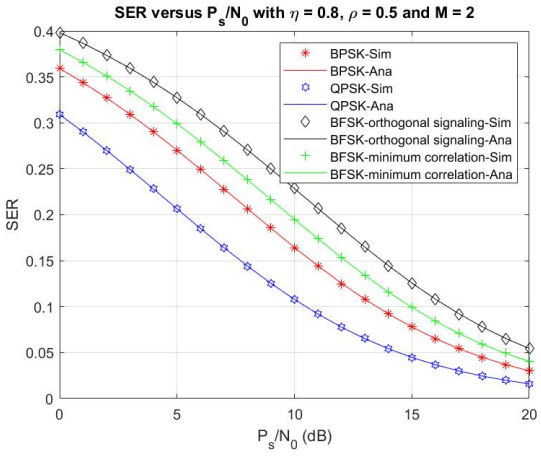


(b) With respect to the source power to noise ratio $P_s/N_0$.

Figure 5.11: SER of the multi-source PSR-based EH FD-DF relay network.

channel is considered. For both model, the closed-form expression of the OP, throughput, and SER are derived mathematically and verified numerically by Monte Carlo simulation. The results can be proposed as a novel approach for the communication network in the near future.

## 5.2 RF Energy Harvesting Under Impact of Interference and Hardware Impairment

To further evaluate the performance of RF EH protocols in wireless cooperative network, I take into account the co-channel interference and hardware impairment. A summary of the results is presented as follows. [HDH03], [HDH09].

### 5.2.1 RF EH in HD Relay Network with Effect of Hardware Impairment

In this section, we introduce a EH-based HD relay network over the different fading environment with the effect of hardware impairment (HI). The system model is investigated with AF relaying strategy and PSR protocols. The system performance analysis in term of the OP, AT, and bit error rate (BER) is demonstrated by their closed-form expressions. Optimal PS factor is determined and the analytical analysis is confirmed by Monte Carlo simulation for all primary parameters. [HDH03]

#### 5.2.1.1 Introduction

Nowadays, wireless powered communication networks (WPCNs) have shown significant advantages in industry and living. The major benefits of WPCNs mainly come from battery charging operations through the air without physical cable connections and recharging, and thus, replacing the battery [63], [64], [87]. Three primary wireless EH techniques have been employed in practice in WPCNs: inductive coupling based on magnetic field induction [79], [88], magnetic

resonant coupling [79], [88], and RF energy transfer, which is suitable for long-distance transfers [63], [79], [89]. EH through RF signals has been studied in cooperative wireless networks, MIMO system, multi-user and multi-hop systems for SWIPT [13], [73], [90]. In these previous papers, the authors have focused on WPCNs using only Rayleigh or Rician fading channel for both transmission hops, while not many papers studied different fading channels for each hop. In addition, hardware impairment (HI) suffers from phase noise, I/Q imbalance, and high-power amplifier nonlinearities [HDH12], [91] is rarely studied in the literature on relay WPCNs.

In this section, we introduce a EH-based HD relay network operating over the different fading environment (Rayleigh and Rician fading channels) with the effect of HI. The system performance is evaluated for AF and PSR protocols. The closed form of OP, AT, and BER of the proposed system are derived in connection with the main primary system parameters. Finally, the correctness of the analytical expressions is validated by Monte Carlo simulation.

#### 5.2.1.2 Network System Model

A basic HD EH relay network as in Fig. 2.5 is considered. The difference between this model and the model in Fig. 2.5 is that different fading environment (Rayleigh and Rician Fading Channel, respectively) are assumed for the $S \to R$ and $R \to D$ links. The PSR protocol such as the one plotted in Fig. 2.6b is applied [92].

To analyze the EH model, the EH part of the signal transferred from S to R in the first time slot $T/2$ can be formulated as

$$y_r = \sqrt{\rho} h(x_s + \mu_s) + n_r, \tag{5.56}$$

where $x_s$ is the energy-transmitted signal with $E\left\{|x_s|^2\right\} = P_s$, $n_r$ is the zero-mean AWGN with variance $N_0$, and $\mu_s$ denotes the distortion error caused by hardware impairment at the source node, which is modeled as a zero-mean Gaussian RV with variance ${P_s\sigma_1}^2$ with $E\left\{|\mu_s|^2\right\} = {P_s\sigma_1}^2$. As analyzed in Section 4.2, the transmitted power at R, which is supplied by the harvested energy, can be calculated as (2.7) (see page 9).

The information transfer (IT) phase is divided into two equal-length sub-intervals with the length of $T/2$. In the first interval, the received signal can be expressed as

$$y_r = \sqrt{1-\rho} h(x_s + \mu_s) + n_r = \sqrt{1-\rho} h x_s + \sqrt{1-\rho} h \mu_s + n_r \tag{5.57}$$

Here, we use the AF protocol for our model. Then, the received signal at R is amplified by a factor $\beta$, which is given by Equation (5.58)

$$\beta = \frac{x_r}{y_r} = \sqrt{\frac{P_r}{(1-\rho)|h|^2 P_s + (1-\rho)|h|^2 P_s \sigma^2 + N_o}} \tag{5.58}$$

In the remaining $T/2$ interval time, R transfers the information to D. Hence, the received signal at D node is formulated by

$$y_d = g(x_r + \mu_r) + n_D = g\beta y_r + g\mu_r + n_d = \underbrace{g\beta\sqrt{1-\rho}hx_s}_{signal} + \underbrace{\sqrt{1-\rho}h\mu_s g\beta + g\beta n_r + g\mu_r + n_D}_{noise} \tag{5.59}$$

where $x_r$ is the transmitted signal, which satisfies $E\left\{|x_r|^2\right\} = P_r$, $\mu_r$ denotes the distortion error caused by hardware impairment at R, which is modeled as a zero-mean Gaussian RV with variance $P_r{\sigma_2}^2$ and $E\left\{|\mu_r|^2\right\} = P_r{\sigma_2}^2$ and $n_r$ is the AWGN noise at R node, $n_d$ is the noise at the destination, which is assumed to have the same power as $n_r$.

The end-to-end SNR at D node can be given by

$$\gamma_{e2e} = \frac{E\left\{(signal)^2\right\}}{E\left\{(noise)^2\right\}} = \frac{(1-\rho)|g|^2\beta^2|h|^2P_s}{|g|^2\beta^2|h|^2P_s{\sigma_1}^2 + |g|^2\beta^2N_o + |g|^2P_r{\sigma_2}^2 + N_o} \tag{5.60}$$

By letting $\varphi_1 = |h|^2, \varphi_2 = |g|^2$ and substituting this into (5.60), we have:

$$\begin{aligned}\gamma_{e2e} &= \frac{(1-\rho)\varphi_1\varphi_2P_s}{\varphi_1\varphi_2P_s{\sigma_1}^2 + \varphi_2N_o + \frac{\varphi_2P_r{\sigma_2}^2}{\beta^2} + \frac{N_0}{\beta^2}} \\ &= ((1-\rho)\varphi_1\varphi_2P_s)/(\varphi_1\varphi_2P_s{\sigma_1}^2 + \varphi_2N_o + (1-\rho)\varphi_1\varphi_2P_s\sigma_2^2 \\ &+ (1-\rho)\varphi_1\varphi_2P_s\sigma_1^2\sigma_2^2 + \varphi_2N_0\sigma_2^2 + \frac{N_0(1-\rho)}{\eta\rho} + \frac{N_0(1-\rho)\sigma_1^2}{\eta\rho} + \frac{N_0^2}{P_r})\end{aligned} \tag{5.61}$$

Because $N_0 << P_r$, then we can reformulate (5.61) as

$$\begin{aligned}\gamma_{e2e} &= \frac{(1-\rho)\varphi_1\varphi_2P_s}{\varphi_1\varphi_2P_s{\sigma_1}^2 + \varphi_2N_o + (1-\rho)\varphi_1\varphi_2P_s\sigma_2^2 + (1-\rho)\varphi_1\varphi_2P_s\sigma_1^2\sigma_2^2 + \varphi_2N_0\sigma_2^2 + \frac{N_0(1-\rho)}{\eta\rho}(1+\sigma_1^2)} \\ &= \frac{(1-\rho)\varphi_1\varphi_2\gamma_0}{\varphi_1\varphi_2\gamma_0{\sigma_1}^2 + \varphi_2 + (1-\rho)\varphi_1\varphi_2\gamma_0\sigma_2^2 + (1-\rho)\varphi_1\varphi_2\gamma_0\sigma_1^2\sigma_2^2 + \varphi_2\sigma_2^2 + \kappa + \kappa\sigma_1^2}\end{aligned} \tag{5.62}$$

where we denote $\kappa = \frac{1-\rho}{\eta\rho}$, $\gamma_0 = \frac{P_s}{N_0}$. In the next section, we analyze the AT, OP and BER in AF mode with the PS protocol [90], [93].

#### 5.2.1.3 System Performance

In this analysis, we consider two scenarios: (1) S-R link is the Rayleigh fading channel, R-D link is Rician fading channel; and (2) S-R link is the Rician fading channel and R-D link is the Rayleigh fading channel.

**Scenario 1: S-R link is Rayleigh fading channel, R-D link is Rician fading channel**

As in previous studies [13], [90], [93], [94], the PDF and CDF of the RV $\varphi_1$ with parameter $\lambda_h$ can be written respectively as

$$f_{\varphi_1}(x) = \lambda_h e^{-\lambda_h x} \tag{5.63}$$

$$F_{\varphi_1}(x) = 1 - e^{-\lambda_h x} \tag{5.64}$$

where $\lambda_h$ is the mean value of RV $\varphi_1$.

Similarly, the PDF of RV $\varphi_2$ with parameter $\lambda_g$ can be obtained as [71]

$$f_{\varphi_2}(x) = \frac{(K+1)e^{-K}}{\lambda_g} e^{-\frac{(K+1)x}{\lambda_g}} I_0\left(2\sqrt{\frac{K(K+1)x}{\lambda_g}}\right) = a\sum_{l=0}^{\infty}\frac{(bK)^l}{(l!)^2}x^l e^{-bx} \tag{5.65}$$

where K denotes the Rician K-factor, and $I_0(\cdot)$ is the zero-th order modified Bessel function of the first kind [71], $a \triangleq \frac{(K+1)e^{-K}}{\lambda_g}$, $b \triangleq \frac{K+1}{\lambda_g}$ and $I_0(x) = \sum\limits_{l=0}^{\infty}\frac{x^{2l}}{2^{2l}(l!)^2}$ [72]. Then the CDF of $\varphi_2$ can be computed like in [77]:

$$F_{\varphi_2}(\varsigma) = \int_0^{\varsigma} f_{\varphi_2}(x)dx = 1 - \frac{a}{b}\sum_{l=0}^{\infty}\sum_{m=0}^{l}\frac{K^l b^m}{l!m!}\varsigma^m e^{-b\varsigma} \tag{5.66}$$

After that, the OP of the proposed system is defined as

$$\begin{aligned} P_{out} &= F_{\gamma_{e2e}}(\gamma) = \Pr(\gamma_{e2e} < \gamma) \\ &= \Pr\left\{\varphi_1\varphi_2\gamma_0[1-\rho-\gamma\sigma_1^2-\gamma(1-\rho)\sigma_2^2-\gamma(1-\rho)\sigma_1^2\sigma_2^2] < \varphi_2(\gamma+\gamma\sigma_2^2)+\gamma\kappa+\gamma\kappa\sigma_1^2\right\} \end{aligned} \tag{5.67}$$

where $\gamma = 2^R - 1$ is the lower threshold for SNR at both R and D, and $R$ is the fixed data transmission rate at S. Let $c_1 = \gamma + \gamma\sigma_2^2$, $c_2 = \gamma\kappa + \gamma\kappa\sigma_1^2$, and $c_3 = \gamma_0[1-\rho-\gamma\sigma_1^2-\gamma(1-\rho)\sigma_2^2-\gamma(1-\rho)\sigma_1^2\sigma_2^2]$. We assume that $c_3$ is positive, otherwise the OP of the system is always equal to 1. Then:

$$P_{out} = \Pr\left\{\varphi_1 < \frac{c_1\varphi_2 + c_2}{c_3\varphi_2}\right\} = \int_0^{\infty} F_{\varphi_1}\left(\frac{c_1\varphi_2 + c_2}{c_3\varphi_2}\right) f_{\varphi_2}(\varphi_2)d\varphi_2 \tag{5.68}$$

By combining (5.68) with (5.64) and (5.65) and using [72, p. 3.471.9], we have:

$$\begin{aligned} P_{out} &= 1 - \int_0^\infty e^{-\lambda_h \frac{c_1\varphi_2 + c_2}{c_3\varphi_2}} a \sum_{l=0}^{\infty} \frac{(bK)^l}{(l!)^2} \varphi_2^l e^{-b\varphi_2} d\varphi_2 \\ &= 1 - ae^{-\frac{\lambda_h c_1}{c_3}} \sum_{l=0}^{\infty} \frac{(bK)^l}{(l!)^2} \int_0^\infty \varphi_2^l e^{-b\varphi_2} e^{-\frac{\lambda_h c_2}{c_3\varphi_2}} d\varphi_2 \\ &= 1 - 2ae^{-\frac{\lambda_h c_1}{c_3}} \sum_{l=0}^{\infty} \frac{(bK)^l}{(l!)^2} \left(\frac{\lambda_h c_2}{c_3 b}\right)^{\frac{l+1}{2}} K_{l+1}\left(2\sqrt{\frac{\lambda_h c_2 b}{c_3}}\right) \end{aligned} \tag{5.69}$$

Then the average throughput of the relay network system can be computed as

$$\tau = (1 - P_{out})\frac{R}{2} = 2ae^{-\frac{\lambda_h c_1}{c_3}} \sum_{l=0}^{\infty} \frac{(bK)^l}{(l!)^2} \left(\frac{\lambda_h c_2}{c_3 b}\right)^{\frac{l+1}{2}} K_{l+1}\left(2\sqrt{\frac{\lambda_h c_2 b}{c_3}}\right) \frac{R}{2} \tag{5.70}$$

Finally, the BER of the proposed system can be formulated by applying (5.18) in Section 5.1

$$BER = E\left[\omega Q(\sqrt{2\theta\gamma}\right] \tag{5.71}$$

where $Q(t) = \frac{1}{\sqrt{2\pi}} \int_t^\infty e^{-x^2/2} dx$ is the Gaussian Q-function, $\omega$ and $\theta$ are constants which are specific for modulation type. Here, we use $(\omega, \theta) = (1, 2)$ for BPSK and $(\omega, \theta) = (1, 1)$ for QPSK. Hence, we begin rewriting the BER expression in Equation (5.71) directly regarding OP at S by using integration as in the equation below

$$BER = \frac{\omega\sqrt{\theta}}{2\sqrt{\pi}} \int_0^\infty \frac{e^{-\theta x}}{\sqrt{x}} F_{\gamma_{e2e}}(x) dx \tag{5.72}$$

**Scenario 2: S-R link is Rician fading channel, R-D link is Rayleigh fading channel**

Similar to scenario 1, the CDF of RV $\varphi_1$ and PDF of RV $\varphi_2$ can be formulated respectively as

$$F_{\varphi_1}(\varsigma) = \int_0^\varsigma f_{\varphi_1}(x) dx = 1 - \frac{a}{b} \sum_{l=0}^{\infty} \sum_{m=0}^{l} \frac{K^l b^m}{l! m!} \varsigma^m e^{-b\varsigma}, \tag{5.73}$$

$$f_{\varphi_2}(x) = \lambda_g e^{-\lambda_g x}. \tag{5.74}$$

The the OP of the proposed system can be found by

$$\begin{aligned}
P_{out} &= \Pr\left\{\varphi_1 < \frac{c_1\varphi_2 + c_2}{c_3\varphi_2}\right\} = \int_0^\infty F_{\varphi_1}\left(\frac{c_1\varphi_2 + c_2}{c_3\varphi_2}\right) f_{\varphi_2}(\varphi_2)d\varphi_2 \\
&= 1 - \int_0^\infty \frac{a}{b}\sum_{l=0}^{\infty}\sum_{m=0}^{l}\frac{K^l b^m}{l!m!}\left(\frac{c_1\varphi_2 + c_2}{c_3\varphi_2}\right)^m e^{-\frac{b(c_1\varphi_2+c_2)}{c_3\varphi_2}}\lambda_g e^{-\lambda_g\varphi_2}d\varphi_2 \\
&= 1 - \lambda_g e^{-\frac{bc_1}{c_3}}\int_0^\infty \frac{a}{b}\sum_{l=0}^{\infty}\sum_{m=0}^{l}\sum_{n=0}^{m}\binom{m}{n}\frac{K^l b^m c_1^{m-n}c_2^n}{l!m!c_3^m}t^{n-2}e^{-\frac{bc_2 t}{c_3}}e^{-\frac{\lambda_g}{t}}dt \\
&= 1 - \lambda_g e^{-\frac{bc_1}{c_3}}\frac{a}{b}\sum_{l=0}^{\infty}\sum_{m=0}^{l}\sum_{n=0}^{m}\frac{K^l b^m c_1^{m-n}c_2^n}{l!n!(m-n)!c_3^m}\int_0^\infty t^{n-2}e^{-\frac{bc_2 t}{c_3}}e^{-\frac{\lambda_g}{t}}dt. \qquad (5.75)
\end{aligned}$$

where the third lineis obtained by applying the equation $(x+y)^m = \sum_{n=0}^{m}\binom{m}{n}x^{m-n}y^n$ and changing variable.

Finally, by using [72, p. 3.471.9], the OP of the proposed system in scenario 2 can be found as

$$\begin{aligned}
P_{out} &= 1 - 2\lambda_g e^{-\frac{bc_1}{c_3}}\frac{a}{b}\sum_{l=0}^{\infty}\sum_{m=0}^{l}\sum_{n=0}^{m}\frac{K^l b^m c_1^{m-n}c_2^n}{l!n!(m-n)!c_3^m}\left(\frac{\lambda_g c_3}{bc_2}\right)^{\frac{n-1}{2}}K_{n-1}\left(2\sqrt{\frac{bc_2\lambda_g}{c_3}}\right) \\
&= 1 - 2ae^{-\frac{bc_1}{c_3}}\sum_{l=0}^{\infty}\sum_{m=0}^{l}\sum_{n=0}^{m}\frac{K^l b^{\frac{2m-n-3}{2}}\lambda_g^{\frac{n+1}{2}}c_1^{m-n}c_2^{\frac{n+1}{2}}c_3^{\frac{n-1-2m}{2}}}{l!n!(m-n)!}K_{n-1}\left(2\sqrt{\frac{bc_2\lambda_g}{c_3}}\right) \qquad (5.76)
\end{aligned}$$

Again, the AT can be derived similar to Scenario 1 as

$$\tau = (1 - P_{out})\frac{R}{2} = aRe^{-\frac{bc_1}{c_3}}\sum_{l=0}^{\infty}\sum_{m=0}^{l}\sum_{n=0}^{m}\frac{K^l b^{\frac{2m-n-3}{2}}\lambda_g^{\frac{n+1}{2}}c_1^{m-n}c_2^{\frac{n+1}{2}}c_3^{\frac{n-1-2m}{2}}}{l!n!(m-n)!}K_{n-1}\left(2\sqrt{\frac{bc_2\lambda_g}{c_3}}\right)\frac{R}{2} \qquad (5.77)$$

and the BER can be derived by using (5.18).

Theoretically, optimal power-splitting factor $\rho^*$ for each scenario can be founded by solving the equation $\frac{d\tau(p)}{d\rho} = 0$, using the AT expression in (5.70) and (5.77). However, due to the complexity of the AT expressions, we cannot find the closed-form of $\rho^*$. Instead, we use the Golden section search algorithm [19], [74], [75], [95], which is popularly used in many global optimization problems, to obtain $\rho^*$ in numerical analysis.

#### 5.2.1.4 Numerical Results

In this part, we investigate the system performance in terms of OP, AT, BER, and the PS factor with respect to the main system parameters: $\eta$, $\rho$, $P_s/N_0$ and $\sigma_1$, $\sigma_2$. The primary simulation parameters are listed in Table 5.3.

Table 5.3: Simulation parameters.

| Symbol | Name | Value |
|---|---|---|
| $\eta$ | EH efficiency | 0.7 |
| $\lambda_h$ | Mean of $\|h\|^2$ | 0.5 |
| $\lambda_g$ | Mean of $\|g\|^2$ | 0.5 |
| $K$ | Rician K-factor | 0.5 |
| $\gamma_{th}$ | SNR threshold | 7 |
| $\mathrm{P}_S/\mathrm{N}_0$ | Source power to noise ratio | 0-30dB |
| $\sigma_1$ | Distortion error | 0.01 |
| $\sigma_2$ | Distortion error | 0.05 |
| $R$ | Source rate | 3 bit/s/Hz |

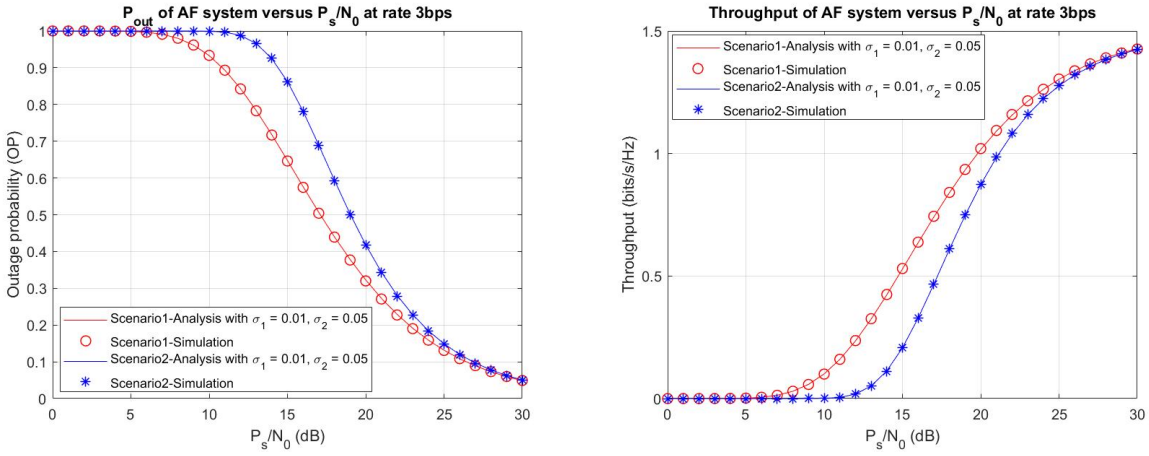


(a) Outage probability

(b) Achievable throughput

Figure 5.12: OP and achievable throughput of the PSR-based EH HD-DF relay network under HI versus ratio of $\mathrm{P}_s/\mathrm{N}_0$.

Fig. 5.12 displays the impact of the ratio $P_s/N_0$ on the OP and AT when the ratio $P_s/N_0$ increases from 0 to 30 dB. From the research results, we can state that the OP decreased and AT increased with the rising of the ratio $P_s/N_0$.

In addition, the OP and AT versus the PS factor $\rho$ are shown in Fig. 5.13. It can be observed that at D the AT increases and OP is reduced with factor $\rho$ from 0 to 0.6. After that, i.e. ratio $\rho$ from 0.6 to 1.0, this effect is reversed. We can find the optimal value of factor $\rho$ between 0.6 and 0.7 in this situation. This can be explained that when $\rho$ is too small, R cannot harvest enough energy from S to operate reliably, but when $\rho$ is too large then the reliability of the communications link from S to R is impaired.

The plots of OP and AT of the proposed system for $\sigma_1 = \sigma_2$ in the range of 0 to 0.2 are showed in Fig. 5.14. Obviously, OP increases and AT decreases with the increasing of $\sigma_1 = \sigma_2$. It is also noted that in all above figures, the simulation and analytical curves agree well with each other.

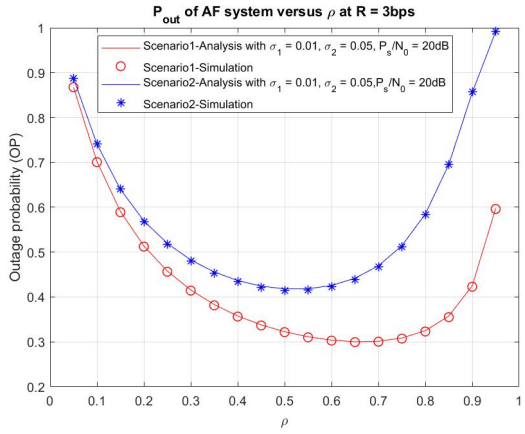


(a) Outage probability

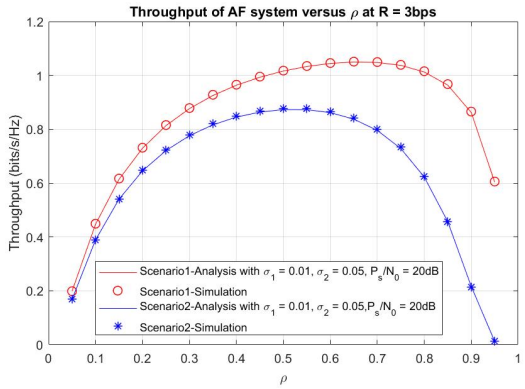


(b) Achievable throughput

Figure 5.13: OP and achievable throughput of the PSR-based EH HD-DF relay network under HI versus power-splitting factor $\rho$.

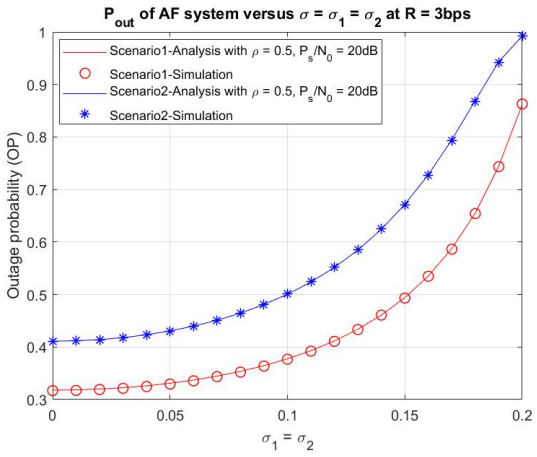


(a) Outage probability

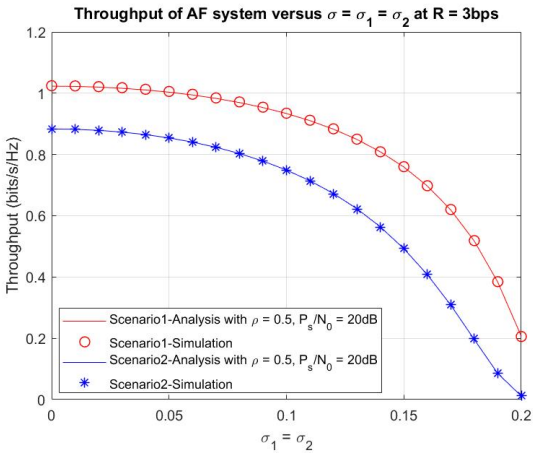


(b) Achievable throughput

Figure 5.14: OP and achievable throughput of the PSR-based EH HD-DF relay network under HI versus HI level $\sigma_1 = \sigma_2$.

Fig. 5.15 shows the optimal power splitting $\rho^*$ factor versus the ratio $P_s/N_0$ in both scenarios. As shown in the figures, $\rho^*$ increases as the ratio $P_s/N_0$ varies from 0 to 30 dB. Finally, Fig. 5.16 plots the dependence of BER on the ratio $P_s/N_0$. The result shows that BER decreases significantly with $P_s/N_0$ from 0 to 20 dB, then approaches to their lower bound.

### 5.2.2 Power Beacon-Assisted Energy Harvesting in a Half-Duplex Communication Network under Co-Channel Interference

Another troublesome factor that degrades the overall performance of wireless networks is the co-channel interference from other RF sources in the surrounding environment. In this part,

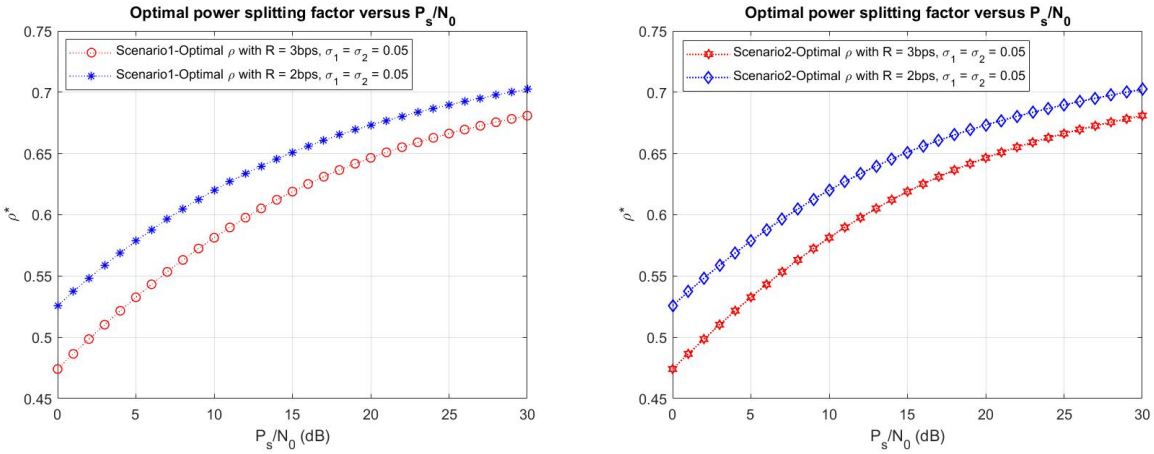


(a) Scenario 1 (b) Scenario 2

Figure 5.15: The optimal power-splitting factor $\rho^*$ versus $P_s/N_0$.

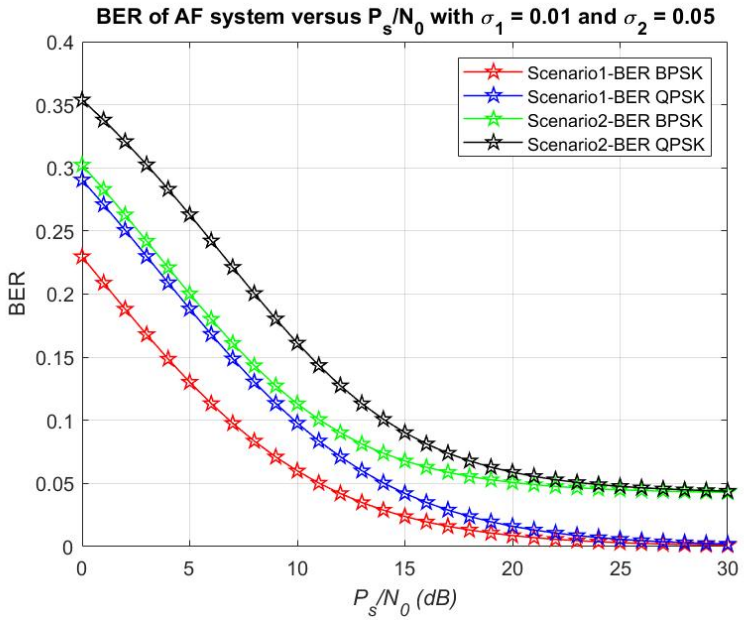


Figure 5.16: BER versus the ratio $P_s/N_0$.

we investigate the impact of co-channel interference on the outage performance and energy efficiency of power beacon (PB) assisted TSR-EH scheme for HD relay network in Rayleigh fading environment. [HDH09].

#### 5.2.2.1 Introduction

Nowadays, the IoT, where all smart devices can work and cooperate over the Internet, is involved in all aspects of civilian life, including transportation, smart grids, security and public safety,

agriculture, logistics, and e-health. In this situation, EH has been considered as a promising solution for extending the lifetime of energy-constrained IoT devices [2], [63], [96]. In the next generation of communication systems, billions of wireless devices will be connected to each other via the IoT system, which will lead to an energy consumption problem. Therefore, energy efficiency (EE), measured in bits per watt, is considered to be an important emerging metric in energy-constrained wireless communication networks due to their energy shortage [97]. The authors of [98] investigated the EE optimization problems in the SWIPT sensor networks, which employs both the PSR and the TSR protocols. In [99], the authors investigated an EE resource allocation algorithm for SWIPT in an OFDMA system, where the receivers employed the PS scheme to harvest energy. The EE in SWIPT based on the IoT distributed antenna system (DAS) is studied in [100]. In [101], a time-slotted large-scale MIMO system for EH and information transmission was studied, where an energy-efficient optimization scheme was proposed by jointly optimizing both transfer duration and transmitted power. The authors of [102] developed a distributed iteration algorithm for power allocation, PS ratio, and relay selection to maximize EE in clustered wireless sensor networks with SWIPT. The authors of [103] considered the EE maximization problem in a WPCN, where multiple users harvest energy from a dedicated power station and then communicate with an information receiving station.

In this research, we propose and investigate a power-beacon-assisted TSR-EH for a HD relay network under co-channel interference and over Rayleigh fading environment. Firstly, the exact and asymptotic form expressions of the OP were derived. Then we investigated the EE of the proposed system and the influence of the primary system parameters on the performance of the proposed system. Finally, the accuracy of the analytical expressions is verified by using Monte Carlo simulation.

#### 5.2.2.2 System Model

Fig. 5.17 displays the proposed system model. In this figure, S and D are the source node and the

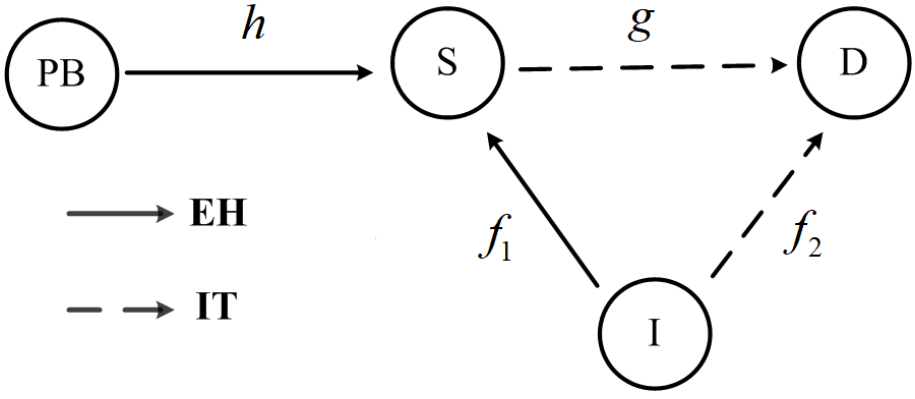


Figure 5.17: System model of a PB-assisted HD network; $f_1$: I-S interference channel; $f_2$: I-D interference channel; $h$: PB-S channel; $g$: S-D channel.

destination node, respectively, PB is a power beacon, and I represents a co-channel interference source from the environment. Let $f_1$ and $f_2$ represent the $I-S$ and $I-D$ interference channels, respectively. Let $h$ and $g$ denote the $PB-S$ and $S-D$ channels. Assume that all channels are Rayleigh block fading channels. The TSR protocol similar to Fig. 2.8a is selected for EH. Specifically, the whole transmission block ($T$) can be divided into parts. S and I scavenge energy from the RF signal received from the PB node S and node I, respectively, during the first interval of length $\alpha T$. Then, the remaining $(1-\alpha)T$ is used for signal transmission from node S to node D, and the interference signal from node I to node D also appears in this interval. Note that all the energy harvested at S and I is consumed for forwarding source information to node D.

In the first phase, let $P_B$ and $P_I$ be the transmit power of the power beacon and the interferer, respectively. The total received energy during the first phase at node S is formulated as

$$E_s = \eta_B |h|^2 P_B \alpha T + \eta_I |f_1|^2 P_I \alpha T \tag{5.78}$$

where $0 < \eta_B, \eta_I < 1$ are the energy conversion efficiencies of the PB and the interferer, respectively. Assume that $\eta_B = \eta_I = \eta$ and let $\kappa = \frac{\eta\alpha}{1-\alpha}$. Then, the average transmit power at node S could be obtained by

$$P_s = \frac{E_s}{(1-\alpha)\,T} = \frac{\eta|h|^2 P_B \alpha T + \eta|f_1|^2 P_I \alpha T}{(1-\alpha)\,T} = \kappa\left(P_B|h|^2 + |f_1|^2 P_I\right) \tag{5.79}$$

In the second phase, node S transmits the signal to node D, and the received signal, $y_D$, at the destination is formulated as:

$$y_D = g x_s + f_2 s_i + n_d = \underbrace{g x_s}_{signal} + \underbrace{f_2 s_i + n_d}_{noise} \tag{5.80}$$

where $x_s$ is the transmit signal by the source with $E\left\{|x_s|^2\right\} = P_s$, $n_d$ is the AWGN with zero-mean and variance $N_0$, $S_i$ is the transmit signal at the interferer, $E\left\{|s_i|^2\right\} = P_I$.

Assume that the power of interferer noise is large such that $P_B \approx P_I$. From (5.79) and (5.80), the end-to-end SINR can be calculated as

$$\gamma_{e2e} = \frac{E\left\{|signal|^2\right\}}{E\left\{|noise|^2\right\}} = \frac{|g|^2 P_s}{|f_2|^2 P_I + N_0} \frac{\kappa|g|^2\left(P_B|h|^2 + |f_1|^2 P_I\right)}{|f_2|^2 P_I + N_0} = \frac{\kappa|g|^2\Delta\left(|h|^2 + |f_1|^2\right)}{|f_2|^2\Delta + 1} \tag{5.81}$$

where $\Delta = \frac{P_B}{N_0} = \frac{P_I}{N_0}$.

#### 5.2.2.3 Performance Analysis

Based on the system model in the above section, we derived the OP throughput performance

and EE of the proposed system. From (5.81) we obtain the OP of the model system as

$$OP = \Pr\left(\gamma_{e2e} < \gamma_0\right) = \Pr\left[\frac{\kappa|g|^2\Delta\left(|h|^2 + |f_1|^2\right)}{|f_2|^2\Delta + 1} < \gamma_0\right] = \Pr\left(XY < \gamma_0\right) = \int_0^\infty F_Y\left(\frac{\gamma_0}{x}\right) f_X(x)dx \tag{5.82}$$

where $\gamma_0 = 2^{2R} - 1$ is the SINR threshold of the system, R is the source rate, $X = |h|^2 + |f_1|^2 = \varphi_1 + \varphi_2$, $Y = \frac{\kappa|g|^2\Delta}{|f_2|^2\Delta+1} = \frac{\kappa\varphi_3\Delta}{1+\Delta\varphi_4}$, and $\varphi_1 = |h|^2$, $\varphi_2 = |f_1|^2$, $\varphi_3 = |g|^2$, $\varphi_4 = |f_2|^2$.

In order to calculate the probability in (5.82), we have to determine the PDF and CDF of X and Y, respectively. The results are stated as in Lemma 5.2.2.3 and Lemma 5.2.2.3.

The CDF of Y can be computed as

$$F_Y(a) = 1 - \frac{\kappa\lambda_3 e^{\frac{-a}{\kappa\Delta\lambda_3}}}{a\lambda_4 + \kappa\lambda_3} \tag{5.83}$$

where $\lambda_3,\ \lambda_4$ are the mean of the RVs $(RV_s)$ $\varphi_3, \varphi_4$, respectively.

**Proof**

$$\begin{aligned} F_Y(a) &= \Pr\left(Y < a\right) = \Pr\left(\frac{\kappa\varphi_3\Delta}{1+\Delta\varphi_4} < a\right) = \Pr\left(\varphi_3 < \frac{a}{\kappa\Delta} + \frac{a\varphi_4}{\kappa}\right) \\ &= \int_0^\infty f_{\varphi_4}(\varphi_4)d\varphi_4 \int_0^{\frac{a}{\kappa\Delta}+\frac{a\varphi_4}{\kappa}} f_{\varphi_3}(\varphi_3)d\varphi_3 = \int_0^\infty F_{\varphi_3}\left(\frac{a}{\kappa\Delta} + \frac{a\varphi_4}{\kappa}\right) f_{\varphi_4}(\varphi_4)d\varphi_4 \\ &= \int_0^\infty f_{\varphi_4}(\varphi_4)d\varphi_4 - \frac{1}{\lambda_4}\int_0^\infty e^{-\frac{a}{\kappa\Delta\lambda_3}-\frac{a\varphi_4}{\kappa\lambda_3}} e^{\frac{-\varphi_4}{\lambda_4}} d\varphi_4 = 1 - \frac{\kappa\lambda_3 e^{-\frac{a}{\kappa\Delta\lambda_3}}}{a\lambda_4 + \kappa\lambda_3} \end{aligned}$$

■

The CDF of X can be expressed as

$$F_X(a) = 1 - e^{\frac{-a}{\lambda_2}} - \frac{e^{\frac{-a}{\lambda_1}}}{\lambda_2}\int_0^a e^{\varphi_2\left(\frac{1}{\lambda_1}-\frac{1}{\lambda_2}\right)} d\varphi_2 \tag{5.84}$$

where $\lambda_1,\ \lambda_2$ are the mean of the $RV_s$ $\varphi_1,\ \varphi_2$, respectively.

**Proof**

$$\begin{aligned} F_X(a) &= \Pr\left[(\varphi_1 + \varphi_2) < a\right] = \Pr\left[\varphi_1 < a - \varphi_2\right] = \int_0^a f_{\varphi_2}(\varphi_2)d\varphi_2 \int_0^{a-\varphi_2} f_{\varphi_1}(\varphi_1)d\varphi_1 \\ &= \frac{1}{\lambda_2}\int_0^a \left[1 - e^{\frac{-a+\varphi_2}{\lambda_1}}\right] e^{\frac{-\varphi_2}{\lambda_2}} d\varphi_2 = 1 - e^{\frac{-a}{\lambda_2}} - \frac{e^{\frac{-a}{\lambda_1}}}{\lambda_2}\int_0^a e^{\varphi_2\left(\frac{1}{\lambda_1}-\frac{1}{\lambda_2}\right)} d\varphi_2 \end{aligned}$$

■

From this point, two cases are considered: Case 1: $\lambda_1 = \lambda_2 = \lambda$, and Case 2: $\lambda_1 \neq \lambda_2$. The exact OPs of the proposed system for these cases are found in Theorem 5.3 below.

**Theorem 5.3** *The exact OP of the proposed PB-assisted TSR-EH HD relay network is*

$$OP = \begin{cases} 1 - \frac{\kappa\lambda_3}{\lambda^2} \int\limits_0^\infty \frac{x^2}{\kappa\lambda_3 x + \gamma_0\lambda_4} \exp\left(-\frac{\gamma_0}{\kappa\Delta\lambda_3 x}\right) \exp\left(-\frac{x}{\lambda}\right) dx & \text{if } \lambda_1 = \lambda_2 = \lambda \\ 1 - \frac{\kappa\lambda_3}{\lambda_2 - \lambda_1} \int\limits_0^\infty \frac{x \exp\left(-\frac{\gamma_0}{\kappa\Delta\lambda_3 x}\right)}{\kappa\lambda_3 x + \gamma_0\lambda_4} \left\{\exp\left(-\frac{x}{\lambda_2}\right) - \exp\left(-\frac{x}{\lambda_1}\right)\right\} dx & \text{if } \lambda_1 \neq \lambda_2 \end{cases} \tag{5.85}$$

**Proof**

**Case 1:** $\lambda_1 = \lambda_2 = \lambda$:

From Equation (5.84), we obtain the CDF and PDF of X in Case 1 as

$$F_X(a) = 1 - \exp\left(-\frac{a}{\lambda}\right) - \frac{a \exp\left(-\frac{a}{\lambda}\right)}{\lambda} \tag{5.86}$$

$$f_X(a) = \frac{\partial F_X(a)}{\partial a} = \frac{a e^{-\frac{a}{\lambda}}}{\lambda^2} \tag{5.87}$$

By combining (5.83), (5.87) and substituting them into (5.82), the OP can be computed as

$$OP = 1 - \int\limits_0^\infty \frac{\kappa\lambda_3 e^{\frac{-\gamma_0}{x\kappa\Delta\lambda_3}}}{\frac{\gamma_0}{x}\lambda_4 + \kappa\lambda_3} \frac{x e^{-\frac{x}{\lambda}}}{\lambda^2} dx = 1 - \frac{\kappa\lambda_3}{\lambda^2} \int\limits_0^\infty \frac{x^2}{\kappa\lambda_3 x + \gamma_0\lambda_4} e^{\frac{-\gamma_0}{\kappa\Delta\lambda_3 x}} e^{\frac{-x}{\lambda}} dx \tag{5.88}$$

**Case 2:** $\lambda_1 \neq \lambda_2$:

Similarly, we can obtain the CDF and the PDF of X as

$$F_X(a) = 1 - \exp\left(-\frac{a}{\lambda_2}\right) - \frac{\lambda_1}{\lambda_2 - \lambda_1}\left[\exp\left(-\frac{a}{\lambda_2}\right) - \exp\left(-\frac{a}{\lambda_1}\right)\right] \tag{5.89}$$

$$f_X(a) = \frac{1}{\lambda_2 - \lambda_1}\left[\exp\left(-\frac{a}{\lambda_2}\right) - \exp\left(-\frac{a}{\lambda_1}\right)\right]. \tag{5.90}$$

By combining (5.83), (5.89), and (5.82), we can obtain the OP in this case as

$$\begin{aligned} OP &= 1 - \int\limits_0^\infty \frac{\kappa\lambda_3 e^{\frac{-\gamma_0}{x\kappa\Delta\lambda_3}}}{\frac{\gamma_0}{x}\lambda_4 + \kappa\lambda_3} \left[\frac{1}{\lambda_2 - \lambda_1}\left(e^{\frac{-x}{\lambda_2}} - e^{\frac{-x}{\lambda_1}}\right)\right] dx \\ &= 1 - \frac{\kappa\lambda_3}{\lambda_2 - \lambda_1} \int\limits_0^\infty \frac{x e^{\frac{-\gamma_0}{\kappa\Delta\lambda_3 x}}}{\kappa\lambda_3 x + \gamma_0\lambda_4}\left(e^{\frac{-x}{\lambda_2}} - e^{\frac{-x}{\lambda_1}}\right) dx \end{aligned} \tag{5.91}$$

■

At high SINR regime, the end-to-end SINR in (5.81) can be approximated as

$$\gamma_{e2e}^{\infty} \approx \frac{\kappa|g|^2\left(|h|^2+|f_1|^2\right)}{|f_2|^2} = ZX \tag{5.92}$$

where $X = |h|^2 + |f_1|^2 = \varphi_1 + \varphi_2$, $Z = \frac{\kappa|g|^2}{|f_2|^2} = \frac{\kappa\varphi_3}{\varphi_4}$

The CDF of Z can be calculated by

$$F_Z(a) = 1 - \frac{\kappa\lambda_3}{a\lambda_4 + \kappa\lambda_3}. \tag{5.93}$$

**Proof**

$$F_Z(a) = \Pr\left(Z < a\right) = \Pr\left(\frac{\kappa\varphi_3}{\varphi_4} < a\right) = \Pr\left(\varphi_3 < \frac{a\varphi_4}{\kappa}\right) = \int_0^{\infty} f_{\varphi_4}(\varphi_4)d\varphi_4 \int_0^{\frac{a\varphi_4}{\kappa}} f_{\varphi_3}(\varphi_3)d\varphi_3$$

$$= 1 - \frac{1}{\lambda_4}\int_0^{\infty} \exp\left(-\frac{a\varphi_4}{\kappa\lambda_3}\right)\exp\left(-\frac{\varphi_4}{\lambda_4}\right)d\varphi_4 = 1 - \frac{\kappa\lambda_3}{a\lambda_4+\kappa\lambda_3}$$

■

The asymptotic OP of the proposed system at high SINR regime is given in Theorem 5.4 below.

**Theorem 5.4** *The asymptotic OP of the proposed PB-assisted TSR-EH HD relay network at high SINR regime is given by*

$$OP^{\infty} = \begin{cases} \frac{\gamma_0\lambda_4\lambda}{\kappa\lambda_3} + \left(\frac{\gamma_0\lambda_4}{\kappa\lambda_3\lambda}\right)^2 \exp\left(\frac{\gamma_0\lambda_4}{\kappa\lambda_3\lambda}\right) Ei\left(-\frac{\gamma_0\lambda_4}{\kappa\lambda_3\lambda}\right) & \text{if } \lambda_1 = \lambda_2 = \lambda \\ \frac{\gamma_0\lambda_4}{\kappa\lambda_3(\lambda_2-\lambda_1)}\left\{\exp\left(\frac{\gamma_0\lambda_4}{\kappa\lambda_3\lambda_1}\right) Ei\left(-\frac{\gamma_0\lambda_4}{\kappa\lambda_3\lambda_1}\right) - \exp\left(\frac{\gamma_0\lambda_4}{\kappa\lambda_3\lambda_2}\right) Ei\left(-\frac{\gamma_0\lambda_4}{\kappa\lambda_3\lambda_2}\right)\right\} & \text{if } \lambda_1 \neq \lambda_2 \end{cases} \tag{5.94}$$

*where* $Ei(-z) = -\int_z^{\infty} e^{-t}t^{-1}dt$ *is the exponential integral function.*

**Proof**

**Case 1:** $\lambda_1 = \lambda_2 = \lambda$:

From (5.87), (5.92), and (5.93), the OP can be computed as

$$OP_1^{\infty} = \Pr\left(\gamma_{e2e}^{\infty} < \gamma_0\right) = \Pr\left(XZ < \gamma_0\right) = \int_0^{\infty} F_Z\left(\frac{\gamma_0}{x}\right) f_X(x)dx = 1 - \frac{1}{\lambda^2}\int_0^{\infty} \frac{x^2 e^{\frac{-x}{\lambda}}}{x + \frac{\gamma_0\lambda_4}{\kappa\lambda_3}}dx \tag{5.95}$$

By applying [72, pp. 3.353, 5], (5.95) can be rewritten as

$$OP^{\infty} = \frac{\gamma_0\lambda_4\lambda}{\kappa\lambda_3} + \left(\frac{\gamma_0\lambda_4}{\kappa\lambda_3\lambda}\right)^2 e^{\frac{\gamma_0\lambda_4}{\kappa\lambda_3\lambda}} \mathrm{Ei}\left(-\frac{\gamma_0\lambda_4}{\kappa\lambda_3\lambda}\right)$$

**Case 2:** $\lambda_1 \neq \lambda_2$:
In this case, based on (5.89), (5.92), and (5.93), the OP can be calculated as

$$\begin{aligned} OP_2^{\infty} &= 1 - \frac{1}{\lambda_2 - \lambda_1} \int_0^{\infty} \frac{x}{x + \frac{\gamma_0\lambda_4}{\kappa\lambda_3}} \left\{ \exp\left(-\frac{x}{\lambda_2}\right) - \exp\left(-\frac{x}{\lambda_1}\right) \right\} dx \\ &= 1 - \frac{1}{\lambda_2 - \lambda_1} \int_0^{\infty} \frac{x \exp\left(-\frac{x}{\lambda_2}\right)}{x + \frac{\gamma_0\lambda_4}{\kappa\lambda_3}} dx + \frac{1}{\lambda_2 - \lambda_1} \int_0^{\infty} \frac{x \exp\left(-\frac{x}{\lambda_1}\right)}{x + \frac{\gamma_0\lambda_4}{\kappa\lambda_3}} dx \end{aligned} \tag{5.96}$$

Similar to Case 1, we apply equation (3.353,5) in [72], then (5.96) can be rewritten as

$$\begin{aligned} OP^{\infty} &= 1 - \frac{\gamma_0\lambda_4}{\kappa\lambda_3\left(\lambda_2 - \lambda_1\right)} e^{\frac{\gamma_0\lambda_4}{\kappa\lambda_3\lambda_2}} \mathrm{Ei}\left(\frac{-\gamma_0\lambda_4}{\kappa\lambda_3\lambda_2}\right) - \frac{\lambda_2}{\lambda_2 - \lambda_1} \\ &\quad + \frac{\gamma_0\lambda_4}{\kappa\lambda_3\left(\lambda_2 - \lambda_1\right)} e^{\frac{\gamma_0\lambda_4}{\kappa\lambda_3\lambda_1}} \mathrm{Ei}\left(\frac{-\gamma_0\lambda_4}{\kappa\lambda_3\lambda_1}\right) + \frac{\lambda_1}{\lambda_2 - \lambda_1} \\ &= \frac{\gamma_0\lambda_4}{\kappa\lambda_3\left(\lambda_2 - \lambda_1\right)} \left[ e^{\frac{\gamma_0\lambda_4}{\kappa\lambda_3\lambda_1}} \mathrm{Ei}\left(\frac{-\gamma_0\lambda_4}{\kappa\lambda_3\lambda_1}\right) - e^{\frac{\gamma_0\lambda_4}{\kappa\lambda_3\lambda_2}} \mathrm{Ei}\left(\frac{-\gamma_0\lambda_4}{\kappa\lambda_3\lambda_2}\right) \right] \end{aligned} \tag{5.97}$$

■

Next, I provide the analysis on energy efficiency (EE), which is defined as a ratio of total information rate C and total power consumption $E_T$ [104]. The result is stated in Theorem 5.5 and Theorem 5.6.

**Theorem 5.5** *The average EE of the proposed PB-assisted TSR-EH HD relay network is*

$$EE_{avg} = \begin{cases} \dfrac{\frac{(1-\alpha)\kappa\lambda_3}{2\lambda^2 \ln 2} \int_0^{\infty}\int_0^{\infty} \frac{x^2}{(\kappa\lambda_3 x + \gamma_0\lambda_4)(1+\gamma_0)} e^{\frac{-\gamma_0}{\kappa\Delta\lambda_3 x}} e^{\frac{-x}{\lambda}} dx d\gamma_0}{(1+\alpha)P/\varepsilon + P_C} & \text{if } \lambda_1 = \lambda_2 = \lambda \\ \dfrac{\frac{(1-\alpha)\kappa\lambda_3}{2(\lambda_2-\lambda_1)\ln 2} \int_0^{\infty}\int_0^{\infty} \frac{x \exp\left(-\frac{\gamma_0}{\kappa\Delta\lambda_3 x}\right)}{(\kappa\lambda_3 x + \gamma_0\lambda_4)(1+\gamma_0)} \left[ e^{\frac{-x}{\lambda_2}} - e^{\frac{-x}{\lambda_1}} \right] dx d\gamma_0}{(1+\alpha)P/\varepsilon + P_C} & \text{if } \lambda_1 \neq \lambda_2 \end{cases} \tag{5.98}$$

**Proof** By definition, the EE of the proposed system is determined as

$$EE = \frac{C}{E_T} = \frac{\frac{(1-\alpha)}{2}\log_2(1+\gamma_{e2e})}{(T+\alpha T)P/\varepsilon + P_C T} = \frac{\frac{(1-\alpha)}{2}\log_2(1+\gamma_{e2e})}{(1+\alpha)P/\varepsilon + P_C}. \tag{5.99}$$

where $P = P_B = P_I$, $\varepsilon$ and $P_C$ denote the power amplifier efficiency of the power beacon and circuit power consumption, respectively.

In order to analyze the EE, we considered calculating the average total information rate, which can be expressed as

$$C_{avg} = \frac{(1-\alpha)}{2\ln 2}\int_0^{\infty}\frac{1-F_{\gamma_{e2e}}(\gamma_0)}{1+\gamma_0}d\gamma_0. \tag{5.100}$$

**Case 1:** $\lambda_1 = \lambda_2 = \lambda$.:
By substituting (5.88) into (5.100), we obtain:

$$C_{avg} = \frac{(1-\alpha)\kappa\lambda_3}{2\lambda^2\ln 2}\int_0^{\infty}\int_0^{\infty}\frac{x^2}{(\kappa\lambda_3 x+\gamma_0\lambda_4)(1+\gamma_0)}e^{\frac{-\gamma_0}{\kappa\Delta\lambda_3 x}}e^{\frac{-x}{\lambda}}dxd\gamma_0 \tag{5.101}$$

Next, by substituting Equation (5.101) into (5.99), the average EE can be given as in (5.98).
**Case 2:** $\lambda_1 \neq \lambda_2$:
From (5.91), the average total information rate of this system can be found as

$$C_{avg} = \frac{(1-\alpha)\kappa\lambda_3}{2(\lambda_2-\lambda_1)\ln 2}\int_0^{\infty}\int_0^{\infty}\frac{xe^{\frac{-\gamma_0}{\kappa\Delta\lambda_3 x}}}{(\kappa\lambda_3 x+\gamma_0\lambda_4)(1+\gamma_0)}\left(e^{\frac{-x}{\lambda_2}}-e^{\frac{-x}{\lambda_1}}\right)dxd\gamma_0 \tag{5.102}$$

Then the average EE can be found by substituting (5.102) into (5.99). ∎

**Theorem 5.6** *The approximated value of the average EE of the proposed system at high SINR regime is given by*

$$EE^{\infty}_{avg} = \begin{cases} \frac{(1-\alpha)\int_0^{\infty}\left[1-\frac{\gamma_0\lambda_4\lambda}{\kappa\lambda_3}-\left(\frac{\gamma_0\lambda_4}{\kappa\lambda_3\lambda}\right)^2 e^{\frac{\gamma_0\lambda_4}{\kappa\lambda_3\lambda}}Ei\left(\frac{-\gamma_0\lambda_4}{\kappa\lambda_3\lambda}\right)\right]d\gamma_0}{2\ln 2[(1+\mu)P/\varepsilon+P_C]1+\gamma_0} & if\ \lambda_1=\lambda_2=\lambda \\ \frac{(1-\alpha)\int_0^{\infty}\left[1-\frac{\gamma_0\lambda_4}{\kappa\lambda_3(\lambda_2-\lambda_1)}\left[e^{\frac{\gamma_0\lambda_4}{\kappa\lambda_3\lambda_1}}Ei\left(\frac{-\gamma_0\lambda_4}{\kappa\lambda_3\lambda_1}\right)-e^{\frac{\gamma_0\lambda_4}{\kappa\lambda_3\lambda_2}}Ei\left(\frac{-\gamma_0\lambda_4}{\kappa\lambda_3\lambda_2}\right)\right]\right]d\gamma_0}{2\ln 2[(1+\alpha)P/\varepsilon+P_C](1+\gamma_0)} & if\ \lambda_1\neq\lambda_2 \end{cases} \tag{5.103}$$

**Proof** By substituting (5.94) into (5.100), the average total information rate can be expressed as

$$C^{\infty}_{avg} = \begin{cases} \frac{(1-\alpha)}{2\ln 2}\int_0^{\infty}\left[1-\left\{\frac{\gamma_0\lambda_4\lambda}{\kappa\lambda_3}+\left(\frac{\gamma_0\lambda_4}{\kappa\lambda_3\lambda}\right)^2 e^{\frac{\gamma_0\lambda_4}{\kappa\lambda_3\lambda}}\mathrm{Ei}\left(\frac{-\gamma_0\lambda_4}{\kappa\lambda_3\lambda}\right)\right\}\right]\frac{d\gamma_0}{1+\gamma_0} & \text{if } \lambda_1=\lambda_2=\lambda \\ \frac{(1-\alpha)}{2\ln 2}\int_0^{\infty}\left\{1-\frac{\gamma_0\lambda_4}{\kappa\lambda_3(\lambda_2-\lambda_1)}\left[e^{\frac{\gamma_0\lambda_4}{\kappa\lambda_3\lambda_1}}\mathrm{Ei}\left(\frac{-\gamma_0\lambda_4}{\kappa\lambda_3\lambda_1}\right)-e^{\frac{\gamma_0\lambda_4}{\kappa\lambda_3\lambda_2}}\mathrm{Ei}\left(\frac{-\gamma_0\lambda_4}{\kappa\lambda_3\lambda_2}\right)\right]\right\}\frac{d\gamma_0}{1+\gamma_0} & \text{if } \lambda_1\neq\lambda_2 \end{cases} \tag{5.104}$$

By combining (5.99) with Equation (5.104), the approximated EE is found as in (5.103). ∎

#### 5.2.2.4 Numerical results and discussion

In this part, we used the Monte Carlo simulation to verify the accuracy of the above analysis.

For each simulation, I first provide the graphs of the OP and the EE obtained by analytical formulas. Secondly, I generate plots of the same OP and EE curves that resulted from the Monte Carlo simulation. To do this, I generated $10^5$ random samples of each channel gain, which are Rayleigh distributed. The analytical curve and the simulation should match together to verify the accuracy of our analysis.

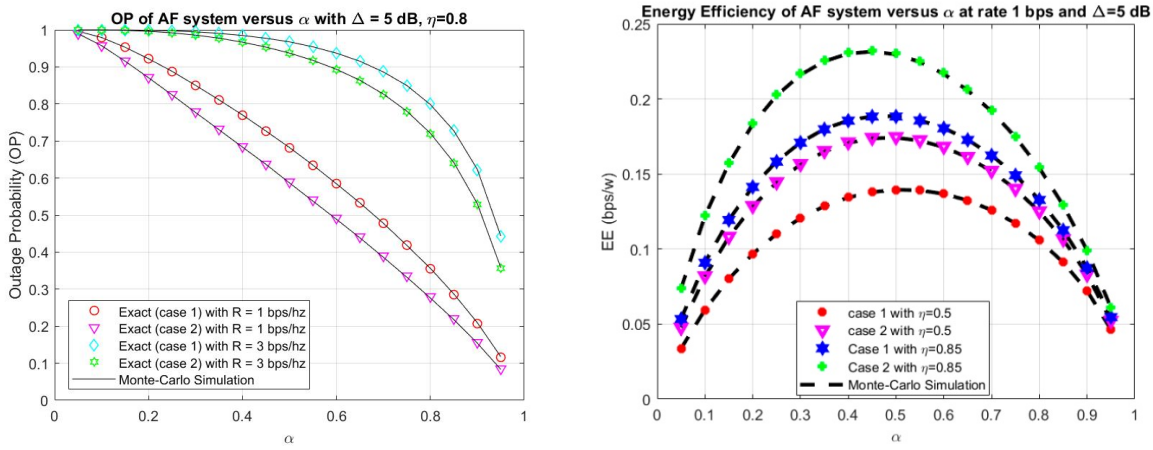


(a) Outage probability (b) Energy efficiency

Figure 5.18: OP and EE of the proposed PB-assisted TSR-EH HD relay network versus TSR factor $\alpha$.

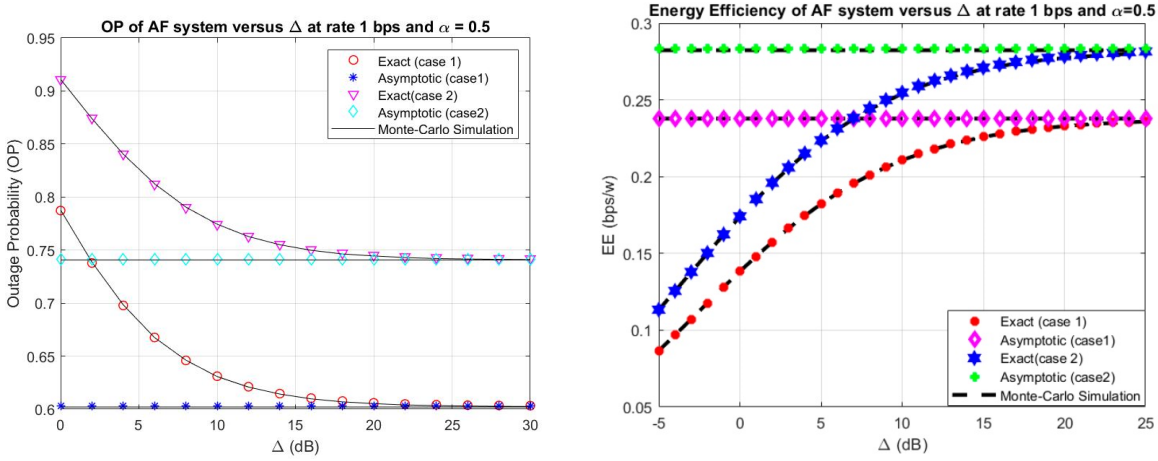


(a) Outage probability (b) Energy efficiency

Figure 5.19: OP and EE of the proposed PB-assisted TSR-EH HD relay network versus $\Delta$.

Fig. 5.18 plots the effect of the TS factor $\alpha$ on the OP and EE in Case 1 and Case 2, respectively. In Fig. 5.18a, I set the primary system parameters as $R = 1, 3bps/Hz$, $\Delta = 5$ dB, and $\eta = 0.8$. From the research results,It can be observed that the OP of the proposed system decreases when $\alpha$ increases from 0 to 1, and the OP of $R = 1bps/Hz$ was not better than that

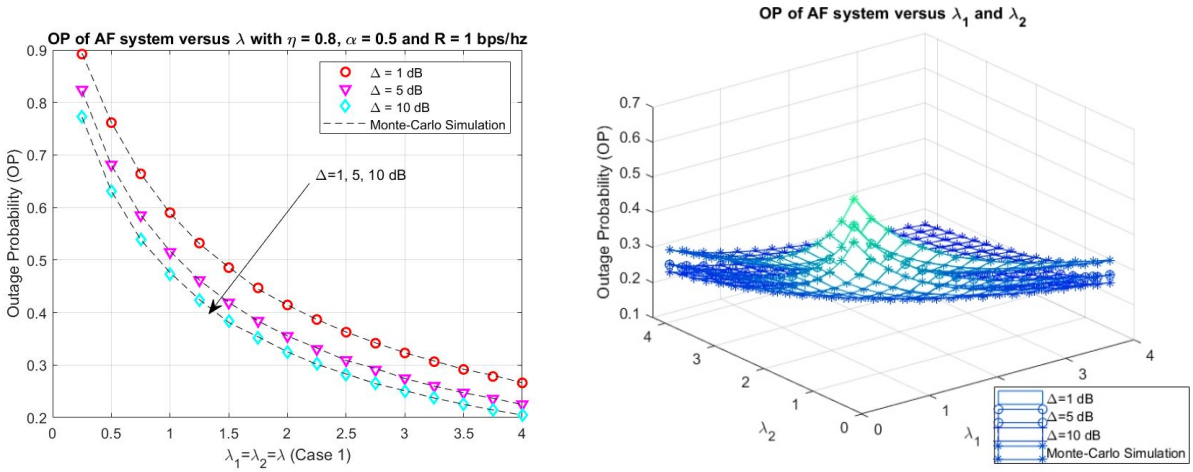


(a) Case 1: $\lambda_1 = \lambda_2 = \lambda$ (b) Case 2: $\lambda_1 \neq \lambda_2$

Figure 5.20: OP of the proposed PB-assisted TSR-EH HD relay network versus average channel power gain.

with $R = 3bps/Hz$. It can be seen that the OP was better with the higher R, and that the OP of Case 2 was better than that of Case 1. In Fig. 5.18b, I set $\eta \in \{0.5, 0.85\}$, $R = 1bps/Hz$, $\Delta = 5$ dB, and $\alpha$ varies from 0 to 1. We canobserve that the EE rises significantly when $\alpha$ rises from 0 to 0.5, after that the EE decreases. The optimal value of EE can be obtained with $\alpha$ from 0.4 to 0.6. Both Case 1 and Case 2 are considered in Fig. 5.18b, and it can be observed that the EE of Case 2 is better than that of Case 1 for different values of $\eta$.

Moreover, the OP and EE versus $\Delta$ is illustrated in Fig. 5.19 in both exact and asymptotic forms. In Fig. 5.19a, I set R = 1 $bps/Hz$ and $\alpha = 0.5$. Similar to Fig. 5.18a, both Case 1 and Case 2 are considered. We can observe that the OP decreases significantly when $\Delta$ increases from -5 to 15 dB and then converges to the asymptotic OP for $\Delta$ from 15 to 25, as shown in Fig. 5.19a. Once again, we see that the OP of Case 2 was better than that of Case 1. In Fig. 5.19b, I set $R = 1bps/Hz$ and $\alpha = 0.5$. Similar to OP, we can see that the exact EE increases with $\Delta$ from -5 to 25 and then converges to the asymptotic curve.

We investigates the influence of $\lambda_1$ and $\lambda_2$ on the OP of the model system, as illustrated in Fig. 5.20. Here, we set $\Delta = 1, 5, 10$ dB, $\eta = 0.8$, $\alpha = 0.5$, and $R = 1bps/Hz$. From Fig. 5.20a, we see that the OP in Case 1 falls with the rising $\lambda$, and the OP was better with a higher value of $\Delta$. In Fig. 5.20b, both $\lambda_1$ and $\lambda_2$ vary from 0 to 4. From the results, we can conclude that the OP of the system falls off when $\lambda_1$ and $\lambda_2$ increase. The optimal value of the system OP is obtained at $\lambda_1 = \lambda_2 = 0$. Finally, from all of the above figures, we can conclude that the simulation results verify the analytical results completely.

### 5.2.3 Summary

In this section, we investigates two practical performance degrading factors: hardware impairment and co-channel interference. For the first model, PSR-based EH HD-DF relay network under HI is considered over different fading channels. In the other model, the PB-assisted TSR-EH for HD relay network under co-channel interference over a Rayleigh fading environment is investigated. Both the exact and asymptotic form expressions for OP, throughput BER, and EE are derived mathematically and verified numerically by Monte Carlo simulation. The results of this section can serve as a practical guide to design better RF-EH-based communication schemes to overcome noise and interference.

## 5.3 Investigation of User Selection and Relay Selection in EH-based Wireless Cooperative Networks

In this section, I present the relay selection and user selection methods to enhance the overall performance of EH-based wireless relay network. These methods are analyzed in Rayleigh and Nakagami-m facding channels. [HDH07], [HDH14].

### 5.3.1 Wireless Power Transfer Wireless Sensor Network with Best AF Relay Selection over Nakagami-m Fading

In this first part, I would like to present the performance analysis of the best relay selection scheme for an EH-based AF relaying wireless sensor network over Nakagami-m fading. Specifically, this considered network consists of one source, multiple energy-constrained relays, and one destination sensor node. The best relay is chosen to amplify and forward the message to the destination after being powered by the source. [HDH14], [HDH17].

#### 5.3.1.1 Introduction

Nowadays, wireless sensor networks (WSNs) present extensive potential in human life, i.e., health monitoring, security and tactical surveillance, intrusion detection, manufacturing control, disaster management, weather monitoring, traceability, farming monitoring, and safety services, especially with the development of 5G and beyond wireless networks and IoT networks. However, the limited energy of sensor nodes degrade the coverage of WSN, reduce the processing ability of the sensor node and decrease the lifetime of the network. RF EH approach may represent a practical trend for WSNs because it's already available in the form of transmitted energy and in small form factor implementation, and low cost [105]. Naturally, the embedding EH into relaying WSNs or cooperative WSNs have attracted a lot of attention from the academia and industry in the recent decade [106].

In [107], the authors derived the analytical expressions of the AT of a block-wise TS-based protocol for EH AF relaying network in two modes of EH at the relay: continuous and discrete time EH. The PS-based protocol was applied at each relay of SWIPT multiple-relay network

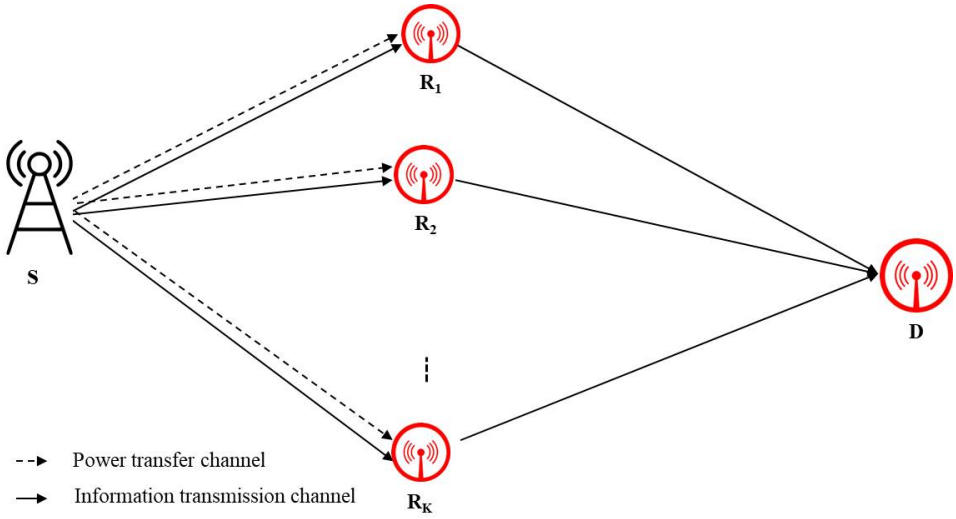


Figure 5.21: System and channel models for EH AF WSNs

to coordinate the received signal energy for information decoding and EH in [108]. By using the interior-point method, the solutions for the optimization problems of PS ratios at the relays were provided for both basic relay schemes, i.e., DF and AF. In the work of [109], the authors proposed a hybrid TS-APS protocol for EH DF relay networks with the discrete-level battery of relays. A TSAPS-OBR protocol based on optimal capacity for EH AF relaying network was proposed in [HDH17] and the optimal power-splitting ratio to maximum the end-to-end SNR was found. However, they have not derived the expression of OP for performance analysis.

Motivate by the work of [HDH17], in this topic I consider an AF multiple-relay wireless sensor networks with RF EH over Nakagami-$m$ fading channels. In order to evaluate the performance of the relay selection algorithm, closed-form expression of OP and throughput are derived in two cases: fixed and adaptive power-splitting ratio. Based on these expressions, I investigate the behavior of this network according to the key parameters such as transmit power, number of relays, TS ratio and the distance for both fixed and adaptive power-splitting ratios.

#### 5.3.1.2 System and Channel Models

In this system model, a best relay selection scheme is presented for an EH-based AF relaying wireless sensor network over Nakagami-$m$ fading. Specifically, this considered network consists of one source node S, $K$ energy-constrained relays $R_k(1 \leq k \leq K)$, and one destination node D as illustrated in Fig. 5.21. The communication protocol for this model is divided into two phases [HDH14] similar to the protocol in Fig. 2.8c, with one modification, i.e. in the second phase, the best relay is selected among $K$ relays to amplify and forward the message from S to D rather than just a fixed relay.

Note that, the power-splitting (PS) ratio can be dynamically adjusted according to the variation of channel coefficient to maximize the end-to-end SNR. The optimal relay is selected

among $K$ relays based on the criteria of maximizing system capacity. The relays can estimate the instantaneous channel gain based on the algorithm of channel estimation in request-to-send (RTS)/clear-to-send (CTS) transmission from the source and the destination [HDH17]. According to [HDH17], in high SNR region, the end-to-end SNR of this considered system is given by

$$\gamma_{e2e}^{*} \sim \frac{c\gamma_0\gamma_1^*\gamma_2^*(1-\rho^*)\rho^*}{\kappa(1-\rho^*)\gamma_2^*+\rho^*} \quad , \tag{5.105}$$

where $\kappa = \dfrac{\eta\alpha}{1-\alpha}$, $\gamma_0 = \dfrac{P_0}{N_0}$, $\gamma_1^* = \dfrac{|h_1|^2}{d_1^\theta}$, $\gamma_2^* = \dfrac{|h_2|^2}{d_2^\theta}$, and the optimal $\rho^*$ was introduced in [HDH17] as

$$\rho^* = \frac{\sqrt{c\gamma_2^*}}{\sqrt{c\gamma_2^*}+1}. \tag{5.106}$$

Assume that the relay node can only split the received signal into two power parts based on a finite discrete set of PS ratios, i.e. $\rho_i^*$ can only receive a value from the following set $\rho_l \in \left\{\dfrac{1}{L}, \dfrac{2}{L}, \cdots, \dfrac{L-1}{L}\right\}$. Here, $L$ is the number of PS ratio levels and $1 \leq l \leq L-1$. Note that, $\rho_l^*$ cannot is selected as zero (no information part) or one (no energy part). From (5.106), we assign $\rho_l^* = \dfrac{l}{L}$ when the channel gain of $R$ - $D$ link satisfies the following condition:

$$b_l = \frac{l^2}{(L-l)^2 c} < \gamma_2^* < b_{l+1} = \frac{(l+1)^2}{(L-l-1)^2 c}, \tag{5.107}$$

where $l \in \{1, 2, \cdots, L-1\}$.

Note that because the links of $S$ - $R$ and $R$ - $D$ undergo the Nakagami-$m$ fading, the CDF and PDF of RVs $\gamma_n$, $n \in \{1, 2\}$, are respectively given by

$$F_{\gamma_n}(x) = 1 - e^{-\frac{m_n}{\lambda_n}x} \sum_{k=0}^{m_n-1} \frac{1}{k!}\left(\frac{m_n}{\lambda_n}x\right)^k, \tag{5.108}$$

$$f_{\gamma_n}(x) = \frac{x^{m_n-1}}{(m_n-1)!}\left(\frac{m_n}{\lambda_n}\right)^{m_n} e^{-\frac{m_n}{\lambda_n}x}, \tag{5.109}$$

where $\lambda_n = \mathbf{E}(\gamma_n)$, $m_n \geq 1/2$ is the fading severity factor, in which $m_n = 1$ corresponds to Rayleigh fading and $m_n = (V+1)^2/(2V+1)$ approximately represents Rician fading with parameter $V$.

#### 5.3.1.3 Performance Analysis

This part presents the derivation of the OP and throughput expressions of this considered WSN system. First, the OP is defined as the probability that the instantaneous capacity ($C$) falls below a predetermined rate threshold $R > 0$, which is expressed as $OP = \Pr(C < R)$. In particular, for this considered system with TSAPS-ORS scheme [HDH17], the overall OP can

be obtained as

$$OP^* \overset{(a)}{=} (P^*_{out})^K = \left[\Pr\left(C^*_{opt} < R\right)\right]^K = \left[\Pr(\gamma^*_{e2e} < 2^{\frac{2R}{1-\alpha}} - 1)\right]^K, \tag{5.110}$$

where $C^*_{opt}$ is the optimal instantaneous capacity for best relay. Note that step (a) is obtained by assuming the channels are modeled as i.i.d. over different relaying channels [109]. The performance analysis of this system is summarized in the following theorems.

**Theorem 5.7** *Under Nakagami-m fading channel assumption, the OP of the proposed system is given by*

$$\begin{aligned} OP^* = \{1 - \sum_{l=1}^{L-1} \sum_{j=0}^{m_1-1} \sum_{i=0}^{j} & \frac{e^{-\frac{m_1\gamma_{th}}{\lambda_1\rho_l\gamma_0}}}{i!(j-i)!(m_2-1)!\kappa^i(1-\rho_l)^i\rho_l^{j-i}} \left(\frac{m_1\gamma_{th}}{\lambda_1\gamma_0}\right)^j \left(\frac{m_2}{\lambda_2}\right)^{m_2} \\ & \times \sum_{p=0}^{\infty} \frac{(-1)^p a_1^p}{p! a_2^{m_2-i-p}} \left[\Gamma(m_2-i-p, a_2 b_l) - \Gamma(m_2-i-p, a_2 b_{l+1})\right]\}^K, \end{aligned} \tag{5.111}$$

*where* $a_1 = \frac{m_1\gamma_{th}}{\lambda_1\kappa(1-\rho_l)\gamma_0}$ *and* $a_2 = \frac{m_2}{\lambda_2}$.

**Proof** Here, we derive the expression of $OP^*$ as in (5.111). Substituting (5.112) into (5.110),

we obtain the closed-form expression of OP for this system.

$$
\begin{aligned}
P_{out}^{*} &= \Pr(\gamma_{e2e}^{*} < 2^{\frac{2R}{1-\alpha}} - 1) = 1 - \sum_{l=1}^{L-1} \Pr\left( \frac{c\gamma_0\gamma_1\gamma_2(1-\rho_l)\rho_l}{c(1-\rho_l)\gamma_2 + \rho_l} > \gamma_{th}, b_l \leq \gamma_2 < b_{l+1} \right) \\
&= 1 - \sum_{l=1}^{L-1} \int_{b_l}^{b_{l+1}} \left[ 1 - F_{\gamma_1}\left( \frac{c(1-\rho_l)\gamma_{th}x + \rho_l\gamma_{th}}{c(1-\rho_l)\rho_l\gamma_0 x} \right) \right] f_{\gamma_2}(x)dx \\
&= 1 - \sum_{l=1}^{L-1} \sum_{j=0}^{m_1-1} \sum_{i=0}^{j} \frac{e^{-\frac{m_1\gamma_{th}}{\lambda_1\rho_l\gamma_0}} \left(\frac{m_1\gamma_{th}}{\lambda_1\gamma_0}\right)^j \left(\frac{m_2}{\lambda_2}\right)^{m_2}}{i!(j-i)!(m_2-1)!c^i(1-\rho_l)^i\rho_l^{j-i}} \int_{b_l}^{b_{l+1}} x^{m_2-i-1} e^{-\frac{m_1\gamma_{th}}{\lambda_1 c(1-\rho_l)\gamma_0 x} - \frac{m_2 x}{\lambda_2}} dx \\
&= 1 - \sum_{l=1}^{L-1} \sum_{j=0}^{m_1-1} \sum_{i=0}^{j} \frac{e^{-\frac{m_1\gamma_{th}}{\lambda_1\rho_l\gamma_0}}}{i!(j-i)!(m_2-1)!c^i(1-\rho_l)^i\rho_l^{j-i}} \left(\frac{m_1\gamma_{th}}{\lambda_1\gamma_0}\right)^j \left(\frac{m_2}{\lambda_2}\right)^{m_2} \\
&\times \left[ \int_{b_l}^{\infty} x^{m_2-i-1} e^{-\frac{m_1\gamma_{th}}{\lambda_1 c(1-\rho_l)\gamma_0 x} - \frac{m_2 x}{\lambda_2}} dx - \int_{b_{l+1}}^{\infty} x^{m_2-i-1} e^{-\frac{m_1\gamma_{th}}{\lambda_1 c(1-\rho_l)\gamma_0 x} - \frac{m_2 x}{\lambda_2}} dx \right] \\
&\overset{(b)}{=} 1 - \sum_{l=1}^{L-1} \sum_{j=0}^{m_1-1} \sum_{i=0}^{j} \frac{e^{-\frac{m_1\gamma_{th}}{\lambda_1\rho_l\gamma_0}}}{i!(j-i)!(m_2-1)!c^i(1-\rho_l)^i\rho_l^{j-i}} \left(\frac{m_1\gamma_{th}}{\lambda_1\gamma_0}\right)^j \left(\frac{m_2}{\lambda_2}\right)^{m_2} \\
&\times \left[ \sum_{p=0}^{\infty} \frac{(-1)^p a_1^p}{p!} \int_{b_l}^{\infty} x^{m_2-i-p-1} e^{-a_2 x} dx - \sum_{q=0}^{\infty} \frac{(-1)^q a_1^q}{q!} \int_{b_{l+1}}^{\infty} x^{m_2-i-q-1} e^{-a_2 x} dx \right] \\
&\overset{(c)}{=} 1 - \sum_{l=1}^{L-1} \sum_{j=0}^{m_1-1} \sum_{i=0}^{j} \frac{e^{-\frac{m_1\gamma_{th}}{\lambda_1\rho_l\gamma_0}}}{i!(j-i)!(m_2-1)!c^i(1-\rho_l)^i\rho_l^{j-i}} \left(\frac{m_1\gamma_{th}}{\lambda_1\gamma_0}\right)^j \left(\frac{m_2}{\lambda_2}\right)^{m_2} \\
&\times \left[ \sum_{p=0}^{\infty} \frac{(-1)^p a_1^p}{p! a_2^{m_2-i-p}} \Gamma(m_2-i-p, a_2 b_l) - \sum_{q=0}^{\infty} \frac{(-1)^q a_1^q}{q! a_2^{m_2-i-q}} \Gamma(m_2-i-q, a_2 b_{l+1}) \right], \qquad (5.112)
\end{aligned}
$$

where $\gamma_{th} = 2^{\frac{2R}{(1-\alpha)}} - 1$. Note that step (b) and (c) are obtained by using (1.211-1) and (3.381-3), respectively, in [72]. ■

The second important and related performance metric is the throughput at the destination This metric is found by evaluating the OP at a fixed source transmission rate − $R$ bps/Hz.

**Theorem 5.8** *Under Nakagami-m fading, the overall throughput ($\tau$) of this considered system under the delay-limited transmission mode is written as*

$$
\begin{aligned}
\tau = \frac{1}{2}(1-\alpha)R \Bigg\{ 1 - \Bigg\{ 1 - \sum_{l=1}^{L-1} \sum_{j=0}^{m_1-1} \sum_{i=0}^{j} \frac{e^{-\frac{m_1\gamma_{th}}{\lambda_1\rho_l\gamma_0}}}{i!(j-i)!(m_2-1)!c^i(1-\rho_l)^i\rho_l^{j-i}} \left(\frac{m_1\gamma_{th}}{\lambda_1\gamma_0}\right)^j \\
\times \left(\frac{m_2}{\lambda_2}\right)^{m_2} \sum_{p=0}^{\infty} \frac{(-1)^p a_1^p}{p! a_2^{m_2-i-p}} \left[ \Gamma(m_2-i-p, a_2 b_l) - \Gamma(m_2-i-p, a_2 b_{l+1}) \right] \Bigg\}^K \Bigg\}. \qquad (5.113)
\end{aligned}
$$

**Proof** Taking into account the fixed source transmission rate $R$ bps/Hz, the effective communication time from the source node to the destination node in the total block time $T$ is $\frac{(1-\alpha)T}{2}$. According to the definition of throughput [29], we have:

$$\tau = (1 - OP^*) R \frac{(1-\alpha)T/2}{T} = \frac{1}{2}(1-\alpha)R(1 - OP^*). \tag{5.114}$$

By substituting (5.111)) into (5.114)), we obtained the throughput of this considered system as (5.113). This ends of our proof. ■

#### 5.3.1.4 Numerical Results and Discussion

In this part, we provide the simulation and analysis results in terms of $OP^*$ and $\tau$ to reveal the impact of key parameters, such as average transmit SNR ($\gamma_0$), number of relays ($N$), TS ratio ($\alpha$), EH efficiency ($\eta$), relay location ($d_1$) and fading severity factor ($m$), on system performance.

The impact of average transmit SNR $\gamma_0$ and the number of relays $K$ on system performance are shown in Fig. 5.22a and Fig. 5.22b. According to these figures, the performance gets better with the increasing of $\gamma_0$ and $K$. This is because the higher transmit power, the better signal and the more energy harvested, leading to the higher power to amplify and retransmit the source signal in the second phase. However, when $\gamma_0$ is large enough, $OP^* \to 0$ and $\tau \to \frac{(1-\alpha)R}{2}$. From these figures, we can also understand that increasing the number of relays can improve the performance of this system because we have more choices to select the best relay to forward the information to the destination sensor node.

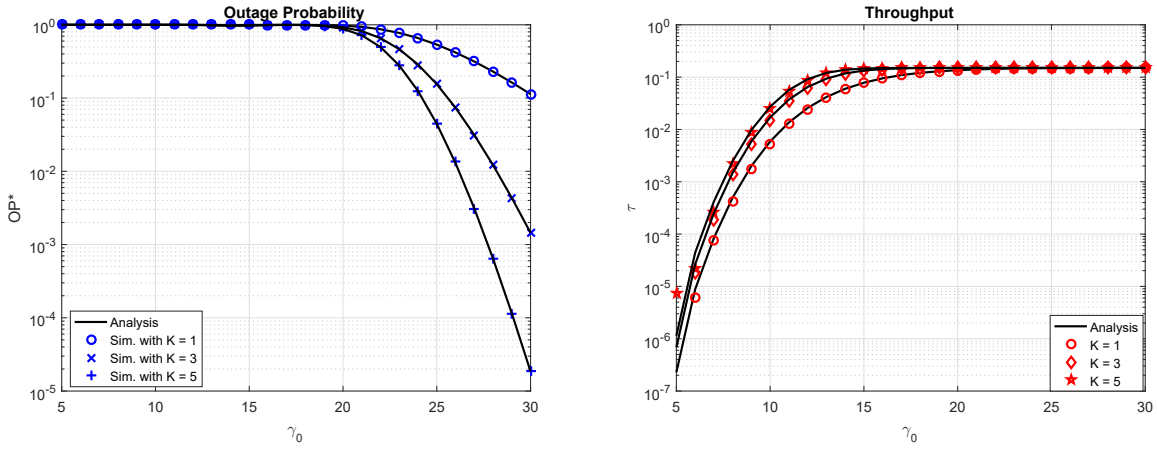


(a) Outage probability (b) Throughput

Figure 5.22: OP and throughput of the proposed EH-based AF relaying WSN versus average transmit $SNR$ $\gamma_0$ with $d_1 = d_2 = 1$, $m_1 = 2$, $m_2 = 25$, $R = 1bps/Hz$, $\theta = 2$, $\alpha = 0.7$, $\eta = 1$, $L = 20$.

Fig. 5.23 plots the OP and throughput of this considered system, respectively, versus TS factor $\alpha$. It is seen from Fig. 5.23a and Fig. 5.23b that when $\alpha$ grows up, $OP^*$ decreases, $\tau$

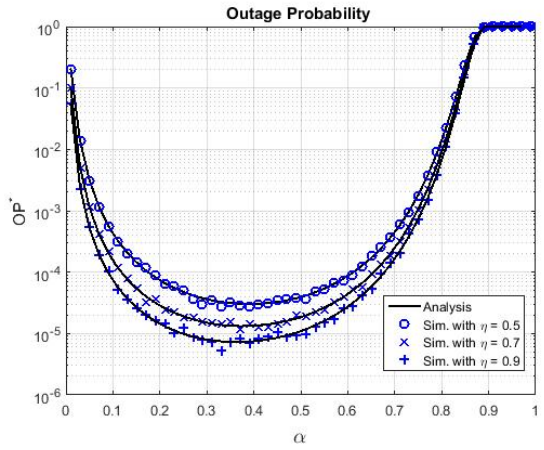


(a) Outage probability

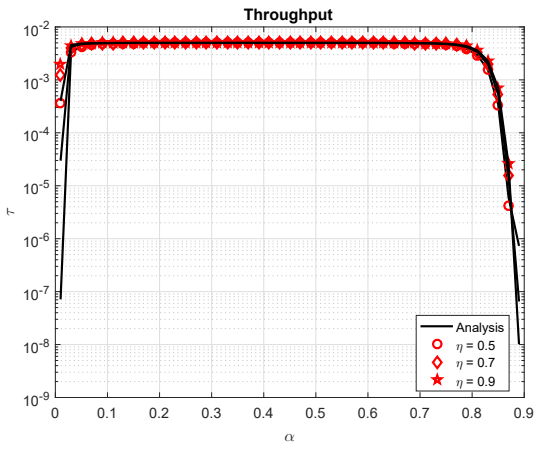


(b) Throughput

Figure 5.23: OP and throughput of the proposed EH-based AF relaying WSN versus $\alpha$ and $\eta$ with $\gamma_0 = 20dB$, $d_1 = d_2 = 1$, $m_1 = 2$, $m_2 = 15$, $R = 1bps/Hz$, $\theta = 2$, $L = 20$.

scales up and the performance is upgraded. This is explained due to more time spent on EH as $\alpha$ grows, which leads to higher transmission power, hence better performance results. However, when $\alpha$ continues to increase, $OP^*$ gets larger, $\tau$ scales down and the performance is degraded. That is because the information time is reduced, which leads to the increasing of real data rate. Overall, there is an optimal value of $\alpha$ that can minimize $OP^*$. This is clearly seen by the single bottom of the $OP^*$ curve plotted in Fig. 5.23a as a function of $\alpha$.

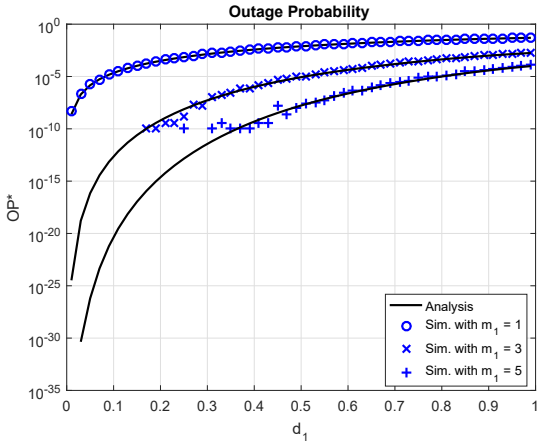


(a) Outage probability

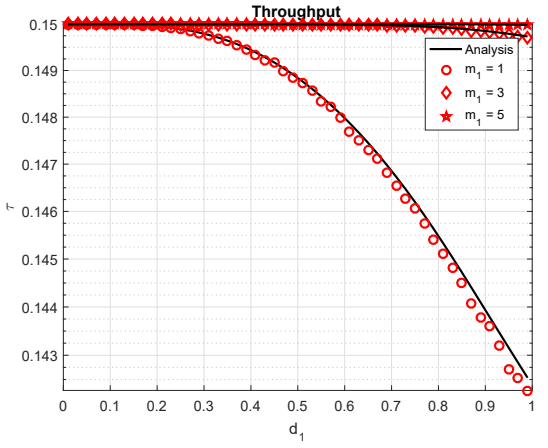


(b) Throughput

Figure 5.24: OP and throughput of the proposed EH-based AF relaying WSN versus $d_1$ and $m_1$ with $\gamma_0 = 20dB$, $d_2 = 2 - d_1$, $m_2 = 25$, $R = 1bps/Hz$, $\theta = 2$, $\alpha = 0.7$, $\eta = 1$, $L = 20$.

The impact of relay location ($d_1$) and fading severity parameters ($m_1$) on OP and throughput are illustrated in Fig. 5.24. In this figure, we see that increasing $d_1$ makes $OP^*$ and $\tau$ worse.

This is because higher values of $d_1^{\theta}$ lead to the smaller values of energy collected as well as poorer received signal strength at the relay nodes. Similarly, we can understand that $OP^*$ decreases and $\tau$ increases with the increasing of $m_1$. This is because the channel quality is better with larger fading severity parameter. Finally, from all above figures we can observe the perfect match between analytical and simulation results at high average transmit SNR, or equivalently at large $P_0$, regime. Reversely, when $\gamma_0$ is low, the analytical and simulation results do not match well because we use the approximated expression for the end-to-end SNR at the destination node as (5.105) [HDH17] and finite terms of (1.211-1) in [72].

### 5.3.2 User Selection Protocol in Cooperative Networks with PSR-Protocol-Based Energy Harvesting Over Nakagami-m/ Rayleigh Channels

In this part, the system performance analysis of cooperative networks with PSR-based EH over Nakagami-$m$/ Rayleigh channels is presented. The research results demonstrate the effectiveness of EH in the network over Nakagami-$m$/ Rayleigh channels. [HDH07].

#### 5.3.2.1 Introduction

IoT is considered a critical research area worldwide and has a significant impact on all activities in daily lives and industry [63], [64]. However, energy limitations are the most significant problem in the long-term operation of wireless IoT networks. Wireless EH using RF is considered a promising solution for prolonging the operating time of devices in wireless, energy-constrained cooperative networks [110]. Especially, in EH cooperative networks, an energy-constrained relay R, by simultaneously harvesting energy and transferring information, can help maintain constant operation and connection without the use of external energy sources. The problem of a two-hop EH cooperative relaying network has been studied in many previous research works. The authors in [111] considered a dual-hop cognitive, inter-vehicular, relay-assisted communication system where all communication links are not line of sight, and their fading is modeled by the binary Rayleigh fading distribution. The authors in [112] presented a general framework for modeling and evaluating the performance of dual-hop, DF relaying schemes over independent and not necessarily identically distributed (INID) Nakagami-$m$ fading channels. The performance of dual-hop MIMO OSTBC transmission with multiple antennas employed at the transceiver and CSI-assisted AF relay over Nakagami-$m$ fading is proposed in [113], and the performance of dual-hop, DF relaying with relay selection over Nakagami fading channels was studied in [77]. In [114], a harvest-then-cooperate (HTC) protocol with AP points for S and R EH was investigated. The authors in [83] investigated two-way relay beamforming optimization to maximize the achievable sum rate of simultaneous wireless information and power transfer (SWIPT) system with a FD-MIMO-AF relay. Moreover, the authors in [115] derived the theoretical symbol error probability (SEP) of cooperative systems with the best relay selection for Nakagami-$m$ fading channels, and the authors in [116] proposed a novel full rate DQOSTBC matrix with embedded adaptive

DAF/amplify-and-forward (AAF) elements for data retransmission with four single-antenna relays.

However, there has been very little research focus on both user selection protocol and EH with different Nakagami-$m$/Rayleigh channels, which are suitable for IoT applications because for example, a sensor node can select the best destination to inform its sensing data. For this purpose, I propose an user selection algorithm for choosing the best-received destination in co-operative networks with PSR-based EH over Nakagami-$m$/Rayleigh channels. The exact-form expressions of the OP and ergodic capacity (EC) is derived using the proposed probabilistic models for wireless channels. Finally, we conduct Monte Carlo simulations to verify the performance analysis of the proposed system.

#### 5.3.2.2 System Model

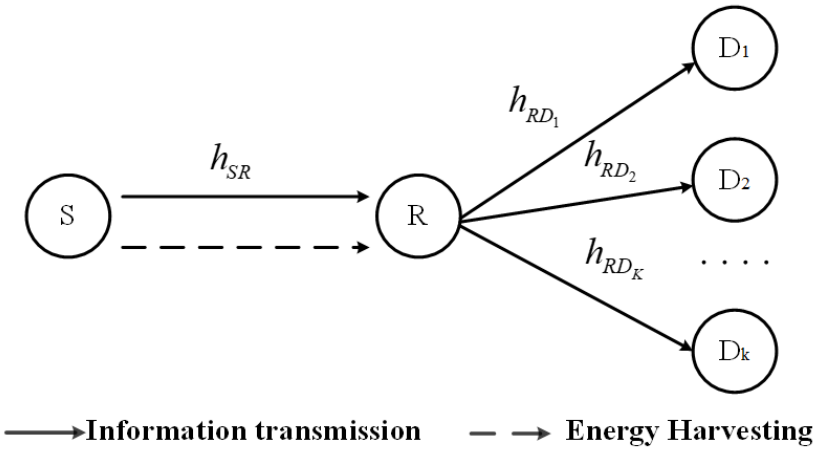


Figure 5.25: System model.

We consider a PSR-based EH relay network for IoT applications with one source node S, one AF relay nodes R, and $K$ destination (user) nodes $D_i, i = 1, 2, ..., K$, as shown in Fig. 5.25 [76], [86]. These destinations represents for multiple sensors to collect the same data to enhance the reliability of the network. In this system model, S, R, and $D_i$ are working in a HD mode with one antenna. The channel gain between node S and the relay R ($h_{SR}$) is a Nakagami-$m$ fading channel, while the one between the relay R and the destinations, $h_{RD_i}, i = 1, ..., K$ is a Rayleigh fading channel. In this model, the direct link between S and D nodes is too weak without the help of a relay. The EH and information transfer follows the PSR protocol as in Fig. 2.6a.

In the first transmission phase, the received signal at R can be formulated by

$$y_r = \frac{1}{\sqrt{d_{SR}^{\theta}}}\sqrt{(1-\rho)}h_{SR}x_s + n_r \tag{5.115}$$

In this equation, $h_{SR}$ is S to R channel gain, $d_{SR}$ is the distance between S and R, and $\theta$ denotes the path loss exponent. Here, $x_s$ is the transmitted signal at S, $n_r$ is the AWGN with variance $N_0$, and $0 < \rho < 1$ is the PS ratio at the relay R. Moreover, $E\left\{|x_s|^2\right\} = P_s$, where $P_s$ is the average transmit power at S.

As analyzed in Section 4.2, the transmit power by the relay, which is provided by EH from S, can be found as

$$P_r = \frac{E_h}{d_{SR}^{\theta}(T/2)} = \frac{\eta\rho P_s|h_{SR}|^2(T/2)}{d_{SR}^{\theta}(T/2)} = \frac{\eta\rho P_s|h_{SR}|^2}{d_{SR}^{\theta}} \tag{5.116}$$

In the second time slot $T/2$, R retransmits the information from S to $D_i$. The received signal at the $i^{th}$ destination during the second phase can be expressed as

$$y_{d_i} = \frac{1}{\sqrt{d_i^{\theta}}} h_{RD_i} x_r + n_{d_i} \tag{5.117}$$

where $i \in (1, 2, ..., K)$, $h_{RD_i}$ is the R to the $D_i$ channel gain, $d_i$ is R-to-D distance, $n_{d_i}$ is the zero-mean AWGN with variance $N_0$, and $E\left\{|x_r|^2\right\} = P_r$. Here, the AF protocol is considered, and the amplifying factor can be given by

$$\beta = \frac{x_r}{y_r} = \sqrt{\frac{P_r}{\frac{(1-\rho)P_s|h_{SR}|^2}{d_{SR}^{\theta}} + N_0}} \tag{5.118}$$

From (5.115), (5.117) and (5.118), the received signal can be rewritten as

$$y_{d_i} = \frac{h_{RD_i}\beta}{\sqrt{d_{RD_i}^{\theta}}}\left[\frac{\sqrt{(1-\rho)}h_{SR}x_s}{\sqrt{d_{SR}^{\theta}}} + n_r\right] + n_{d_i} = \underbrace{\frac{\sqrt{(1-\rho)}h_{SR}x_s h_{RD_i}\beta}{\sqrt{d_i^{\theta}}\sqrt{d_{SR}^{\theta}}}}_{signal} + \underbrace{\frac{h_{RD_i}\beta n_r}{\sqrt{d_i^{\theta}}} + n_{d_i}}_{noise} \tag{5.119}$$

Therefore, the overall signal to noise ratio (SNR) from S to D can be given by

$$SNR = \frac{E\left\{|signal|^2\right\}}{E\left\{|noise|^2\right\}} = \frac{\frac{(1-\rho)P_S|h_{SR}|^2\left|h_{RD_i}\right|^2\beta^2}{d_i^{\theta}d_{SR}^{\theta}}}{\frac{\left|h_{RD_i}\right|^2\beta^2 N_0}{d_i^{\theta}} + N_0} = \frac{(1-\rho)P_S|h_{SR}|^2|h_{RD_i}|^2}{|h_{RD_i}|^2 d_{SR}^{\theta}N_0 + \frac{N_0 d_i^{\theta}d_{SR}^{\theta}}{\beta^2}} \tag{5.120}$$

After doing some algebra, using (5.116) and the fact that $N_0 << P_R$, and denoting $\gamma_1 = |h_{SR}|^2, \gamma_i = |h_{RD_i}|^2$, (5.120) can be rewritten as

$$SNR = \frac{(1-\rho)P_s P_r|h_{SR}|^2|h_{RD_i}|^2}{|h_{RD_i}|^2 d_{SR}^{\theta}P_r N_0 + (1-\rho)P_s|h_{SR}|^2 N_0 d_i^{\theta}} = \frac{\eta\rho(1-\rho)\psi|h_{SR}|^2|h_{RD_i}|^2}{\eta\rho|h_{RD_i}|^2 d_{SR}^{\theta} + (1-\rho)d_i^{\theta}} \tag{5.121}$$

where $\psi = P_s/N_0$.

#### 5.3.2.3 Performance Analysis

The closed-form expressions of OP and EC of this system model are derived in this section. At first, I determine the PDF and CDF of RVs $|h_{SR}|^2, |h_{RD_i}|^2$. As shown in [117] and using [72, Eq. 8.353.4], the PDF and CDF of RV $\gamma_1$ can be calculated by

$$f_{|h_{SR}|^2}(x) = \frac{x^{m_{|h_{SR}|^2}-1}}{(m_{|h_{SR}|^2}-1)!(\Omega_{|h_{SR}|^2})^{m_{|h_{SR}|^2}}} \exp(-\frac{x}{\Omega_{|h_{SR}|^2}}) \tag{5.122}$$

$$F_{|h_{SR}|^2}(x) = 1 - \exp(-\frac{x}{\Omega_{|h_{SR}|^2}}) \sum_{t=0}^{m_{|h_{SR}|^2}-1} \frac{x^t}{t!(\Omega_{|h_{SR}|^2})^t} \tag{5.123}$$

where $\Omega_{|h_{SR}|^2} = \frac{\lambda_{SR}}{m_{|h_{SR}|^2}}$; $m_{|h_{SR}|^2}$ is the Nakagami-$m$ parameter and note that the case of $m_{|h_{SR}|^2} = 1$ corresponds to Rayleigh fading; $\lambda_{SR} = \frac{E\{|h_{SR}|^2\}}{d_{SR}^{\theta}}$ is the mean of RV $|h_{SR}|^2$. Furthermore, we have the PDF and CDF of RV $|h_{RD_i}|^2$ as shown in [6] as

$$f_{|h_{RD_i}|^2}(x) = \frac{1}{\lambda_{RD_i}} e^{-x/\lambda_{RD_i}} \tag{5.124}$$

$$F_{|h_{RD_i}|^2}(x) = 1 - e^{-x/\lambda_{RD_i}} \tag{5.125}$$

where $\lambda_{RD_i} = \frac{E\left\{|h_{RD_i}|^2\right\}}{d_i^{\theta}}$ is the mean of RV $|h_{RD_i}|^2$.

In this system model, the best selection user $US_q$ is selected if and only if

$$|h_{RD_q}|^2 = \max_{i=1,2,\ldots,K} (|h_{RD_i}|^2) \tag{5.126}$$

For simplicity, from now on we denote $h_{RD} = h_{RD_q}$. According to [118], the CDF and PDF of $|h_{RD}|^2$ can be given respectively by

$$F_{|h_{RD}|^2}(y) = \sum_{p=0}^{K} (-1)^p \binom{K}{p} e^{-py/\lambda_{RD}}, \tag{5.127}$$

$$f_{|h_{RD}|^2}(y) = \frac{1}{\lambda_{RD}} \sum_{p=0}^{K-1} (-1)^p \binom{K-1}{p} K e^{-(p+1)y/\lambda_{RD}} \tag{5.128}$$

where $\lambda_{RD}$ is the mean of RV $|h_{RD}|^2$.

Now, we can state the following theorem on the closed-form of OP.

**Theorem 5.9 (OP—Closed Form)** *The closed-form expression of the OP of the proposed*

*model system can be formulated as*

$$P_{out} = 1 - 2\exp\left[-\frac{zd_{SR}^{\theta}}{\Omega_{|h_{SR}|^2}(1-\rho)\psi}\right]\sum_{t=0}^{m_{\gamma_1}-1}\sum_{n=0}^{t}\sum_{p=0}^{K-1}\frac{(-1)^p K\binom{K-1}{p} z^{\frac{n+t+1}{2}}(\lambda_{RD})^{\frac{n-t-1}{2}}}{(t-n)!n!\left(\Omega_{|h_{SR}|^2}\psi\right)^{\frac{n+t+1}{2}}(p+1)^{\frac{n-t+1}{2}}}$$
$$\times\left(\frac{d_i^{\theta}}{\eta\rho}\right)^{\frac{t-n+1}{2}}\left[\frac{d_{SR}^{\theta}}{(1-\rho)}\right]^n K_{n-t+1}\left(2\sqrt{\frac{zd_i^{\theta}(p+1)}{\Omega_{|h_{SR}|^2}\eta\rho\psi\lambda_{RD}}}\right) \tag{5.129}$$

**Proof** OP can be calculated as

$$\begin{aligned}
P_{out} &= \Pr\left(SNR < z\right) = \Pr\left(\frac{\eta\rho(1-\rho)\psi|h_{SR}|^2|h_{RD}|^2}{\eta\rho|h_{RD}|^2 d_{SR}^{\theta} + (1-\rho)d_i^m} < z\right)\\
&= \Pr\left\{\eta\rho(1-\rho)\psi|h_{SR}|^2|h_{RD}|^2 < z\eta\rho|h_{RD}|^2 d_{SR}^{\theta} + z(1-\rho)d_i^{\theta}\right\}\\
&= \Pr\left[|h_{SR}|^2 < \frac{z\eta\rho|h_{RD}|^2 d_{SR}^{\theta} + z(1-\rho)d_i^{\theta}}{\eta\rho(1-\rho)\psi|h_{RD}|^2}\right] = \Pr\left[|h_{SR}|^2 < \frac{zd_i^{\theta}}{\eta\rho\psi|h_{RD}|^2} + \frac{zd_{SR}^{\theta}}{(1-\rho)\psi}\right]\\
&= \int_0^{\infty} F_{|h_{SR}|^2}\left(\frac{zd_i^{\theta}}{\eta\rho\psi y} + \frac{zd_{SR}^{\theta}}{(1-\rho)\psi}\right) f_{|h_{RD}|^2}(y)dy
\end{aligned} \tag{5.130}$$

where $z = 2^{2R} - 1$ is the SNR threshold, and R is the source data rate.

From Equations (5.123) and (5.129), we can rewrite (5.130) as

$$\begin{aligned}
P_{out} &= 1 - \int_0^{\infty}\exp\left[-\frac{\frac{zd_i^{\theta}}{\eta\rho\psi y} + \frac{zd_{SR}^{\theta}}{(1-\rho)\psi}}{\Omega_{|h_{SR}|^2}}\right]\sum_{t=0}^{m_{\gamma_1}-1}\frac{\left[\frac{zd_i^{\theta}}{\eta\rho\psi y} + \frac{zd_{SR}^{\theta}}{(1-\rho)\psi}\right]^t}{t!\left(\Omega_{|h_{SR}|^2}\right)^t}\frac{1}{\lambda_q}\sum_{p=0}^{K-1}(-1)^p\binom{K-1}{p}Ke^{\frac{-(p+1)y}{\lambda_q}}dy\\
&= 1 - \frac{e^{\frac{-zd_{SR}^{\theta}}{\Omega_{|h_{SR}|^2}(1-\rho)\psi}}}{\lambda_{RD}}\int_0^{\infty}\sum_{t=0}^{m_{\gamma_1}-1}\frac{\left[\frac{zd_i^{\theta}}{\eta\rho\psi y} + \frac{zd_{SR}^{\theta}}{(1-\rho)\psi}\right]^t}{t!\left(\Omega_{|h_{SR}|^2}\right)^t}e^{\frac{zd_i^{\theta}}{\Omega_{|h_{SR}|^2}\eta\rho\psi y}}\sum_{p=0}^{K-1}(-1)^p\binom{K-1}{p}Ke^{\frac{-(p+1)y}{\lambda_{RD}}}dy
\end{aligned} \tag{5.131}$$

Now by applying $(x+y)^m = \sum_{n=0}^{m} \binom{m}{n} x^{m-n} y^n$, the OP in (5.131) can be found as

$$
\begin{aligned}
P_{out} &= 1 - \frac{e^{\frac{-zd_{SR}^{\theta}}{\Omega_{|h_{SR}|^2(1-\rho)\psi}}}}{\lambda_{RD}} \int_0^{\infty} \sum_{t=0}^{m_{\gamma_1}-1} \sum_{n=0}^{t} \binom{t}{n} \frac{z^t}{t!\left(\Omega_{|h_{SR}|^2}\right)^t} \left(\frac{d_i^{\theta}}{\eta\rho\psi y}\right)^{t-n} \left[\frac{d_{SR}^{\theta}}{(1-\rho)\psi}\right]^n e^{\frac{-zd_i^{\theta}}{\Omega_{|h_{SR}|^2\eta\rho\psi y}}} \\
&\times \sum_{p=0}^{K-1} (-1)^p \binom{K-1}{p} K e^{\frac{-(p+1)y}{\lambda_{RD}}} dy \\
&= 1 - \frac{e^{\frac{-zd_{SR}^{\theta}}{\Omega_{|h_{SR}|^2(1-\rho)\psi}}}}{\lambda_{RD}} \sum_{t=0}^{m_{\gamma_1}-1} \sum_{n=0}^{t} \sum_{p=0}^{K-1} \frac{(-1)^p K \binom{K-1}{p} z^t}{(t-n)!n!\left(\Omega_{|h_{SR}|^2}\right)^t \psi^t} \left(\frac{d_i^{\theta}}{\eta\rho}\right)^{t-n} \left[\frac{d_{SR}^{\theta}}{(1-\rho)}\right]^n \\
&\times \int_0^{\infty} y^{n-t} e^{\frac{-zd_i^{\theta}}{\Omega_{\gamma_1}\eta\rho\psi y}} e^{\frac{-(p+1)}{\lambda_{RD}}} dy
\end{aligned} \tag{5.132}
$$

By using [72, pp. 3.471, 9] and (5.132), we obtain the OP as in (5.129). ∎

In this part, we will find the PS factor to maximize capacity. The overall capacity from source to destination is given by

$$
C_{s,d} = \frac{1}{2}\log_2(1+SNR) = \frac{1}{2}\log_2\left[1 + \frac{\eta\rho(1-\rho)\psi|h_{SR}|^2|h_{RD}|^2}{\eta\rho|h_{RD}|^2 d_{SR}^{\theta} + (1-\rho)d_i^{\theta}}\right] \tag{5.133}
$$

Therefore, to maximize capacity, we need to maximize SNR. From (5.121), SNR is a concave function of $\rho$.

**Theorem 5.10 (EC closed-form)** *a. The optimal $\rho$ that maximize the SNR can be given as*

$$
\rho^* = \frac{1}{1 + |h_{RD}|\sqrt{\frac{\eta d_{SR}^{\theta}}{d_i^{\theta}}}} \tag{5.134}
$$

*b. The closed-form expression of the EC of the proposed system in optimal condition can be expressed as*

$$
C_{AF} = \frac{1}{\ln 2} \sum_{v=1}^{N_p} \omega_v \frac{1 - F_{SNR_{\max}}(x_v)}{1+x_v} \tag{5.135}
$$

*where* $x_v = \tan\left(\frac{\pi}{4}\cos\left[\frac{2v-1}{2N_p}\pi\right] + \frac{\pi}{4}\right)$, *and* $\omega_v = \frac{\pi^2 \sin\left(\frac{2v-1}{2N_p}\pi\right)}{4N_p \cos^2\left(\frac{\pi}{4}\cos\left[\frac{2v-1}{2N_p}\pi\right]+\frac{\pi}{4}\right)}$ *and*

$$F_{SNR_{\max}}(z) = 1 - 2e^{-\frac{zd_{SR}^{\theta}}{\Omega_{|h_{SR}|^2}\psi}}$$
$$\times \sum_{t=0}^{m_{|h_{SR}|^2}-1} \sum_{n=0}^{2t} \sum_{p=0}^{K-1} \sum_{q=0}^{\infty} \frac{(-1)^p \binom{K-1}{p} K(-2)^q (2t)! \left(d_{SR}^{\theta}\right)^{\frac{q+n}{2}} \left(d_i^{\theta}\right)^{\frac{q-n-2t+2}{4}}}{n!t!(2t-n)!q!\eta^{\frac{2t-n+q+2}{4}}(p+1)^{\frac{n-2t-q+2}{4}}(\lambda_{RD})^{\frac{2t-n+q+2}{4}}}$$
$$\times \left(\frac{z}{\Omega_{|h_{SR}|^2}\psi}\right)^{\frac{n+2t+3q+2}{4}} K_{\frac{n-2t-q+2}{2}}\left(2\sqrt{\frac{zd_i^{\theta}(p+1)}{\Omega_{|h_{SR}|^2}\eta\psi\lambda_{RD}}}\right), \tag{5.136}$$

**Proof** a. It is easy to observe that $\frac{\partial^2 SNR}{\partial \rho^2}$ is negative for $0 < \rho < 1$. Hence, SNR is a concave function of $\rho(0 < \rho < 1)$. We can find the value of $\rho$ that maximizes SNR by differentiating the SNR with respect to $\rho$, and then equate it to zero. After some algebraic calculations, we have two possible solutions for $\rho^*$: $\rho^* = \frac{1}{1+|h_{RD}|\sqrt{\frac{\eta d_{SR}^{\theta}}{d_i^{\theta}}}}$ or $\rho^* = \frac{1}{1-|h_{RD}|\sqrt{\frac{\eta d_{SR}^{\theta}}{d_i^{\theta}}}}$.

Since $\rho^* = \frac{1}{1-|h_{RD}|\sqrt{\frac{\eta d_{SR}^{\theta}}{d_i^{\theta}}}}$ results in a value of $\rho^* > 1$ or $\rho^* < 0$, we choose $\rho^* = \frac{1}{1+|h_{RD}|\sqrt{\frac{\eta d_{SR}^{m}}{d_i^{m}}}}$ as the solution. By substituting this into (5.121), $SNR_{max}$ can be obtained as

$$SNR_{max} = \frac{\eta\psi|h_{SR}|^2|h_{RD}|^2}{\left(1+|h_{RD}|\sqrt{\frac{\eta d_{SR}^{\theta}}{d_i^{\theta}}}\right)^2 d_i^{\theta}}. \tag{5.137}$$

The CDF of $SNR_{max}$ can be derived as

$$F_{SNR_{\max}}(z) = \Pr\left(SNR_{\max} < z\right) = \Pr\left[\frac{\eta\psi|h_{SR}|^2|h_{RD}|^2}{\left(1+|h_{RD}|\sqrt{\frac{\eta d_{SR}^{\theta}}{d_i^{\theta}}}\right)^2 d_i^{\theta}} < z\right]$$
$$= \Pr\left[|h_{SR}|^2 < \frac{\left(1+|h_{RD}|\sqrt{\frac{\eta d_{SR}^{\theta}}{d_i^{\theta}}}\right)^2 z d_i^{\theta}}{\eta\psi|h_{RD}|^2}\right] = \int_0^{\infty} F_{|h_{SR}|^2}\left(\frac{\left(1+\sqrt{\frac{\eta y d_{SR}^{\theta}}{d_i^{\theta}}}\right)^2 z d_i^{\theta}}{\eta\psi y}\right) f_{|h_{RD}|^2}(y)\, dy$$
$$= 1 - \frac{1}{\lambda_{RD}} \int_0^{\infty} e^{\frac{-\left(1+\sqrt{\frac{\eta y d_{SR}^{\theta}}{d_i^{\theta}}}\right)^2 z d_i^{m}}{\Omega_{|h_{SR}|^2}\eta\psi y}} \sum_{t=0}^{m_{|h_{SR}|^2}-1} \frac{1}{t!\left(\Omega_{|h_{SR}|^2}\right)^t} \left[\frac{\left(1+\sqrt{\frac{\eta y d_{SR}^{\theta}}{d_i^{\theta}}}\right)^2 z d_i^{\theta}}{\eta\psi y}\right]^t$$
$$\times \sum_{p=0}^{K-1} (-1)^p \binom{K-1}{p} K e^{\frac{-(p+1)y}{\lambda_{RD}}} dy \tag{5.138}$$

In Equation (5.138), we consider

$$A = e^{\frac{-\left(1+\sqrt{\frac{\eta y d_{SR}^{\theta}}{d_i^{\theta}}}\right)^2 z d_i^{\theta}}{\Omega_{|h_{SR}|^2}\eta\psi y}} = e^{\frac{-zd_i^{\theta}+2z\sqrt{\eta y d_{SR}^{\theta} d_i^{\theta}}+zy\eta d_{SR}^{\theta}}{\Omega_{|h_{SR}|^2}\eta\psi y}} = e^{\frac{-zd_i^{\theta}}{\Omega_{|h_{SR}|^2}\eta\psi y}} e^{\frac{-2z\sqrt{d_{SR}^{\theta} d_i^{\theta}}}{\Omega_{|h_{SR}|^2}\psi\sqrt{\eta y}}} e^{\frac{-zd_{SR}^{\theta}}{\Omega_{|h_{SR}|^2}\psi}} \quad (5.139)$$

We then apply a Taylor series as follows:

$$e^{\frac{-2z\sqrt{d_{SR}^{\theta} d_i^{\theta}}}{\Omega_{|h_{SR}|^2}\psi\sqrt{\eta y}}} = \sum_{q=0}^{\infty} \frac{\left(-\frac{2z\sqrt{d_{SR}^{\theta} d_i^{\theta}}}{\Omega_{|h_{SR}|^2}\psi\sqrt{\eta y}}\right)^q}{q!} = \sum_{q=0}^{\infty} \frac{(-1)^q \left(\frac{2z\sqrt{d_{SR}^{\theta} d_i^{\theta}}}{\Omega_{|h_{SR}|^2}\psi\sqrt{\eta}}\right)^q}{q!} y^{-q/2} \quad (5.140)$$

Then, (5.139) can be rewritten as

$$A = \sum_{q=0}^{\infty} \frac{(-1)^q \left(\frac{2z\sqrt{d_{SR}^{\theta} d_i^{\theta}}}{\Omega_{|h_{SR}|^2}\psi\sqrt{\eta}}\right)^q}{q!} y^{-q/2} e^{\frac{-zd_{SR}^{\theta}}{\Omega_{|h_{SR}|^2}\psi}} e^{\frac{-zd_i^{\theta}}{\Omega_{|h_{SR}|^2}\eta\psi y}} \quad (5.141)$$

By substituting (5.141) into (5.138) and using the formula $(x+y)^m = \sum_{n=0}^{m} \binom{m}{n} x^{m-n} y^n$, we get

$$\begin{aligned}
F_{SNR_{\max}}(z) &= 1 - \frac{1}{\lambda_{RD}} \int_0^{\infty} \sum_{q=0}^{\infty} \frac{(-1)^q \left(\frac{2z\sqrt{d_{SR}^{\theta} d_i^{\theta}}}{\Omega_{|h_{SR}|^2}\psi\sqrt{\eta}}\right)^q}{q!} y^{-q/2} e^{\frac{-zd_{SR}^{\theta}}{\Omega_{|h_{SR}|^2}\psi}} e^{\frac{-zd_i^{\theta}}{\Omega_{|h_{SR}|^2}\eta\psi y}} \\
&\times \sum_{t=0}^{m_{|h_{SR}|^2}-1} \frac{\left(zd_i^{\theta}\right)^t}{t!\left(\Omega_{|h_{SR}|^2}\eta\psi y\right)^t} \sum_{n=0}^{2t} \binom{2t}{n} \left[\sqrt{\frac{\eta y d_{SR}^{\theta}}{d_i^{\theta}}}\right]^n \sum_{p=0}^{K-1} (-1)^p \binom{K-1}{p} K e^{\frac{-(p+1)y}{\lambda_{RD}}} dy \\
&= 1 - \frac{1}{\lambda_{RD}} \sum_{t=0}^{m_{|h_{SR}|^2}-1} \sum_{n=0}^{2t} \sum_{p=0}^{K-1} \sum_{q=0}^{\infty} \int_0^{\infty} e^{\frac{-zd_{SR}^{\theta}}{\Omega_{|h_{SR}|^2}\psi}} e^{\frac{-zd_i^{\theta}}{\Omega_{|h_{SR}|^2}\eta\psi y}} \\
&\times \frac{(-2)^q (2t)! (z)^{t+q} y^{\frac{n-2t-q}{2}} \left(d_{SR}^{\theta}\right)^{\frac{q}{2}} \left(d_i^{\theta}\right)^{\frac{q}{2}}}{n!t!(2t-n)!q!\left(\Omega_{|h_{SR}|^2}\psi\right)^{t+q} \eta^{t+q/2}} \left(\frac{\eta d_{SR}^{\theta}}{d_i^{\theta}}\right)^{\frac{n}{2}} (-1)^p \binom{K-1}{p} K e^{\frac{-(p+1)y}{\lambda_{RD}}} dy \\
&= 1 - \frac{e^{-\frac{zd_{SR}^{\theta}}{\Omega_{|h_{SR}|^2}\psi}}}{\lambda_{RD}} \sum_{t=0}^{m_{|h_{SR}|^2}-1} \sum_{n=0}^{2t} \sum_{p=0}^{K-1} \sum_{q=0}^{\infty} \frac{(-1)^p \binom{K-1}{p} K (-2)^q (2t)! (z)^{t+q} \left(d_{SR}^{\theta}\right)^{\frac{q+n}{2}} \left(d_i^{\theta}\right)^{\frac{q-n}{2}}}{n!t!(2t-n)!q!\left(\Omega_{|h_{SR}|^2}\psi\right)^{t+q} \eta^{t+q/2-n/2}} \\
&\times \int_0^{\infty} y^{\frac{n-2t-q}{2}} e^{\frac{-zd_i^{\theta}}{\Omega_{|h_{SR}|^2}\eta\psi y}} e^{\frac{-(p+1)y}{\lambda_{RD}}} dy
\end{aligned} \quad (5.142)$$

Table 5.4: Simulation parameters.

| Symbol | Name | Value |
|---|---|---|
| $\eta$ | EH efficiency | 0.8 |
| $\lambda_{SR}$ | Mean of $\|h_{SR}\|^2$ | 0.5 |
| $\lambda_{RD}$ | Mean of $\|h_{RD}\|^2$ | 0.5 |
| $m_{\gamma_1}$ | Nakagami m-factor | 3 |
| $z$ | SNR threshold | 1 |
| $\mathrm{P}_S/\mathrm{N}_0$ | Source power to noise ratio | 0-20dB |
| $R$ | Source rate | 0.5 bit/s/Hz |
| $K$ | Number of sources | 1-6 |
| $\theta$ | Pathloss exponent | 3 |
| $d_{SR} = d_i$ | the distance of S-R link and R-D link, respectively | 0.85 |

By using equation [3.471.9] in [72], (5.142) can be rewritten as

$$F_{SNR_{\max}}(z) = 1 - \frac{2e^{-\frac{zd_{SR}^{\theta}}{\Omega_{|h_{SR}|^2}\psi}}}{\lambda_{RD}} \sum_{t=0}^{m_{|h_{SR}|^2}-1} \sum_{n=0}^{2t} \sum_{p=0}^{K-1} \sum_{q=0}^{\infty} \frac{(-1)^p \binom{K-1}{p} K(-2)^q (2t)! (z)^{t+q} \left(d_{SR}^{\theta}\right)^{\frac{q+n}{2}} \left(d_i^{\theta}\right)^{\frac{q-n}{2}}}{n!t!(2t-n)!q! \left(\Omega_{|h_{SR}|^2}\psi\right)^{t+q} \eta^{t+q/2-n/2}}$$
$$\times \left[\frac{zd_i^{\theta}\lambda_{RD}}{(p+1)\Omega_{|h_{SR}|^2}\eta\psi}\right]^{\frac{n-2t-q+2}{4}} K_{\frac{n-2t-q+2}{2}} \left(2\sqrt{\frac{zd_i^{\theta}(p+1)}{\Omega_{|h_{SR}|^2}\eta\psi\lambda_{RD}}}\right). \quad (5.143)$$

By doing some simplifications, we get (5.136). Now, the ergodic capacity can be found by

$$C_{AF} = \int_0^{\infty} f_{SNR_{\max}}(z) \log_z(1+z) dz = \frac{1}{\ln 2} \int_0^{\infty} \frac{1 - F_{SNR_{\max}}(z)}{1+z} dz \quad (5.144)$$

We can observe that the involving integral in Equation (5.144) is difficult to solve in a closed form. However, by changing the variable $z = \tan\phi$ in the integration (5.144), we have:

$$C_{AF} = \frac{1}{\ln 2} \int_0^{\infty} \frac{1 - F_{SNR_{\max}}(z)}{1+z} dz = \frac{1}{\ln 2} \int_0^{\pi/2} \frac{1 - F_{SNR_{\max}}(\tan\phi)}{1+\tan\phi} \sec^2\phi d\phi \quad (5.145)$$

We can then apply an efficient NP-point Gauss–Chebyschev quadrature (GCQ) formula [119, Eq. (25.4.39)] from [84] to numerically derive (5.135). ∎

#### 5.3.2.4 Numerical Results and Discussion

Like in previous studies [73], [120], I conduct Monte Carlo simulations to verify analytical expressions of the OP and EC of the proposed system in the above section. In addition, we investigated the effect of the primary system parameter on the system performance in terms of OP and EC. All other simulation parameters are listed in Table 5.4.

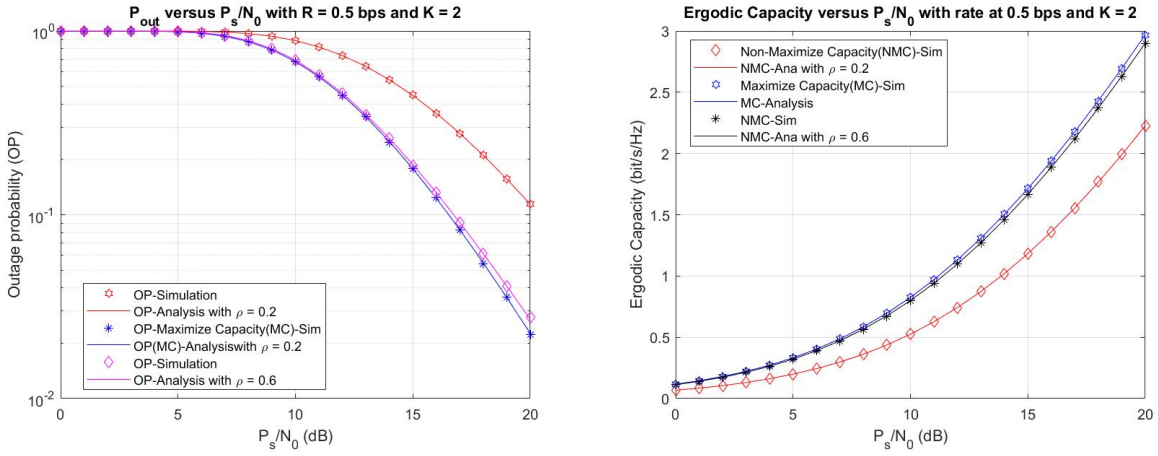


(a) Outage probability (b) Ergodic capacity

Figure 5.26: OP and ergodic capacity of the proposed multi-destination PSR-based EH versus $P_s/N_0$ while K = 2.

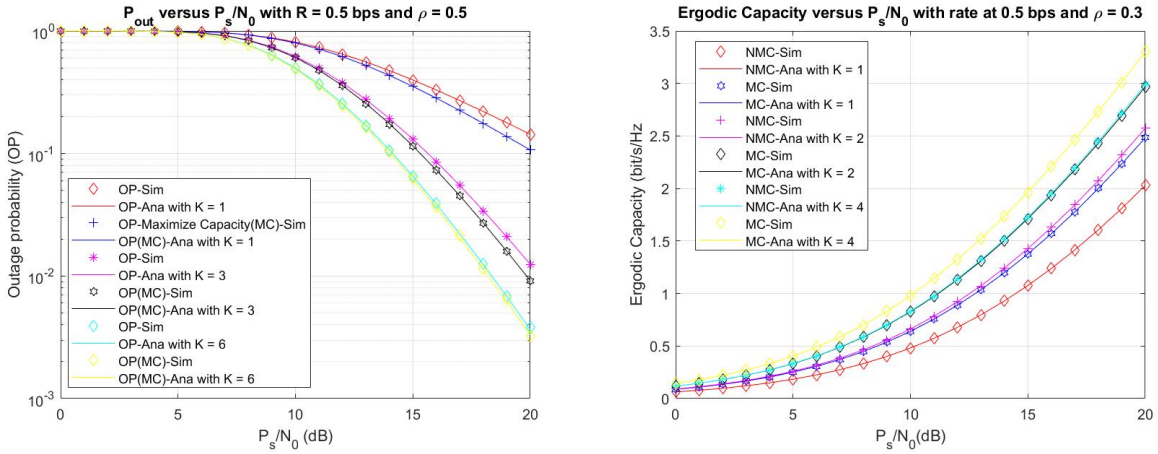


(a) Outage probability (b) Ergodic capacity

Figure 5.27: OP and ergodic capacity of the proposed multi-destination PSR-based EH versus $P_s/N_0$ while $\rho = 0.5$.

Fig. 5.26 illustrates the influence of $P_s/N_0$ on the OP and EC of the proposed system. The main parameters in this figure are as follows: K = 2, R = 0.5, and $\rho = 0.2$ and 0.6. In this figure, the OP of the cases $\rho = 0.2$ and 0.6 and the maximum capacity are provided for comparison. We can observe that OP decreases and EC increases as $\rho$ varies from 0.2 and 0.6. When $P_s/N_0$ increases from 0 to 20 dB, OP decreases and EC significantly increases. Furthermore, the higher the value of $\rho$ is, the faster the OP decreases and the EC increases. In addition, we can see that the OP and EC in the maximum capacity case is better than other cases, i.e. with other values of $\rho$. This can be explained by looking at the mathematical analysis in (5.129) and (5.135).

Fig. 5.27 depicts the effect of $P_s/N_0$ on the OP and the EC for different values of K. I set

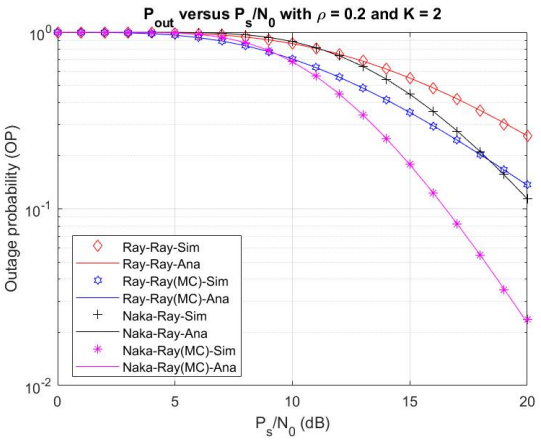


(a) Outage probability with $\rho = 0.2$ and $K = 2$

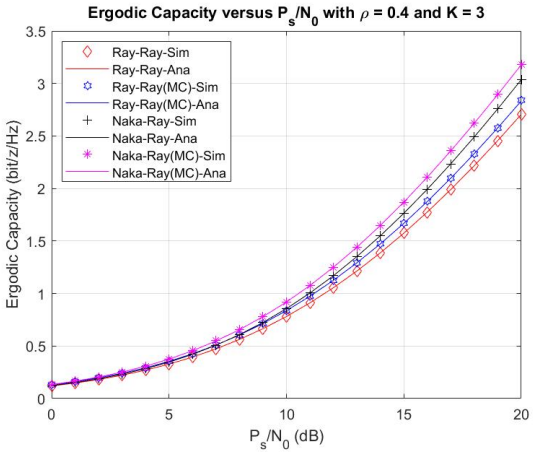


(b) Ergodic capacity with $\rho = 0.4$ and $K = 3$

Figure 5.28: OP and ergodic capacity of the proposed multi-destination PSR-based EH versus $P_s/N_0$ with different channel environments.

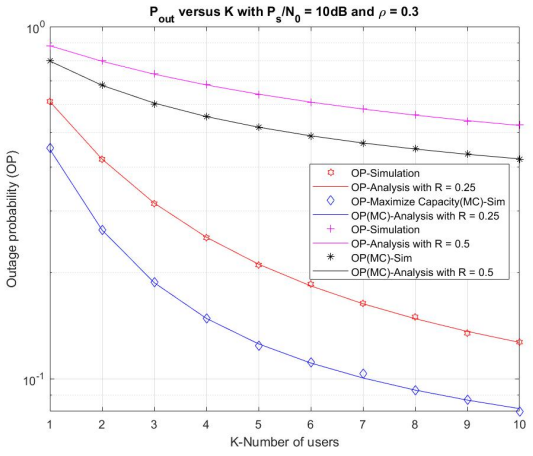


(a) Outage probability

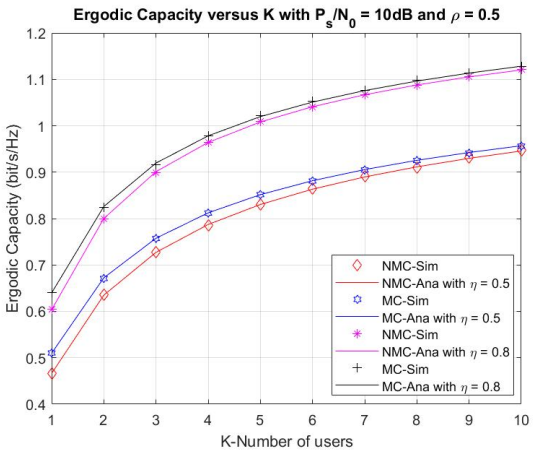


(b) Ergodic capacity

Figure 5.29: OP and ergodic capacity of the proposed multi-destination PSR-based EH versus number of users.

R = 0.5 bps, $\rho = 0.5$, and K = 1, 3, and 6. From Fig. 5.27a, the OP decreases when $P_s/N_0$ increases from 0 to 20 dB, and OP decreases faster with a higher K. On the other hand, the EC increases significantly when $P_s/N_0$ rises from 0 to 20 dB. Furthermore, the EC is higher with higher value of K.

Moreover, Fig. 5.28 displays the influence of the ratio $P_s/N_0$ on the OP and the EC of the model system for different channel conditions. Here, the cases Ray-Ray, Naka-Ray in the non-maximize and maximize modes are compared with each other in the same system condition. In particular, I let the ratio $P_s/N_0$ vary from 0 to 20 dB, and set $\rho = 0.2$, K = 2 in Fig 5.28a and $\rho = 0.4$, K = 3 in Fig 5.28b, respectively. Fig. 5.28a shows that OP decreases faster in the

Naka-Ray case with maximum capacity than in other cases. Similarly, EC increases faster in the Ray-Ray case with non-maximum capacity than in other cases in Fig. 5.28b. Here, we can see that the system performance in the maximum capacity case is better than in the non-maximum capacity case.

The OP and EC of the proposed system with respect to the number of users are presented in Fig. 5.29. Again, OP decreases and EC increases as the number of users varies from 0 to 10, and get better values in the maximum capacity case. Finally, it is observed that in all above figures, simulation and analytical results match well with each other.

### 5.3.3 Summary

This section extends the study of EH in wireless cooperative networks to the case of multiple relays or multiple destinations. I propose a best relay selection method for EH-based AF relaying WSN and a user selection protocol for PSR-based EH over Nakagami-$m$ and Rayleigh channels. In both models, the analytical closed-form expressions for the OP, throughput, and EC are derived. In the second model, the performance analysis is also applied for both fixed PS ratio and adaptive (optimal) PS ratio. Finally, Monte Carlo simulations confoirms the correctness of analytical expressions.

## 5.4 Hybrid TSR and PSR Protocol for RF Energy Harvesting in Alternate-Relay Network over Rician Fading Channels

All of the works mentioned above use either TSR or PSR EH protocol, each of which has its own advantages. In this section, I investigate a hybrid TSR–PSR alternative EH that can exploit the benefits from both conventional protocols. For this analysis, the AF mode and Rician fading channels are selected. [HDH12].

### 5.4.1 Introduction

Currently, EH from green environmental sources and the conversion of this energy into the electrical energy used to supply communication network devices is considered to be a leading research direction. In the series of primary environmentally green energy sources, such as solar, wind, geothermal, and mechanical energy, RF signals can be considered as a prospective energy source in the future. The research direction of RF-powered mobile networks has received significant attention during the last decade in wireless sensor networks (WSNs) and cooperative communication systems from both academia and industry [121], [122]. In cooperative networks, references [123] developed two new EH-based relaying protocols based on the receiver structures at R, termed time-switching-based receiver (TSR) and power-splitting-based receiver (PSR). From [124], the TSR and PSR protocols have some drawbacks; for instance, TSR loses information in the switching process to the harvesting mode, and PSR has a low coverage area. Furthermore, PSR requires a complicated hardware structure to make sure that a proper portion

of energy from the source signal is extracted for EH. In contrast, TSR can simplify the hardware at the expense of the throughput or achievable rate of the system. Based on the fact that both TSR and PSR protocols have their drawbacks, a method to combine these two protocols to get the best out of them should be considered. This solution is obtained in this paper by using an adaptive relaying protocol [125], [126]. From the other point of view, Tran et al. [127] proposed a general hybrid TSR-PSR protocol and provided its performance analysis. However, they just consider a simple network model.

The main objective of this section is to propose and investigate the performance (in terms of the OP and SER) alternative hybrid TSR–PSR EH relaying networks over Rician fading channels. In this model, two relays R1 and R2 are alternatively used for EH and data transmission process from S to D. In the first step, the exact and asymptotic expressions of the OP and SER are derived. Then, the influence of all system parameters on the system performance is investigated, and the Monte Carlo simulation verifies all results. Finally, the system performance of TSR–PSR, TSR, and PSR cases are compared in connection with all system parameters.

### 5.4.2 System Model

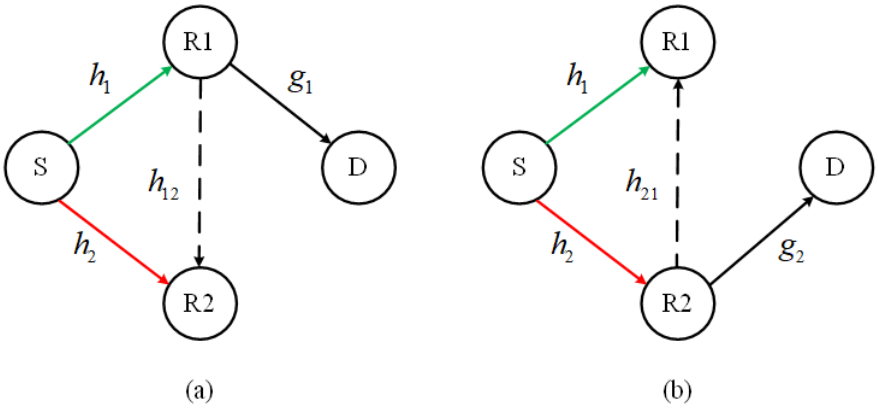


Figure 5.30: The system model. The green, red and black lines represent the first-hop and second-hop transmissions, respectively. The green and dashed back lines represent data transmission (DT) and EH, respectively. (a) $R_1$: DT and $R_2$: EH; (b) $R_2$: DT and $R_1$: EH.

Fig. 5.30 describes my considered network model, which consists of one source node S, one destination node D, and two alternative relays $R_1$ and $R_2$. Each device works with a single antenna and in a HD mode, and there is no direct link between S and D. In this model, S, and D have their own stable power supplies, while $R_1$ and $R_2$ operate by RF harvested energy and alternately forward source signal to destination following AF relaying strategy. We denote that $h_1$ and $h_2$ are the fading channel gains from the source to relays, $g_1$ and $g_2$ are the fading channel gain from the relays $R_1$ and $R_2$ to the destination D, and $h_{12}$ and $h_{21}$ are the channel gains between $R_1$ and $R_2$, respectively.

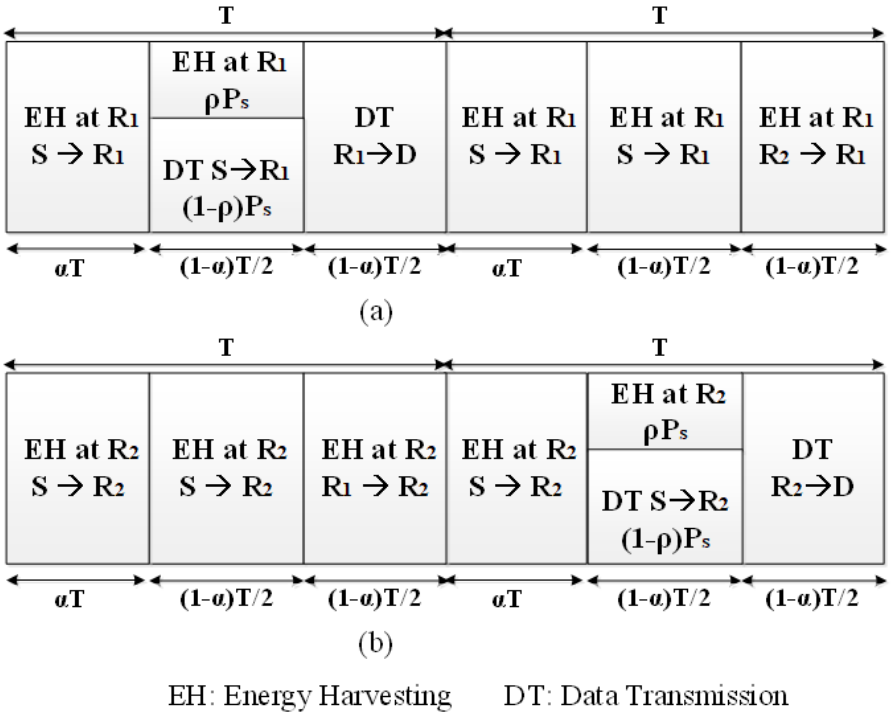


Figure 5.31: The information transmission and EH process.

Moreover, Fig. 5.31 shows the division of the transmission time. In the first interval time $\alpha T$ with $0 \leq \alpha \leq 1$, S transfers energy by signal to $R_1$ and $R_2$. After that, S simultaneously transfers energy (with power $\rho P_s$) and information (with power $(1-\rho)P_s$) to $R_1$ in the next interval of length $(1-\alpha)T/2$. In the same interval time, $R_2$ harvests energy from S. In the final interval of length $(1-\alpha)T/2$, $R_1$ transfers information to D and $R_2$ harvests energy from $R_1$ [6], [73], [111], [124]. For the next transmission block, the roles of $R_1$ and $R_2$ are reversed. Thus, $R_1$ and $R_2$ will alternately forward source data in every transmission block. Please note that $R_1$ and $R_2$ always harvest energy from the received RF signals in all of the first transmission blocks. Compared with TSR or PSR single-relay system, more energy can be harvested by relays in our protocol [73], [124], [128].

### 5.4.3 System Performance

In this part, we analyze and investigate the EH and data transmission processes in the two relays in the hybrid TSR–PSR protocol. In the system model, the inter-relay channel is assumed to be symmetric, i.e., $h_{12} = h_{21}$. Rician block fading is assumed, so all the channels are circularly-symmetric jointly-Gaussian complex RVs, i.e. $h_i \approx \mathcal{CN}(0,1)$, $g_i \sim \mathcal{CN}(0,1)$ and $h_{12} \sim \mathcal{CN}(0,1)$, where $i \in \{1,2\}$. In the hybrid TSR–PSR alternative relaying, the source provides an energy signal to both $R_1$ and $R_2$ in $\alpha T$ and $(1-\alpha)T/2$ blocks. In the $(1-\alpha)T/2$ block, $R_1$ allocates $0 \leq \rho < 1$ ($\rho$ is the PS factor) as part of the received source signal for the EH (EH). Therefore,

the total harvested energy at $R_1$ and $R_2$ can be given by

$$E_{r1a} = E_{r2a} = \eta\alpha T P_s + \frac{\eta\rho(1-\alpha)TP_s}{2}, \tag{5.146}$$

where $E\left\{|h_i|^2\right\} = 1$, $0 < \eta < 1$, $0 < \rho < 1$ and $0 \leq \alpha < 1$ are the energy conversion efficiency, power-splitting factor, and time-switching factor, respectively. In this model, small-scale channel fading is omitted.

When S sends data to $R_1$, after splitting a portion $\rho$ of the received signal for EH, the remaining signa at $R_1$ can be obtained as

$$y_{r1} = \sqrt{1-\rho}h_1 x_s + n_{r1} \tag{5.147}$$

where $n_{r1}$ is the zero-mean AWGN with variance $N_0$ at $R_1$, and $E\left\{|x_s|^2\right\} = P_s$.

Then, $R_1$ amplifies and forwards the signal to D in the next stage. The transmitted signal from $R_1$ can be expressed as $x_{r1} = \beta y_{r1}$, where $\beta$ is the amplifying factor, which is determined as

$$\beta = \frac{\sqrt{P_{r1}}}{\sqrt{(1-\rho)P_s|h_1|^2 + N_0}}. \tag{5.148}$$

Then, the received signal at D can be formulated as

$$y_{1d} = g_1 x_{r1} + n_{1d} = \beta g_1\left[\sqrt{1-\rho}h_1 x_s + n_{r1}\right] + n_{1d} = \underbrace{\beta g_1\sqrt{1-\rho}h_1 x_s}_{signal} + \underbrace{\beta g_1 n_{r1} + n_{1d}}_{noise} \tag{5.149}$$

where $n_{1d}$ is the AWGN with variance $N_0$ at D, $E\{|x_{r1}|^2\} = P_{r1}$, and $P_{r1}$ is the average transmit power of $R_1$.

In this case, when $R_1$ performs the delay-tolerant (DT) transmission mode, the end to end signal to noise ratio (SNR) at D can be calculated as

$$\gamma_{e2e1} = \frac{E\{|signal|^2\}}{E\{|noise|^2\}} = \frac{\beta^2|g_1|^2|h_1|^2 P_s(1-\rho)}{\beta^2|g_1|^2 N_0 + N_0} \approx \frac{(1-\rho)P_s P_{r1}|h_1|^2|g_1|^2}{|g_1|^2 N_0 + (1-\rho)P_s|h_1|^2 N_0} \tag{5.150}$$

where the last approximation is obtained by using (5.148) and the fact that $N_0 << P_r$.

In this tranmission block, $R_2$ can harvest energy from S in $\alpha T + (1-\alpha)T/2$ blocks, i.e., $\frac{T}{2}(1+\alpha)$ blocks, and $R_2$ can also harvest energy from $R_1$ in $(1-\alpha)T/2$ blocks. Therefore, the total harvested energy at $R_2$ when $R_1$ joins in the data transmission (DT) can be calculated by

$$E_{r2b} = \frac{\eta(1+\alpha)TP_s}{2} + \frac{\eta(1-\alpha)TP_{r1}}{2} \tag{5.151}$$

Similar to $R_2$, the total harvested energy at $R_1$ when $R_2$ joins in the DT can be obtained as

$$E_{r1b} = \frac{\eta(1+\alpha)TP_s}{2} + \frac{\eta(1-\alpha)TP_{r2}}{2} \tag{5.152}$$

where $P_{r2}$ is the average transmit power of $R_2$.

From the EH process at $R_1$ in the previous transmission block and current transmmission block, the total harvested energy of $R_1$ for DT can be obtained as

$$E_{r1} = E_{r1a} + E_{r1b} = \frac{\eta T\left[(3\alpha - \alpha\rho + 1)P_s + \rho + (1-\alpha)P_{r2}\right]}{2} \tag{5.153}$$

Similarly, the total harvested energy of $R_2$ also can be obtained as

$$E_{r2} = E_{r2a} + E_{r2b} = \frac{\eta T\left[(3\alpha - \alpha\rho + 1)P_s + \rho + (1-\alpha)P_{r1}\right]}{2} \tag{5.154}$$

From (5.153), (5.154) and using the law of energy conservation, the average transmitted power of $R_1$ and $R_2$ can be calculated as

$$P_{r1} = \frac{E_{r1}}{(1-\alpha)T/2} = \eta\left[\frac{(3\alpha - \alpha\rho + 1)P_s + \rho}{1-\alpha} + P_{r2}\right] \tag{5.155}$$

$$P_{r2} = \frac{E_{r2}}{(1-\alpha)T/2} = \eta\left[\frac{(3\alpha - \alpha\rho + 1)P_s + \rho}{1-\alpha} + P_{r1}\right] \tag{5.156}$$

By substituting (5.156) into (5.155), we obtain:

$$P_{r1} = \frac{\eta\Psi}{1-\eta} \tag{5.157}$$

where we denote $\Psi \triangleq \frac{(3\alpha-\alpha\rho+1)P_s+\rho}{1-\alpha}$. Finally, the SNR of the proposed system in (5.150) can be rewritten as

$$\gamma_{e2e1} = \frac{(1-\rho)P_sP_{r1}|h_1|^2|g_1|^2}{|g_1|^2N_0 + (1-\rho)P_s|h_1|^2N_0} = \frac{(1-\rho)P_sP_{r1}\varphi_1\varphi_2}{\varphi_2N_0 + (1-\rho)P_s\varphi_1N_0} \tag{5.158}$$

where $\varphi_1 = |h_1|^2, \varphi_2 = |g_1|^2$ and $P_{r1}$ is defined by (5.157).

#### 5.4.3.1 Exact Outage Probability Analysis

The PDF of the RV $\varphi_i$ (where $i \in \{1,2\}$) as in [73] is given by

$$f_{\varphi_i}(x) = a\sum_{l=0}^{\infty}\frac{(bK)^l}{(l!)^2}x^le^{-bx} \tag{5.159}$$

where we denote $\varphi_1 = |h_1|^2, \varphi_2 = |g_1|^2$, $a = \frac{(K+1)e^{-K}}{\lambda_i}, b = \frac{K+1}{\lambda_i}$, in which $\lambda_i$ is the unit mean value of RV $\varphi_i$ where $i = \{1, 2\}$, respectively, because we consider the small-scale power fading $|h_1|^2, |g_1|^2$ in the derivation. Therefore, a and b can be re-denoted as $a = (K+1)e^{-K}$, $b = K+1$, K is the Rician K-factor defined as the ratio of the power of the line-of-sight (LOS) component to the scattered components.

The CDF of RV $\varphi_i$, where $i \in \{1, 2\}$, can be computed as [125]

$$F_{\varphi_i}(\varsigma) = \int_0^{\varsigma} f_{\varphi_i}(x)dx = 1 - \frac{a}{b}\sum_{l=0}^{\infty}\sum_{n=0}^{l}\frac{K^l b^n}{l!n!}\varsigma^n e^{-b\varsigma} = 1 - \sum_{l=0}^{\infty}\sum_{n=0}^{l}\frac{K^l b^n e^{-K}}{l!n!}\varsigma^n e^{-b\varsigma} \tag{5.160}$$

**Theorem 5.11 (Exact Outage Probability)** *The expression of the exact OP of the proposed alternative hybrid TPSR EH relay network can be formulated by*

$$P_{out}^1 = 1 - \sum_{l=0}^{\infty}\sum_{m=0}^{\infty}\sum_{n=0}^{l}\sum_{k=0}^{n+m}\binom{n+m}{k}\frac{2ae^{-K}e^{\frac{-b\gamma_{th}N_0}{P_{r1}P_s(1-\rho)}}e^{\frac{-b\gamma_{th}N_0}{P_{r1}}}K^{l+m}b^{n+m}(\gamma_{th}N_0)^{n+m+1}}{l!(m!)^2 n! {P_{r1}}^{n+m+1}[P_s(1-\rho)]^{\frac{2n+m-k+1}{2}}}$$
$$\times K_{m-k+1}\left(\frac{2b\gamma_{th}N_0}{P_{r1}\sqrt{P_s(1-\rho)}}\right) \tag{5.161}$$

*where $K_v(\cdot)$ is the modified Bessel function of the second kind and $v^{th}$ order.*

**Proof** The OP of the model system can be calculated as

$$\begin{aligned}
P_{out}^1 &= \Pr\left(\gamma_{e2e1} < \gamma_{th}\right) = \Pr\left[\frac{(1-\rho)P_s P_{r1}\varphi_1\varphi_2}{\varphi_2 N_0 + (1-\rho)P_s\varphi_1 N_0} < \gamma_{th}\right] \\
&= \Pr\left[(1-\rho)P_s\varphi_1\left(P_{r1}\varphi_2 - \gamma_{th}N_0\right) < \gamma_{th}\varphi_2 N_0\right] \\
&= \Pr\left\{\varphi_1 < \frac{\gamma_{th}\varphi_2 N_0}{P_s(1-\rho)\left[P_{r1}\varphi_2 - \gamma_{th}N_0\right]}, \varphi_2 > \frac{\gamma_{th}N_0}{P_{r1}}\right\} + \Pr\left(\varphi_2 \le \frac{\gamma_{th}N_0}{P_{r1}}\right) \\
&= \int_0^{\frac{\gamma_{th}N_0}{P_{r1}}} f_{\varphi_2}(\varphi_2)d\varphi_2 + \int_{\frac{\gamma_{th}N_0}{P_{r1}}}^{\infty} F_{\varphi_1}\left\{\frac{\gamma_{th}\varphi_2 N_0}{P_s(1-\rho)\left[P_{r1}\varphi_2 - \gamma_{th}N_0\right]}|\varphi_2\right\} f_{\varphi_2}(\varphi_2)d\varphi_2
\end{aligned} \tag{5.162}$$

where $\gamma_{th} = 2^{2R} - 1$ is the SNR threshold and R is the source transmission rate.

From (5.160), the OP can be rewritten as

$$P_{out}^{1} = \int_{0}^{\frac{\gamma_{th}N_0}{P_{r1}}} f_{\varphi_2}(\varphi_2)d\varphi_2 + \int_{\frac{\gamma_{th}N_0}{P_{r1}}}^{\infty} \left\{1 - \sum_{l=0}^{\infty}\sum_{n=0}^{l} \frac{K^l b^n e^{-K}}{l!n!}\left[\frac{\gamma_{th}\varphi_2 N_0}{P_s(1-\rho)\left(P_{r1}\varphi_2 - \gamma_{th}N_0\right)}\right]^n e^{\frac{-b\gamma_{th}\varphi_2 N_0}{P_s(1-\rho)(P_{r1}\varphi_2 - \gamma_{th}N_0)}}\right\} f_{\varphi_2}(\varphi_2)d\varphi_2 \tag{5.163}$$

Furthermore, by using (5.159), we obtain

$$\begin{aligned} P_{out}^{1} &= 1 - \int_{\frac{\gamma_{th}N_0}{P_{r1}}}^{\infty} \left\{\sum_{l=0}^{\infty}\sum_{n=0}^{l} \frac{K^l e^{-K}}{l!n!}\left[\frac{b\gamma_{th}\varphi_2 N_0}{P_s(1-\rho)(P_{r1}\varphi_2 - \gamma_{th}N_0)}\right]^n e^{\frac{-b\gamma_{th}\varphi_2 N_0}{P_s(1-\rho)(P_{r1}\varphi_2 - \gamma_{th}N_0)}}\right\} f_{\varphi_2}(\varphi_2)d\varphi_2 \\ &= 1 - \int_{\frac{\gamma_{th}N_0}{P_{r1}}}^{\infty} \left\{\sum_{l=0}^{\infty}\sum_{n=0}^{l} \frac{aK^l e^{-K}}{l!n!}\left[\frac{b\gamma_{th}\varphi_2 N_0}{P_s(1-\rho)(P_{r1}\varphi_2 - \gamma_{th}N_0)}\right]^n e^{\frac{-b\gamma_{th}\varphi_2 N_0}{P_s(1-\rho)(P_{r1}\varphi_2 - \gamma_{th}N_0)}}\right\} \sum_{m=0}^{\infty} \frac{(bK\varphi_2)^m}{(m!)^2} e^{-b\varphi_2} d\varphi_2 \\ &= 1 - ae^{-K} \sum_{l=0}^{\infty}\sum_{m=0}^{\infty}\sum_{n=0}^{l} \frac{K^{l+m}b^{n+m}}{l!(m!)^2 n!} \int_{\frac{\gamma_{th}N_0}{P_{r1}}}^{\infty} \left[\frac{\gamma_{th}\varphi_2 N_0}{P_s(1-\rho)(P_{r1}\varphi_2 - \gamma_{th}N_0)}\right]^n e^{\frac{-b\gamma_{th}\varphi_2 N_0}{P_s(1-\rho)(P_{r1}\varphi_2 - \gamma_{th}N_0)} - b\varphi_2} \varphi_2^m d\varphi_2 \end{aligned} \tag{5.164}$$

By changing a variable $t = P_{r1}\varphi_2 - \gamma_{th}N_0$ in to (5.164), we obtain

$$\begin{aligned} P_{out}^{1} &= 1 - \frac{ae^{-K}}{P_{r1}} \sum_{l=0}^{\infty}\sum_{m=0}^{\infty}\sum_{n=0}^{l} \frac{K^{l+m}b^{n+m}}{l!(m!)^2 n!} \\ &\quad \times \int_{0}^{\infty} \left[\frac{\gamma_{th}\frac{t+\gamma_{th}N_0}{P_{r1}}N_0}{P_s(1-\rho)t}\right]^n e^{\frac{-b\gamma_{th}\left[\frac{t+\gamma_{th}N_0}{P_{r1}}\right]N_0}{P_s(1-\rho)t}} \left(\frac{t+\gamma_{th}N_0}{P_{r1}}\right)^m e^{-b\frac{t+\gamma_{th}N_0}{P_{r1}}} dt \\ &= 1 - \frac{ae^{-K} e^{\frac{-b\gamma_{th}N_0}{P_{r1}P_s(1-\rho)}} e^{\frac{-b\gamma_{th}N_0}{P_{r1}}}}{P_{r1}} \sum_{l=0}^{\infty}\sum_{m=0}^{\infty}\sum_{n=0}^{l} \frac{K^{l+m}b^{n+m}\left(\gamma_{th}N_0\right)^n}{l!(m!)^2 n! {P_{r1}}^{n+m} {P_s}^n (1-\rho)^n} \\ &\quad \times \int_{0}^{\infty} t^{-n} e^{-\frac{b\gamma_{th}^2 N_0^2}{P_{r1}P_s(1-\rho)t}} (t+\gamma_{th}N_0)^{n+m} e^{-\frac{bt}{P_{r1}}} dt \end{aligned} \tag{5.165}$$

Now, by applying $(x+y)^n = \sum_{k=0}^{n} \binom{n}{k} x^{n-k} y^k$ to (5.165), the OP can be rewritten as

$$P_{out}^{1} = 1 - \frac{ae^{-K} e^{\frac{-b\gamma_{th}N_0}{P_{r1}P_s(1-\rho)}} e^{\frac{-b\gamma_{th}N_0}{P_{r1}}}}{P_{r1}} \sum_{l=0}^{\infty}\sum_{m=0}^{\infty}\sum_{n=0}^{l}\sum_{k=0}^{n+m} \binom{n+m}{k} \frac{K^{l+m} b^{n+m} (\gamma_{th}N_0)^{n+k}}{l!(m!)^2 n! {P_{r1}}^{n+m} {P_s}^n (1-\rho)^n} \times \int_0^{\infty} t^{m-k} e^{\frac{-b\gamma_{th}^2 N_0^2}{P_{r1}P_s(1-\rho)t} - \frac{bt}{P_{r1}}} dt. \tag{5.166}$$

By apply [72, pp. 3.471, 9], we get (5.167) below. Then (5.161) follows directly.

$$P_{out}^{1} = 1 - \frac{2ae^{-K} e^{\frac{-b\gamma_{th}N_0}{P_{r1}P_s(1-\rho)}} e^{\frac{-b\gamma_{th}N_0}{P_{r1}}}}{P_{r1}} \sum_{l=0}^{\infty}\sum_{m=0}^{\infty}\sum_{n=0}^{l}\sum_{k=0}^{n+m} \binom{n+m}{k} \frac{K^{l+m} b^{n+m} (\gamma_{th}N_0)^{n+k}}{l!(m!)^2 n! {P_{r1}}^{n+m} {P_s}^n (1-\rho)^n} \times \left[\frac{\gamma_{th}^2 N_0^2}{P_s(1-\rho)}\right]^{\frac{m-k+1}{2}} K_{m-k+1}\left(\frac{2b\gamma_{th}N_0}{P_{r1}\sqrt{P_s(1-\rho)}}\right). \tag{5.167}$$

■

#### 5.4.3.2 Asymptotic Outage Probability Analysis

From (5.158), at the high SNR regime, the end to end SNR can be approximated as

$$\gamma_{\gamma_{e2e1}}^{\infty} = \frac{(1-\rho)P_s P_{r1}\varphi_1\varphi_2}{\varphi_2 N_0 + (1-\rho)P_s\varphi_1 N_0} \approx \frac{P_{r1}\varphi_2}{N_0} \tag{5.168}$$

Then, the asymptotic OP can be formulated as

$$P_{out}^{1,\infty} = \Pr\left(\frac{P_{r1}\varphi_2}{N_0} < \gamma_{th}\right) = \Pr\left(\varphi_2 < \frac{\gamma_{th}N_0}{P_{r1}}\right) = 1 - \sum_{l=0}^{\infty}\sum_{n=0}^{l} \frac{K^l b^n e^{-K}}{l!n!}\left(\frac{\gamma_{th}N_0}{P_{r1}}\right)^n e^{-\frac{b\gamma_{th}N_0}{P_{r1}}} \tag{5.169}$$

#### 5.4.3.3 SER Analysis

In this part, we obtain new expressions for the SER at the destination, which is given in (5.18). The CDF of $\gamma_{e2e1}$ is needed for analyzing the SER performance. In particular, (5.18) can be rewritten using integration as

$$SER_1 = \frac{\phi\sqrt{\theta}}{2\sqrt{\pi}} \int_0^{\infty} \frac{e^{-\theta x}}{\sqrt{x}} F_{\gamma_{e2e1}}(x) dx \tag{5.170}$$

**Theorem 5.12 (Exact SER)** *The exact SER of the proposed TPSR-based EH AF HD relay*

*network is calculated as*

$$SER_1 = \frac{\phi}{2} - ae^{-K}\phi\sqrt{\theta}\sum_{l=0}^{\infty}\sum_{m=0}^{\infty}\sum_{n=0}^{l}\sum_{k=0}^{n+m}\binom{n+m}{k}\frac{4^{m-k+1}K^{l+m}b^{n+2m-k+1}(N_0)^{n+2m-k+2}}{l!(m!)^2 n! {P_{r1}}^{n+2m-k+2}[P_s(1-\rho)]^{\frac{2n+3m-3k+3}{2}}}$$
$$\times \frac{1}{\left[\theta + \frac{3bN_0}{P_{r1}\sqrt{P_s(1-\rho)}} + \frac{bN_0}{P_{r1}}\right]^{n+2m-k+5/2}} \frac{\Gamma\left(n+2m-k+\frac{5}{2}\right)\Gamma\left(n+k+\frac{1}{2}\right)}{\Gamma\left(n+m+2\right)}$$
$$\times F\left(n+2m-k+\frac{5}{2}, m-k+\frac{3}{2}; n+m+2; \frac{\theta - \frac{bN_0}{P_{r1}\sqrt{P_s(1-\rho)}} + \frac{bN_0}{P_{r1}}}{\theta + \frac{3bN_0}{P_{r1}\sqrt{P_s(1-\rho)}} + \frac{bN_0}{P_{r1}}}\right) \tag{5.171}$$

*where* $\Gamma(\cdot)$ *is the gamma function, and* $F(\upsilon, \beta; \gamma; z)$ *is a hypergeometric function.*

**Proof** By substituting (5.159) into (5.178), we have:

$$SER_1 = \frac{\phi\sqrt{\theta}}{2\sqrt{\pi}}\int_0^{\infty}\frac{e^{-\theta x}}{\sqrt{x}}dx - \frac{\phi\sqrt{\theta}}{2\sqrt{\pi}}\sum_{l=0}^{\infty}\sum_{m=0}^{\infty}\sum_{n=0}^{l}\sum_{k=0}^{n+m}\binom{n+m}{k}\frac{2ae^{-K}K^{l+m}b^{n+m}}{l!(m!)^2 n! {P_{r1}}^{n+m+1}[P_s(1-\rho)]^{\frac{2n+m-k+1}{2}}}$$
$$\times \int_0^{\infty}\frac{e^{-\theta x}}{\sqrt{x}}(xN_0)^{n+m+1}e^{\frac{-bxN_0}{P_{r1}P_s(1-\rho)}}e^{\frac{-bxN_0}{P_{r1}}}K_{m-k+1}\left(\frac{2bxN_0}{P_{r1}\sqrt{P_s(1-\rho)}}\right)dx \tag{5.172}$$

The first term of (5.172) can be calculated by using in [72, Eq. (3.361, 1)]

$$I_1 = \frac{\phi\sqrt{\theta}}{2\sqrt{\pi}}\int_0^{\infty}\frac{e^{-\theta x}}{\sqrt{x}}dx = \frac{\phi\sqrt{\theta}}{2\sqrt{\pi}}\frac{\sqrt{\pi}}{\sqrt{\theta}} = \frac{\phi}{2} \tag{5.173}$$

The second term of (5.172) can be calculated as

$$I_2 = \frac{ae^{-K}\phi\sqrt{\theta}}{\sqrt{\pi}}\sum_{l=0}^{\infty}\sum_{m=0}^{\infty}\sum_{n=0}^{l}\sum_{k=0}^{n+m}\binom{n+m}{k}\frac{K^{l+m}b^{n+m}(N_0)^{n+m+1}}{l!(m!)^2 n! {P_{r1}}^{n+m+1}[P_s(1-\rho)]^{\frac{2n+m-k+1}{2}}}$$
$$\times \int_0^{\infty}(x)^{n+m+1}\frac{e^{-\theta x}}{\sqrt{x}}e^{-\frac{bxN_0}{P_{r1}P_s(1-\rho)}}e^{-\frac{bxN_0}{P_{r1}}}K_{m-k+1}\left(\frac{2bxN_0}{P_{r1}\sqrt{P_s(1-\rho)}}\right)dx$$
$$= \frac{ae^{-K}\phi\sqrt{\theta}}{\sqrt{\pi}}\sum_{l=0}^{\infty}\sum_{m=0}^{\infty}\sum_{n=0}^{l}\sum_{k=0}^{n+m}\binom{n+m}{k}\frac{K^{l+m}b^{n+m}(N_0)^{n+m+1}}{l!(m!)^2 n! {P_{r1}}^{n+m+1}[P_s(1-\rho)]^{\frac{2n+m-k+1}{2}}}$$
$$\times \int_0^{\infty}x^{n+m+1/2}e^{-x\left[\theta+\frac{bN_0}{P_{r1}P_s(1-\rho)}+\frac{bN_0}{P_{r1}}\right]}K_{m-k+1}\left(\frac{2bxN_0}{P_{r1}\sqrt{P_s(1-\rho)}}\right)dx \tag{5.174}$$

By using (6.621.3) in [72], the integral in (5.174) can be calculated as

$$J_1 = \int_0^{\infty} x^{n+m+1/2} e^{-x\left[\theta+\frac{bN_0}{P_{r1}P_s(1-\rho)}+\frac{bN_0}{P_{r1}}\right]} K_{m-k+1}\left(\frac{2bxN_0}{P_{r1}\sqrt{P_s(1-\rho)}}\right) dx$$
$$= \frac{\sqrt{\pi}\left[\frac{4bN_0}{P_{r1}\sqrt{P_s(1-\rho)}}\right]^{m-k+1}}{\left[\theta+\frac{3bN_0}{P_{r1}\sqrt{P_s(1-\rho)}}+\frac{bN_0}{P_{r1}}\right]^{n+2m-k+5/2}} \frac{\Gamma\left(n+2m-k+\frac{5}{2}\right)\Gamma\left(n+k+\frac{1}{2}\right)}{\Gamma\left(n+m+2\right)}$$
$$\times F\left(n+2m-k+\frac{5}{2}, m-k+\frac{3}{2}; n+m+2; \frac{\theta-\frac{bN_0}{P_{r1}\sqrt{P_s(1-\rho)}}+\frac{bN_0}{P_{r1}}}{\theta+\frac{3bN_0}{P_{r1}\sqrt{P_s(1-\rho)}}+\frac{bN_0}{P_{r1}}}\right) \tag{5.175}$$

where $\Gamma(\cdot)$ is the gamma function, and $F(\upsilon, \beta; \gamma; z)$ is a hypergeometric function. Then:

$$I_2 = \frac{ae^{-K}\phi\sqrt{\theta}}{\sqrt{\pi}} \sum_{l=0}^{\infty}\sum_{m=0}^{\infty}\sum_{n=0}^{l}\sum_{k=0}^{n+m}\binom{n+m}{k} \frac{K^{l+m}b^{n+m}(N_0)^{n+m+1}}{l!(m!)^2 n! {P_{r1}}^{n+m+1}[P_s(1-\rho)]^{\frac{2n+m-k+1}{2}}}$$
$$\times \frac{\sqrt{\pi}\left[\frac{4bN_0}{P_{r1}\sqrt{P_s(1-\rho)}}\right]^{m-k+1}}{\left[\theta+\frac{3bN_0}{P_{r1}\sqrt{P_s(1-\rho)}}+\frac{bN_0}{P_{r1}}\right]^{n+2m-k+5/2}} \frac{\Gamma\left(n+2m-k+\frac{5}{2}\right)\Gamma\left(n+k+\frac{1}{2}\right)}{\Gamma\left(n+m+2\right)}$$
$$\times F\left(n+2m-k+\frac{5}{2}, m-k+\frac{3}{2}; n+m+2; \frac{\theta-\frac{bN_0}{P_{r1}\sqrt{P_s(1-\rho)}}+\frac{bN_0}{P_{r1}}}{\theta+\frac{3bN_0}{P_{r1}\sqrt{P_s(1-\rho)}}+\frac{bN_0}{P_{r1}}}\right) \tag{5.176}$$

$$I_2 = ae^{-K}\phi\sqrt{\theta} \sum_{l=0}^{\infty}\sum_{m=0}^{\infty}\sum_{n=0}^{l}\sum_{k=0}^{n+m}\binom{n+m}{k} \frac{4^{m-k+1}K^{l+m}b^{n+2m-k+1}(N_0)^{n+2m-k+2}}{l!(m!)^2 n! {P_{r1}}^{n+2m-k+2}[P_s(1-\rho)]^{\frac{2n+3m-3k+3}{2}}}$$
$$\times \frac{1}{\theta\left[\phi+\frac{3bN_0}{P_{r1}\sqrt{P_s(1-\rho)}}+\frac{bN_0}{P_{r1}}\right]^{n+2m-k+5/2}} \frac{\Gamma\left(n+2m-k+\frac{5}{2}\right)\Gamma\left(n+k+\frac{1}{2}\right)}{\Gamma\left(n+m+2\right)}$$
$$\times F\left(n+2m-k+\frac{5}{2}, m-k+\frac{3}{2}; n+m+2; \frac{\theta-\frac{bN_0}{P_{r1}\sqrt{P_s(1-\rho)}}+\frac{bN_0}{P_{r1}}}{\theta+\frac{3bN_0}{P_{r1}\sqrt{P_s(1-\rho)}}+\frac{bN_0}{P_{r1}}}\right) \tag{5.177}$$

By substituting (5.173) and (5.177) into (5.172), we complete the proof. ∎

**Theorem 5.13 (Asymptotic SER Analysis)** *The asymptotic SER of the proposed system can be found as*

$$SER_1^{\infty} = \frac{\phi}{2} - \frac{e^{-K}\phi\sqrt{\theta}}{2\sqrt{\pi}} \sum_{l=0}^{\infty}\sum_{n=0}^{l} \frac{K^l b^n}{l!n!}\left(\frac{N_0}{P_{r1}}\right)^n \left(\theta+\frac{bN_0}{P_{r1}}\right)^{-n-1/2}\Gamma\left(n+\frac{1}{2}\right) \tag{5.178}$$

Table 5.5: Simulation parameters.

| Symbol | Value |
|---|---|
| $0 < \eta \leq 1$ | 0.7 |
| $\lambda_1$ | 1 |
| $\lambda_2$ | 1 |
| $\mathrm{P}_S/\mathrm{N}_0$ | 0-20dB |
| $K$ | 3 |
| $R$ | 0.5 bps |

**Proof** Using (5.169), we can rewrite SER at high SNR regime as

$$\begin{aligned} SER_1^{\infty} &= \frac{\phi\sqrt{\theta}}{2\sqrt{\pi}} \int_0^{\infty} \frac{e^{-\theta x}}{\sqrt{x}} \left\{ 1 - \sum_{l=0}^{\infty} \sum_{n=0}^{l} \frac{K^l b^n e^{-K}}{l!n!} \left( \frac{xN_0}{P_{r1}} \right)^n e^{-\frac{bxN_0}{P_{r1}}} \right\} dx \\ &= \frac{\phi\sqrt{\theta}}{2\sqrt{\pi}} \int_0^{\infty} \frac{e^{-\theta x}}{\sqrt{x}} dx - \frac{e^{-K}\phi\sqrt{\theta}}{2\sqrt{\pi}} \sum_{l=0}^{\infty} \sum_{n=0}^{l} \frac{K^l b^n}{l!n!} \left( \frac{N_0}{P_{r1}} \right)^n \int_0^{\infty} x^n \frac{e^{-\theta x}}{\sqrt{x}} e^{-\frac{bxN_0}{P_{r1}}} dx \end{aligned} \tag{5.179}$$

By using the (3.381.4) in [72], the integral in (5.179) can be computed as

$$I_3 = \int_0^{\infty} x^n \frac{e^{-\theta x}}{\sqrt{x}} e^{-\frac{bxN_0}{P_{r1}}} dx = \int_0^{\infty} x^{n-1/2} e^{-x\left(\theta + \frac{bN_0}{P_{r1}}\right)} dx = \left( \theta + \frac{bN_0}{P_{r1}} \right)^{-n-1/2} \Gamma\left( n + \frac{1}{2} \right). \tag{5.180}$$

By substituting (5.180) into (5.179), we obtain the expected result. ∎

### 5.4.4 Numerical Results and Discussion

For validation of the correctness of the derived OP and SER expressions, as well as investigation of the effect of various parameters on the system performance, a set of Monte Carlo simulations are conducted and presented in this section. For each simulation, we first provide the graphs of the OP and SER obtained by the analytical formulas. Secondly, we plot the same OP and SER curves that result from the Monte Carlo simulation. To do this, we generate $10^6$ random samples of each channel gain, which are Rician distributed. The analytical curve and the simulation curve should match to verify the correctness of our analysis. All simulation parameters are listed in Table 5.5.

The function of the OP with respect to K and R is presented in Fig. 5.32. In Fig. 5.32a, I set $\mathrm{P}_S/\mathrm{N}_0 = 10$ dB, $\rho = 0.5$ and $\alpha = 0.5$, and the OP decreases remarkably while K varies from 0 to 4. On another hand, the influence of R on the OP in three cases TSR, PSR, TSR–PSR, is also investigated in Fig. 5.32b with $\mathrm{P}_S/\mathrm{N}_0 = 15$ dB, $\rho = 0.7$ and $\alpha = 0.3$. The OP significantly increases with R from 0 to 4.

Fig. 5.33 plots the analytical and simulation results of the system OP and SER with respect to the ratio $\mathrm{P}_S/\mathrm{N}_0$. In Fig. 5.33a, both the exact and asymptotic OP in cases TSR, PSR, and

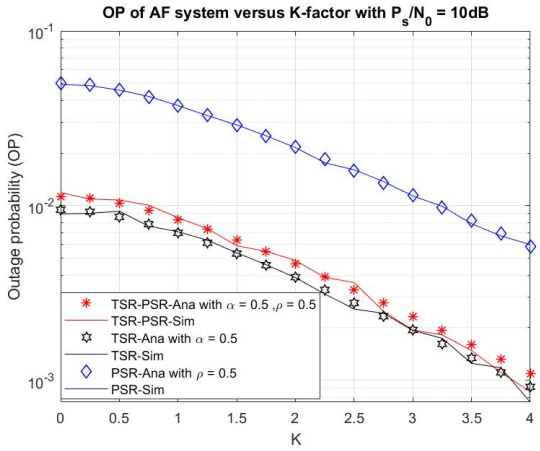


(a) Versus fading parameter

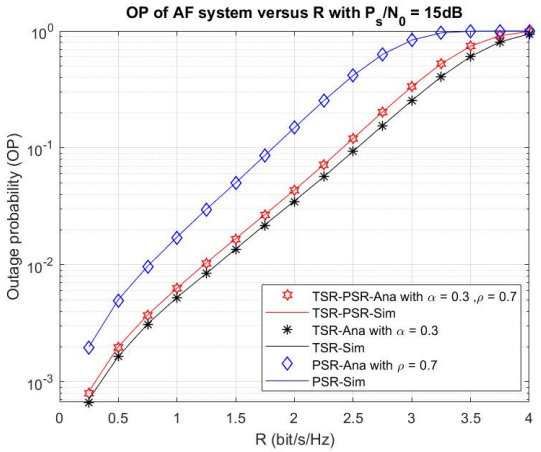


(b) Versus data transmission rate

Figure 5.32: OP of the proposed hybrid TPSR EH alternative-relay AF HD relay network versus fading parameter $K$ and data transmission rate $R$.

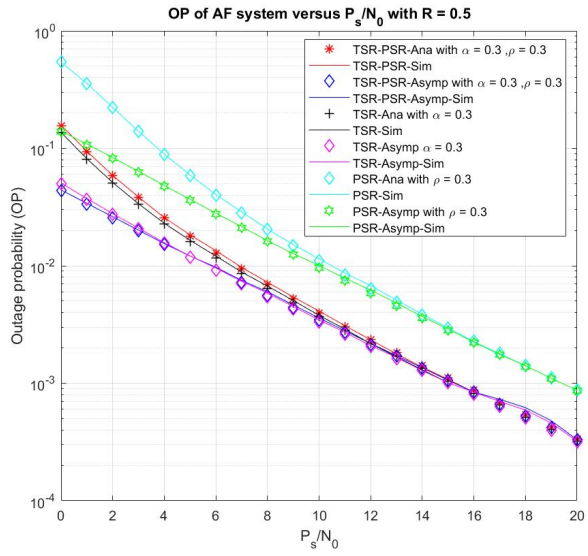


(a) Outage probability versus $P_s/N_0$ in the cases TSR, PSR, and TSR–PSR.

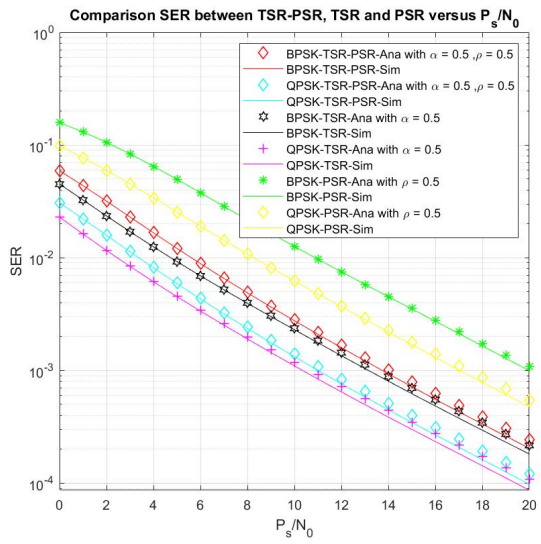


(b) SER versus $P_s/N_0$ in the cases TSR, PSR, and TSR–PSR.

Figure 5.33: OP and SER of the proposed hybrid TPSR EH alternative-relay AF HD relay network versus $P_s/N_0$.

TSR–PSR are illustrated. The main parameters are set as R = 0.5, $\rho$ = 0.3 and $\alpha$ = 0.3. From the results, the exact OP decreases and comes close to the asymptotic line when the ratio $P_S/N_0$ increases from 0 to 20 dB. Furthermore, Fig. 5.33b, shows the comparison SER of three cases TSR, PSR, and TSR–PSR versus $P_S/N_0$ with specific for the modulation type BPSK and QPSK.

Fig. 5.34 Outage probability and SER numerical results. In Fig. 5.34a illustrates the nu-

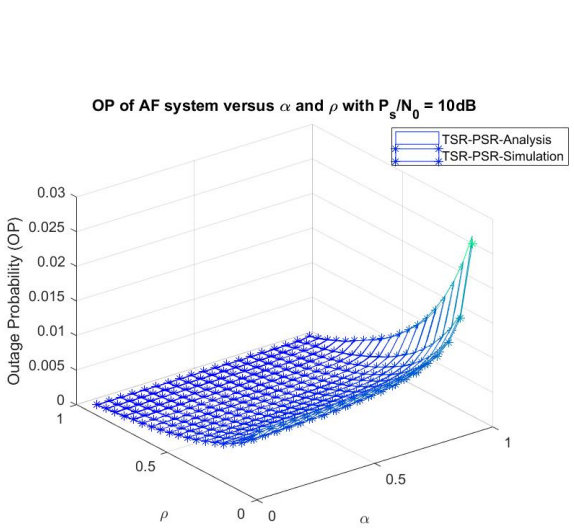


(a) Outage probability versus $\rho$ and $\alpha$.

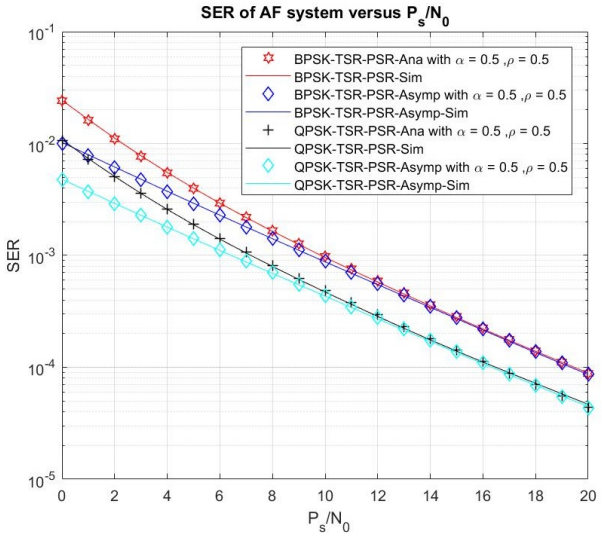


(b) The exact and asymptotic SER versus $P_s/N_0$ in the cases TSR–PSR.

Figure 5.34: Outage probability and SER numerical results.

merical and simulation results of the system OP concerning $\alpha$ and $\rho$ with $P_S/N_0 = 10$ dB. It is clearly shown that the OP increases with increasing $\alpha$ and $\rho$, and the minimum OP can be obtained with $\alpha = 0$ and $\rho = 1$. Furthermore, Fig. 5.34b the comparison of the exact and asymptotic SER of TSR–PSR versus $P_S/N_0$ with specific for the modulation type BPSK and QPSK.

We can see that the hybrid TPSR outperforms the other 2 protocols. Last but not least, the results indicate that all the simulation and analytical values agree well with each other.

### 5.4.5 Conclusions

In this section, the hybrid TSR–PSR alternate EH relay network over AF-based Rician fading channels is presented and investigated. The system model consists of one source, one destination and two alternative relays for signal transmission from the source to the destination. We derive the exact and asymptotic expressions of the OP and SER and investigate the influence of all system parameters on the system performance using the Monte Carlo simulation. The research results indicate that the alternative hybrid TSR–PSR has better performance in comparison with the TSR and PSR cases. The research results can provide essential recommendations for communication network research and practice directions.

# 6 Design secrecy protocols at the physical layer and propose methods of calculating and analyzing secrecy performance of wireless networks

In this section, to fulfil the second aim of this dissertation, I propose two advanced model for enhance the security at physical layer. In the first model, I design a novel harvest-to-jam protocol to enhance the security and reliability of a multi-hop LEACH wireless sensor network. This protocol can provide good security and reliability performance even with the presence of hardware noise [HDH18]. For the second model, I design a protocol to improve the security of the LEACH sensor networks by integrating multi-hop communications, jammer selection with RF EH. [HDH02], [HDH19].

## 6.1 Harvest-to-Jam Protocol for Improving Security and Reliability of Multi-hop LEACH Sensor Networks under Impact of Hardware Noises

In this section, I propose a protocol to enhance the security of multi-hop low-energy adaptive clustering hierarchy (LEACH) networks. In the proposed protocol, a source sends its data to a destination using multi-hop relaying method in presence of an eavesdropper. All of the nodes including source, destination and relays are cluster heads (CHs), and the data transmission is split into orthogonal time slots. To protect the data at each hop, harvest-to-jam and randomize-and-forward methods are employed by CHs and cooperative jammers, respectively. Each jammer which is randomly selected at each cluster harvests energy from the previous CHs to transmit jamming signals to the eavesdropper. [HDH18].

### 6.1.1 Introduction

Due to the widely applications in different areas such as environment, agriculture, military, healthcare, industry, and IoT, WSNs have been developed rapidly during last two decades [129]. The main components of WSNs are small energy-constrained sensor nodes that are installed in the certain locations to sense data and information to send to the base station (sink) via radio links. However, these tiny sizes of low-cost wireless sensor nodes are strongly affected to the life-time of WSNs. Then, one of the most considerable challenges of WSNs is the strategy to efficiently utilise the energy of those small electronic nodes to extend the life-time of the systems. There are the number of solutions for this challenge proposed in [130] including RF - EH, low-energy adaptive clustering hierarchy (LEACH) protocol, and multi-hop relaying communications.

Due to the limited energy, prolonging the lifetime for WSNs has become a critical issue. Recently, the RF-EH method [74], [131] has been gained much attention as a potential solution, where sensor nodes can harvest energy from ambient RF signals for communication. In addition, both data and energy can be supported for the RF-EH receivers at the same time and the same

RF bands. In [131], [132], the authors proposed efficient RF-EH schemes in which power stations are deployed in a certain area to simultaneously serve wireless devices.

For power consumption efficiency, the sensors can be divided into several groups of nodes called clusters, using the LEACH protocol [133], [134]. Then, each cluster is led by a cluster head (CH), which is also a sensor node that collects the data from all of other alive-nodes in the group to send to neighbor CHs. Moreover, to improve the data rate, extend the network coverage, and mitigate effect of fading environments, multi-hop relaying approach is often employed to communicate between non-adjacent clusters. In [134], the source data is sent to the destination via multi-hop approach, where intermediate nodes are also CHs. Different with [134], each cluster in [135] selects the best receiver (a cluster node) to forward the data to next hop to enhance the reliability of the data transmission. However, the implementation of the protocol in [135] is complex due to requirement of high synchronization, perfect CSI estimation and high power consumption for the relay selection process.

Due to the broadcast nature of wireless medium as well as the communication over multi-hop, the source data can be overheard by eavesdroppers. Therefore, the security and privacy issues are the considerable challenges in WSNs. Conventionally, the original information will be ciphered by crypto codes before sending to the end users. This scheme coding is generally performed in the high-layer in the communication systems. However, this is computational complexity in coded and decoded algorithms, so it normally needs a large capacity of memories and storages, which may not be suitable for sensor nodes. Recently, PLS has been widely developed to satisfy the secrecy requirements and also to reduce the computation in wireless communication systems [136]. In [137], the transmitters adjust their transmit power so that the active eavesdroppers cannot successfully receive the data at each hop. Then, efficient path-selection methods are proposed to improve the end-to-end performance, in terms of OP. Reference [131] proposed a joint transmit and receive diversity method, i.e., transmit antenna selection (TAS)/selection combining (SC) to enhance quality of the data channels in cognitive WSNs under joint constraint of co-channel interference and hardware impairments. In [135], the authors analyzed the trade-off between OP and IP in cluster-based multi-hop cognitive radio networks with relay selection at each hop.

To further enhance secrecy performance, cooperative jamming technique can be used efficiently, where friendly jammers are employed to only generate artificial noises on the eavesdroppers [138], [139]. For the authorized receivers, they can cooperate with the jammers to remove the interference from the received signals. The authors of [138], [139] proposed joint relay and jammer selection methods to obtain the best secrecy performance for dual-hop relaying networks. Furthermore, the jammers in [139] can harvest energy from the RF signals of the source to transmit the jamming signals.

In this section, we propose a secured communication protocol in multi-hop LEACH networks using the harvest-to-jam method at each hop to protect the data under the presence of an eavesdropper. Different with [134], the jammer in the proposed protocol harvests energy from the

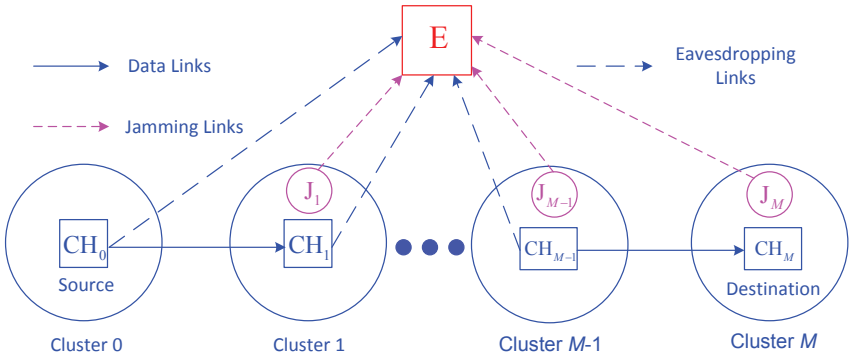


Figure 6.1: System model of the proposed protocol.

RF signals of the previous CH for the jamming process. For performance evaluation, we derive exact and asymptotic closed-form expressions of the end-to-end OP and IP over Rayleigh fading channel and in presence of hardware imperfection. We then perform Monte Carlo simulations to verify the theoretical results. The results presented the trade-off between OP and IP, which can be improved by carefully designing the system parameters such as the number of hops, hardware impairment levels and fraction of time used for the EH phase.

### 6.1.2 System Model

Fig. 6.1 presents the system model of the proposed protocol, where the source node (CH of cluster 0) wants to transmit its data to the destination node (CH of cluster $M$) via the multi-hop LEACH approach with the assistance of multiple relays (CHs of intermediate clusters denoted by Cluster 1, Cluster 2,..., Cluster ($M$-1). In this network, the eavesdropper E attempts to illegally receive the data over all of the hops. Hence, the CHs must cooperate together to confuse the eavesdropper by generating random codebooks so that the eavesdropper cannot combine the received signals with maximal ratio combining (MRC) [140], [141].

Assume that all of CHs are equipped with a single antenna, operate on HD mode. Hence, the data transmission between the source and the destination is performed via $M$ orthogonal time slots, follows a time-division multiple access (TDMA) schedule. Let us denote T as the total transmission time; and hence the duration allocated for each time slot is $\delta = \mathrm{T}/M$.

Let us consider the $k-$th time slot, where the CH of the cluster $(k-1)$ (denoted by $\mathrm{CH}_{k-1}$) sends the source data to that of the cluster $k$ (denoted $\mathrm{CH}_k$), where $k = 1, 2, ..., M$. To protect the data at this hop, a cluster node (denoted by $\mathrm{J}_k$) is randomly selected by $\mathrm{CH}_k$ to play a role as the cooperative jammer. In addition, $\mathrm{J}_k$ will harvest energy from $\mathrm{CH}_{k-1}$ to generate the jamming signals.

Let us denote $\psi_{\mathrm{X,Y}}$ as channel gain between nodes X and Y, where $(\mathrm{X}, \mathrm{Y}) \in \{\mathrm{CH}_{k-1}, \mathrm{CH}_k, \mathrm{J}_k, \mathrm{E}\}$. Assume that all of the channels are Rayleigh fading, the channel gain $\psi_{\mathrm{X,Y}}$ is an exponential

RV. Hence, CDF and PDF of $\psi_{\mathrm{X,Y}}$ can be given, respectively as

$$\begin{aligned} F_{\psi_{\mathrm{X,Y}}}(x) &= 1 - \exp\left(-\Omega_{\mathrm{X,Y}} x\right), \\ f_{\psi_{\mathrm{X,Y}}}(x) &= \Omega_{\mathrm{X,Y}} \exp\left(-\Omega_{\mathrm{X,Y}} x\right), \end{aligned} \tag{6.1}$$

where $\Omega_{\mathrm{X,Y}} = 1/\mathcal{E}\{\psi_{\mathrm{X,Y}}\}$, and $\mathcal{E}\{.\}$ is an expected operator. To take path-loss into account, the parameter $\Omega_{\mathrm{X,Y}}$ can be modeled as [72]: $\Omega_{\mathrm{X,Y}} = d_{\mathrm{X,Y}}^{\theta}$, where $d_{\mathrm{X,Y}}$ is distance between X and Y, and $\theta$ is path-loss exponent.

Again, we consider the data transmission at the $k-$th time slot, which is split into two sub-time slots: the first one ($\alpha\tau$) is used for the RF-EH operation, and the second one ($(1-\alpha)\tau$) is used for the data transmission, where $0 \leq \alpha \leq 1$. As analyzed in (2.4), after the EH phase, the average transmit power that $\mathrm{J}_k$ can use in the second sub-time slot is obtained by

$$Q_k = \frac{E_{\mathrm{J}_k}}{(1-\alpha)\delta} = \kappa P \psi_{\mathrm{CH}_{k-1},J_k}, \tag{6.2}$$

where $\eta$ is energy conversion efficiency, $P$ is transmit power of $\mathrm{CH}_{k-1}$ for all $k$, and $\kappa = \eta\alpha/(1-\alpha)$.

It is worth noting that because $\mathrm{CH}_k$ and $\mathrm{J}_k$ are in the same cluster, $\mathrm{CH}_k$ can know the jamming signals of $\mathrm{J}_k$ for the interference cancelation, but the eavesdropper E cannot. Hence, under impact of hardware impairment, the channel capacity of the $\mathrm{CH}_{k-1} \to \mathrm{CH}_k$ link can be given as

$$C_{\mathrm{D},k} = (1-\alpha)\delta \log_2\left(1 + \frac{P\psi_{\mathrm{CH}_{k-1},\mathrm{CH}_k}}{\tau_{\mathrm{D}}^2 P\psi_{\mathrm{CH}_{k-1},\mathrm{CH}_k} + N_0}\right) = (1-\alpha)\delta \log_2\left(1 + \frac{\Delta\psi_{\mathrm{CH}_{k-1},\mathrm{CH}_k}}{\tau_{\mathrm{D}}^2 \Delta\psi_{\mathrm{CH}_{k-1},\mathrm{CH}_k} + 1}\right), \tag{6.3}$$

where $N_0$ is variance of Gaussian noise, $\Delta = P/N_0$ is transmit SNR, and $\tau_{\mathrm{D}}^2$ is total hardware impairment level of the $\mathrm{CH}_{k-1} \to \mathrm{CH}_k$ link for all $k$.

For the $\mathrm{CH}_{k-1} \to \mathrm{E}$ link, the channel capacity can be expressed as

$$\begin{aligned} C_{\mathrm{E},k} &= (1-\alpha)\delta \log_2\left(1 + \frac{P\psi_{\mathrm{CH}_{k-1},\mathrm{E}}}{\tau_{\mathrm{E}}^2 P\psi_{\mathrm{CH}_{k-1},\mathrm{E}} + Q_k\psi_{\mathrm{J}_k,\mathrm{E}} + N_0}\right) \\ &= (1-\alpha)\delta \log_2\left(1 + \frac{\Delta\psi_{\mathrm{CH}_{k-1},\mathrm{E}}}{\tau_{\mathrm{E}}^2 \Delta\psi_{\mathrm{CH}_{k-1},\mathrm{E}} + \kappa\Delta\psi_{\mathrm{CH}_{k-1},J_k}\psi_{\mathrm{J}_k,\mathrm{E}} + 1}\right), \end{aligned} \tag{6.4}$$

where $\tau_{\mathrm{E}}^2$ is total hardware impairment level of the $\mathrm{CH}_{k-1} \to \mathrm{E}$ link for all $k$.

Next, due to the DF relaying method, the end-to-end channel capacity of the data link can be given as

$$C_{\mathrm{D}}^{\mathrm{e2e}} = \min_{k=1,2,\ldots,M}\left(C_{\mathrm{D},k}\right). \tag{6.5}$$

Since CHs employ the randomize and forward method to confuse E, the obtained channel capacity of the eavesdropping links can be formulated as

$$C_{\mathrm{E}}^{\mathrm{e2e}} = \max_{k=1,2,\ldots,M} \left(C_{\mathrm{E},k}\right). \tag{6.6}$$

Then, we define the OP and intercept probability (IP), respectively as

$$\begin{aligned} \mathrm{OP} &= \Pr\left(C_{\mathrm{D}}^{\mathrm{e2e}} < C_{\mathrm{th}}\right), \\ \mathrm{IP} &= \Pr\left(C_{\mathrm{E}}^{\mathrm{e2e}} \geq C_{\mathrm{th}}\right), \end{aligned} \tag{6.7}$$

where $C_{\mathrm{th}}$ is a pre-determined threshold.

### 6.1.3 Performance evaluation

In this part, we derive exact and asymptotic closed-form expression of the end-to-end OP and IP for the proposed protocol.

#### 6.1.3.1 Outage probability (OP)

Firstly, from (6.5) and (6.7), OP of the data link can be formulated as

$$\mathrm{OP} = \Pr\left(\min_{k=1,2,\ldots,M} \left(C_{\mathrm{D},k}\right) < C_{\mathrm{th}}\right) = 1 - \prod_{k=1}^{M} \left(1 - \mathrm{OP}_k\right), \tag{6.8}$$

where $\mathrm{OP}_k = \Pr\left(C_{\mathrm{D},k} < C_{\mathrm{th}}\right)$ is OP at the $k-$th hop. Using (6.3), we can obtain

$$\mathrm{OP}_k = \Pr\left(\frac{\Delta\psi_{\mathrm{CH}_{k-1},\mathrm{CH}_k}}{\tau_{\mathrm{D}}^2 \Delta\psi_{\mathrm{CH}_{k-1},\mathrm{CH}_k} + 1} < \rho\right) = \Pr\left(\left(1 - \tau_{\mathrm{D}}^2\rho\right)\Delta\psi_{\mathrm{CH}_{k-1},\mathrm{CH}_k} < \rho\right), \tag{6.9}$$

where $\rho = 2^{\frac{C_{\mathrm{th}}}{(1-\alpha)\delta}} - 1$.

Next, we can observe from (6.9) that if $1 - \tau_{\mathrm{D}}^2\rho \leq 0$, then $\mathrm{OP}_k = 1$ and OP =1, and if $1 - \tau_{\mathrm{D}}^2\rho > 0$, using (6.1), we can compute $\mathrm{OP}_k$ exactly as

$$\mathrm{OP}_k = \Pr\left(\psi_{\mathrm{CH}_{k-1},\mathrm{CH}_k} < \frac{\rho}{\left(1 - \tau_{\mathrm{D}}^2\rho\right)\Delta}\right) = 1 - \exp\left(-\frac{\Omega_{\mathrm{CH}_{k-1},\mathrm{CH}_k}\rho}{\left(1 - \tau_{\mathrm{D}}^2\rho\right)\Delta}\right). \tag{6.10}$$

Substituting (6.10) into (6.8), which yields

$$\mathrm{OP} = 1 - \prod_{k=1}^{M} \exp\left(-\frac{\Omega_{\mathrm{CH}_{k-1},\mathrm{CH}_k}\rho}{\left(1 - \tau_{\mathrm{D}}^2\rho\right)\Delta}\right). \tag{6.11}$$

At high transmit SNR, i.e., $\Delta \to +\infty$, we can approximate $\mathrm{OP}_k$ as

$$\mathrm{OP}_k \approx \frac{\Omega_{\mathrm{CH}_{k-1},\mathrm{CH}_k}\rho}{\left(1-\tau_{\mathrm{D}}^2\rho\right)\Delta}. \tag{6.12}$$

Hence, OP can be approximated as

$$\mathrm{OP} \approx \sum_{k=1}^{M} \mathrm{OP}_k = \frac{\Omega_{\mathrm{CH}_{k-1},\mathrm{CH}_k}\rho}{\left(1-\tau_{\mathrm{D}}^2\rho\right)\Delta}. \tag{6.13}$$

Therefore, the diversity gain can be determined as

$$\mathrm{DG} = -\lim_{\Delta\to+\infty} \frac{\log\left(\mathrm{OP}\right)}{\log\left(\Delta\right)} = 1. \tag{6.14}$$

#### 6.1.3.2 Intercept Probability (IP)

From (6.6) and (6.7), we can write

$$\mathrm{IP} = \Pr\left(\max_{k=1,2,\ldots,M}\left(C_{\mathrm{E},k}\right) \geq C_{\mathrm{th}}\right) = 1 - \prod_{k=1}^{M} \Pr\left(C_{\mathrm{E},k} < C_{\mathrm{th}}\right). \tag{6.15}$$

From (6.15), our next objective is to calculate the probability $\Pr\left(C_{\mathrm{E},k} < C_{\mathrm{th}}\right)$. Using (6.4), we can obtain

$$\Pr\left(C_{\mathrm{E},k} < C_{\mathrm{th}}\right) = \Pr\left(\left(1-\tau_{\mathrm{E}}^2\rho\right)\Delta\psi_{\mathrm{CH}_{k-1},\mathrm{E}} < \kappa\rho\Delta\psi_{\mathrm{CH}_{k-1},J_k}\psi_{\mathrm{J}_k,\mathrm{E}} + \rho\right). \tag{6.16}$$

Similarly, if $1-\tau_{\mathrm{E}}^2\rho \leq 0$, $\Pr\left(C_{\mathrm{E},k} < C_{\mathrm{th}}\right) = 1$ and $\mathrm{IP} = 1$. Otherwise, equation (6.16) can be rewritten as

$$\begin{aligned}\Pr\left(C_{\mathrm{E},k} < C_{\mathrm{th}}\right) &= \Pr\left(\psi_{\mathrm{CH}_{k-1},\mathrm{E}} < \omega_1 + \omega_2\psi_{\mathrm{CH}_{k-1},J_k}\psi_{\mathrm{J}_k,\mathrm{E}}\right) \\ &= \int_0^{+\infty}\int_0^{+\infty} F_{\psi_{\mathrm{CH}_{k-1},\mathrm{E}}}\left(\omega_1+\omega_2 yz\right), f_{\psi_{\mathrm{CH}_{k-1},J_k}}\left(y\right) f_{\psi_{\mathrm{J}_k,\mathrm{E}}}\left(z\right) dydz, \end{aligned} \tag{6.17}$$

where $\omega_1 = \frac{\rho}{\left(1-\tau_{\mathrm{E}}^2\rho\right)\Delta}, \omega_2 = \frac{\kappa\rho}{1-\tau_{\mathrm{E}}^2\rho}$.

Substituting (6.1) into (6.17), after some manipulations, we obtain

$$\Pr\left(C_{\mathrm{E},k} < C_{\mathrm{th}}\right) = 1 - \phi_k \exp\left(\phi_k - \Omega_{\mathrm{CH}_{k-1},\mathrm{E}}\omega_1\right) E_1\left(\phi_k\right), \tag{6.18}$$

where $E_1\left(.\right)$ is exponential integral function [72], and $\phi_k = \frac{\Omega_{\mathrm{CH}_{k-1},\mathrm{J}_k}\Omega_{\mathrm{J}_k,\mathrm{E}}}{\Omega_{\mathrm{CH}_{k-1},\mathrm{E}}\omega_2}$.

Substituting (6.18) into (6.15), IP at the eavesdropper can be expressed as

$$\mathrm{IP} = 1 - \prod_{k=1}^{M}\left[1 - \phi_k \exp\left(\phi_k - \Omega_{\mathrm{CH}_{k-1},\mathrm{E}}\omega_1\right) E_1\left(\phi_k\right)\right], \tag{6.19}$$

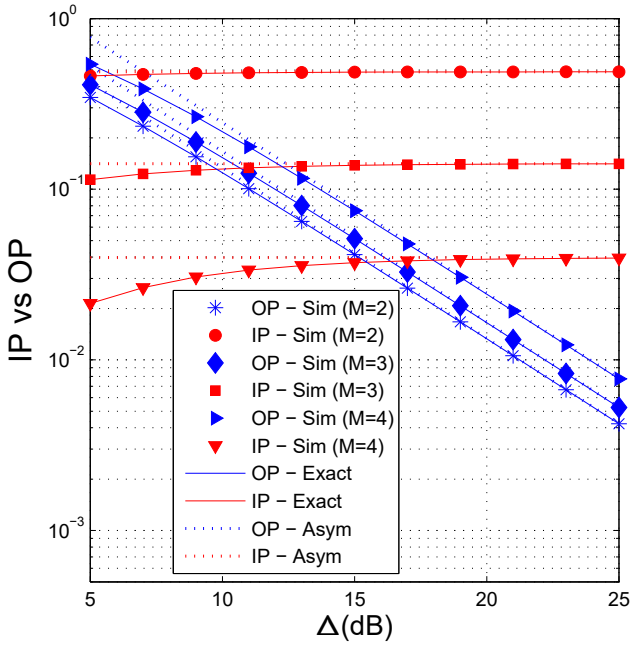


Figure 6.2: OP and IP as a function of $\Delta$ (dB) when $x_{\mathrm{E}} = 0.5$, $y_{\mathrm{E}} = 0.3$, $\alpha = 0.25$, and $\tau_{\mathrm{D}}^2 = \tau_{\mathrm{E}}^2 = 0$.

Next, at high transmit SNR, we can approximate (6.4) as

$$C_{\mathrm{E},k} \approx (1-\alpha)\,\delta\log_2\left(1+\frac{\Delta\psi_{\mathrm{CH}_{k-1},\mathrm{E}}}{\tau_{\mathrm{E}}^2\Delta\psi_{\mathrm{CH}_{k-1},\mathrm{E}}+\kappa\Delta\psi_{\mathrm{CH}_{k-1},J_k}\psi_{\mathrm{J}_k,\mathrm{E}}}\right), \tag{6.20}$$

With the same manner as deriving (6.18), we can obtain the asymptotic expression of $\Pr\left(C_{\mathrm{E},k} < C_{\mathrm{th}}\right)$. Then, the asymptotic expression of IP can be expressed as

$$\mathrm{IP} \approx 1 - \prod_{k=1}^{M}\left[1-\phi_k \exp\left(\phi_k\right) E_1\left(\phi_k\right)\right]. \tag{6.21}$$

We can observe from (6.21) that at high transmit SNR, IP does depend on $\Delta$.

### 6.1.4 Simulation Results

In this part, Monte-Carlo simulations are presented to validate the analyzes in part 6.1.3. In the simulations, we place all the nodes into a two-dimensional Oxy plane. In particular, the nodes in the cluster $k$ have same positions of $(k/M, 0)$, and the eavesdropper is located at $(x_{\mathrm{E}}, y_{\mathrm{E}})$, where $k = 0, 1, ..., M$. In all simulations, the path-loss exponent $(\theta)$ is fixed at 3, the target rate $(C_{\mathrm{th}})$ is fixed at 1, the energy conversion efficiency $(\eta)$ is set to 1, and and the total delay time (T) is set by 1.

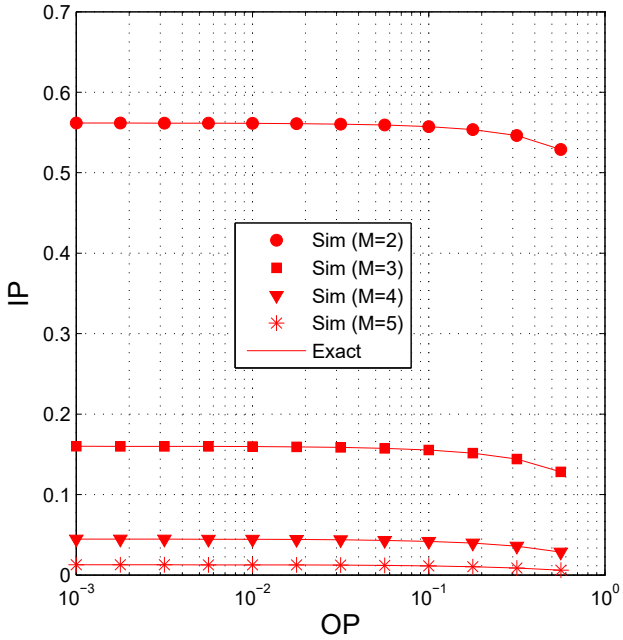


Figure 6.3: IP as a function of OP when $x_{\mathrm{E}} = 0.5$, $y_{\mathrm{E}} = 0.25$, $\alpha = 0.25$, and $\tau_{\mathrm{D}}^2 = \tau_{\mathrm{E}}^2 = 0$.

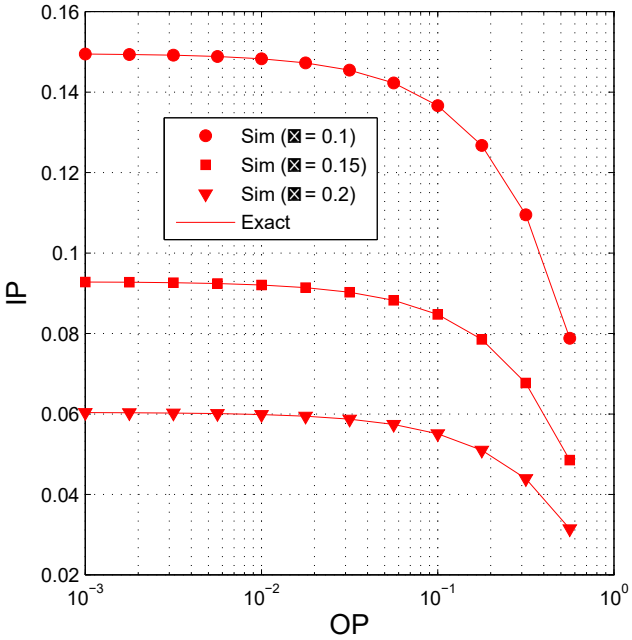


Figure 6.4: IP as a function of OP when $M = 4$, $x_{\mathrm{E}} = 0.5$, $y_{\mathrm{E}} = 0.3$, and $\tau_{\mathrm{D}}^2 = \tau_{\mathrm{E}}^2 = 0$.

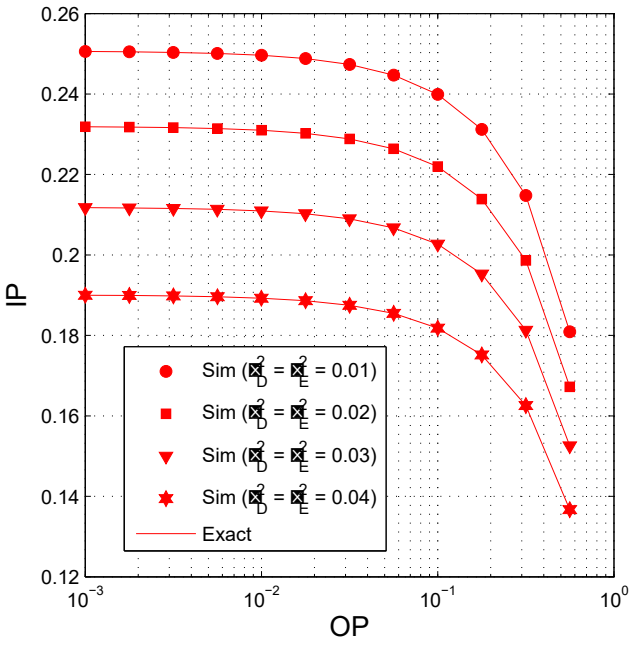


Figure 6.5: IP as a function of OP when $M = 3$, $x_{\mathrm{E}} = 0.5$, $y_{\mathrm{E}} = 0.3$, and $\alpha = 0.15$.

In Fig. 6.2, we present OP and IP as a function of the transmit SNR $\Delta$ in dB with different number of hops. In this figure, the eavesdropper is located at (0.5, 0.3), the fraction of time for the EH phase ($\alpha$) is 0.25, and the transceiver hardware of all the nodes is assumed to be perfect, i.e., $\tau_{\mathrm{D}}^2 = \tau_{\mathrm{E}}^2 = 0$. As shown in Fig. 6.2, as $\Delta$ increases, the OP values decrease, while the IP values increase at the small and medium $\Delta$ regions, and converge to constant at high $\Delta$ values. We also see that the slope of the OP curves equals 1, and hence the obtained diversity order is 1, as proved in Section 6.1.3. It is seen from Fig. 6.2 that with higher number of hops, the OP performance and the intercept possibility of the eavesdropper are worse. It is worth noting that the simulation results (Sim) match well with the theory (Exact), and the exact results nicely converge to asymptotic ones (Asym) at high $\Delta$ regimes.

For showing more clearly the trade-off between the security and reliability, Fig. 6.3 presents IP as a function of OP with different values of $M$. As we can see, at the same value of OP, the IP value reduces as increasing the number of hops. Moreover, the value of IP as $M = 2$ is much higher than that in the remaining cases. As we can see, at low OP regions, the IP values converge to a constant. Again, the simulation results validate the theoretical ones.

Fig. 6.4 presents IP as a function of OP with various values of $\alpha$. Different from Fig. 6.3, IP significantly decreases at high OP values. As we can see, the IP values decrease as increasing $\alpha$ from 0.1 to 0.2. It is due to the fact that the transmit power of the cooperative jammer nodes is higher with high value of $\alpha$, which degrades the IP performance of the eavesdropper. However, it is worth noting that when $\alpha$ is high, the time used for the data transmission reduces, and the

OP performance is worse.

Fig. 6.5 investigates the impact of hardware impairments on the IP-OP trade-off. In this figure, we assume that the hardware impairment levels of the data and eavesdropping links are same, i.e., $\tau_{\mathrm{D}}^2 = \tau_{\mathrm{E}}^2$. We can see that the IP-OP trade-off is better as the hardware impairment levels increase. This means that the hardware noises impact on the IP performance higher that on the OP performance.

### 6.1.5 Conclusions

In this section, investigated the trade-off between the security and reliability for harvest-to-jam based multi-hop leach networks under impact of hardware noises. The results presented that the IP-OP trade-off can be enhanced via increasing the number of hops, and the fraction of time used for the EH phase. Moreover, the hardware impairment levels also significantly impact on the IP-OP trade-off. In future works, i will evaluate the other performance metrics such as secrecy OP, probability of non-zero secrecy capacity, and ASC over more generalized fading channels, i.e., Nakagami-$m$, Rician, etc.

## 6.2 Secrecy Outage Performance of Multi-hop LEACH Networks Using Power Beacon Aided Cooperative Jamming With Jammer Selection Methods

In this section, we evaluate secrecy performance of cooperative jamming (CJ) aided secure transmission for Multi-hop Low-Energy Adaptive Clustering Hierarchy (M-LEACH) networks with the presence of an eavesdropper. Data transmission between a source and a destination is performed via cluster heads (CHs) of intermediate clusters. To protect the source information at each hop, each CH selects one or many cluster nodes to realize the CJ technique. We propose EH-based jammer selection methods named MAX-EH, MAX-IP and ALL-CJ, where the selected jammer(s) has to harvest wireless energy from a dedicated power beacon to generate jamming noises. [HDH02]

### 6.2.1 Introduction

Recently, PLS has been introduced as a promising technique to guarantee security for wireless systems [58], [60]. Performance of PLS methods is evaluated via secrecy capacity, i.e., average secrecy rate (ASR), SOP, probability of non-zero secrecy rate (NZSR). In [141], the authors considered secure connection approaches for dual-hop relay networks using DF and randomize-and-forward (RF) methods. In the RF method, the source and relay nodes randomly generate code-books to prevent the eavesdroppers from using maximal ratio combining (MRC). Therefore, the RF method outperforms the conventional DF one, in terms of secrecy performance. Reference [142] studied the RF-based secure connectivity with random presence of eavesdroppers who cooperate to decode the source data. The authors in [143] proposed a cooperative communication approach to improve the e2e SOP performance. The authors of [144] proposed relay selection

schemes to improve secrecy performance for both DF and AF relay networks in limited co-channel interference environments. In [145], SOP of cognitive radio networks (CRNs) was evaluated. Operating on underlay mode, the secondary transmitters in [145] must adapt transmit power to guarantee QoS for the primary network. Different than [145], the authors in [146] proposed a spectrum sharing approach, where secondary users help the primary network protect the data so that they have opportunities to access the licensed bands. In [147], the authors investigated secure communication for FD wireless powered systems, in presence of multiple eavesdroppers. The authors of [148] proposed an analog cooperative beam-forming method to enhance the secrecy performance for three-dimensional Gaussian distributed WSNs. Unlike [141], [148], published works [149], [150] analyzed intercept behavior at the eavesdropper defined as the probability that the instantaneous secrecy capacity equals to zero.

So far, almost published literature related to the efficient PLS methods mainly focus on single-hop or dual-hop relay networks. There have been several reports of multi-hop secure transmission ones such as [134], [137], [151] and references therein. In [151], the authors derived exact closed-form expressions of the e2e NZSR and SOP for multi-hop RF relay networks with multiple eavesdroppers over Nakagami-$m$ fading channels. Different than [151], published work [152] considered impact of hardware imperfection on the e2e NZSR performance. Reference [153] studied impact of co-channel interference on the e2e secrecy performance of cluster-based multi-hop networks. In [154], optimal transmit power allocation strategies were presented to enhance the e2e secrecy capacity for in multi-hop DF relay networks. In [155], the secrecy performance of multi-hop AF relay networks using compressed sensing was studied. The authors of [156] proposed an online control method for multi-hop secure transmission networks with security constraint. In [134], a random jammer selection was proposed to protect Fountain encoded packets. Reference [157] studied the e2e secrecy performance of a WPT based multi-hop networks, where transmitters harvest wireless energy from multiple power beacons.

In PLS, cooperative jamming is an efficient method to protect the transmitted data, where trusted jammers are employed to generate jamming signals only on eavesdroppers. In [158], power beacons not only support wireless energy for transmitters but also play a role as friendly jammers. Reference [159] evaluated the secrecy capacity of secure AF relay networks using wireless powered cooperative jamming. In [160], the authors studied optimal power allocation for PLS systems with assistance of a FD jammer. Published work [161] proposed a PLS-based multi-user broadcast protocol, and designed an optimal pre-coding matrix at a multi-antenna base station as well as a jamming covariance matrix at a jammer node to minimize total transmit power under a secrecy constraint. Reference [162] considered a CJ method in multi-eavesdropper environment with finite alphabet inputs. In [163], harvest-to-jam (H2J) method was proposed, where the jammer nodes harvest wireless energy for generating the artificial noises. Moreover, the authors in [139] proposed various relay and jammer selection strategies to enhance the secrecy performance for dual-hop relay networks.

This section concerns with the PLS issue in M-LEACH networks, where the source-destination

communication is realized via CHs of intermediate clusters, in presence of an eavesdropper. To protect the source information, CHs can select one or many cluster nodes to perform the CJ operation, using the H2J technique. Although reference [134] also considers the M-LEACH network with CJ, the jammer nodes use their power to transmit the artificial noises. Under total transmit power constraint, the authors of [164] provided a sub-optimal solution of transmit power allocation to maximize lower bound of the end-to-end instantaneous secrecy capacity in multi-hop FD relay systems. Similar to [134], the jammer nodes in [164] do not use H2T technique. In [165], a multi-hop DF relay network was considered, where the HD relays allocate a part of total transmit power for generating the jamming noises. In [HDH18], the random jammer selection and the RF technique are employed to protect the source data in M-LEACH networks. However, in [HDH18], the selected jammer node harvests the wireless energy from CH of the previous cluster. References [157] considered power beacon-aided multi-hop relaying protocols. In [166], the authors proposed a multi-hop EH WSNs employing non-orthogonal multiple access (NOMA) and CJ techniques under presence of multiple eavesdroppers. Moreover, the relay and jammer nodes in [166] are powered by power transfer stations deployed in the network. However, unlike [157], the source data is relayed via full-energy CHs, while friendly jammers are cluster nodes which are powered by PB. Moreover, because each CH and the selected jammer(s) are in the same cluster, they can surely exchange information about the jamming noises. Therefore, we can assume that CHs can perfectly remove the interference generated by the jammer(s), but the eavesdropper cannot.

Also different than [134], I propose three H2J jammer selection methods named Max-EH, MAX-IP and ALL-CJ. In MAX-EH, the cluster node obtained the MAXimum Energy Harvested from the power beacon is chosen. In MAX-IP, the selected jammer is the cluster node providing the MAXimum Interference Power to the eavesdropper. In ALL-CJ, ALL cluster nodes in the clusters take part in the CJ operation. For performance evaluation, we derive expressions of the end-to-end (e2e) SOP for the proposed methods over Rayleigh fading channels. Particularly, for RAND and MAX-EH, exact closed-form expressions of the e2e SOP are derived. For MAX-IP, an exact integral-form formula and an lower-bound closed-form expression of the e2e SOP are provided. For ALL-CJ, a lower-bound expression of the e2e SOP is derived. We then perform Monte-Carlo based computer simulations to verify the theoretical results. The results show that the proposed methods outperform the RANDom jammer selection (RAND) and the corresponding method Without using the CJ technique (WO-CJ). The impact of the system parameters such as the number of hops, the number of nodes at each cluster, the fraction of time spent for the EH process on the e2e SOP of the proposed methods is also investigated.

### 6.2.2 System Model

Fig. 6.6 presents system model of the proposed secure transmission protocol. Here, the source ($\mathrm{T}_0$) (CH of cluster 0), attempts to send its data to the destination ($\mathrm{T}_M$) (CH of cluster $M$), via CHs of the intermediate clusters. It can be assumed that there are $(M-1)$ clusters between the

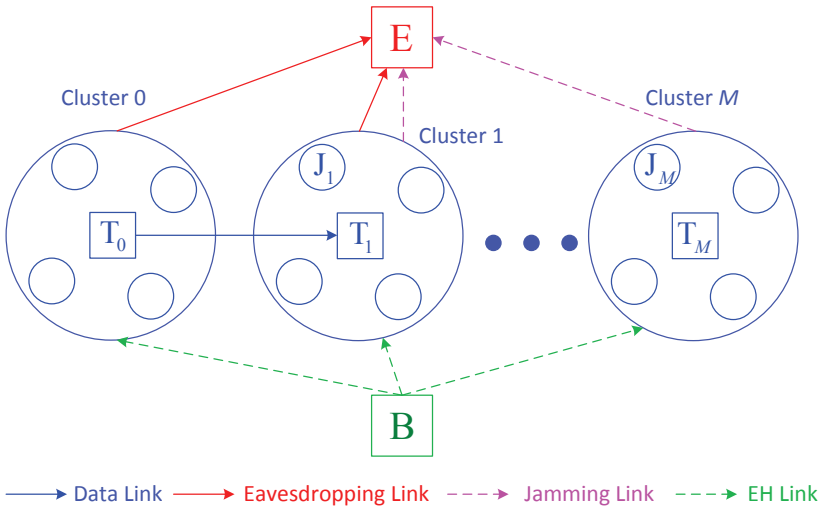


Figure 6.6: System model of the PLS protocol in M-LEACH networks using CJ.

cluster 0 and the cluster $M$. Let $\mathrm{T}_m$ denote CH of the $m^{th}$ cluster, where $m = 1, 2, ..., M-1$. The node $\mathrm{T}_m$ receives the source data from the previous node $\mathrm{T}_{m-1}$, decodes, re-encodes, and then transmits the encoded data to the next node $\mathrm{T}_{m+1}$. To protect the source data, $\mathrm{T}_0$ and $\mathrm{T}_m$ employ the RF technique to confuse the eavesdropper E [141], [142]. Furthermore, at each cluster, the CJ process is performed to reduce quality of the eavesdropping channel. To support wireless energy for all of the nodes, a power beacon (B) is deployed in the network. The node B can generate wireless signals using a specific frequency band which differs with the frequency used for the data transmission. We assume that all the terminals are single-antenna devices, and the data transmission is split into $M$ orthogonal time slots. We denote $L$ as a maximal delay time for each data transmission. As a result, the time spent for each time slot is equally allocated as $\tau = L/M$.

Considering the $m^{th}$ time slot in which $\mathrm{T}_{m-1}$ transmits the data to $\mathrm{T}_m$, E overhears the transmitted data, and the selected jammer(s) transmits the jamming noises on E. In this time slot, a duration of $\alpha\tau$ is used for harvesting the wireless energy from B, and a duration of $(1-\alpha)\tau$ is spent for the $\mathrm{T}_{m-1} \rightarrow \mathrm{T}_m$ transmission, where $0 \leq \alpha \leq 1$. Assume that there are $N$ nodes in each cluster, and the cluster nodes in the $m^{th}$ cluster are named by $\mathrm{R}_{m,n}$, where $n = 1, 2, ..., N$.

Before describing the channel and system models, we would like to summarize the notations used through this section (see Table 6.1).

Next, the transmit power of node $\mathrm{R}_{m,n}$ can be obtained from the harvested energy from B

Table 6.1: Mathematical notations.

| Symbol | Meaning |
|---|---|
| $M$ | Number of hops or number of clusters |
| $L$ | Maximum delay time between $\mathrm{T}_0$ and $\mathrm{T}_\mathrm{M}$ |
| $\tau = L/M$ | Time allocated for each time slot |
| $\alpha$ | Fraction of time spent for EH phases |
| $P_\mathrm{T}$, $P_\mathrm{B}$ | Transmit power of cluster heads and power beacon, respectively |
| $\eta$ | Energy conversion efficiency |
| $\sigma_0^2$ | Variance of additive white Gaussian noise |
| $\Delta = P_\mathrm{T}/\sigma_0^2$, $\Lambda = P_\mathrm{B}/\sigma_0^2$ | Transmit signal-to-noise ratios |
| $F_U(.)$, $f_U(.)$ | CDF and PDF of random variable $U$, respectively |
| $\gamma_{\mathrm{X,Y}}$ | Channel gain between X and Y |
| $\lambda_{\mathrm{X,Y}}$ | Parameter of channel gain $\gamma_{\mathrm{X,Y}}$ |

and can be found by similar approach as in (2.4):

$$P_{\mathrm{R}_{m,n}} = \frac{\mathrm{EH}_{\mathrm{R}_{m,n}}}{(1-\alpha)\,\tau} = \kappa P_\mathrm{B} \gamma_{\mathrm{B,R}_{m,n}}, \tag{6.22}$$

where $\eta$ is an energy conversion efficiency $(0 < \eta < 1)$, $P_\mathrm{B}$ is transmit power of B, $\gamma_{\mathrm{B,R}_{m,n}}$ is channel gain between B and $\mathrm{R}_{m,n}$, $\kappa = \eta\alpha/(1-\alpha)$.

As mentioned above, because $\mathrm{T}_m$ and $\mathrm{R}_{m,n}$ are close to each other, they can securely exchange information about the jamming noises so that $\mathrm{T}_m$ can remove them from the received signals. Hence, the instantaneous channel capacity of the $\mathrm{T}_{m-1} \to \mathrm{T}_m$ link can be given as

$$C_{\mathrm{D},m} = (1-\alpha)\,\tau \log_2\left(1 + \frac{P_\mathrm{T}\gamma_{\mathrm{T}_{m-1},\mathrm{T}_m}}{\sigma_0^2}\right) = (1-\alpha)\,\tau \log_2\left(1 + \Delta\gamma_{\mathrm{T}_{m-1},\mathrm{T}_m}\right), \tag{6.23}$$

where $P_\mathrm{T}$ is transmit power of all of CHs, $\gamma_{\mathrm{T}_{m-1},\mathrm{T}_m}$ is channel gain of the $\mathrm{T}_{m-1} \to \mathrm{T}_m$ link, $\sigma_0^2$ is variance of AWGN, and $\Delta = P_\mathrm{T}/\sigma_0^2$ is the transmit SNR.

Because E cannot remove the jamming noises, the instantaneous channel capacity of the $\mathrm{T}_{m-1} \to \mathrm{E}$ channel can be given by

$$C_{\mathrm{E},m} = (1-\alpha)\,\tau \log_2\left(1 + \frac{P_\mathrm{T}\gamma_{\mathrm{T}_{m-1},\mathrm{E}}}{P_{\mathrm{R}_{m,n}}\gamma_{\mathrm{R}_{m,n},\mathrm{E}} + \sigma_0^2}\right) = (1-\alpha)\,\tau \log_2\left(1 + \frac{\Delta\gamma_{\mathrm{T}_{m-1},\mathrm{E}}}{\kappa\Lambda\gamma_{\mathrm{B,R}_{m,n}}\gamma_{\mathrm{R}_{m,n},\mathrm{E}} + 1}\right), \tag{6.24}$$

where $\gamma_{\mathrm{T}_{m-1},\mathrm{E}}$ and $\gamma_{\mathrm{R}_{m,n},\mathrm{E}}$ are channel gains of the $\mathrm{T}_{m-1} \to \mathrm{E}$ and $\mathrm{R}_{m,n} \to \mathrm{E}$ links, respectively, and $\Lambda = P_\mathrm{B}/\sigma_0^2$.

From (6.23) and (6.24), the secrecy capacity obtained at the $m^{th}$ time slot can be given as

$$\mathrm{SC}_m = [C_{\mathrm{D},m} - C_{\mathrm{E},m}]^+ = \left[ (1-\alpha)\,\tau \log_2 \left( \frac{1 + \Delta\gamma_{\mathrm{T}_{m-1},\mathrm{T}_m}}{1 + \frac{\Delta\gamma_{\mathrm{T}_{m-1},\mathrm{E}}}{\kappa\Lambda\gamma_{\mathrm{B},\mathrm{R}_{m,n}}\gamma_{\mathrm{R}_{m,n},\mathrm{E}}+1}} \right) \right]^+, \tag{6.25}$$

where $[x]^+ = \max(x, 0)$.

Due to the RF technique used, the e2e instantaneous secrecy capacity can be formulated as

$$\mathrm{SC}_{\mathrm{e2e}} = \min_{m=1,2,\ldots,M} (\mathrm{SC}_m). \tag{6.26}$$

Assume that all the channels are Rayleigh fading, therefore $\gamma_{\mathrm{X,Y}}$ follows an exponential RV, and its CDF are expressed as

$$F_{\gamma_{\mathrm{X,Y}}}(u) = 1 - \exp(-\lambda_{\mathrm{X,Y}} u), f_{\gamma_{\mathrm{X,Y}}}(u) = \lambda_{\mathrm{X,Y}} \exp(-\lambda_{\mathrm{X,Y}} u), \tag{6.27}$$

where $(\mathrm{X}, \mathrm{Y}) \in \{\mathrm{T}_m, \mathrm{B}, \mathrm{E}\}$, $\lambda_{\mathrm{X,Y}} = 1/\mathcal{E}\{\gamma_{\mathrm{X,Y}}\} = d^{\theta}_{\mathrm{X,Y}}$ [HDH18],[137], $\mathcal{E}\{.\}$ is an expected operator, $d_{\mathrm{X,Y}}$ is distance between X and Y, $\theta$ is path-loss exponent, $F_U(.)$ is cumulative distribution function (CDF) of RV $U$, and $f_U(.)$ is PDF of RV $U$.

**Remark 6.1** Firstly, in M-LEACH, the data transmission is performed via CHs which often have high residual energy [167], [168], and hence we can assume that they can transmit the data with the maximum power $P_{\mathrm{T}}$. Secondly, we assume that E only overhears and illegally decodes the source data, and an jamming-attack model as in [169] is out of scope of this paper. Thirdly, for ease of presentation and analysis as well as for clearly observing the impact of $N$ and $\alpha$ on the secrecy performance, we can assume the number of nodes at each cluster ($N$) is same, and the fraction time used for the EH phase ($\alpha$) at each hop is the same. It is worth noting that the analysis in this work can be easily extended to the scheme with different values of $N$ at each cluster, and different values of $\alpha$ at each hop. Next, before $\mathrm{T}_{m-1}$ transmits the data to $\mathrm{T}_m$, we can assume that $\mathrm{T}_{m-1}$ has already reserved the channel, which means that the other transmitter/receiver pairs in the network are not allowed to be active on the reserved channel. Indeed, the channel reservation has to be performed to avoid impact of the jamming noises on the other receivers. Finally, because the nodes in each cluster are close together, it can be assumed that $d_{\mathrm{X},\mathrm{T}_m} = d_{\mathrm{X},\mathrm{R}_{m,n}}$ for all X, $m$ and $n$. Therefore, in the following, we use the following notations:

$$\lambda_{\mathrm{T}_{m-1},\mathrm{T}_m} = \lambda_{\mathrm{T}_{m-1},\mathrm{R}_{m,n}} = \lambda_{\mathrm{D},m}, \lambda_{\mathrm{T}_m,\mathrm{E}} = \lambda_{\mathrm{R}_{m,n},\mathrm{E}} = \lambda_{\mathrm{E},m}, \lambda_{\mathrm{B},\mathrm{R}_{m,n}} = \lambda_{\mathrm{B},m}. \tag{6.28}$$

Next, we introduce jammer selection methods proposed in this part. At first, we denote the selected jammer at the $m^{th}$ cluster as $\mathrm{J}_m$, where $\mathrm{J}_m \in \{\mathrm{R}_{m,1}, \mathrm{R}_{m,2}, ..., \mathrm{R}_{m,N}\}$.

#### 6.2.2.1 RAND method

In RAND, each CH randomly selects one of its members for the CJ operation [HDH18], [134]. The implementation of RAND is simplest, e.g., the cluster nodes are sequentially chosen, follows their ID. In addition, this method also avoids the case where only one node is always selected for the CJ phases. However, the performance of RAND is worst than that of MAX-EH, MAX-IP and ALL-CJ.

#### 6.2.2.2 MAX-EH method

In this method, the CH node $\mathrm{T}_m$ selects the candidate obtained the highest energy harvested from B. Mathematically, we can write

$$\mathrm{J}_m = \arg \max_{n=1,2,\ldots,N} \left(\mathrm{EH}_{\mathrm{R}_{m,n}}\right). \tag{6.29}$$

Combining (6.22) and (6.29), we obtain (6.30) as

$$\mathrm{J}_m = \arg \max_{n=1,2,\ldots,N} \left(P_{\mathrm{R}_{m,n}}\right) = \arg \max_{n=1,2,\ldots,N} \left(\gamma_{\mathrm{B},\mathrm{R}_{m,n}}\right). \tag{6.30}$$

Equation (6.30) implies that among members of the $m^{th}$ cluster, $\mathrm{J}_m$ is the node having the highest transmit power or having the highest channel gain between itself and B.

**Remark 6.2** The implementation of MAX-EH can be realized as follows: the cluster members $\mathrm{R}_{m,n}$ send the value of $\mathrm{EH}_{\mathrm{R}_{m,n}}$ (or $P_{\mathrm{R}_{m,n}}$ or $\gamma_{\mathrm{B},\mathrm{R}_{m,n}}$) to $\mathrm{T}_m$ so that $\mathrm{T}_m$ can select the best node by using (6.29) or (6.30). As a result, MAX-EH is more complex than RAND because it requires more overhead, time and energy for estimating and exchanging the information. Moreover, RAND and MAX-EH can be applied for passive-eavesdropper schemes [170] in which the instantaneous CSI of the eavesdropping links are not available.

#### 6.2.2.3 MAX-IP method

When the eavesdropper is active [137], [171], the cluster members $\mathrm{R}_{m,n}$ are assumed to be able to estimate the instantaneous CSI between themselves and E. In this case, we propose the MAX-IP method in which the jammer at the $m^{th}$ cluster is selected as

$$\mathrm{J}_m = \arg \max_{n=1,2,\ldots,N} \left(\kappa\Lambda\gamma_{\mathrm{B},\mathrm{R}_{m,n}}\gamma_{\mathrm{R}_{m,n},\mathrm{E}}\right) = \arg \max_{n=1,2,\ldots,N} \left(\gamma_{\mathrm{B},\mathrm{R}_{m,n}}\gamma_{\mathrm{R}_{m,n},\mathrm{E}}\right). \tag{6.31}$$

Equation (6.31) implies that the node providing the highest interference power on E is selected, which also means that

$$\gamma_{\mathrm{B},\mathrm{J}_m}\gamma_{\mathrm{J}_m,\mathrm{E}} = \max_{n=1,2,\ldots,N} \left(\gamma_{\mathrm{B},\mathrm{R}_{m,n}}\gamma_{\mathrm{R}_{m,n},\mathrm{E}}\right). \tag{6.32}$$

**Remark 6.3** Since the jammer selection in MAX-IP considers both the EH and eavesdropping links, MAX-IP provides higher performance than MAX-EH. However, the implementation of MAX-IP which requires perfect CSIs of the eavesdropping links is very complex. As mentioned above, this method is only applied when the eavesdropper is active. Moreover, to perform the jammer selection, all the nodes $\mathrm{R}_{m,n}$ have to send the values of $\gamma_{\mathrm{B},\mathrm{R}_{m,n}}\gamma_{\mathrm{R}_{m,n},\mathrm{E}}$ to $\mathrm{T}_m$, which can spend a lot of energy and time.

#### 6.2.2.4 ALL-CJ method

Unlike RAND, MAX-EH and MAX-IP, the CH $\mathrm{T}_m$ in ALL-CJ selects all the cluster nodes to join in the CJ operation. Hence, the channel capacity of the $\mathrm{T}_{m-1} \to \mathrm{E}$ link is given as

$$C_{\mathrm{E},m} = (1-\alpha)\,\tau\log_2\left(1+\frac{P_{\mathrm{T}}\gamma_{\mathrm{T}_{m-1},\mathrm{E}}}{\sum\limits_{n=1}^{N} P_{\mathrm{R}_{m,n}}\gamma_{\mathrm{R}_{m,n},\mathrm{E}}+\sigma_0^2}\right) = (1-\alpha)\,\tau\log_2\left(1+\frac{\Delta\gamma_{\mathrm{T}_{m-1},\mathrm{E}}}{\sum\limits_{n=1}^{N} \kappa\Lambda\gamma_{\mathrm{B},\mathrm{R}_{m,n}}\gamma_{\mathrm{R}_{m,n},\mathrm{E}}+1}\right). \tag{6.33}$$

Hence, the secrecy capacity obtained at the $m^{th}$ hop in ALL-CJ can be written as

$$\mathrm{SC}_m^{\mathrm{ALL-CJ}} = \left[(1-\alpha)\,\tau\log_2\left(\frac{1+\Delta\gamma_{\mathrm{T}_{m-1},\mathrm{T}_m}}{1+\frac{\Delta\gamma_{\mathrm{T}_{m-1},\mathrm{E}}}{\sum\limits_{n=1}^{N}\kappa\Lambda\gamma_{\mathrm{B},\mathrm{R}_{m,n}}\gamma_{\mathrm{R}_{m,n},\mathrm{E}}+1}}\right)\right]^+. \tag{6.34}$$

**Remark 6.4** Until now, almost published works related to the jammer selection methods have only considered the single-node selection, which motivates us to propose the ALL-CJ protocol. Moreover, as shown in part 6.2.4, ALL-CJ provides the highest SOP performance, as compared with the remaining protocols. However, due to the requirement of high synchronization between the nodes in each cluster, ALL-CJ uses a lot of energy and time. In addition, using all of the nodes in each cluster for the CJ operation also reduces spectrum efficiency. Finally, unlike MAX-IP, ALL-CJ does not require CSIs of the eavesdropping links.

#### 6.2.2.5 WO-CJ method

For performance comparison, we also consider the conventional secure transmission method in which the CJ technique is not used at each hop. Because the EH phase does not need to use, the secrecy capacity at the $m^{th}$ time slot in WO-CJ can be calculated as

$$\mathrm{SC}_m^{\mathrm{WO-CJ}} = \left[\tau\log_2\left(\frac{1+\Delta\gamma_{\mathrm{T}_{m-1},\mathrm{T}_m}}{1+\Delta\gamma_{\mathrm{T}_{m-1},\mathrm{E}}}\right)\right]^+. \tag{6.35}$$

### 6.2.3 Performance Analysis

In this part, we analyze the e2e SOP of RAND, MAX-EH, MAX-IP, All-CJ over Rayleigh fading channel, which is defined as

$$\mathrm{SOP}_{\mathrm{e2e}}^{\mathrm{Z}} = \Pr\left(\mathrm{SC}_{\mathrm{e2e}}^{\mathrm{Z}} < C_{\mathrm{th}}\right), \tag{6.36}$$

where $C_{\mathrm{th}}$ is a positive threshold, and $Z \in \{\mathrm{RAND}, \mathrm{MAX-EH}, \mathrm{MAX-IP}, \mathrm{ALL-CJ}, \mathrm{WO-CJ}\}$. Combining (6.26) and (6.36), we have

$$\mathrm{SOP}_{\mathrm{e2e}}^{\mathrm{Z}} = \Pr\left(\min_{m=1,2,\ldots,M}\left(\mathrm{SC}_{m}^{\mathrm{Z}}\right) < C_{\mathrm{th}}\right) = 1 - \prod_{m=1}^{M}\left(1 - \mathrm{SOP}_{m}^{\mathrm{Z}}\right), \tag{6.37}$$

where $\mathrm{SOP}_{m}^{\mathrm{Z}} = \Pr\left(\mathrm{SC}_{m}^{\mathrm{Z}} < C_{\mathrm{th}}\right)$ is SOP at the $m^{th}$ hop. Therefore, to obtain $\mathrm{SOP}_{\mathrm{e2e}}^{\mathrm{Z}}$, we have to calculate $\mathrm{SOP}_{m}^{\mathrm{Z}}$.

When $\mathrm{Z} \neq \mathrm{WO-CJ}$, using (6.25) and (6.34), we can express $\mathrm{SOP}_{m}^{\mathrm{Z}}$ in the following form:

$$\mathrm{SOP}_{m}^{\mathrm{Z}} = \Pr\left(\gamma_{\mathrm{T}_{m-1},\mathrm{T}_{m}} < \phi_1 + \phi_2 U_{m}^{\mathrm{Z}}\right), \tag{6.38}$$

where

$$\begin{aligned}
&\rho = 2^{\frac{C_{\mathrm{th}}}{(1-\alpha)\tau}}, \phi_1 = \frac{\rho - 1}{\Delta}, \phi_2 = \frac{\rho}{\Delta}, \\
&U_{m}^{\mathrm{Z}} = \begin{cases} \frac{\Delta\gamma_{\mathrm{T}_{m-1},\mathrm{E}}}{\kappa\Lambda\gamma_{\mathrm{B},\mathrm{J}_m}\gamma_{\mathrm{J}_m,\mathrm{E}}+1}, & \mathrm{Z} \in \{\mathrm{RAND}, \mathrm{MAX-EH}, \mathrm{MAX-IP}\} \\ \frac{\Delta\gamma_{\mathrm{T}_{m-1},\mathrm{E}}}{\kappa\Lambda\sum_{n=1}^{N}\gamma_{\mathrm{B},\mathrm{R}_{m,n}}\gamma_{\mathrm{R}_{m,n},\mathrm{E}}+1}, & \mathrm{Z} = \mathrm{ALL-CJ} \end{cases}
\end{aligned} \tag{6.39}$$

Using CDF of $\gamma_{\mathrm{T}_{m-1},\mathrm{T}_{m}}$ given by (6.27), we can rewrite (6.38) as

$$\begin{aligned}
\mathrm{SOP}_{m}^{\mathrm{Z}} &= \int_{0}^{+\infty} F_{\gamma_{\mathrm{T}_{m-1},\mathrm{T}_{m}}}\left(\phi_1 + \phi_2 u\right) f_{U_{m}^{\mathrm{Z}}}\left(u\right) du \\
&= 1 - \exp\left(-\lambda_{\mathrm{D},m}\phi_1\right) \int_{0}^{+\infty} \exp\left(-\lambda_{\mathrm{D},m}\phi_2 u\right) f_{U_{m}^{\mathrm{Z}}}\left(u\right) du \\
&= 1 - \lambda_{\mathrm{D},m}\phi_2 \exp\left(-\lambda_{\mathrm{D},m}\phi_1\right) \int_{0}^{+\infty} \exp\left(-\lambda_{\mathrm{D},m}\phi_2 u\right) F_{U_{m}^{\mathrm{Z}}}\left(u\right) du,
\end{aligned} \tag{6.40}$$

where $f_{U_{m}^{\mathrm{Z}}}\left(u\right)$ and $F_{U_{m}^{\mathrm{Z}}}\left(u\right)$ are PDF and CDF of $U_{m}^{\mathrm{Z}}$, respectively.

#### 6.2.3.1 WO-CJ method

In this method, $\mathrm{SOP}_m^{\mathrm{WO-CJ}}$ can be computed exactly as

$$\begin{aligned}\mathrm{SOP}_m^{\mathrm{WO-CJ}} &= \Pr\left(\gamma_{\mathrm{T}_{m-1},\mathrm{T}_m} < \frac{2^{C_{\mathrm{th}}/\tau}-1}{\Delta} + 2^{C_{\mathrm{th}}/\tau}\gamma_{\mathrm{T}_{m-1},\mathrm{E}}\right)\\ &= \int_0^{+\infty} F_{\gamma_{\mathrm{T}_{m-1},\mathrm{T}_m}}\left(\frac{2^{C_{\mathrm{th}}/\tau}-1}{\Delta} + 2^{C_{\mathrm{th}}/\tau}x\right) f_{\gamma_{\mathrm{T}_{m-1},\mathrm{E}}}(x)\,dx\\ &= 1 - \frac{\lambda_{\mathrm{E},m}}{\lambda_{\mathrm{E},m} + \lambda_{\mathrm{D},m}2^{C_{\mathrm{th}}/\tau}} \exp\left(-\frac{\lambda_{\mathrm{D},m}}{\Delta}\left(2^{C_{\mathrm{th}}/\tau}-1\right)\right). \end{aligned} \tag{6.41}$$

Then, substituting (6.41) into (6.37), which yields

$$\mathrm{SOP}_{\mathrm{e2e}}^{\mathrm{WO-CJ}} = 1 - \prod_{m=1}^{M}\left[\frac{\lambda_{\mathrm{E},m}}{\lambda_{\mathrm{E},m} + \lambda_{\mathrm{D},m}2^{C_{\mathrm{th}}/\tau}} \exp\left(-\frac{\lambda_{\mathrm{D},m}}{\Delta}\left(2^{C_{\mathrm{th}}/\tau}-1\right)\right)\right]. \tag{6.42}$$

Next, we analyze the e2e SOP of the proposed methods. As observed from (6.40), we have to obtain CDF of $U_m^{\mathrm{Z}}$, which can be formulated as

$$F_{U_m^{\mathrm{Z}}}(u) = \Pr\left(U_m^{\mathrm{Z}} < u\right) = \Pr\left(\gamma_{\mathrm{T}_{m-1},\mathrm{E}} < \frac{\kappa\Lambda}{\Delta}V_m^{\mathrm{Z}}u + \frac{u}{\Delta}\right) = \int_0^{+\infty} F_{\gamma_{\mathrm{T}_{m-1},\mathrm{E}}}\left(\phi_3 v u + \frac{u}{\Delta}\right) f_{V_m^{\mathrm{Z}}}(v)\,dv, \tag{6.43}$$

where $\phi_3 = \kappa\Lambda/\Delta$, $f_{V_m^{\mathrm{Z}}}(v)$ is PDF of $V_m^{\mathrm{Z}}$, with

$$V_m^{\mathrm{Z}} = \begin{cases} \gamma_{\mathrm{B},\mathrm{J}_m}\gamma_{\mathrm{J}_m,\mathrm{E}}, \ \mathrm{Z} \in \{\mathrm{RAND}, \mathrm{MAX-EH}, \mathrm{MAX-IP}\} \\ \sum\limits_{n=1}^{N} \gamma_{\mathrm{B},\mathrm{R}_{m,n}}\gamma_{\mathrm{R}_{m,n},\mathrm{E}}, \ \mathrm{Z} = \mathrm{ALL-CJ} \end{cases} \tag{6.44}$$

From (6.27) and (6.44), we can write

$$\begin{aligned} F_{U_m^{\mathrm{Z}}}(u) &= 1 - \exp\left(-\lambda_{\mathrm{E},m}\frac{u}{\Delta}\right)\int_0^{+\infty}\exp\left(-\lambda_{\mathrm{E},m}\phi_3 u v\right) f_{V_m^{\mathrm{Z}}}(v)\,dv\\ &= 1 - \lambda_{\mathrm{E},m}\phi_3 u \exp\left(-\phi_{4,m}u\right)\int_0^{+\infty}\exp\left(-\lambda_{\mathrm{E},m}\phi_3 u v\right) F_{V_m^{\mathrm{Z}}}(v)\,dv, \end{aligned} \tag{6.45}$$

where $\phi_{4,m} = \lambda_{\mathrm{E},m}/\Delta$, and $F_{V_m^{\mathrm{Z}}}(v)$ is CDF of $V_m^{\mathrm{Z}}$.

Then, substituting (6.45) into (6.40), after some manipulation, we arrive at

$$\begin{aligned}\mathrm{SOP}_m^{\mathrm{Z}} &= 1 - e^{-\lambda_{\mathrm{D},m}\phi_1} + \\ &+ \lambda_{\mathrm{D},m}\lambda_{\mathrm{E},m}\phi_2\phi_3 e^{-\lambda_{\mathrm{D},m}\phi_1}\int_0^{+\infty} F_{V_m^{\mathrm{Z}}}(v)\left[\int_0^{+\infty} u e^{-\left(\lambda_{\mathrm{D},m}\phi_2+\phi_{4,m}\right)u} e^{-\lambda_{\mathrm{E},m}\phi_3 vu} du\right] dv \\ &= 1 - e^{-\lambda_{\mathrm{D},m}\phi_1} + \lambda_{\mathrm{D},m}\lambda_{\mathrm{E},m}\phi_2\phi_3 e^{-\lambda_{\mathrm{D},m}\phi_1}\int_0^{+\infty} \frac{F_{V_m^{\mathrm{Z}}}(v)\, dv}{\left(\left(\lambda_{\mathrm{D},m}\phi_2+\phi_{4,m}\right)+\lambda_{\mathrm{E},m}\phi_3 v\right)^2} \\ &= 1 - e^{-\lambda_{\mathrm{D},m}\phi_1} + \phi_{5,m} e^{-\lambda_{\mathrm{D},m}\phi_1}\int_0^{+\infty} \frac{F_{V_m^{\mathrm{Z}}}(v)\, dv}{\left(\phi_{6,m}+v\right)^2}, \end{aligned} \tag{6.46}$$

where $\phi_{5,m} = \frac{\lambda_{\mathrm{D},m}\phi_2}{\lambda_{\mathrm{E},m}\phi_3}$, $\phi_{6,m} = \frac{\lambda_{\mathrm{D},m}\phi_2+\phi_{4,m}}{\lambda_{\mathrm{E},m}\phi_3}$.

Next, we attempt to find CDF of $V_m^{\mathrm{Z}}$, and then substituting it into (6.46) to obtain $\mathrm{SOP}_m^{\mathrm{Z}}$.

#### 6.2.3.2 RAND method

In RAND, CDF of $V_m^{\mathrm{RAND}}$ is expressed as

$$\begin{aligned} F_{V_m^{\mathrm{RAND}}}(v) &= \Pr\left(\gamma_{\mathrm{B},\mathrm{J}_m}\gamma_{\mathrm{J}_m,\mathrm{E}} < v\right) = \int_0^{+\infty} F_{\gamma_{\mathrm{B},\mathrm{J}_m}}\left(\frac{v}{x}\right) f_{\gamma_{\mathrm{J}_m,\mathrm{E}}}(x)\, dx \\ &= 1 - \lambda_{\mathrm{E},m+1}\int_0^{+\infty} \exp\left(-\frac{\lambda_{\mathrm{B},m}v}{x}\right)\exp\left(-\lambda_{\mathrm{E},m+1}x\right) dx. \end{aligned} \tag{6.47}$$

Using [72, eq. (3.324.1)] for (6.47), we can obtain

$$F_{V_m^{\mathrm{RAND}}}(v) = 1 - 2\sqrt{\lambda_{\mathrm{B},m}\lambda_{\mathrm{E},m+1}v}K_1\left(2\sqrt{\lambda_{\mathrm{B},m}\lambda_{\mathrm{E},m+1}v}\right) = 1 - \phi_{7,m}\sqrt{v}K_1\left(\phi_{7,m}\sqrt{v}\right), \tag{6.48}$$

where $\phi_{7,m} = 2\sqrt{\lambda_{\mathrm{B},m}\lambda_{\mathrm{E},m+1}}$, and $K_1(.)$ is a modified Bessel function of the second kind [72]. Combining (6.46) and (6.48), we arrive at

$$\mathrm{SOP}_m^{\mathrm{RAND}} = 1 - \frac{\phi_{6,m}-\phi_{5,m}}{\phi_{6,m}} e^{-\lambda_{\mathrm{D},m}\phi_1} - \phi_{5,m}\phi_{7,m} e^{-\lambda_{\mathrm{D},m}\phi_1}\int_0^{+\infty} \frac{\sqrt{v}}{\left(\phi_{6,m}+v\right)^2} K_1\left(\phi_{7,m}\sqrt{v}\right) dv. \tag{6.49}$$

By changing variable $t = \sqrt{v}$, we obtain

$$\mathrm{SOP}_m^{\mathrm{RAND}} = 1 - \frac{\phi_{6,m}-\phi_{5,m}}{\phi_{6,m}} e^{-\lambda_{\mathrm{D},m}\phi_1} - 2\phi_{5,m}\phi_{7,m} e^{-\lambda_{\mathrm{D},m}\phi_1}\int_0^{+\infty} \frac{t^2 K_1\left(\phi_{7,m}t\right) dt}{\left(\phi_{6,m}+t^2\right)^2}. \tag{6.50}$$

Combining [72, eq. (6.565.7)], [72, eq. (9.34.6)] and (6.50), we obtain an exact closed-form

expression of $\mathrm{SOP}_m^{\mathrm{RAND}}$ as

$$\mathrm{SOP}_m^{\mathrm{RAND}} = 1 - \frac{\phi_{6,m} - \phi_{5,m}}{\phi_{6,m}} e^{-\lambda_{\mathrm{D},m}\phi_1} - \frac{\phi_{5,m}(\phi_{7,m})^2}{4} e^{-\lambda_{\mathrm{D},m}\phi_1} G_{1,3}^{3,1}\left( \frac{\phi_{6,m}(\phi_{7,m})^2}{4} \middle\| \begin{matrix} -1 & - & - \\ -1 & 0 & 0 \end{matrix} \right), \tag{6.51}$$

where $G_{\cdot,\cdot}^{\cdot,\cdot}(.|.)$ is Meijer-G function [72].

#### 6.2.3.3 MAX-EH method

Because $\gamma_{\mathrm{B,J}_m} = \max\limits_{n=1,2,\ldots,N}(\gamma_{\mathrm{B,R}_{m,n}})$ (see (6.30)), CDF of $\gamma_{\mathrm{B,J}_m}$ is determined by

$$F_{\gamma_{\mathrm{B,J}_m}}(x) = \Pr\left( \max_{n=1,2,\ldots,N}(\gamma_{\mathrm{B,R}_{m,n}}) < x \right) = \left(1 - e^{-\lambda_{\mathrm{B},m}x}\right)^N = 1 + \sum_{t=1}^{N} (-1)^t \binom{N}{t} e^{-t\lambda_{\mathrm{B},m}x}, \tag{6.52}$$

where $\binom{N}{t} = \frac{N!}{t!(N-t)!}$ is a binomial coefficient. Then, CDF of $V_m^{\mathrm{MAX-EH}}$ can be formulated as

$$\begin{aligned} F_{V_m^{\mathrm{MAX-EH}}}(v) &= \int_0^{+\infty} F_{\gamma_{\mathrm{B,J}_m}}\left(\frac{v}{x}\right) f_{\gamma_{\mathrm{J}_m,\mathrm{E}}}(x)\, dx \\ &= 1 + \sum_{t=1}^{N} (-1)^t \binom{N}{t} \lambda_{\mathrm{E},m+1} \int_0^{+\infty} e^{-t\lambda_{\mathrm{B},m}\frac{v}{x}} e^{-\lambda_{\mathrm{E},m+1}x} dx. \end{aligned} \tag{6.53}$$

Again, using [72, eq. (3.324.1)] to calculate the integral in (6.53), we obtain (6.54) as

$$F_{V_m^{\mathrm{MAX-EH}}}(v) = 1 + \sum_{t=1}^{N} (-1)^t \binom{N}{t} \sqrt{t}\phi_{7,m}\sqrt{v} K_1\left(\sqrt{t}\phi_{7,m}\sqrt{v}\right). \tag{6.54}$$

Substituting (6.54) into (6.46), similar to (6.49)-(6.50), we can obtain an exact closed-form expression of $\mathrm{SOP}_m^{\mathrm{MAX-EH}}$ as

$$\begin{aligned} \mathrm{SOP}_m^{\mathrm{MAX-EH}} &= 1 - \frac{\phi_{6,m} - \phi_{5,m}}{\phi_{6,m}} e^{-\lambda_{\mathrm{D},m}\phi_1} \\ &+ \phi_{5,m}\phi_{7,m} e^{-\lambda_{\mathrm{D},m}\phi_1} \sum_{t=1}^{N} (-1)^t \binom{N}{t} \sqrt{t} \int_0^{+\infty} \frac{\sqrt{v} K_1\left(\sqrt{t}\phi_{7,m}\sqrt{v}\right)}{(\phi_{6,m} + v)^2} dv \\ &= 1 - \frac{\phi_{6,m} - \phi_{5,m}}{\phi_{6,m}} e^{-\lambda_{\mathrm{D},m}\phi_1} + \phi_{5,m}\phi_{7,m} e^{-\lambda_{\mathrm{D},m}\phi_1} \sum_{t=1}^{N} (-1)^t 2C_N^t \sqrt{t} \int_0^{+\infty} \frac{u^2 K_1\left(\sqrt{t}\phi_{7,m}u\right)}{(\phi_{6,m} + u^2)^2} du \\ &= 1 - \frac{\phi_{6,m} - \phi_{5,m}}{\phi_{6,m}} e^{-\lambda_{\mathrm{D},m}\phi_1} + \frac{\phi_{5,m}(\phi_{7,m})^2 e^{-\lambda_{\mathrm{D},m}\phi_1}}{4} \sum_{t=1}^{N} (-1)^t \binom{N}{t} t G_{1,3}^{3,1}\left( \frac{t\phi_{6,m}(\phi_{7,m})^2}{4} \middle| \begin{matrix} -1 & - & - \\ -1 & 0 & 0 \end{matrix} \right). \end{aligned} \tag{6.55}$$

#### 6.2.3.4 MAX-IP method

Because $\gamma_{\mathrm{B,J}_m}\gamma_{\mathrm{J}_m,\mathrm{E}} = \max\limits_{n=1,2,\ldots,N}\left(\gamma_{\mathrm{B,R}_{m,n}}\gamma_{\mathrm{R}_{m,n},\mathrm{E}}\right)$ (see (6.48)), using (6.32), CDF of $V_m^{\mathrm{MAX-IP}}$ can be obtained as

$$\begin{aligned} F_{V_m^{\mathrm{MAX-IP}}}(v) &= \Pr\left(\max_{n=1,2,\ldots,N}\left(\gamma_{\mathrm{B,R}_{m,n}}\gamma_{\mathrm{R}_{m,n},\mathrm{E}}\right) < v\right) = \left[\Pr\left(\gamma_{\mathrm{B,R}_{m,n}}\gamma_{\mathrm{R}_{m,n},\mathrm{E}} < x\right)\right]^N \\ &= \left[1 - \phi_{7,m}\sqrt{v}K_1\left(\phi_{7,m}\sqrt{v}\right)\right]^N. \end{aligned} \tag{6.56}$$

Substituting (6.56) into (6.46), an exact expression of $\mathrm{SOP}_m^{\mathrm{MAX-IP}}$ is given as

$$\mathrm{SOP}_m^{\mathrm{MAX-IP}} = 1 - e^{-\lambda_{\mathrm{D},m}\phi_1}\phi_{5,m}e^{-\lambda_{\mathrm{D},m}\phi_1}\int\limits_0^{+\infty}\frac{\left[1 - \phi_{7,m}\sqrt{v}K_1\left(\phi_{7,m}\sqrt{v}\right)\right]^N}{\left(\phi_{6,m}+v\right)^2}dv. \tag{6.57}$$

It is worth noting that the integral in (6.57) can be calculated by computer software such as MATLAB and MATHEMATICA. Moreover, we also attempt to derive a lower-bound closed-form expression for $\mathrm{SOP}_m^{\mathrm{MAX-IP}}$. At first, we have the following inequality:

$$V_m^{\mathrm{MAX-IP}} \le \max_{n=1,2,\ldots,N}\left(\gamma_{\mathrm{B,R}_{m,n}}\right)\max_{n=1,2,\ldots,N}\left(\gamma_{\mathrm{R}_{m,n},\mathrm{E}}\right) = W_{\mathrm{B,R}}^{\max}W_{\mathrm{R,E}}^{\max}, \tag{6.58}$$

where $W_{\mathrm{B,R}}^{\max} = \max\limits_{n=1,2,\ldots,N}\left(\gamma_{\mathrm{B,R}_{m,n}}\right)$, $W_{\mathrm{R,E}}^{\max} = \max\limits_{n=1,2,\ldots,N}\left(\gamma_{\mathrm{R}_{m,n},\mathrm{E}}\right)$.

Similar to (6.52), CDF of $W_{\mathrm{B,R}}^{\max}$ is obtained as

$$F_{W_{\mathrm{B,R}}^{\max}}(x) = 1 + \sum_{t=1}^{N}(-1)^t\binom{N}{t}e^{-t\lambda_{\mathrm{B},m}x}. \tag{6.59}$$

In addition, PDF of $W_{\mathrm{R,E}}^{\max}$ can be written by

$$\begin{aligned} f_{W_{\mathrm{R,E}}^{\max}}(y) &= \frac{\partial\left(1 - e^{-\lambda_{\mathrm{E},m+1}y}\right)^N}{\partial y} = N\lambda_{\mathrm{E},m+1}e^{-\lambda_{\mathrm{E},m+1}y}\left(1 - e^{-\lambda_{\mathrm{E},m+1}y}\right)^{N-1} \\ &= \sum_{r=0}^{N-1}(-1)^r N\binom{N-1}{r}\lambda_{\mathrm{E},m+1}e^{-(r+1)\lambda_{\mathrm{E},m+1}y}. \end{aligned} \tag{6.60}$$

Hence, if $W_m^{\mathrm{MAX-IP}} = W_{\mathrm{B,R}}^{\max}V_{\mathrm{R,E}}^{\max}$, using (6.59), (6.60) and [72, eq. (3.324.1)], CDF of $W_m^{\mathrm{MAX-IP}}$ is exactly computed as

$$\begin{aligned} F_{W_m^{\mathrm{MAX-IP}}}(v) &= \int_0^{+\infty}F_{W_{\mathrm{B,R}}^{\max}}\left(\frac{v}{y}\right)f_{V_{\mathrm{R,E}}^{\max}}(y)\,dy \\ &= 1 + \sum_{t=1}^{N}\sum_{r=0}^{N-1}(-1)^{t+r}N\binom{N}{t}\binom{N-1}{r}\sqrt{\frac{t}{r+1}}\phi_{7,m}\sqrt{v}K_1\left(\sqrt{t\left(r+1\right)}\phi_{7,m}\sqrt{v}\right). \end{aligned} \tag{6.61}$$

Combining (6.46), (6.58) and (6.61), $\mathrm{SOP}_m^{\mathrm{MAX-IP}}$ is bounded by a closed-form formula as

$$\begin{aligned}
&\mathrm{SOP}_m^{\mathrm{MAX-IP}} \geq 1 - \frac{\phi_{6,m} - \phi_{5,m}}{\phi_{6,m}} e^{-\lambda_{\mathrm{D},m}\phi_1} + \\
&\phi_{5,m} e^{-\lambda_{\mathrm{D},m}\phi_1} \sum_{t=1}^{N} \sum_{r=0}^{N-1} (-1)^{t+r} N \binom{N}{t} \binom{N-1}{r} \sqrt{\frac{t}{r+1}} \phi_{7,m} \int_0^{+\infty} \frac{\sqrt{v} K_1\left(\sqrt{t\,(r+1)}\phi_{7,m}\sqrt{v}\right)}{\left(\phi_{6,m}+v\right)^2} dv \\
&\geq 1 - \frac{\phi_{6,m} - \phi_{5,m}}{\phi_{6,m}} e^{-\lambda_{\mathrm{D},m}\phi_1} + \\
&\frac{\phi_{5,m}(\phi_{7,m})^2}{4} e^{-\lambda_{\mathrm{D},m}\phi_1} \sum_{t=1}^{N} \sum_{r=0}^{N-1} (-1)^{t+r} N t \binom{N}{t} \binom{N-1}{r} G_{1,3}^{3,1}\left( \frac{t\,(r+1)\,\phi_{6,m}(\phi_{7,m})^2}{4} \middle| \begin{matrix} -1 & - & - \\ -1 & 0 & 0 \end{matrix} \right).
\end{aligned} \tag{6.62}$$

#### 6.2.3.5 ALL-CJ method

In this method, it is impossible to find exact closed-form expression of $\mathrm{SOP}_m^{\mathrm{ALL-CJ}}$, which motivates us to find a lower-bound closed-form one. At first, we use the following inequality:

$$V_m^{\mathrm{ALL-CJ}} \leq \max_{n=1,2,\ldots,N} \left(\gamma_{\mathrm{B,R}_{m,n}}\right) \sum_{n=1}^{N} \gamma_{\mathrm{R}_{m,n},\mathrm{E}} = \underbrace{W_{\mathrm{B,R}}^{\max} W_{\mathrm{R,E}}^{\mathrm{sum}}}_{W_m^{\mathrm{ALL-CJ}}}, \tag{6.63}$$

where $W_{\mathrm{R,E}}^{\mathrm{sum}} = \sum_{n=1}^{N} \gamma_{\mathrm{R}_{m,n},\mathrm{E}}$ and $W_m^{\mathrm{ALL-CJ}} = W_{\mathrm{B,R}}^{\max} W_{\mathrm{R,E}}^{\mathrm{sum}}$. Moreover, because $W_{\mathrm{R,E}}^{\mathrm{sum}}$ is a summation of independent and identical exponential RVs, its PDF can be obtained by using [144, eq. (382)]:

$$f_{W_{\mathrm{R,E}}^{\mathrm{sum}}}(y) = \frac{\lambda_{\mathrm{E},m+1}^{N}}{(N-1)!} y^{N-1} \exp\left(-\lambda_{\mathrm{E},m+1} y\right). \tag{6.64}$$

Using (6.59) and (6.64), we can write CDF of $W_m^{\mathrm{ALL-CJ}}$ as

$$\begin{aligned}
F_{W_m^{\mathrm{ALL-CJ}}}(v) &= \int_0^{+\infty} F_{W_{\mathrm{B,R}}^{\max}}\left(\frac{v}{y}\right) f_{W_{\mathrm{R,E}}^{\mathrm{sum}}}(y)\, dy \\
&= 1 + \sum_{t=1}^{N} \frac{(-1)^t \binom{N}{t}}{(N-1)!} \lambda_{\mathrm{E},m+1}^{N} \int_0^{+\infty} y^{N-1} e^{-t\lambda_{\mathrm{B},m}\frac{v}{y}} e^{-\lambda_{\mathrm{E},m+1} y} dy.
\end{aligned} \tag{6.65}$$

Applying [72, eq. (3.471.9)] for the integral in (6.65), which yields

$$F_{W_m^{\mathrm{ALL-CJ}}}(v) = 1 + \sum_{t=1}^{N} \frac{(-1)^t \binom{N}{t}}{(N-1)!} \frac{t^{\frac{N}{2}}}{2^{N-1}} (\phi_{7,m})^N v^{\frac{N}{2}} K_N\left(\sqrt{t}\phi_{7,m}\sqrt{v}\right). \tag{6.66}$$

Combining (6.46), (6.63) and (6.66), $\mathrm{SOP}_m^{\mathrm{ALL-CJ}}$ can be bounded by a closed-form expression as

$$\begin{aligned}\mathrm{SOP}_m^{\mathrm{ALL-CJ}} &\geq 1-\frac{\phi_{6,m}-\phi_{5,m}}{\phi_{6,m}}e^{-\lambda_{\mathrm{D},m}\phi_1}\\ &\quad-\phi_{5,m}e^{-\lambda_{\mathrm{D},m}\phi_1}\sum_{t=1}^{N}\frac{(-1)^t\binom{N}{t}}{(N-1)!}\frac{t^{\frac{N}{2}}}{2^{N-1}}(\phi_{7,m})^N\int_0^{+\infty}\frac{v^{\frac{N}{2}}K_N\left(\sqrt{t}\phi_{7,m}\sqrt{v}\right)}{(\phi_{6,m}+v)^2}dv\\ &\geq 1-\frac{\phi_{6,m}-\phi_{5,m}}{\phi_{6,m}}e^{-\lambda_{\mathrm{D},m}\phi_1}\\ &\quad-\frac{\phi_{5,m}(\phi_{7,m})^N}{2^{N-2}}e^{-\lambda_{\mathrm{D},m}\phi_1}\sum_{t=1}^{N}\frac{(-1)^t\binom{N}{t}t^{\frac{N}{2}}}{(N-1)!}\int_0^{+\infty}\frac{x^{N+1}K_N\left(\sqrt{t}\phi_{7,m}x\right)}{(\phi_{6,m}+x^2)^2}dx. \end{aligned}\tag{6.67}$$

Again, using [72, eq. (6.565.7)] and [72, eq. (9.34.6)] for (6.67), we obtain

$$\begin{aligned}\mathrm{SOP}_m^{\mathrm{ALL-CJ}} &\geq 1-\frac{\phi_{6,m}-\phi_{5,m}}{\phi_{6,m}}e^{-\lambda_{\mathrm{D},m}\phi_1}-\frac{\phi_{5,m}}{2^{N+1}}(\phi_{6,m})^{\frac{N-1}{2}}(\phi_{7,m})^{N+1}e^{-\lambda_{\mathrm{D},m}\phi_1}\\ &\quad\times\sum_{t=1}^{N}(-1)^t\frac{\binom{N}{t}}{(N-1)!}t^{\frac{N+1}{2}}G_{1,3}^{3,1}\left(\frac{t\phi_{6,m}(\phi_{7,m})^2}{4}\middle|\begin{matrix}-\frac{N+1}{2} & - & -\\ -\frac{N+1}{2} & \frac{N-1}{2} & \frac{1-N}{2}\end{matrix}\right).\end{aligned}\tag{6.68}$$

**Remark 6.5** By substituting (6.51), (6.55), (6.57), (6.62), (6.68) into (6.37), we obtain exact or lower-bound closed-form expressions of the e2e SOP of the proposed protocols.

### 6.2.4 Simulation Results

This part provides Monte-Carlo simulations to validate the expressions derived above, and to compare the e2e SOP performance of the considered methods. Both simulation and analysis of theoretical results are carried out in MATLAB. In each simulation, $5*10^5-10^6$ trials are realized, where Rayleigh fading channel coefficients of the links are generated. For the theoretical results, the derived formulas are used to illustrate.

In the simulation environment, the nodes in the $m^{th}$ cluster are assumed to locate at the same co-ordinate, i.e., $(m/M, 0)$. Hence, the positions of the source and the destination are (0,0) and (1,0), respectively, and the link distance between two adjacent clusters is $d_{\mathrm{T}_{m-1},\mathrm{T}_m}=1/M$, where $m=0,1,...,M$. For the nodes B and E, their positions are $(x_{\mathrm{B}},y_{\mathrm{B}})$ and $(x_{\mathrm{E}},y_{\mathrm{E}})$, respectively. To focus on the impact of the system parameters, i.e., the number of hops ($M$), EH time-switching factor ($\alpha$), the number of nodes in each cluster ($N$), on the e2e secrecy performance, we fix the energy conversion efficiency ($\eta$) by 0.2, the total delay time ($L$) by 1, the path-loss exponential ($\theta$) by 3, the target rate ($C_{\mathrm{th}}$) by 1, the co-ordinates of B by $x_{\mathrm{B}}=0.5$, $y_{\mathrm{B}}=-0.2$. Moreover, the transmit SNRs $\Delta$ and $\Lambda$ are set to be identical in the simulations, i.e., $\Delta=\Lambda$. It is worth noting that the derived expressions in part 6.2.3 can be used for any values of the system

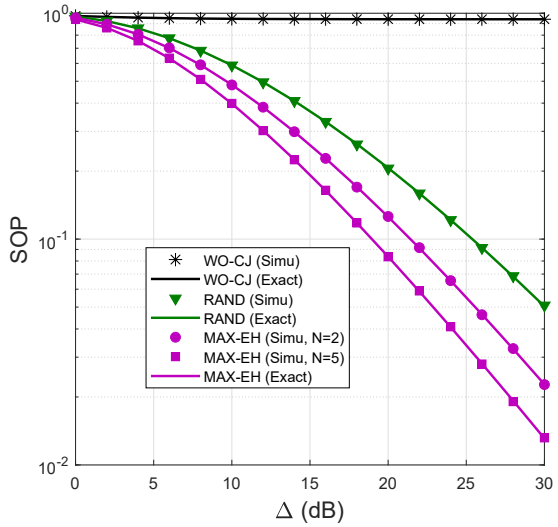


(a) MAX-EH, RAND, and WO-CJ

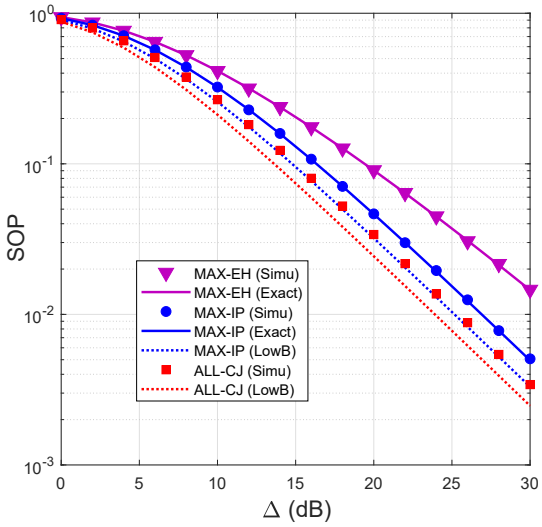


(b) MAX-EH, MAX-IP, and ALL-CJ

Figure 6.7: E2e SOP as a function of $\Delta$ (dB) when $M = 3$, $\alpha = 0.25$, $x_{\mathrm{E}} = y_{\mathrm{E}} = 0.5$.

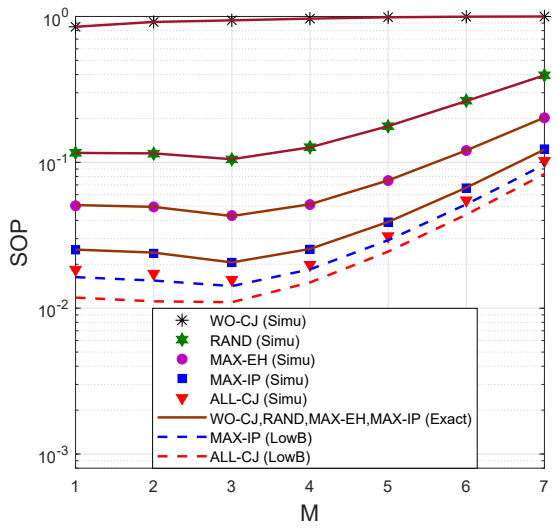


(a) As a function of number of hops

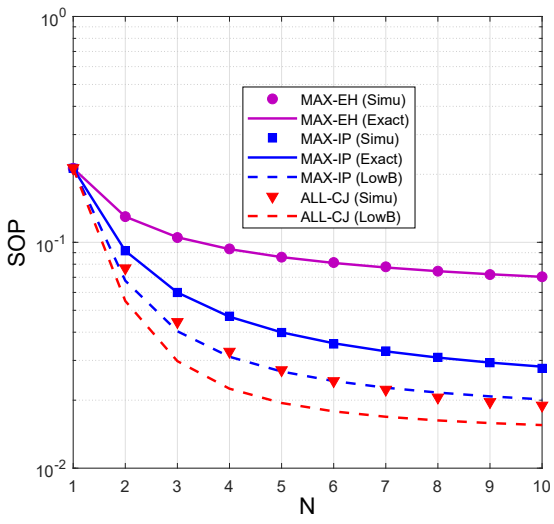


(b) As a function of number of nodes in a cluster

Figure 6.8: E2e SOP as a function of number of hops and number of nodes in a cluster when $\Delta$ = 20 (dB), $M = 3$, $\alpha = 0.2$, $x_{\mathrm{E}} = y_{\mathrm{E}} = 0.5$.

parameters. Moreover, it can be expected that the system performance is better with higher energy conversion efficiency, lower target rate or shorter distance between B and the nodes in the clusters.

In Fig. 6.7, we compare the e2e SOP of WO-CJ, RAND, MAX-EH, MAX-IP, and ALL-CJ when $M = 3$, $\alpha = 0.25$, and $x_{\mathrm{E}} = y_{\mathrm{E}} = 0.5$. As we can see, the secrecy performance of RAND,

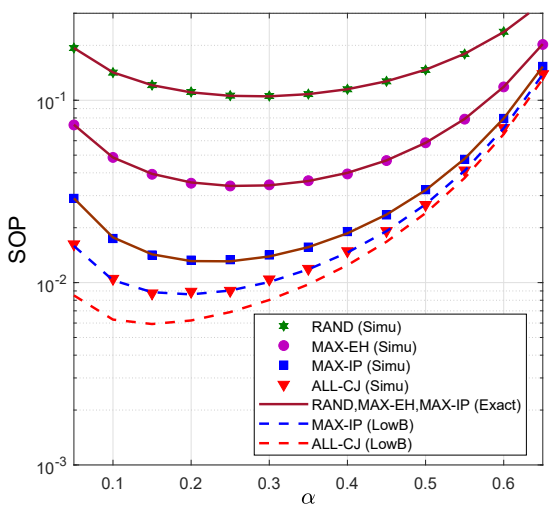


(a) As a function of $\alpha$ when $x_{\mathrm{E}} = y_{\mathrm{E}} = 0.5$.

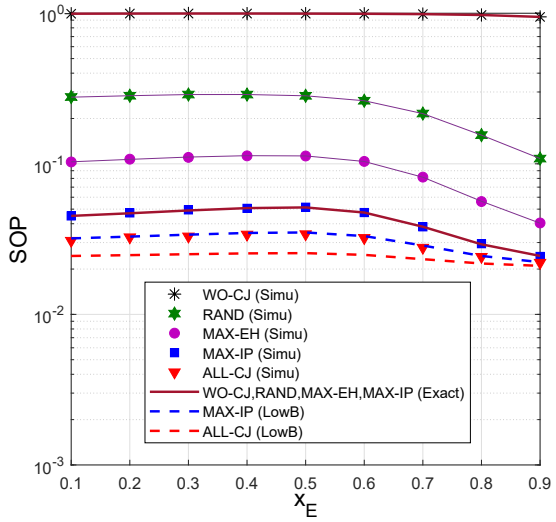


(b) As a function of location $x_E$ of eavesdropper when $\alpha = 0.3$, $y_{\mathrm{E}} = 0.3$.

Figure 6.9: E2e SOP as a function of $\alpha$ and location of eavesdropper.

MAX-EH is much better than that of WO-CJ due to the usage of the CJ technique. It can be observed that the e2e SOP of RAND and MAX-EH decreases with the increasing of $\Delta$, while the e2e SOP of WO-CJ converges to a constant as $\Delta$ is high enough. Indeed, from (6.35), we can obtain

$$\mathrm{SC}_m^{\mathrm{WO-CJ}} \overset{\Delta \to +\infty}{\to} \left[\tau \log_2 \left(\frac{\gamma_{\mathrm{T}_{m-1},\mathrm{T}_m}}{\gamma_{\mathrm{T}_{m-1},\mathrm{E}}}\right)\right]^+. \tag{6.69}$$

We can observe from (6.69) that at high $\Delta$ values, $\mathrm{SC}_m^{\mathrm{WO-CJ}}$ does not depend on $\Delta$, and this is the reason why the e2e SOP of WO-CJ does not depend on $\Delta$ when $\Delta \to +\infty$. We also see from Fig. 6.7a that the e2e SOP of MAX-EH is lower than that of RAND for all $N$ values. It is worth noting that because of the random jammer selection, the secrecy performance of RAND does not depend on $N$. For MAX-EH, the value of SOP is lower with high number of cluster node ($N$). Fig. 6.7b presents the e2e SOP of MAX-EH, MAX-IP and ALL-CJ as a function of $\Delta$ in dB when $M = 3$, $N = 4$, $\alpha = 0.25$, and $x_{\mathrm{E}} = y_{\mathrm{E}} = 0.5$. This figure shows that ALL-CJ obtains the best performance, while the performance of MAX-IP is between those of ALL-CJ and MAX-EH. However, as discussed above, the implementation of ALL-CJ is very complex because it requires a lot of overhead, energy and delay time.

Fig. 6.8 studies the impact of the number of hops ($M$) and number of nodes in a cluster ($N$) on the e2e SOP of all of the considered methods when $\Delta = 25$ (dB), $N = 3$, $\alpha = 0.3$, and $x_{\mathrm{E}} = y_{\mathrm{E}} = 0.5$. As seen in Fig. 6.8a, the e2e SOP of WO-CJ is very high, and increases with the increasing of $M$. We can see that the e2e SOP of WO-CJ almost equals to 1 as $M \geq 4$.

For the proposed CJ methods, the e2e SOP obtains the lowest value when $M = 3$, and rapidly increase when $M$ ($M > 3$) increases. In Fig. 6.8b, we see that the values of $N$ does not affect on the secrecy performance of WO-CJ and RAND. As expected, we can see from Fig. 6.8b that the secrecy performance of MAX-EH, MAX-IP and ALL-CJ is better when increasing the number of nodes in each cluster. It is also seen that the performance gap between MAP-IP (ALL-CJ) and MAX-EH increases with higher value of $N$.

In Fig. 6.9a, we study the impact of the fraction $\alpha$ on the e2e SOP of the proposed methods when $\Delta = 25$ (dB), $M = 3$, $N = 5$, and $x_{\mathrm{E}} = y_{\mathrm{E}} = 0.5$. As we can see from Fig. 6.9a, there exist an optimal value of $\alpha$ so that the e2e SOP of RAND, MAX-EH, MAX-IP and ALL-CJ is lowest. Hence, $\alpha$ is important parameter which should be designed appropriately to optimize the system performance. In Fig. 6.9b, we change position of the eavesdropper by fixing $y_{\mathrm{E}} = 0.3$, and changing $x_{\mathrm{E}}$ from 0.1 to 0.9. The remaining parameters are set by $\Delta = 20$ (dB), $M = 3$, $N = 7$, and $\alpha = 0.3$. As observed, the e2e SOP of all of the methods vary, follows the position of the E nodes. We also see that when $x_{\mathrm{E}}$ is about 0.5, the secrecy performance of the considered methods is highest.

Finally, we see that in all figures the simulation results (Simu) match very well with the theoretical ones (Exact), which validates our derived expressions of the e2e SOP of WO-CJ, RAND and MAX-EH.

### 6.2.5 Conclusion

In this section, we proposed EH based jammer selection methods where the selected jammer(s) has to harvest wireless energy from a power beacon to generate jamming noises. The secrecy performance of the proposed methods was evaluated via both simulations and analyzes, in terms of the e2e SOP. The results showed that the proposed methods outperform the corresponding method without using the cooperative jamming technique and the random jammer selection technique. Moreover, the number of hops, the number of cluster nodes, and the fraction of time used for the EH operation significantly affect the secrecy performance, and should be appropriately designed to optimize the system performance.

# 7 Integrate energy harvesting together with other advanced techniques to further strengthen network security and reliability

To complete the third goal of the dissertation, I plan to recommend an advanced model that combine PLS and RF EH protocol. In particular, I introduce a two-way HD relaying network that employ hybrid TPSR EH protocol at relay nodes in the presence of eavesdroppers near one of the sources. To enhance both security and reliability, I integrate relay selection technique in this system and exploit the help of friendly jammers.

In recent years, PLS has been considered as an effective method to enhance the information security beside the cryptographic techniques that are used in upper layers. In this section, we provide the security analysis for a two-way HD relay network, where the two sources can only communicate through the intermediate relay nodes. In particular, we consider the scenario that there is an eavesdropper in the vicinity of one source node. Both reliability and security aspects are taken into consideration in our work. To enhance the reliability of communication, the intermediate relays are supplied with the energy harvested from the sources' RF signals using hybrid TPSR protocol. Also, we apply the relay selection technique to select the best relay for the information exchange between two sources. Regarding security, the secrecy of information is improved with the help of friendly jammers nearby the eavesdropper. [HDH01], [HDH05], [HDH13].

## 7.1 Introduction

Secrecy is always a critical issue in wireless communications because of the information leakage resulting from the broadcast nature of the wireless medium. It leaves unprotected information vulnerable. Besides conventional cryptographic techniques to improve the security, the pioneering work by Wyner [58] on the wiretap channel and subsequent works [59], [60] show that the secrecy can also be guaranteed along with reliability by introducing randomness in coding or signaling to confuse the eavesdropper at the physical layer. This is known as physical layer security (PLS). During the last decade, PLS has experienced a resurgence of interest from a lot of scientists [61] due to its potential to enhance the quality of communication to satisfy the vast demand of mobile users. PLS has been applied in relay networks [172], cellular networks [173], [174], cognitive radio networks [138], IoT networks [175], and massive MIMO networks [176]. In multi-user networks, PLS can be improved by node cooperation. Relay nodes can actively relay the source signal - cooperative relay (CR) or passively jam the eavesdropper - cooperative jamming (CJ).

In CR scheme, relay not only listens and forwards messages from the source to the destination, but also prevent the information from leaking to eavesdroppers [25], [172]. For example, in [172], the authors proposed a generalized multi-relay selection scheme to improve the security in a cooperative relay network. They derived a semi-closed-form expression of the SOP and

jointly optimize the power allocation factor and the number of relay to minimize the SOP. On the other hand, relays in the CJ scheme do not only forward the messages from the source to the destinations, but also generate signals to interfere with the eavesdroppers. CJ scheme includes artificial-noise (AN) and noise forwarding (NF) schemes. In AN scheme, the cooperative jammers generate Gaussian AN to interfere with the eavesdropper such as in [177], [178]. In [178], the authors conceived an AN aided two-way opportunistic relay selection scheme for enhancing the security of a two-way multiple-relay network. For NF scheme, the helpers can send dummy codewords which are independent of the source messages and can be decoded reliably at the destination [179]. Later, Chiang and Lehnert [180] jointly designed the optimal co-variance matrices of the multiple-antenna signals at the source and helper to maximize the secrecy rate of the NF scheme. Recently, Lee and Khisti [181] exploited a NF scheme to establish the secure degrees of-freedom of the Gaussian diamond-wiretap channel with rate-limited relay cooperation, where the eavesdropper not only listens the relay transmission but also wiretaps some of communication links among relays.

The concept of EH, that represents the direct using of available energy in the surroundings through energy conversion from a given physical domain into electricity, has been raised a decade ago and is now an intensive research and application field [182]. In fact, the main focus for wireless networks has been shifted from spectral efficiency and QoS constraints to energy efficiency and green communication [183], especially in the fifth generation (5G) and sixth generation (6G) networks to reduce the power consumption [184]. EH from RF signals has emerged as a promising solution and attracted a lot of attention in recent years, especially because RF signals can be utilized for both energy and information transmission simultaneously. This idea was first raised in the seminal paper of Varshney in 2008 [12]. Nasir [6], [14] has significantly contributed to the development of RF EH. He introduced two practical protocol for RF EH in relay networks, namely TSR and PSR protocols and derived the analytical expression for key performance factors of these protocols. Later, the hybrid time-switching and power-splitting (TPSR) protocol was introduced and its performance was evaluated in [127]. In 2020, Ngo et al. [185] analyzed a two-hop single-relay networks using hybrid TPSR EH protocol in the presence of an eavesdropper near the relay. The authors have derived the closed-form expressions of OP and intercept probability in their model.

Two-way relay channel (TWRC), in which two users exchange their messages with each other, has long been a typical model to study the performance of novel communication methods, protocols, or algorithms, including the wireless EH technique, for several decades. The classical two-way communication channel was first presented in the seminal paper of Shannon [186] in 1961. During the fist decade of this century, research on TWRC has been resurged by the paper of [187] and since then has drawn much research attention again. In 2006, Katti et al. [188] proposed the digital network coding scheme for TWRC, in which the relay decodes the packets from different sources separately and broadcasts the XOR-ed version of them to both sources and saves one transmission time slot. Then in 2007, Katti et al. [189] again presented and

analog network coding, in which the relays can receives signals from both source simultaneously and then broadcasts the sum of two signals back to the sources. This method even improve the throughput of TWRC compared to digital network coding by saving one more time slot of the communication. These two network coding techniques have been the main focus of TWRC for last decade. With the advance research of TWRC, the PLS in spectrally-efficient TWR networks has been extensively researched in the literature [173], [174]. In particular, Shukla [174] and Pandey [173] investigated the secrecy outage performance of a FD cellular multi-user two-way AF relay network, where a multi-antenna base station using transmit antennas selection communicates with one of the several users by the assistance of a relay in the presence of a passive eavesdropper that employs maximal ratio combining.

Naturally, the application of wireless EH via RF signals in TWCN have been well studied. In 2015, the authors in [190] proposed and analyzed the EH transmission strategies for TWRC to maximize the sum-throughput of the system. In [191], the authors analyzed the performance of a wireless-powered communication network, in which a multiple-antenna two-way AF relay transfers power to multi-pair of single antenna users and then helps the users exchange their data. Zhou and Li [97] provided a jointly optimal design of relay precoding matrices and PS ration to maximize the energy efficiency for SWIPT in MIMO two-way AF relay networks, where the relay harvests energy from both sources to forward sources messages. An adaptive EH protocol for two-way AF relay network over the Rician fading environment was also introduced in [78]. On the other hand, partial relay selection (PRS) has been selected as a simple but effective method to enhance the reliability of data transmission at the cooperative phase in EH-based two-way relay networks, such as in [74].

To the best of our knowledge, the study of PLS in RF EH-based networks have not been investigated much in literature. The most recent results of PLS in EH-based networks [185], which was published in early 2020, only considered a simple relay network with single relay. Motivated by these above facts, in this chapter I provide a thorough analysis on the reliability and security performance of a two-way relay networks using the hybrid TPSR EH protocol and PRS in the presence of an eavesdropper near one of the source nodes.

The main contributions of this chapter are summarized as follows:

- We derive the closed-form and semi-closed form expressions of key performance factors for our proposed model, including the OP of the legitimate communications, the intercept probability of the eavesdropper (IP), the secrecy outage probability of the system (SOP), and the average secrecy capacity (ASC). In fact, this is a challenging problem because the probability analysis involves a lot of RVs, which makes the derivation more complicated.

- This work also provides an insightful analysis of the effect of various system parameters on the reliability and security performance. It is worth to notice that there should be optimal values of the EH parameters like time-switching factor and PS factor for each relay and jammer configuration. It's also concluded from the analysis that increasing the number

of available relay nodes can improve the overall performance better than increasing the number of jammer, except for very high values of transmit power.

- Finally, the Monte Carlo simulations are also conducted to verify the correctness of our analysis and the effectiveness of the proposed scheme. From numerical results, we provide the recommendation on selecting the configurations and appropriate values of system parameters to obtain the reliable and secure transmission without paying too much for the complexity of the system.

## 7.2 System Model

### 7.2.1 Energy harvesting and scheduling protocols

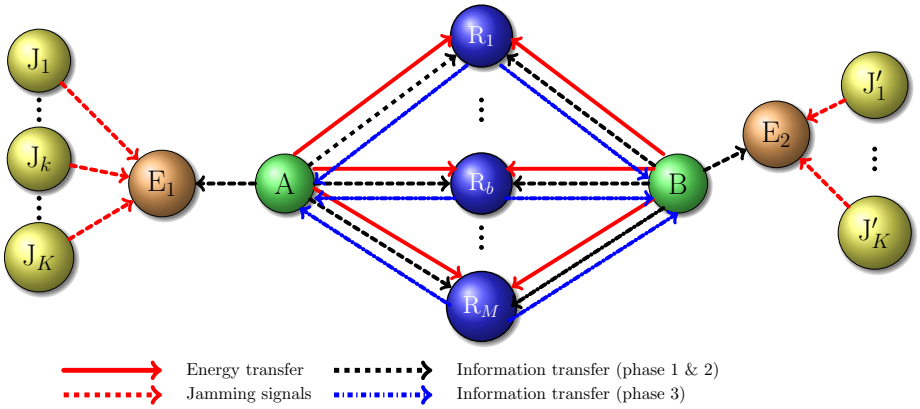


Figure 7.1: System model of the proposed EH scheme.

Our proposed system model is illustrated by Fig. 7.1. Here, we consider a multiple-relay ($M$ relay nodes) two-way relay networks, in which the relay nodes are equipped with RF EH capability and help two sources A and B exchange their information. The relay nodes are assumed to be located in a cluster, that means the distances from every available relay nodes to a source node are approximately the same. This assumption is reasonable in practice, especially for IoT device networks or wireless sensor networks. PRS is applied in our model, where only the relay with best channel to the source (without loss of generality, we consider the best channel gain to the source A) is selected. All nodes in this model are single-antenna devices and operates on HD mode. For EH protocol, we apply the hybrid time-switching and power-splitting (TPSR) protocol [127], [192], [193] (see Fig. 7.2). In this protocol, the information exchange between two source nodes is accomplished after three distinct phases using DF relaying strategy. For the first two phases, the sources A and B take turns to broadcast their messages, say $x_1$ and $x_2$, respectively, to the relay and the other source. The relay node uses a power divider to split the received signal in each source into two portions: the first portion is used to extracted the energy and stored at the relay, whereas the second portion of the signal is used for decoding the

information message. We denote $\beta$, with $0 < \beta < 1$, as the PS factor. Then in the final phase, the relay combines two message (using XOR operator) and broadcasts this XOR-ed message $x_{\oplus} = x_1 \oplus x_2$ to both sources. Now, each source, with knowledge about its own message, can retrieve the desired message sent to it. We assume that the direct link between two sources is not available for communicating due to long distance and obstacles in surroundings such as buildings or mountains. For simplicity but without loss of practicality, the PS factors for both sources' signals are set to be equal to each other. In addition, the duration of Phase 1 and Phase 2 are assumed to be the same, which is equal to $\alpha T$, where $T$ is the total duration of a single transmission block and $0 < \alpha < 0.5$ is the TS factor.

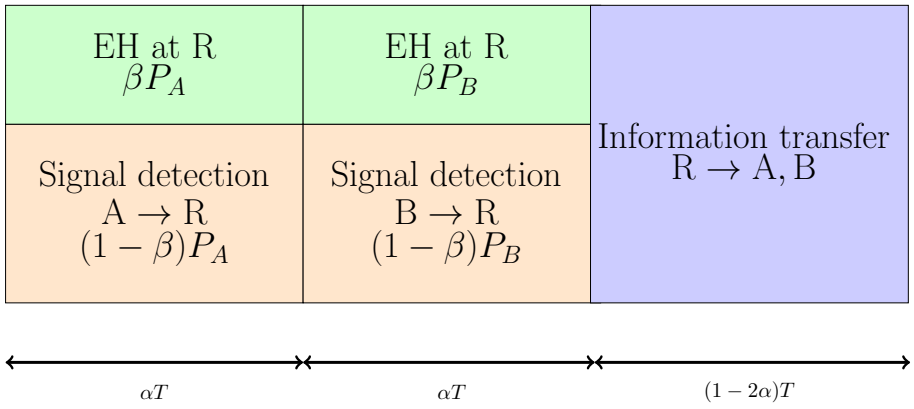


Figure 7.2: EH and scheduling protocol for the proposed model.

Regarding the eavesdropping strategy, we intend to adopt a single eavesdropper near each source to retrieve the information transmitted by that source, i.e. an eavesdropper $E_1$ in the vicinity of the source A and an eavesdropper $E_2$ in the vicinity of the source B. In fact, eavesdropping strategy may involve multiple eavesdroppers, however, more eavesdroppers require higher cost and higher probability of being detected. Regarding the position of eavesdropper, many scenarios may be employed in practice: near the source(s) [194] or in the middle of the communication link [195]. For two-way communications, the analysis in [196] confirmed that the eavesdropper has a better chance to eavesdrop the message when it is close to one of the transmitters. Furthermore, in practical applications such as in military or IoT sensor networks, the relay node is not fixed, but can be changed among available nodes between source and destination. Therefore, locating the eavesdropper near one relay node may not be reasonable. To conclude, our eavesdropping strategy are totally applicable in practice, especially in military communications, where the eavesdropper is usually put near each command center.

The eavesdropper $E_1$ tries to retrieves the information sent from A to any other node. Because E is close to A, it is assumed that the direct link from the source B to E is not available either. Therefore, even if it can receive the signal from a relay node, it cannot remove the message sent by B from the received signal. That means the signal received from the relay

node is not useful for the eavesdropper. Similarly, the eavesdropper $E_1$ tries to retrieves the information sent by B. To enhance the security of communications, many friendly jammers are used to suppress the received signal at the eavesdropper. In particulars, when A broadcasts its message, the jammers also transmits the artificial noise to the eavesdropper. This artificial noise is known by the relay nodes, so we can ignore any negative effect caused by this signal to the relay nodes. [HDH01].

Now we are going through the mathematical representation of the entire process. First, the source A uses the first time slot to send its packet to both relay and the second source B. The received signal at the relay $R$ and the source $S_2$ can be expressed, respectively, as

$$y_{A,R_i} = h_{A,R_i} x_A + n_{r_i}^{(1)}, \tag{7.1}$$

where $E\{|x_A|^2\} = P_A$ ($P_A$ represents the average transmit power at A), $n_{r_i}^{(1)}$ denotes the zero-mean AWGN with variances $N_0$.

In the second time slot, B transmits $x_2$ to the relay nodes $R_i$. Therefore, the received signals at the relay $R_i$ can be expressed as

$$y_{B,R_i} = h_{B,R_i} x_A + n_{r_i}^{(2)}, \tag{7.2}$$

where $E\{|x_2|^2\} = P_2$ is the average transmit power at the $S_2$, $n_{r_i}^{(2)}$ is zero-mean AWGN with variance $N_0$.

Using the same approach as in (2.9) in Section 4.2, the average transmit power of the relay node during the third time slot can be given as

$$P_{R_i} = \frac{E_R}{T(1-2\alpha)} = \frac{\eta\beta\alpha TP\left(|h_{AR_i}|^2 + |h_{BR_i}|^2\right)}{T(1-2\alpha)} = \kappa P\left(|h_{AR_i}|^2 + |h_{BR_i}|^2\right), \tag{7.3}$$

where $\kappa \triangleq \frac{\eta\beta\alpha}{1-2\alpha}$, $0 < \eta \leq 1$ is the effective energy conversion efficiency (which takes into account the energy loss by harvesting circuits and also by decoding and processing circuits). For simplicity, we assume that the average transmit powers from sources $S_1$ and $S_2$ are both equal to $P$.

The signals received at $R_i$ from A and B will be decoded and re-encoded by using the network coding scheme [197]. Let $\hat{x}_A$ and $\hat{x}_B$ denote the decoded messages from A and B, respectively. Then during the third time slot, the relay uses its power $P_{R_i}$ to broadcast the exclusive-OR of the decoded message $x_{R_i} = \hat{x}_A \oplus \hat{x}_B$ to both sources A and B. The received signals at A and B can be expressed, respectively, as

$$\begin{aligned} y_A &= h_{R_iA} x_{R_i} + n_A, \\ y_B &= h_{R_iB} x_{R_i} + n_B, \end{aligned} \tag{7.4}$$

where $\mathrm{E}\left\{|x_{R_i}|^2\right\} = P_{R_i}$; $n_A$ and $n_B$ are i.i.d. AWGN noise terms, which have zero mean and variance of $N_0$.

From (7.1) and (7.2), the received SNRs at the relay for decoding the messages $x_A$ and $x_B$ can be obtained respectively as

$$\gamma_{AR_i} = \frac{(1-\beta)|h_{AR_i}|^2 P}{N_0} = (1-\beta)|h_{AR_i}|^2 \Psi, \tag{7.5}$$

$$\gamma_{BR_i} = \frac{(1-\beta)|h_{BR_i}|^2 P}{N_0} = (1-\beta)|h_{BR_i}|^2 \Psi, \tag{7.6}$$

where $\Psi \triangleq \frac{P}{N_0}$ is the transmit-signal-power-to-noise-ratio. In this section, we assume that the channels are reciprocal, so $h_{BR_i} = h_{R_iB}$ and $h_{AR_i} = h_{R_iA}$.

During the third phase, the source nodes A and B need to decode successfully the received signal from the relay $\mathrm{R}_i$, then with the knowledge on its transmitted message, it can recover the message sent by the other source. Without loss of generality, we can only consider the decoding performance at the source B. The SNR at this node during the third time-slot can be calculated as

$$\gamma_{R_iB} = \frac{|h_{R_iB}|^2 P_R}{N_0} = \frac{\kappa P \left(|h_{AR_i}|^2 + |h_{BR_i}|^2\right)|h_{R_iB}|^2}{N_0} = \kappa\Psi \left(|h_{AR_i}|^2 + |h_{BR_i}|^2\right)|h_{R_iB}|^2. \tag{7.7}$$

For the DF relaying strategy at the relay, there is a minor modification from the traditional protocol because digital network coding is used in this case. Specifically, the transmit message from the relay node during the third phase of transmission block should depend on the decoding results of $x_1$ and $x_2$ in the previous two phases. There are three possible situations as follows:

(1) The relay successfully decodes both $x_1$ and $x_2$ in the first two phases, then it will broadcast the message $x_1 \oplus x_2$ during the third phase.

(2) The relay decodes $x_2$ successfully but not $x_1$. In this case, it only broadcasts $x_1$ during the third phase without applying XOR operation.

(3) the relay cannot decode neither $x_1$ nor $x_2$, then no message is broadcasted in the third phase and the communication fails.

For both cases (1) and (2), both links from A to R and from R to B must be good to ensure the communication by the relayed path. Therefore, the equivalent signal-to-noise ratio (SNR) computed at the source B can be obtained as

$$\gamma_{DF} = \min\left\{\gamma_{AR_i}, \gamma_{R_iB}\right\} = \Psi \min\left\{(1-\beta)|h_{AR_i}|^2, \kappa\left(|h_{AR_i}|^2 + |h_{BR_i}|^2\right)|h_{R_iB}|^2\right\}. \tag{7.8}$$

Now, let's consider the received signal at the eavesdroppers. For simplicity, we only consider the eavesdropper at A because of two reasons: (1) two eavesdroppers at A and B cannot communicate together due to the long distance, so their operations are independent; (2) the roles of

these two eavesdroppers are similar, so the intercept probability analysis for one eavesdropper can be found by exchanging A and B in the analysis for the other. The eavesdropper $E_1$ tries to overhear the signals transmitted by A during the first phase of our communication protocol. However, during this phase, it also receives the artificial noises from the $K$ jammers ($J_k$, for $k = 1, 2, ..., K$). It should be noted that we don't consider the overhearing of signal from the relay during the broadcasting phase (third time slot) because the message sent by the relay is a combination of messages from A and B. Without knowledge of the message from B (it's too far to eavesdrop from B), the information from relay is just useless to the eavesdropper (the signal from the relay nodes during phase 3 is only useful for retrieving the message from B, but for that purpose, the eavesdropper near B, i.e. $E_2$, should do better). As a result, the eavesdropper must rely on the received signal during phase 1, which can be expressed as

$$y_E = h_{AE}x_s + \sum_{k=1}^{K} h_{J_kE}x_k + n_E, \tag{7.9}$$

where $x_s$ is the message transmitted by A; $x_k$ is the artificial noise transmitted by the jammer $J_k$, which satisfies $E(|x_k|^2) = P_J$ is the transmit power of each jammer; and $n_E$ is the AWGN noise at E, which has zero mean and variance of $N_0$.

From (7.9), it is easy to derive the received signal-to-interference-and-noise ratio SINR at the eavesdropper:

$$\gamma_E = \frac{P_s|h_{AE}|^2}{\sum\limits_{k=0}^{K} |h_{J_kE}|^2 P_J + N_0} = \frac{\Psi|h_{AE}|^2}{\sum\limits_{k=1}^{K} |h_{J_kE}|^2 \Psi_J + 1}, \tag{7.10}$$

where $\Psi_J \triangleq \frac{P_J}{N_0}$.

Assume that the channels between two arbitrary nodes are block Rayleigh fading [6], [14], [191], [198], where channel coefficients remain constant during one transmission block and change independently across different transmission blocks. Therefore, the channel power gains $X_i = |h_{AR_i}|^2 = |h_{R_iA}|^2$, $Y_i = |h_{BR_i}|^2 = |h_{R_iB}|^2$, $Z = |h_{AE}|^2$, and $T = |h_{J_kE}|^2$ are independent exponential RVs whose PDF and CDFs has the following form:

$$f_U(u) = \begin{cases} \lambda e^{-\lambda_u u} & \text{if } x \geq 0 \\ 0 & \text{if } x < 0 \end{cases} \tag{7.11}$$

$$F_U(u) = 1 - e^{-\lambda_u u}, \tag{7.12}$$

where $U \in \{X_i, Y_i, Z, T\}$ and $\lambda_u \in \{\lambda_1, \lambda_2, \lambda_3, \lambda_4\}$, correspondingly ($\lambda_u$ is the mean of the exponential RV $U$). To take path-loss into account, we can model these parameters as $\lambda_1 = d^{\theta}_{AR_i}$, $\lambda_2 = d^{\theta}_{BR_i}$, $\lambda_3 = d^{\theta}_{AE}$, and $\lambda_4 = d^{\theta}_{J_kE}$. Here, $d_{AR_i}, d_{BR_i}, d_{AE}$ and $d_{J_kE}$ are the link distances of

the $\mathrm{A} \to \mathrm{R}_i, \mathrm{B} \to \mathrm{R_i}, \mathrm{A} \to \mathrm{E}$ and $\mathrm{E} \to \mathrm{J}_k$, respectively, and $\theta$ is the path-loss exponent whose value may range from 2 to 6. For simplicity, we assume that all jammers are at approximately equal distance to the eavesdropper. Similarly, all relay nodes belong to a cluster such that the distances from each source to all relay nodes are approximately the same.

### 7.2.2 Partial relay selection

In our system, we apply the partial relay selection (PRS) method[1] to enhance the quality of communication. It means that the cooperative relay can be selected among $M$ relay nodes by the following criterion:

$$R_b = \underset{\{R_i : i=\overline{1,M}\}}{\arg\max} |h_{AR_i}|^2. \tag{7.13}$$

In other words, the relay which provides the highest channel gain between itself and A in the third time slot is selected for the cooperative communications.

**Remark 7.1** In PRS protocol, it will require the channel sate information (CSI) between A and the relay nodes. In practice, A can estimate CSI via local control message and hence it can be easily determine the best candidate as in (7.13). Moreover, it is worth noting that without loss of generality, we assume $d_1 > d_2$, so the relay selection should be performed based on the quality of the first-hop links to enhance the overall performance.

According to the result from the paper [112], the CDF and PDF of $X = |h_{AR_b}|^2$ can be given by

$$F_X(x) = \sum_{j=0}^{M} (-1)^j \binom{M}{j} e^{-j\lambda_1 x} \tag{7.14}$$

and

$$f_X(x) = \lambda_1 \sum_{j=0}^{M-1} (-1)^j \binom{M-1}{j} e^{-(j+1)\lambda_1 x}. \tag{7.15}$$

## 7.3 Performance Analysis

In this part, we derive the key performance factors of our proposed system, including OP, IP, SOP and the average secrecy capacity (ASC) of the system.

[1] Another selection method is optimal relay selection (ORS), in which the relay that maximizes the secrecy capacity is selected. ORS can provide better performance, but we consider PRS here because its simplicity to implement.

### 7.3.1 Outage probability

First, we have the achievable data rate of the legitimate communication link A $\rightarrow$ B and the eavesdropper link given respectively as

$$C_B = (1-\alpha)\log_2\left(1+\gamma_{DF}\right), \tag{7.16}$$

$$C_E = (1-\alpha)\log_2\left(1+\gamma_E\right), \tag{7.17}$$

where $\gamma_{DF}$ is given by (7.8).

Assume that the relay node $\mathrm{R}_b$ is selected for the cooperative communications and let $X = |h_{AR_b}|^2, Y = |h_{BR_i}|^2$, then we can rewrite the equivalent SNR at the receiver B as

$$\gamma_{DF} = \min\left\{(1-\beta)X\Psi, \kappa\Psi\left(X+Y\right)Y\right\}. \tag{7.18}$$

The OP occurs when the data rate of the system exceeds the achievable data rate of the link, i.e. $C_B < R$, where $R$ is the data transmission rate. Therefore, it can be expressed as

$$\mathrm{OP} = \Pr\left\{\mathrm{C_B} < \mathrm{R}\right\} = \Pr\left\{\min\left\{(1-\beta)\Psi\mathrm{X}, \kappa\Psi\left(\mathrm{X}+\mathrm{Y}\right)\mathrm{Y}\right\} < \gamma_{\mathrm{th}}\right\} \tag{7.19}$$

where $\gamma_{th} \triangleq 2^{\frac{R}{(1-\alpha)}} - 1$ is the SNR threshold of B, which is the solution of the equation $C_B = R$.

Now we can state the Theorem 7.1 on the OP of our proposed system as follows.

**Theorem 7.1** *The* OP *of the proposed two-way relay networks with partial relay selection and power-splitting EH at relay nodes can be found as*

$$\begin{aligned}\mathrm{OP} = 1 &+ \sum_{j=1}^{M}(-1)^j\binom{M}{j}e^{-j\lambda_1\frac{\gamma_{th}}{(1-\beta)\Psi}-\lambda_2\xi} + \sum_{n=0}^{\infty}\sum_{j=1}^{M}\frac{(-1)^j(j\lambda_1-\lambda_2)^n(j\lambda_1\gamma_{th})^{n+1}\lambda_2}{n!\left(\kappa\Psi\right)^{n+1}}\binom{M}{j} \\ &\times\Gamma\left(-n-1, \frac{j\lambda_1\gamma_{th}}{\kappa\Psi\xi}\right).\end{aligned} \tag{7.20}$$

*where $M$ is the number of available relay nodes, $\gamma_{th}$ is the* SNR *threshold of receiver, $\kappa \triangleq \frac{\eta\beta\alpha}{1-2\alpha}$, $\Psi \triangleq \frac{P}{N_0}$, $\xi = \frac{1}{2}\left[\sqrt{\frac{\gamma_{th}^2}{(1-\beta)^2\Psi^2} + \frac{4\gamma_{th}}{\kappa\Psi}} - \frac{\gamma_{th}}{(1-\beta)\Psi}\right]$, and $\Gamma(s,x) \triangleq \int_x^{\infty} t^{s-1}e^{(}-t)dt$ is the incomplete Gamma function.*

**Proof** We can rewrite the equation (7.19) as

$$\begin{aligned}\mathrm{OP} &= \Pr\left\{\min\left\{(1-\beta)\Psi X, \kappa\Psi\left(X+Y\right)Y\right\} < \gamma_{th}\right\} = 1 - \Pr\left\{(1-\beta)\Psi X \geq \gamma_{th}, \kappa\Psi\left(X+Y\right)Y \geq \gamma_{th}\right\} \\ &= 1 - \Pr\left\{X \geq \frac{\gamma_{th}}{(1-\beta)\Psi}, X \geq \frac{\gamma_{th}}{\kappa\Psi Y} - Y\right\} \\ &= 1 - \underbrace{\Pr\left(\frac{\gamma_{th}}{\kappa\Psi Y} - Y \geq \tilde{\gamma}_{th}, X \geq \frac{\gamma_{th}}{\kappa\Psi Y} - Y\right)}_{P_1} - \underbrace{\Pr\left(\frac{\gamma_{th}}{\kappa\Psi Y} - Y \leq \tilde{\gamma}_{th}, X \geq \tilde{\gamma}_{th}\right)}_{P_2}. \end{aligned} \tag{7.21}$$

where $\tilde{\gamma}_{th} \triangleq \frac{\gamma_{th}}{(1-\beta)\Psi}$.

Let $\xi = \frac{1}{2}\left(\sqrt{\left(\tilde{\gamma}_{th}\right)^2 + \frac{4\gamma_{th}}{\kappa\Psi}} - \tilde{\gamma}_{th}\right)$ be the positive solution of the equation $\frac{\gamma_{th}}{\kappa\Psi y} - y = \tilde{\gamma}_{th}$, the probability terms in (7.21) can be rewritten as

$$\begin{aligned} P_1 &= \int_0^{\xi} \Pr\left(X \geq \frac{\gamma_{th}}{\kappa\Psi y} - y\right) f_Y(y)dy = \int_0^{\xi} \left[1 - F_X\left(\frac{\gamma_{th}}{\kappa\Psi y} - y\right)\right] f_Y(y)dy \\ &= -\int_0^{\xi} \left\{\sum_{j=1}^{M} (-1)^j \binom{M}{j} e^{-j\lambda_1\left(\frac{\gamma_{th}}{\kappa\Psi y} - y\right)}\right\} f_Y(y)dy = -\sum_{j=1}^{M} (-1)^j \binom{M}{j} \lambda_2 \int_0^{\xi} e^{y(j\lambda_1 - \lambda_2)} e^{-\frac{j\lambda_1\gamma_{th}}{\kappa\Psi y}} dy, \end{aligned} \tag{7.22}$$

$$\begin{aligned} P_2 &= \int_{\xi}^{\infty} \Pr\left(X \geq \tilde{\gamma}_{th}\right) f_Y(y)dy = \int_{\xi}^{\infty} \left[1 - F_X\left(\tilde{\gamma}_{th}\right)\right] f_Y(y)dy = \sum_{j=1}^{M} (-1)^{j+1} \binom{M}{j} . e^{-j\lambda_1\tilde{\gamma}_{th}} \int_{\xi}^{\infty} f_Y(y)dy \\ &= \sum_{j=1}^{M} (-1)^{j+1} \binom{M}{j} e^{-j\lambda_1\tilde{\gamma}_{th} - \lambda_2\xi}. \end{aligned} \tag{7.23}$$

The integral in $P_1$ can be solved by changing variable $t = 1/y$ and applying Taylor's series expansion $e^x = \sum_{n=0}^{\infty} \frac{x^n}{n!}$ for $x = \frac{j\lambda_1 - \lambda_2}{t}$:

$$\begin{aligned} P_1 &= -\sum_{j=1}^{M} (-1)^j \binom{M}{j} \lambda_2 \int_{1/\xi}^{\infty} t^{-2} e^{\frac{(j\lambda_1 - \lambda_2)}{t}} e^{-j\frac{\lambda_1\gamma_{th}t}{\kappa\Psi}} dt \\ &= -\sum_{n=0}^{\infty} \sum_{j=1}^{M} \frac{(-1)^j (j\lambda_1 - \lambda_2)^n \lambda_2}{n!} \binom{M}{j} \int_{1/\xi}^{\infty} \frac{e^{-j\lambda_1\gamma_{th}t}}{\kappa\Psi t^{n+2}} dt \\ &= \sum_{n=0}^{\infty} \sum_{j=1}^{M} \frac{(-1)^{j+1} (j\lambda_1 - \lambda_2)^n (j\lambda_1\gamma_{th})^{n+1} \lambda_2}{n!(\kappa\Psi)^{n+1}} \binom{M}{j} \times \Gamma\left(-n-1, \frac{j\lambda_1\gamma_{th}}{\kappa\Psi\xi}\right). \end{aligned} \tag{7.24}$$

where the last equality comes from [72, p. 3.462.16].

By substituting (7.15), (7.23) and (7.24) into (7.21), we finally get (7.20). ∎

### 7.3.2 Intercept probability (IP)

The IP at the eavesdropper E is defined as the probability that capacity of the legitimate link falls below the wiretap link's capacity, i.e. $C_E > C_B$. By using the result of the OP analysis, we obtain the Theorem 7.2.

**Theorem 7.2** *The IP at the eavesdropper E in the proposed two-way relay networks with jamming by artificial noise is given by* (7.25)*, as shown at the bottom of the page, where K is the number of jammers,* $\Psi \triangleq \frac{P}{N_0}$*, and* $\Psi_J \triangleq \frac{P_J}{N_0}$*, and* $\tilde{\xi}_x = \frac{1}{2}\left[\sqrt{\frac{x^2}{(1-\beta)^2} + \frac{4x}{\kappa}} - \frac{x}{(1-\beta)}\right]$.

**Proof** By definition and using (7.8) and (7.10), the IP by the eavesdropper E can be found as

$$\begin{aligned}\mathrm{IP} = 1 &+ \int_0^\infty \left\{ \sum_{n=0}^{\infty} \sum_{j=1}^{M} \frac{(-1)^j (j\lambda_1 - \lambda_2)^n [j\lambda_1 x]^{n+1} \lambda_2}{n!(\kappa)^{n+1}} \binom{M}{j} \Gamma\left(-n-1, \frac{j\lambda_1 x}{\kappa \tilde{\xi}_x}\right) \right\} \\ &\times \frac{e^{-\lambda_3 x}\left[(\lambda_3)^2 \frac{\Psi_J}{\lambda_4} x + \lambda_3 + \frac{\lambda_3 \Psi_J K}{\lambda_4}\right]}{\left(1 + \frac{\lambda_3 \Psi_J x}{\lambda_4}\right)^{K+1}} dx \\ &+ \int_0^\infty \left\{ \sum_{j=1}^{M} (-1)^j \binom{M}{j} e^{-\frac{j\lambda_1(x)}{(1-\beta)} - \lambda_2 \tilde{\xi}_x} \right\} \frac{e^{-\lambda_3 x}\left[(\lambda_3)^2 \frac{\Psi_J}{\lambda_4} x + \lambda_3 + \frac{\lambda_3 \Psi_J K}{\lambda_4}\right]}{\left(1 + \frac{\lambda_3 \Psi_J x}{\lambda_4}\right)^{K+1}} dx. \end{aligned} \tag{7.25}$$

$$\mathrm{IP} = \Pr\left(C_E \geq C_B\right) = \Pr\left(\gamma_E \geq \gamma_{DF}\right) = \Pr\left(\frac{Z}{\Psi_J T + 1} \geq \min\left\{(1-\beta)X\Psi, \kappa\Psi\left(X + Y\right)Y\right\}\right). \tag{7.26}$$

where $\Psi_J \triangleq P_J/N_0$, $Z = |h_{AE}|^2$, $T = \sum_{k=1}^{K} |h_{J_k E}|^2$.

Let's denote $V = \min\left\{(1-\beta)X, \kappa\left(X + Y\right)Y\right\}$ and $U = \frac{Z}{\Psi_J T + 1}$. Then (7.26) can be rewritten as

$$\mathrm{IP} = \Pr\left(U \geq V\right) = \int_0^\infty f_U(u)du \int_0^u f_V(v)dv = \int_0^\infty f_U(u).F_V(u)du. \tag{7.27}$$

By using (7.10), the CDF of $U$ can be written as

$$F_U(u) = \Pr\left\{U \leq u\right\} = \Pr\left\{\frac{Z}{\Psi_J T + 1} \leq u\right\} = \Pr\left\{Z < u\left(T\Psi_J + 1\right)\right\} = \int_0^\infty F_Z\left(u\left(t\Psi_J + 1\right)\right) f_T(t)dt, \tag{7.28}$$

where $F_Z(\cdot)$ and $f_T(\cdot)$ are the CDF of $Z$ and PDF of $T$, respectively.

As mentioned in the previous section, $Z$ is an exponential RV with parameter $\lambda_3$, while $T$ is the sum of $K$ i.i.d. exponential RV with parameter $\lambda_4$. As a result, the CDF of $Z$ is given by

(7.12) and $T$ is a gamma RV with the parameters $K$ and $\lambda_4$, whose PDF is given by [144]

$$f_T(t) = \frac{\lambda_4^K}{(K-1)!} t^{K-1} e^{-\lambda_4 t}. \tag{7.29}$$

By substituting (7.12) and (7.33) into (7.28), we can rewrite $F_U(u)$ as

$$\begin{aligned} F_U(u) &= \int_0^\infty F_Z\left(u\left(t\Psi_J+1\right)\right) f_T(t)dt = \int_0^\infty f_T(t)dt - \frac{\lambda_4^K e^{-\lambda_3 u}}{(K-1)!}\int_0^\infty t^{K-1} e^{-t(\lambda_4+\lambda_3 u\Psi_J)}dt \\ &= 1 - \frac{\lambda_4^K \Gamma\left(K\right) e^{-\lambda_3 u}}{(K-1)!(\lambda_4+\lambda_3 u\Psi_J)^K} = 1 - \frac{\lambda_4^K e^{-\lambda_3 u}}{(\lambda_4+\lambda_3 u\Psi_J)^K}, \end{aligned} \tag{7.30}$$

where the second last equality is obtained by using [72, p. 3.381.4] and the last equality is obtained by replacing $\Gamma(K) = (K-1)!$.

By taking the derivative of (7.34), we obtain the PDF of $U$ as

$$f_U(u) = \frac{e^{-\lambda_3 u}\left[(\lambda_3)^2 \frac{\Psi_J}{\lambda_4} u + \lambda_3 + \frac{\lambda_3 \Psi_J K}{\lambda_4}\right]}{\left(1+\frac{\lambda_3 u\Psi_J}{\lambda_4}\right)^{K+1}}. \tag{7.31}$$

On the other hand, the CDF of $V$ is obtained by using the result of Theorem 7.1 (substituting $\gamma_{th}$ by $v\Psi$ in (7.20)):

$$\begin{aligned} F_V(v) = \Pr\left(V \le v\right) = \Pr\left(\frac{\gamma_{DF}}{\Psi} \le v\right) &= 1 + \sum_{j=1}^{M} (-1)^j \binom{M}{j} e^{-\frac{j\lambda_1 v}{(1-\beta)} - \lambda_2 \tilde{\xi}_v} \\ &+ \sum_{n=0}^{\infty}\sum_{j=1}^{M} \frac{(-1)^j (j\lambda_1 - \lambda_2)^n (j\lambda_1 v)^{n+1} \lambda_2}{n!\left(\kappa\right)^{n+1}} \binom{M}{j} \Gamma\left(-n-1, \frac{j\lambda_1 v}{\kappa\tilde{\xi}_v}\right). \end{aligned} \tag{7.32}$$

where $\tilde{\xi}_v = \frac{1}{2}\left[\sqrt{\frac{v^2}{(1-\beta)^2} + \frac{4v}{\kappa}} - \frac{v}{(1-\beta)}\right]$. By substituting (7.31) and (7.32) into (7.27), we obtain (7.25). The proof is complete. ∎

**Remark 7.2** It can be seen from (7.25) that the IP does not depend on $\Psi$.

**Remark 7.3** It is worth noting that our analytical results in this section can be easily extended to the general case when there exist hardware noise terms at both relay and primary transmitters. In fact, each SINR formula for the hardware imperfection case is a one-to-one mapping of the corresponding SINR for perfect hardware case presented above. For example, the received signal at relay and its corresponding SINR in hardware imperfection case can be rewritten respectively

as

$$y_{A,R_i} = h_{A,R_i}(x_A + \eta_A^{\mathrm{t}}) + \eta_{\mathrm{R}_i}^{\mathrm{r}} + n_{r_i}^{(1)},$$
$$\gamma_{AR_i}^{HI} = \frac{(1-\beta)|h_{AR_i}|^2 P}{|h_{\mathrm{AR_i}}|^2 k_{\mathrm{AR_i}}^2 P + N_0} = \frac{(1-\beta)}{k_{\mathrm{AR_i}}^2 + \frac{1}{|h_{AR_i}|^2 \Psi}} = \frac{1}{\frac{k_{\mathrm{AR_i}}^2}{1-\beta} + \frac{1}{\gamma_{AR_i}}}.$$

where $\eta_A^{\mathrm{t}} \sim C\mathcal{N}(0, (k_{\mathrm{A}}^{\mathrm{t}})^2 P)$ and $\eta_{R_i}^{\mathrm{r}} \sim C\mathcal{N}(0, (k_{\mathrm{R_i}}^{\mathrm{r}})^2 P_{R_i})$ are HI noise terms caused by the transmitter impairment at A and receiver impairment at $\mathrm{R_i}$, respectively; $k_{\mathrm{AR_i}}^2 = (k_{\mathrm{A}}^{\mathrm{t}})^2 + (k_{\mathrm{R_i}}^{\mathrm{r}})^2$ denotes the aggregated HI level at both transmitter A ($k_{\mathrm{A}}^{\mathrm{t}}$) and receiver $\mathrm{R_i}$ ($k_{\mathrm{R_i}}^{\mathrm{r}}$) [199].

Then, to derive $P(\gamma_{AR_i}^{HI} < \gamma_{th})$, we can use:

$$P(\gamma_{AR_i}^{HI} < \gamma_{th}) = P\left(\frac{1}{\frac{k_{\mathrm{AR_i}}^2}{1-\beta} + \frac{1}{\gamma_{AR_i}}} < \gamma_{th}\right) = P\left(\gamma_{AR_i} < \frac{1-\beta-k_{\mathrm{AR_i}}^2}{(1-\beta)\gamma_{th}}\right)$$

By replacing $\gamma_{th}$ in our original analysis by $\frac{1-\beta-k_{\mathrm{AR_i}}^2}{(1-\beta)\gamma_{th}}$, we can obtain the result for hardware imperfection case.

### 7.3.3 Secrecy outage probability (SOP)

In the literature on PLS, such as [180], the researchers are interested in the possibility of conveying confidential messages at a positive rate, termed secrecy rate, between a source and a legitimate destination while keeping an eavesdropper ignorant if the source-destination channel is better than the source-eavesdropper channel. In addition, the larger the difference of the channel strengths between the two channels, the higher the achieved secrecy rate. This secrecy rate is defined as

$$C_{sec} = \max\{C_B - C_E, 0\}, \tag{7.33}$$

where $C_B = (1-\alpha)\log_2(1+\gamma_{DF})$ is the achievable data rate at the node B.

The secrecy rate must be maintained above certain threshold to guarantee the confidentiality of the message. An secrecy outage occurs if the achievable secrecy rate falls below the threshold:

$$\mathrm{SOP} = \Pr\{C_{\mathrm{sec}} < R\} = \Pr\left\{\frac{1+\gamma_{DF}}{1+\gamma_E} < \gamma_{sc,th}\right\}, \tag{7.34}$$

where $R$ is the threshold of the secrecy rate, and $\gamma_{sc,th} \triangleq 2^{\frac{R}{(1-\alpha)}}$.

The closed-form expression of this SOP can be found in the following theorem.

**Theorem 7.3** *The SOP (*SOP*) of the proposed two-way wireless relay networks with partial relay selection, EH at relay nodes, and friendly jammers is given by* (7.35) *on the next page,*

*where* $a = \frac{j\lambda_1\gamma_{sc,th}}{(1-\beta)\Psi} + \frac{\lambda_3}{\Psi}, b = \frac{\lambda_3\Psi_J}{\lambda_4\Psi}$, $\tilde{\gamma}_{th} \triangleq 2^{\frac{3R}{\alpha T}} - 1$ *is the* SNR *threshold at* E, *and* $\Gamma(s,x) \triangleq \int_x^\infty t^{s-1}e^{-t}dt$ *is the incomplete gamma function.*

**Proof** To begin, we can rewrite (7.34) as

$$\begin{aligned}\text{SOP} = 1 + \int_0^\infty \Bigg\{ \sum_{n=0}^{\infty}\sum_{j=1}^{M} \frac{(-1)^j(j\lambda_1-\lambda_2)^n[j\lambda_1(\tilde{\gamma}+\gamma_{sc,th}x)]^{n+1}\lambda_2}{n!(\kappa\Psi)^{n+1}}\binom{M}{j}\Gamma\left(-n-1, \frac{j\lambda_1(\tilde{\gamma}+\gamma_{sc,th}x)}{\kappa\Psi\Xi_x}\right)\Bigg\} \\ \times \frac{e^{-\frac{\lambda_3 x}{\Psi}}\left[\left(\frac{\lambda_3}{\Psi}\right)^2\frac{\Psi_J}{\lambda_4}x + \frac{\lambda_3}{\Psi} + \frac{\lambda_3\Psi_J K}{\Psi\lambda_4}\right]}{\left(1+\frac{\lambda_3\Psi_J x}{\Psi\lambda_4}\right)^{K+1}}dx \\ + \int_0^\infty \left\{\sum_{j=1}^{M}(-1)^j\binom{M}{j}e^{-\frac{j\lambda_1(\tilde{\gamma}+\gamma_{sc,th}x)}{(1-\beta)\Psi}-\lambda_2\Xi_x}\right\}\frac{e^{-\frac{\lambda_3 x}{\Psi}}\left[\left(\frac{\lambda_3}{\Psi}\right)^2\frac{\Psi_J}{\lambda_4}x + \frac{\lambda_3}{\Psi} + \frac{\lambda_3\Psi_J K}{\Psi\lambda_4}\right]}{\left(1+\frac{\lambda_3\Psi_J x}{\Psi\lambda_4}\right)^{K+1}}dx. \qquad (7.35)\end{aligned}$$

$$\text{SOP} = \Pr\left\{\frac{1+\gamma_{DF}}{1+\gamma_E} < \gamma_{sc,th}\right\} = \Pr\{\gamma_{DF} < (1+\gamma_E)\gamma_{sc,th} - 1\} = \int_0^\infty F_{\gamma_{DF}}((1+x)\gamma_{sc,th}-1)\, f_{\gamma_E}(x)dx \qquad (7.36)$$

where $F_{\gamma_{DF}}(\cdot)$ and $f_{\gamma_E}(\cdot)$ are the CDF of $\gamma_{DF}$ and PDF of $\gamma_E$, respectively.

By applying the result of Theorem 7.2 (just substitute $u$ by $\frac{x}{\Psi}$ in (7.34)), the CDF and the PDF of $\gamma_E$ can be found by

$$F_{\gamma_E}(x) = \Pr\{\gamma_E < x\} = 1 - \frac{e^{\frac{-\lambda_3 x}{\Psi}}}{\left(1+\frac{\lambda_3\Psi_J x}{\Psi\lambda_4}\right)^K} \qquad (7.37)$$

and

$$f_{\gamma_E}(x) = \frac{df_{\gamma_E}}{dx} = \frac{e^{-\frac{\lambda_3 x}{\Psi}}\left[\left(\frac{\lambda_3}{\Psi}\right)^2\frac{\Psi_J}{\lambda_4}x + \frac{\lambda_3}{\Psi} + \frac{\lambda_3\Psi_J K}{\Psi\lambda_4}\right]}{\left(1+\frac{\lambda_3\Psi_J x}{\Psi\lambda_4}\right)^{K+1}}. \qquad (7.38)$$

On the other hand, the CDF of $\gamma_{DF}$ is obtained by using the result of Theorem 7.1 (substituting $\gamma_{th}$ by $y$ in (7.20)).

$$\begin{aligned}F_{\gamma_{DF}}(y) = 1 + \sum_{j=1}^{M}(-1)^j\binom{M}{j}e^{-j\lambda_1\frac{y}{(1-\beta)\Psi}-\lambda_2\xi} + \sum_{n=0}^{\infty}\sum_{j=1}^{M}\frac{(-1)^j(j\lambda_1-\lambda_2)^n(j\lambda_1 y)^{n+1}\lambda_2}{n!\,(\kappa\Psi)^{n+1}}\binom{M}{j} \\ \times\Gamma\left(-n-1, \frac{j\lambda_1 y}{\kappa\Psi\xi_y}\right). \qquad (7.39)\end{aligned}$$

where $\xi_y = \frac{1}{2}\left[\sqrt{\frac{y^2}{(1-\beta)^2\Psi^2} + \frac{4y}{\kappa\Psi}} - \frac{y}{(1-\beta)\Psi}\right]$.

Let's denote $\tilde{\gamma} \triangleq \gamma_{sc,th} - 1$ and $\Xi_x = \xi_{\gamma_{sc,th}(1+x)-1} = \sqrt{\frac{(x\gamma_{sc,th}+\tilde{\gamma})^2}{4(1-\beta)^2\Psi^2} + \frac{(x\gamma_{sc,th}+\tilde{\gamma})}{\kappa\Psi}} - \frac{(x\gamma_{sc,th}+\tilde{\gamma})}{2(1-\beta)\Psi}$.

Now, by substituting (7.39) with $y = x\gamma_{sc,th} + \tilde{\gamma}$ into (7.36), we have (7.40) below. Finally, by substituting (7.38) into (7.40), we get (7.35).

$$\text{SOP} = \int_0^\infty \left\{ \sum_{n=0}^{\infty} \sum_{j=1}^{M} \frac{(-1)^j (j\lambda_1 - \lambda_2)^n [j\lambda_1(\tilde{\gamma} + \gamma_{sc,th}x)]^{n+1} \lambda_2}{n!(\kappa\Psi)^{n+1}} \binom{M}{j} \Gamma\left(-n-1, \frac{j\lambda_1(\tilde{\gamma} + \gamma_{sc,th}x)}{\kappa\Psi\Xi_x}\right) \right\}$$
$$\times f_{\gamma_E}(x)dx + 1 + \int_0^\infty \left\{ \sum_{j=1}^{M} (-1)^j \binom{M}{j} e^{-\frac{j\lambda_1(\tilde{\gamma}+\gamma_{sc,th}x)}{(1-\beta)\Psi} - \lambda_2\Xi_x} \right\} f_{\gamma_E}(x)dx. \tag{7.40}$$

■

### 7.3.4 Average secrecy capacity (ASC)

The secrecy capacity of the proposed system depends on the SNRs of the legitimate link and the wire-tap link, which are RVs. The ASC is defined as the expected value of the secrecy capacity [200]:

$$C_{avg} = \mathrm{E}\left[C_{\text{Sec}}\right] = (1-\alpha) \iint\limits_{\substack{x,y>0 \\ y \geq x}} \log_2\left(\frac{1+y}{1+x}\right) f_{\gamma_{DF}}(y) f_{\gamma_E}(x) dxdy$$
$$= (1-\alpha) \int_0^\infty f_{\gamma_E}(x)dx \int_x^\infty \log_2\left(\frac{1+y}{1+x}\right) f_{\gamma_{DF}}(y)dy. \tag{7.41}$$

where $f_{\gamma_E}(\cdot)$ and $f_{\gamma_{DF}}(\cdot)$ are the PDF of $\gamma_E$ and $\gamma_{DF}$, respectively.

We now state the following theorem on the ASC of the proposed system.

**Theorem 7.4** *The average secrecy capacity $C_{avg}$ of the proposed two-way relay network with PRS, EH at relay nodes, and friendly jammers is given by* (7.42).

$$C_{avg} = (1-\alpha) \sum_{n=0}^{\infty} \sum_{j=1}^{M} \frac{(-1)^j (j\lambda_1 - \lambda_2)^n \lambda_2}{n!} \binom{M}{j} \int_0^\infty \frac{(n+1)e^{-\frac{\lambda_3 x}{\Psi}} \Lambda_x}{\left(1 + \frac{\lambda_3 \Psi_J x}{\Psi \lambda_4}\right)^{K+1}} dx \int_x^\infty \log_2\left(\frac{1+y}{1+x}\right)$$
$$\times \left[ \frac{y^n (j\lambda_1)^{n+1}}{(\kappa\Psi)^{n+1}} \Gamma\left(-n-1, \frac{j\lambda_1 y}{\kappa\Psi\xi_y}\right) \right] dy - (1-\alpha) \sum_{n=0}^{\infty} \sum_{j=1}^{M} \frac{(-1)^j (j\lambda_1 - \lambda_2)^n \lambda_2}{n!} \binom{M}{j}$$
$$\times \int_0^\infty \frac{e^{-\frac{\lambda_3 x}{\Psi}} \Lambda_x}{\left(1 + \frac{\lambda_3 \Psi_J x}{\Psi \lambda_4}\right)^{K+1}} dx \int_x^\infty \log_2\left(\frac{1+y}{1+x}\right) \left[ e^{\frac{-j\lambda_1 y}{\kappa\Psi\xi_y}} \xi_y^{n+1} \left(\frac{1}{y} - \frac{\Upsilon_y}{\xi_y}\right) \right] dy$$
$$+ (1-\alpha) \sum_{j=1}^{M} \binom{M}{j} \int_0^\infty \frac{(-1)^{j+1} e^{-\frac{\lambda_3 x}{\Psi}} \Lambda_x}{\left(1 + \frac{\lambda_3 \Psi_J x}{\Psi \lambda_4}\right)^{K+1}} dx \int_x^\infty \log_2\left(\frac{1+y}{1+x}\right) e^{-\left[\frac{j\lambda_1 y}{(1-\beta)\Psi} + \lambda_2 \xi_y\right]} \left[ \frac{j\lambda_1}{(1-\beta)\Psi} + \lambda_2 \Upsilon_y \right] dy \tag{7.42}$$

*where* $\Lambda_x \triangleq \left(\frac{\lambda_3}{\Psi}\right)^2 \frac{\Psi_J}{\lambda_4} x + \frac{\lambda_3}{\Psi} + \frac{\lambda_3 \Psi_J K}{\Psi \lambda_4}$ *and* $\Upsilon_y \triangleq \frac{\frac{y}{\{(1-\beta)\Psi\}^2} + \frac{2}{\kappa\Psi}}{2\sqrt{\left(\frac{y}{(1-\beta)\Psi}\right)^2 + \frac{4y}{\kappa\Psi}}} - \frac{1}{2(1-\beta)\Psi}$.

**Proof** The CDF of $\gamma_{DF}$ has been given in (7.39). By taking the derivative of (7.39), we get the PDF of $\gamma_{DF}$ as

$$
\begin{aligned}
f_{\gamma_{DF}}(y) &= \frac{\partial F_{\gamma_{DF}}(y)}{\partial y} \\
&= \sum_{n=0}^{\infty} \sum_{j=1}^{M} \frac{(-1)^j (j\lambda_1 - \lambda_2)^n (j\lambda_1)^{n+1} \lambda_2}{n! (\kappa\Psi)^{n+1}} \binom{M}{j} \frac{\partial}{\partial y} \left[ y^{n+1} \Gamma\left(-n-1, \frac{j\lambda_1 y}{\kappa\Psi\xi_y}\right) \right] \\
&+ \sum_{j=1}^{M} (-1)^j \binom{M}{j} \frac{\partial}{\partial y} \left[ e^{\frac{-j\lambda_1 y}{(1-\beta)\Psi} - \lambda_2 \xi_y} \right] \\
&= \sum_{n=0}^{\infty} \sum_{j=1}^{M} \frac{(-1)^j (j\lambda_1 - \lambda_2)^n \lambda_2}{n!} \binom{M}{j} \left[ \frac{(n+1) y^n (j\lambda_1)^{n+1}}{(\kappa\Psi)^{n+1}} \Gamma\left(-n-1, \frac{j\lambda_1 y}{\kappa\Psi\xi_y}\right) - e^{\frac{-j\lambda_1 y}{\kappa\Psi\xi_y}} \xi_y^{n+1} \left(\frac{1}{y} - \frac{\Upsilon_y}{\xi_y}\right) \right] \\
&+ \sum_{j=1}^{M} (-1)^{j+1} \binom{M}{j} e^{-\left[\frac{j\lambda_1 y}{(1-\beta)\Psi} + \lambda_2 \xi_y\right]} \left[ \frac{j\lambda_1}{(1-\beta)\Psi} + \lambda_2 \Upsilon_y \right]. \qquad (7.43)
\end{aligned}
$$

where $\Upsilon_y \triangleq \frac{\frac{y}{\{(1-\beta)\Psi\}^2} + \frac{2}{\kappa\Psi}}{2\sqrt{\left(\frac{y}{(1-\beta)\Psi}\right)^2 + \frac{4y}{\kappa\Psi}}} - \frac{1}{2(1-\beta)\Psi}$, and the last equality is obtained by using [201, p. 8.8.13].

By substituting (7.43) and (7.38) into (7.41) we obtain (7.42). ∎

## 7.4 Numerical Results and Discussion

In this part, some Monte Carlo simulations are presented to validate the derived expressions of OP, IP, SOP, and ASC. Moreover, the effect of various system parameters, such as transmit-power-to-noise-ratio, TS factor, PS factor, number of relay nodes, number of jammers, and spectrum efficiency, on the system performance is investigated through these simulation results. All Monte Carlo simulations are generated using $10^5$ samples of each channel gain. The settings of simulation parameters are listed in Table 7.1. Regarding to the channel settings, we adopt a simplified path loss model, i.e., $\lambda_i = d_i^{\theta}$, for $i \in \{1, 2, 3, 4\}$, where $d_1$, $d_2$, $d_3$, $d_4$ are the distances between A and the relay cluster, between B and the relay cluster, between A and the eavesdropper, and between the eavesdropper and the jamming cluster, respectively; $\theta$ denotes the path loss exponent, respectively. For illustrative purpose, we set $d_1 = 0.85$, $d_2 = 0.5$, $d_3 = d_4 = 2$, and $\theta = 2$, which leads to the values of $\lambda_i, i \in \{1, 2, 3, 4\}$ as in Table 7.1.

Firstly, we examine the reliability and security performance of the proposed model in terms of OP and IP. Fig. 7.3 plots OP and IP versus the ratio between transmission power of the source A and the noise power density $N_0$, which is denoted by $\Psi$, for four different cluster size of the relay cluster and jamming clusters. It can be seen from these figures that the analytical results and the simulation results exactly match together. As expected, OP decreases with $\Psi$, while the IP does not depend on $\Psi$ as stated in the Remark 7.2. It can also be observed that

Table 7.1: Simulation parameters.

| Symbol | Parameter name | Fixed value | Varying range |
|---|---|---|---|
| $R$ | Spectrum efficiency | 0.25 bps/Hz | 0.1 to 1 (bps/Hz) |
| $\eta$ | EH efficiency | 0.8 | none |
| $\alpha$ | Time division factor | 0.3 | 0 to 0.5 |
| $\beta$ | Power splitting factor | 0.5 | 0 to 1 |
| $\lambda_1$ | Mean of $\|h_{AR_i}\|^2$ | 0.7225 | none |
| $\lambda_2$ | Mean of $\|h_{BR_i}\|^2$ | 0.258 | none |
| $\lambda_3$ | Mean of $\|h_{AE}\|^2$ | 4 | none |
| $\lambda_4$ | Mean of $\|h_{J_kE}\|^2$ | 4 | none |
| $\Psi$ | Transmit-power-to-noise-ratio | 15 dB | 0 to 30 (dB) |
| $\Psi_J$ | Jammer-power-to-noise-ratio | 15 dB | 0 to 30 (dB) |
| $M$ | No. of relay nodes | 1; 3; 5; 7 | none |
| $K$ | No. of jamming nodes | 1; 3; 5; 7 | none |

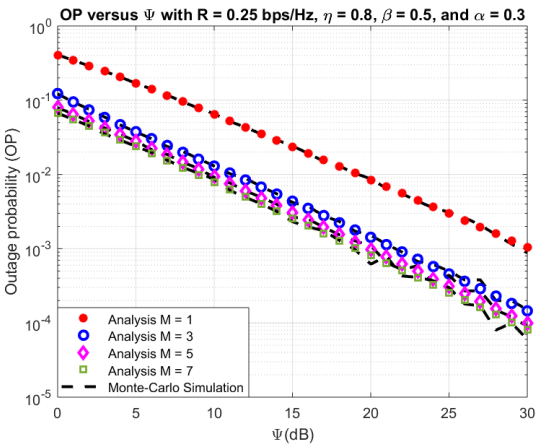


(a) OP for different number of relays.

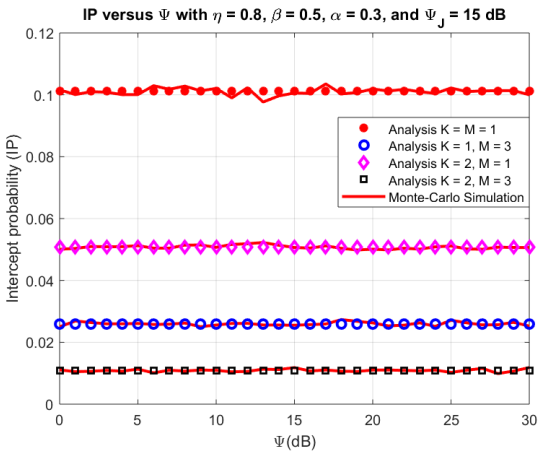


(b) IP for different number of jammers and jammer power levels.

Figure 7.3: OP and IP versus transmit-power-to-noise-ratio.

both reliability and security performance can be improved by increasing the number of relay nodes and jammer nodes. However, when the number of relay nodes is sufficient, adding more nodes to the relay cluster does not significantly improve the outage performance (we can see the gaps among the cases $M = 3, M = 5$, and $M = 7$ are small). This can be explained as follows. Because the relays are located in a cluster, they are closed to each others. With PRS, the more relays added to the cluster, the less likely that the newly added relay has best channel gain. After a certain number of relays, keep increasing the number of relays does not improve much. So it is recommended that we use a moderate number of relays, let's say $M = 3$, and use cooperative jammers, for example $K = 2$, to obtain a desired performance.

The effect of the EH TS factor on the outage and security performance is shown in Fig. 7.4.

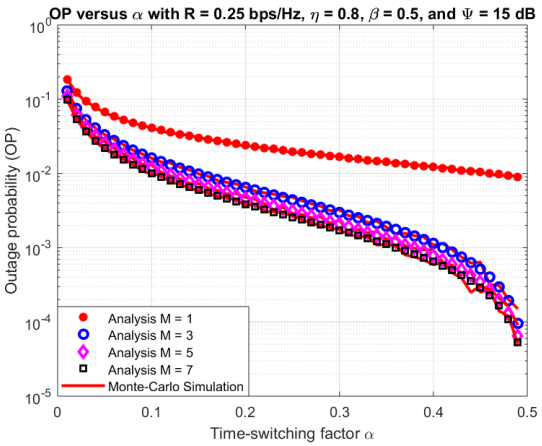


(a) OP for different number of relays.

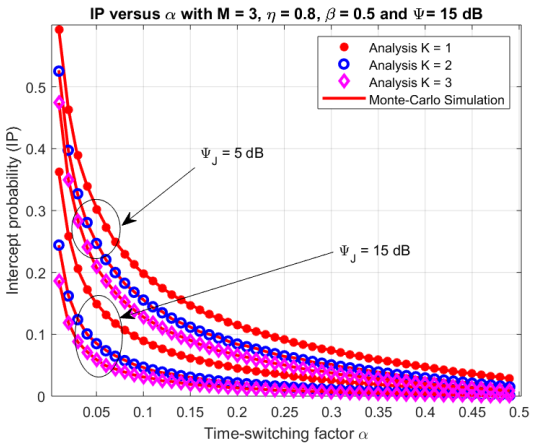


(b) IP for different number of jammers and jammer power levels.

Figure 7.4: OP and IP versus versus time-switching factor.

I consider again four cluster sizes of the relay and jammer clusters, i.e., $M \in \{1, 3, 5, 7\}, K \in \{1, 2, 3\}$. As observed from Fig. 7.4a, OP decreases with $\alpha$. This can be explained as follows. For small $\alpha$, the EH time is limited, so the relay nodes do not harvest much energy for their transmission. Therefore, increasing $\alpha$ would improve the quality of transmission. Again, it can be seen that increasing the number of relays $M \geq 3$ does not improve much on performance. On other aspect, Fig. 7.4b shows that IP decreases with $\alpha$. It is obvious because increasing $\alpha$ means increasing the duration of EH time by the relay, which results in the better legitimate link condition, while the wire-tap link condition is not improved by increasing $\alpha$. From these two figures, it is recommended that we choose $\alpha$ large enough and choose a proper number of jammers (for example, $K = 2$) and relays (for example, $M = 3$). Adding more jammers and relays after these certain numbers cannot bring significant benefit. In addition, the transmit power of jammer is not necessarily too large, with $\Psi_J = 5dB$ and with sufficient large $\alpha$, we can achieve an acceptable performance.

Fig. 7.5 plots the OP and IP versus the PS factor $\beta$. There is a trade-off between the energy using to supply the relay nodes and to guarantee the transmission of the message from source A. That means there exists an optimal $\beta$ to minimize the OP or IP for each number of relay nodes. From Fig. 7.5a, when the number of relay nodes is increased, the optimal value of $\beta$ tend to approach 1 ($\beta = 0.46$, 0.87, 0.95, and 0.97 for $M = 1, 3, 5$, and 7, respectively). This is because when the number of relays increases, the quality of the link between A and the selected relay nodes is improved so that we do not worry much about the transmit power for message signal and can use more energy to supply the relay node. It is reasonable to see that there is also an optimal value of $\beta$ that minimize the IP for each scenario. This is because the wiretap-link condition does not depend on $\beta$, while the OP of the main link from A $\rightarrow$ B get a single minimum at shown in Fig. 7.5b. However, it is worth noting that the optimal value of $\beta$ for

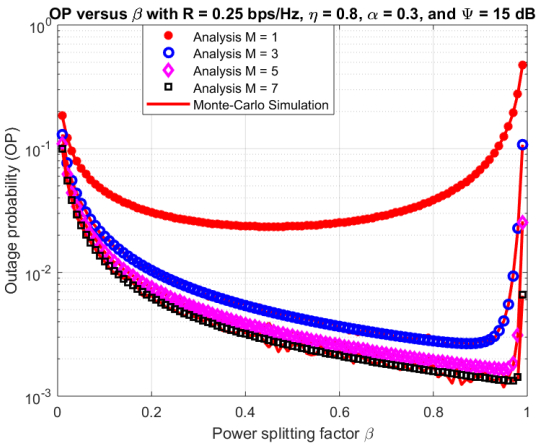


(a) OP for different number of relays.

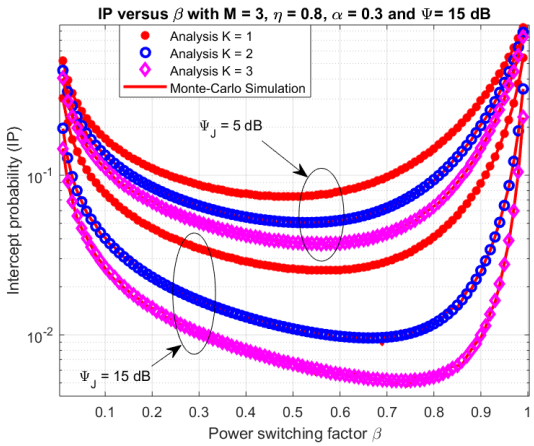


(b) IP for different number of jammers and jammer power levels.

Figure 7.5: OP and IP versus versus PS factor.

minimizing IP is different from the one that minimizing OP. In fact, the optimal $\beta$ in this case (minimizing IP should depend on the number of jammers, too, and also tend to increases when the number of jammers increases. In particular, the optimal values of $\beta^*$ for $K = \{1, 2, 3\}$ and $\Psi_J = 5dB$ are 0.49, 0.53, and 0.56 respectively. For $\Psi_J = 15dB$, the optimal values $\beta^*$ for $K = \{1, 2, 3\}$ are 0.56, 0.66, and 0.73, respectively. Here, because $\alpha$ is not large enough, the IP is significantly impacted by $\Psi_J$.

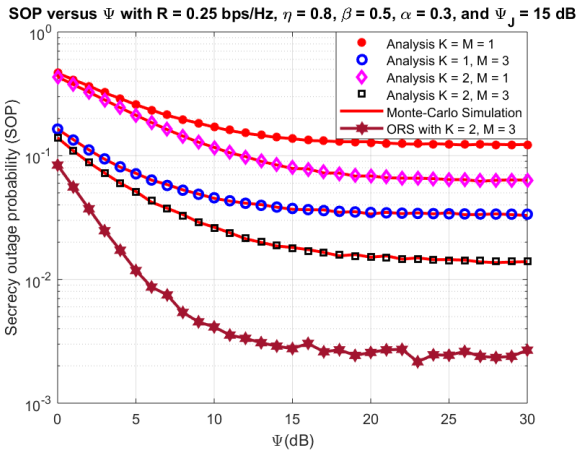


(a) Secrecy outage probability

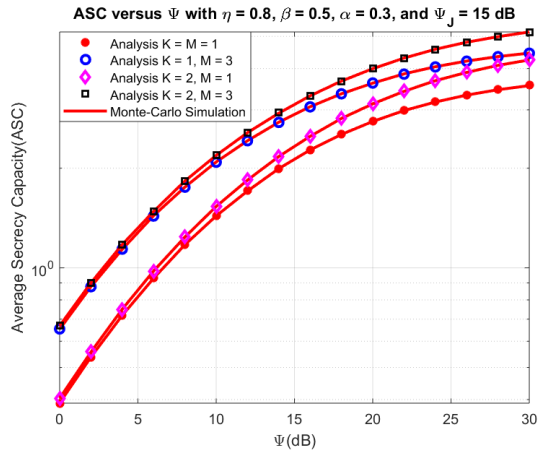


(b) Average secrecy capacity

Figure 7.6: SOP and ASC versus transmit-power-to-noise-ratio for different configurations of relay and jammer nodes.

Fig. 7.6 depicts the impact of transmit-power-to-noise-ratio on the secrecy outage performance of our proposed systems. In Fig. 7.6a, we can observe that SOP decreases when $\Psi$ increases,

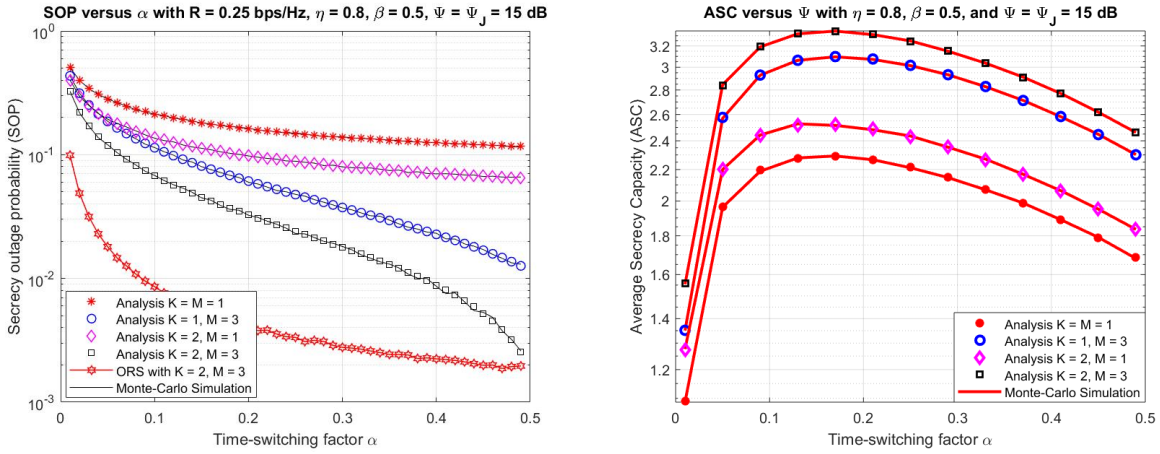


(a) Secrecy outage probability (b) Average secrecy capacity

Figure 7.7: SOP and ASC versus TS factor for different configurations of relay and jammer nodes.

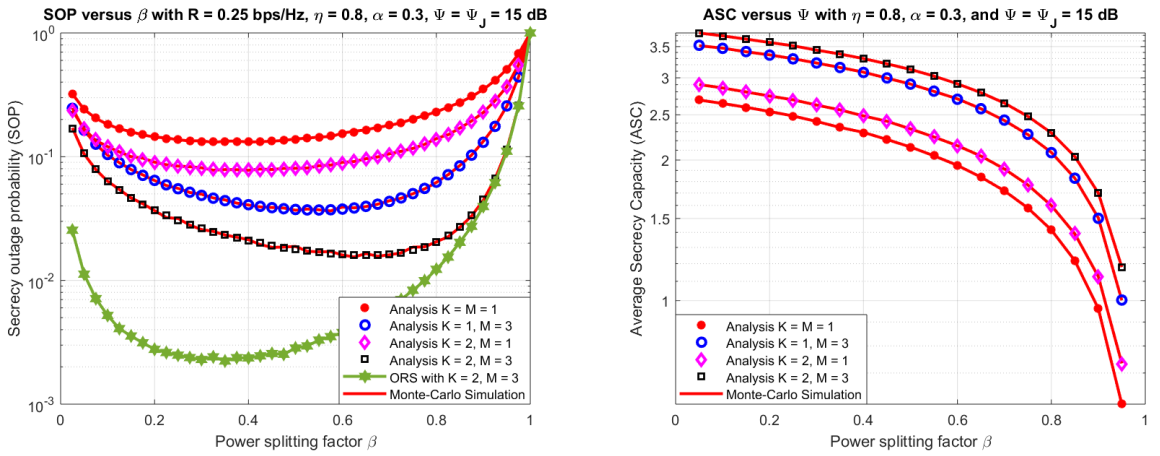


(a) Secrecy outage probability (b) Average secrecy capacity

Figure 7.8: SOP and ASC versus PS factor for different configurations of relay and jammer nodes.

similar to OP in Fig. 7.3a but faster. It is interesting to note that there always exists an outage floor in each simulation case. That means when $\Psi$ is large enough, the increasing of $\Psi$ does not result in notably change in SOP. This floor is lower when more relay nodes and jammer nodes are considered for helping. In Fig. 7.6b we can see that ASC increases with the transmit-power-to-noise ratio (SINR). It is obvious that the secrecy capacity is improved if we add more available-to-help relay nodes and more jammers. It seems that adding more available relay can bring more improvement that adding jammers, except for sufficiently high SINR regime, which makes the source-relay communications good enough.

Fig. 7.7 shows the effect of TS factor $\alpha$ on the secrecy performance. First, the SOP tends

to decreases when $\alpha$ increases. Please note that the secrecy rate in this case is defined as difference in capacity between the source-relay link and the source-eavesdropper link. When $\alpha$ increases, the outage performance of source-relay link is slightly degraded because the SINR threshold increases, while the performance of relay-destination link is significantly improved due to higher harvested energy and smaller transmission time (so, transmit power becomes larger). On the other hand, increasing $\alpha$ does not improve the capacity of the source-eavesdropper link. That's why SOP decreases with $\alpha$. It is shown in Fig. 7.7a that $K = 2$, $M = 3$ should be an appropriate choice for the numbers of relays and jammers, respectively. Secondly, the ASC is a concave function with respect to the time-switching factor $\alpha$, which can be explained as follows. For small $\alpha$, the transmission duration is large enough, while the SOP decreases with $\alpha$ as we explained in Fig. 7.7a, so the ASC increases with $\alpha$. However, when $\alpha$ passed some certain threshold, the transmission time becomes smaller and has bad impact on the overall capacity. So the ASC starts to decrease. As seen from Fig. 7.7b, the optimal $\alpha$ for 4 considered cases are very close together (around 0.17). Again, adding more available relays or adding more jammers can improve the ASC, where the former is better because here we have $\Psi = 15dB$.

As expected, there exists an optimal value of PS factor $\beta$ that minimizes SOP, as shown in Fig. 7.8a. This can be explained by the same argument as in Fig. 7.5b. We can also observe that the optimal value of $\beta$ increases from the scheme with less relays and jammers to the scheme with larger number of relays and jammers. Specifically, the optimal values of $\beta$ for the cases $K = M = 1$, $K = 2$, $M = 1$, $K = 1$, $M = 3$, and $K = 2$, $M = 3$ are 0.375, 0.4, 0.55, and 0.65 respectively. It's difficult to derive the closed-form formula for the optimal value of $\beta$, which is the solution of the equation $\frac{\partial(\text{SOP})}{\partial\beta} = 0$ because the integral form of SOP. However, because the SOP is a single-minimum function with respect to $\beta$, it is easy to develop an iterative algorithm to find the optimal $\beta$ numerically, for example, using Golden section search algorithm [75]. On the other hand, it is easily to see that larger $\beta$ results in smaller ASC because in (7.42), increasing $\beta$ leads to decreasing of the exponential terms and then the decreasing of ASC. By intuition, increasing $\beta$ makes the chance of successful decoding the message at relay reduced, so the overall capacity is reduced. Fig. 7.8b confirms this argument, as we see that ASC falls to zero when $\beta$ approaches 1.

The 3-D plot of SOP function versus $\alpha$ and $\beta$ for the case that $K = 2$ and $M = 3$ is shown in Fig. 7.9. We can find the global minimum of SOP, which is equal to 0.00168, obtained as $\alpha$ approaches 0.5 and $\beta = 0.34$[2]. It's worth noting that in all above figures, all analytical curves match perfectly with the corresponding simulation curves, which validate the correctness of our analysis. In Fig. 7.6a, Fig. 7.7a, and Fig. 7.8a, the SOP for optimal relay selection (ORS) is also given by simulation as a benchmark to compare with the partial relay selection (PRS) strategy. However, in this section, we prefer PRS because its simplicity to implement.

[2]An adaptive TPSR protocol, in which $\alpha$ and $\beta$ are regularly and optimally updated according to the channel states, can be implemented, with the trade-off on complexity and cost.

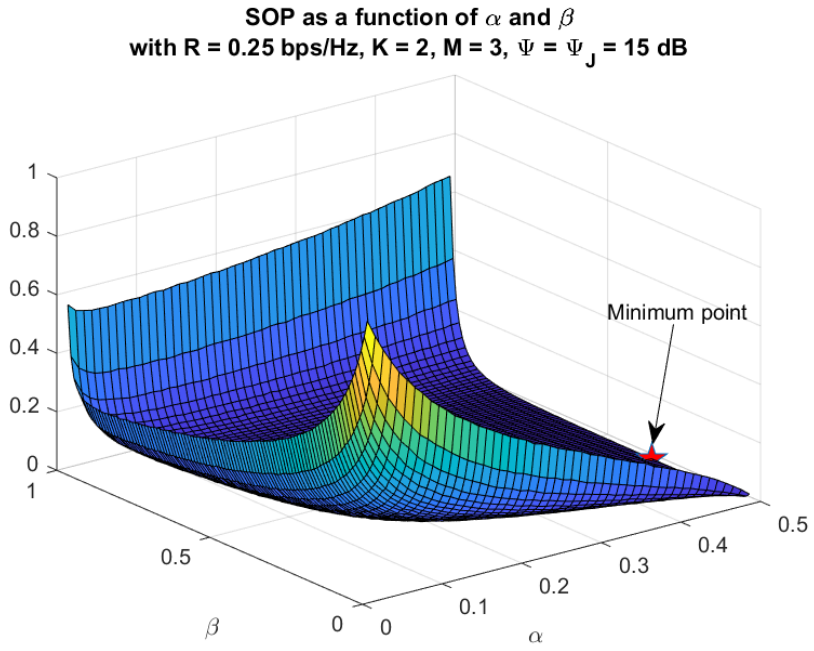


Figure 7.9: 3-D graph of SOP of A $\rightarrow$ B link versus $\alpha$ and $\beta$.

### 7.4.1 Conclusion

In this section, we propose a two-way HD wireless relay networks in Rayleigh fading environment with partial relay selection and hybrid-TPSR-based EH at relay node, in which there is an eavesdropper in the vicinity of one source node. To enhance the security of the networks, some friendly jammers are employed to degrade the received signals at eavesdropper. We derive the closed-form expression of OP at the legitimate destination node, the intercept probability at eavesdropper, the SOP, and the ASC of the system. All analytical results are verified by Monte Carlo simulations. From the numerical results, we show that adding more available-to-help relay nodes or adding more jammers can improve the reliability and security performance of the system significantly, in which the former method can provide larger improvement in average-to-high SINR regime. For very high SINR, adding more jammers would be more beneficial. Secondly, there exists a unique optimal value for either time-switching or PS factor to minimize the OP, while the intercept probability increases with time-switching factor but does not depend on PS factor. For the SOP, there may exist an outage floor if $M$ and $K$ is small. Therefore, it's recommended that we select $\alpha$ around 0.3 with $M = 3$ relay nodes and $K = 5$ or 7 jammers to obtain the desired performance but not to complicate the system. The results of this paper can find good applications in military communications as well as in IoT networks for smart cities, where the security of the messages is utmost important. For future work, we can extend the analysis to the case that multiple antennas are equipped at source nodes or eavesdroppers.

# 8 Conclusions and future work

This section is divided in two parts. In the first one, I summarize outcomes of this dissertation and the second is devoted to the future plans.

## 8.1 Summary of results and insights

In this dissertation, I study advanced EH protocols and various physical layer security strategies, and then propose some new communication schemes that integrate these two techniques together with other attracting techniques, with the ultimate goal to enhance both security and reliability of wireless relay networks in the presence of eavesdroppers. My wireless networks model consists of single or multiple sources, single or multiple destinations, and single or multiple intermediate relay nodes to help forwarding information from the sources to the destinations. There also exist some eavesdroppers in the surrounding environment, who may also want to receive the information from the sources illegally. To enhance the security of the networks, in this dissertation, I recommend to integrate many techniques to design a new physical layer security protocols based on RF EH. These techniques include relay selection, user selection, NOMA, multi-hop communications, FD communications, and cooperative jamming. This PhD dissertation thesis has introduced the framework for the design, analysis, and simulation of various EH-based physical layer security (PLS) schemes in wireless relay networks. To summary, the methodology to do the following works were demonstrated during this dissertation thesis in order to carry out the goals of the dissertation:

- The most important contribution of my dissertation is the proposal of two novel EH-based physical layer security network models: the first one is using friendly jammers together with hybrid TPSR protocol and partial relay selection and the second one is using cooperative jamming with jammer selection and multi-hop relaying.
- Closed-form or at least integral-form formulas of the key performance factors on security and reliability, including OP, throughput, symbol-error-rate, secrecy capacity, SOP, intercept probability, etc. have been derived rigorously for each EH or PLS or EH-PLS scheme that has been proposed in this dissertation. Beside the basic relaying model such as HD and FD relaying, some advanced relaying models has been proposed to serve specific applications, for example, the two-way relaying, multi-source relaying, or multi-hop relaying schemes for wireless sensor networks or wireless ad hoc networks.
- The effect of channel, transceiver, and attacker's parameters on the system performance is also an important contribution of this project. By taking into account the co-channel interference and hardware impairment, I investigate the robustness and the secure of the proposed network model to evaluate the possibility for their practical implementation.

- Finally, all analytical expressions of key performance factors as well as the impact of channel conditions, hardware noise, jammer and eavesdroppers configurations are verified carefully through Monte Carlo simulation. From the numerical results, the beast feasible configurations of the proposed network model can be recommended for practical applications.

To conclude, I confirm that my purpose is to provide a thorough analysis of EH and physical layer security combining solution for wireless relay networks from multiple perspectives: theoretical framework, simulation results, practical consideration, the variety of the strategies to serve for different applications, as well as the variety of the channel and transceiver conditions to be studied.

## 8.2 Future work

In the future, this work can also be extended to more complicated network models, for example, multi-hop relaying, multiple eavesdroppers, or correlation channels, as well as more advanced techniques such as massive MIMO. In addition, more specific applications can be investigated, for example, unmanned aerial vehicle (UAV) communication or underwater communications, which is out of the current scope of my dissertation.

## Candidate's published results cited in this work


[HDH01] **Ha, D.-H.**, Nguyen, T.N., Tran, M.H.Q., Li, X., Tran, P.T., Voznak, M. Security and reliability analysis of a two-way half-duplex wireless relaying network using partial relay selection and hybrid TPSR energy harvesting at relay nodes (2020) IEEE Access, 8, pp. 187165-187181. DOI: 10.1109/ACCESS.2020.3030794. **IF 3.745**.

[HDH02] **Ha. D.-H.**, Duy, T.T., Voznak, M. Secrecy outage performance of multi-hop LEACH networks using power beacon aided cooperative jamming with jammer selection methods (2020) AEU - International Journal of Electronics and Communications, 124, art. no. 153357. DOI: 10.1016/j.aeue.2020.153357. **IF 2.924**.

[HDH03] **Ha, D.-H.**, Dong, S.T.C., Nguyen, T.N., Trang, T.T., Voznak, M. Half-duplex energy harvesting relay network over different fading environment: System performance with effect of hardware impairment (2019) Applied Sciences (Switzerland), 9 (11), art. no. 2283. DOI: 10.3390/app9112283. **IF 2.217**.

[HDH04] Phu, T.T., Phan, D.-V., **Ha, D.-H.**, Nguyen, T.N., Tran, M., Voznak, M. Non-linear energy harvesting based power splitting relaying in full-duplex AF and DF relaying networks: System performance analysis (2020) Proceedings of the Estonian Academy of Sciences, 69 (4), pp. 368-381. DOI: 10.3176/proc.2020.4.06. **IF 0.883**.

[HDH05] Huynh, T.-P., **Ha, D.-H.**, Tuong, T.C., Fazio, P., Voznak, M. Secrecy outage probability of a NOMA scheme and impact imperfect channel state information in underlay cooperative cognitive networks (2020) Sensors (Switzerland), 20 (3), art. no. 895. DOI: 10.3390/s20030895. **IF 3.031**.

[HDH06] Nguyen, T.N., Tran, M., **Ha, D.-H.**, Trang, T.T., Voznak, M. Multi-source in DF cooperative networks with the PSR protocol based full-duplex energy harvesting over a Rayleigh fading channel: Performance analysis (2019) Proceedings of the Estonian Academy of Sciences, 68 (3), pp. 264-275. DOI: 10.3176/proc.2019.3.03 **IF 0.883**.

[HDH07] Nguyen, T.N., Tran, M., Nguyen, T.-L., **Ha, D.-H.**, Voznak, M. Performance analysis of a user selection protocol in cooperative networks with power splitting protocol-based energy harvesting over nakagami-m/rayleigh channels (2019) Electronics (Switzerland), 8 (4), art. no. 448. DOI: 10.3390/electronics8040448. **IF 1.764**.

[HDH08] Nguyen, T.N., Tran, M., Nguyen, T.-L., **Ha, D.-H.**, Voznak, M. Multisource power splitting energy harvesting relaying network in half-duplex system over block rayleigh fading channel: System performance analysis (2019) Electronics (Switzerland), 8 (1), art. no. 67. DOI: 10.3390/electronics8010067. **IF 1.764**.

[HDH09] Phan, V.-D., Nguyen, T.N., Tran, M., Trang, T.T., Voznak, M., **Ha, D.-H.**, Nguyen, T.-L. Power beacon-assisted energy harvesting in a half-duplex communication network under co-channel interference over a Rayleigh fading environment: Energy efficiency and outage probability analysis (2019) Energies, 12 (13), art. no. 2579. DOI: 10.3390/en12132579. **IF 2.707**.

[HDH10] Nguyen, T.N., Tran, M., **Ha, D.-H.**, Nguyen, T.-L., Voznak, M. Energy harvesting based two-way full-duplex relaying network over a rician fading environment: Performance analysis (2019) Proceedings of the Estonian Academy of Sciences, 68 (1), pp. 111-123. DOI: 10.3176/proc.2019.1.11 **IF 0.883**.

[HDH11] Nguyen, T.N., Tran, M., Tran, P.T., Tin, P.T., Nguyen, T.-L., **Ha, D.-H.**, Voznak, M. On the Performance of Power Splitting Energy Harvested Wireless Full-Duplex Relaying Network with Imperfect CSI over Dissimilar Channels (2018) Security and Communication Networks, 2018, art. no. 6036087. DOI: 10.1155/2018/6036087. **IF 1.288**.

[HDH12] Nguyen, T.N., Tin, P.T., **Ha, D.-H.**, Voznak, M., Tran, P.T., Tran, M., Nguyen, T.-L. Hybrid TSR-PSR alternate energy harvesting relay network over rician fading channels: Outage probability and SER analysis (2018) Sensors (Switzerland), 18 (11), art. no. 3839. DOI: 10.3390/s18113839. **IF 3.031**.

[HDH13] **Ha, D.-H.**, Ha, D.-B., Voznak, M. On secure cooperative non-orthogonal multiple access network with RF power transfer (2019) Lecture Notes of the Institute for Computer Sciences, Social-Informatics and Telecommunications Engineering, LNICST, 293, pp. 117-129. DOI: 10.1007/978-3-030-30149-1_10.

[HDH14] **Ha, D.-H.**, Ha, D.-B., Vo, V.-A., Voznak, M. Performance analysis on wireless power transfer wireless sensor network with best AF relay selection over Nakagami-m fading (2019) Lecture Notes of the Institute for Computer Sciences, Social-Informatics and Telecommunications Engineering, LNICST, 293, pp. 193-204. DOI: 10.1007/978-3-030-30149-1_16.

[HDH15] **Ha, D.-H.**, Ha, D.-B., Zdralek, J., Voznak, M. A New Protocol based on Optimal Capacity for Energy Harvesting Amplify-and-Forward Relaying Networks (2019) NICS 2018 - Proceedings of 2018 5th NAFOSTED Conference on Information and Computer Science, art. no. 8606829, pp. 11-16. DOI: 10.1109/NICS.2018.8606829.

[HDH16] **Ha, D.-H.**, Ha, D.-B., Zdralek, J., Voznak, M. Performance Analysis of Hybrid Energy Harvesting AF Relaying Networks over Nakagami-m Fading Channels (2018) International Conference on Advanced Technologies for Communications, 2018-October, art. no. 8587424, pp. 157-162. DOI: 10.1109/ATC.2018.8587424.

[HDH17] **Ha, D.-H.**, Ha, D.-B., Zdralek, J., Voznak, M., Nguyen, T.N. A new protocol for energy harvesting decode-and-forward relaying networks (2020) Lecture Notes in Electrical Engineering, 554, pp. 693-704. DOI: 10.1007/978-3-030-14907-9_67.

[HDH18] Anh, N.T., **Ha, D.-H.**, Duy, T.T., Hai, H.D., Minh, N.C. Reliability-Security Analysis for Harvest-to-Jam based Multi-hop LEACH Networks under Impact of Hardware Noises (2019) International Conference on Advanced Technologies for Communications, 2019-October, art. no. 8924531, pp. 174-178. DOI: 10.1109/ATC.2019.8924531.

[HDH19] Ha, D.-B., Truong, V.-T., **Ha, D.-H.** A Novel Secure Protocol for Mobile Edge Computing Network Applied Downlink NOMA (2020) Lecture Notes of the Institute for Computer Sciences, Social-Informatics and Telecommunications Engineering, LNICST, 334, pp. 324-336. DOI: 10.1007/978-3-030-63083-6_25.

# Overview of candidate's research results and activities

## Publication activities

I provide the following overview of indexed results in relevant scientific databases, in order to document my research activities within the entire period of my doctoral study:

- Articles in journals with non-zero impact factor indexed in Web of Science: 12.
- Conference papers indexed in WoS/Scopus: 7.
- Citations: 75 in Scopus and 65 in Web of Science.
- ORCID: 0000-0001-6980-7273
- Research ID: G-2213-2019

## Project memberships and participations

- Proj. reg. no. SP2020/65 - Networks and Communications Technologies for Smart Cities III., Student Grant Competition of VSB-TUO (2020).
- Proj. reg. no. SP2019/41 - Networks and Communications Technologies for Smart Cities II., Student Grant Competition of VSB-TUO (2019).
- Proj. reg. no. SP2018/59 - Networks and Communications Technologies for Smart Cities I., Student Grant Competition of VSB-TUO (2018).

## References


[1] H. Alves, R. D. Souza, M. Debbah, and M. Bennis, "Performance of transmit antenna selection physical layer security schemes", 6, vol. 19, 2012, pp. 372–375.

[2] K. Huang and V. K. N. Lau, "Enabling wireless power transfer in cellular networks: Architecture, modeling and deployment", 2, vol. 13, 2014, pp. 902–912.

[3] G. Gui, M. Liu, F. Tang, N. Kato, and F. Adachi, "6g: Opening new horizons for integration of comfort, security, and intelligence", *IEEE Wireless Communications*, vol. 27, no. 5, pp. 126–132, 2020. DOI: 10.1109/MWC.001.1900516.

[4] K. David and H. Berndt, "6g vision and requirements: Is there any need for beyond 5g?", *IEEE Vehicular Technology Magazine*, vol. 13, no. 3, pp. 72–80, 2018. DOI: 10.1109/MVT.2018.2848498.

[5] A. Dogra, R. K. Jha, and S. Jain, "A survey on beyond 5g network with the advent of 6g: Architecture and emerging technologies", *IEEE Access*, pp. 1–1, 2020. DOI: 10.1109/ACCESS.2020.3031234.

[6] A. A. Nasir, X. Zhou, S. Durrani, and R. A. Kennedy, "Relaying protocols for wireless energy harvesting and information processing", *IEEE Transactions on Wireless Communications*, vol. 12, no. 7, pp. 3622–3636, 2013. DOI: 10.1109/TWC.2013.062413.122042.

[7] R. Vahidnia, A. Anpalagan, and J. Mirzaei, "Achievable rate region for energy harvesting asynchronous two-way relay networks", *IEEE Access*, vol. 4, pp. 951–958, 2016. DOI: 10.1109/ACCESS.2016.2535486.

[8] D. W. K. Ng, T. Q. Duong, C. Zhong, and R. Schober, *Wireless information and power transfer: theory and practice*. John Wiley & Sons, 2019.

[9] S. Atapattu and J. Evans, "Optimal energy harvesting protocols for wireless relay networks", *IEEE Transactions on Wireless Communications*, vol. 15, no. 8, pp. 5789–5803, 2016. DOI: 10.1109/TWC.2016.2569097.

[10] Q. Wu, M. Tao, D. W. Kwan Ng, W. Chen, and R. Schober, "Energy-efficient resource allocation for wireless powered communication networks", *IEEE Transactions on Wireless Communications*, vol. 15, no. 3, pp. 2312–2327, 2016. DOI: 10.1109/TWC.2015.2502590.

[11] H. Ju and R. Zhang, "Throughput maximization in wireless powered communication networks", *IEEE Transactions on Wireless Communications*, vol. 13, no. 1, pp. 418–428, 2014-01, ISSN: 1558-2248. DOI: 10.1109/TWC.2013.112513.130760.

[12] L. R. Varshney, "Transporting information and energy simultaneously", in *2008 IEEE International Symposium on Information Theory*, 2008-07, pp. 1612–1616. DOI: 10.1109/ISIT.2008.4595260.

[13] R. Zhang and C. K. Ho, "Mimo broadcasting for simultaneous wireless information and power transfer", *IEEE Transactions on Wireless Communications*, vol. 12, no. 5, pp. 1989–2001, 2013.

[14] A. A. Nasir, X. Zhou, S. Durrani, and R. A. Kennedy, "Throughput and ergodic capacity of wireless energy harvesting based df relaying network", in *2014 IEEE International Conference on Communications (ICC)*, 2014, pp. 4066–4071.

[15] C. R. Valenta and G. D. Durgin, "Harvesting wireless power: Survey of energy-harvester conversion efficiency in far-field, wireless power transfer systems", *IEEE Microwave Magazine*, vol. 15, no. 4, pp. 108–120, 2014.

[16] T. N. Nguyen, P. Tran Tin, D. H. Ha, M. Voznak, P. T. Tran, M. Tran, and T.-L. Nguyen, "Hybrid tsr–psr alternate energy harvesting relay network over rician fading channels: Outage probability and ser analysis", *Sensors*, vol. 18, no. 11, p. 3839, 2018.

[17] H. Alves, R. D. Souza, and M. Debbah, "Enhanced physical layer security through transmit antenna selection", in *2011 IEEE GLOBECOM Workshops (GC Wkshps)*, 2011, pp. 879–883.

[18] R. Zhang, L. Song, Z. Han, and B. Jiao, "Physical layer security for two-way untrusted relaying with friendly jammers", *IEEE Transactions on Vehicular Technology*, vol. 61, no. 8, pp. 3693–3704, 2012.

[19] A. Goldsmith, *Wireless Communications*. Cambridge University Press: Cambridge, UK, 2009.

[20] L. Vandenberghe, S. Boyd, and K. Comanor, "Generalized chebyshev bounds via semidefinite programming", *SIAM review*, vol. 49, no. 1, pp. 52–64, 2007.

[21] L. Wang, N. Yang, M. Elkashlan, P. L. Yeoh, and J. Yuan, "Physical layer security of maximal ratio combining in two-wave with diffuse power fading channels", *IEEE Transactions on Information Forensics and Security*, vol. 9, no. 2, pp. 247–258, 2014. DOI: 10.1109/TIFS.2013.2296991.

[22] J. Barros and M. R. D. Rodrigues, "Secrecy capacity of wireless channels", in *2006 IEEE International Symposium on Information Theory*, 2006, pp. 356–360.

[23] I. F. Akyildiz, W. Lee, M. C. Vuran, and S. Mohanty, "A survey on spectrum management in cognitive radio networks", *IEEE Communications Magazine*, vol. 46, no. 4, pp. 40–48, 2008. DOI: 10.1109/MCOM.2008.4481339.

[24] B. R. Marks and G. P. Wright, "A general inner approximation algorithm for nonconvex mathematical programs", *Operations research*, vol. 26, no. 4, pp. 681–683, 1978.

[25] L. Dong, Z. Han, A. P. Petropulu, and H. V. Poor, "Improving wireless physical layer security via cooperating relays", *IEEE Transactions on Signal Processing*, vol. 58, no. 3, pp. 1875–1888, 2010-03, ISSN: 1941-0476. DOI: 10.1109/TSP.2009.2038412.

[26] A. Afana, A. Ghrayeb, V. Asghari, and S. Affes, "Distributed beamforming for spectrum-sharing systems with af cooperative two-way relaying", *IEEE Transactions on Communications*, vol. 62, no. 9, pp. 3180–3195, 2014. DOI: 10.1109/TCOMM.2014.2345406.

[27] U. Rashid, H. D. Tuan, and H. H. Nguyen, "Relay beamforming designs in multi-user wireless relay networks based on throughput maximin optimization", *IEEE Transactions on Communications*, vol. 61, no. 5, pp. 1739–1749, 2013. DOI: 10.1109/TCOMM.2013.022713.120129.

[28] D. W. K. Ng, E. S. Lo, and R. Schober, "Robust beamforming for secure communication in systems with wireless information and power transfer", *IEEE Transactions on Wireless Communications*, vol. 13, no. 8, pp. 4599–4615, 2014. DOI: 10.1109/TWC.2014.2314654.

[29] D.-B. H. Ha, D.-D. Tran, V. Tran-Ha, and E.-K. Hong, "Performance of amplify-and-forward relaying with wireless power transfer over dissimilar channels", *Elektronika ir Elektrotechnika*, vol. 21, no. 5, pp. 90–95, 2015.

[30] E. Tekin and A. Yener, "The general gaussian multiple-access and two-way wiretap channels: Achievable rates and cooperative jamming", *IEEE Transactions on Information Theory*, vol. 54, no. 6, pp. 2735–2751, 2008. DOI: 10.1109/TIT.2008.921680.

[31] P. Lin, S. Lai, S. Lin, and H. Su, "On secrecy rate of the generalized artificial-noise assisted secure beamforming for wiretap channels", *IEEE Journal on Selected Areas in Communications*, vol. 31, no. 9, pp. 1728–1740, 2013. DOI: 10.1109/JSAC.2013.130907.

[32] A. Wiesel, Y. C. Eldar, and S. Shamai, "Linear precoding via conic optimization for fixed mimo receivers", *IEEE Transactions on Signal Processing*, vol. 54, no. 1, pp. 161–176, 2006. DOI: 10.1109/TSP.2005.861073.

[33] G. Zheng, I. Krikidis, J. Li, A. P. Petropulu, and B. Ottersten, "Improving physical layer secrecy using full-duplex jamming receivers", *IEEE Transactions on Signal Processing*, vol. 61, no. 20, pp. 4962–4974, 2013. DOI: 10.1109/TSP.2013.2269049.

[34] U. Maurer and S. Wolf, "Secret-key agreement over unauthenticated public channels .i. definitions and a completeness result", *IEEE Transactions on Information Theory*, vol. 49, no. 4, pp. 822–851, 2003.

[35] R. Ahlswede and I. Csiszar, "Common randomness in information theory and cryptography. i. secret sharing", *IEEE Transactions on Information Theory*, vol. 39, no. 4, pp. 1121–1132, 1993.

[36] C. Chen and M. A. Jensen, "Secrecy extraction from increased randomness in a time-variant mimo channel", in *GLOBECOM 2009 - 2009 IEEE Global Telecommunications Conference*, 2009, pp. 1–6.

[37] Lun Dong, Z. Han, A. P. Petropulu, and H. V. Poor, "Secure wireless communications via cooperation", in *2008 46th Annual Allerton Conference on Communication, Control, and Computing*, 2008, pp. 1132–1138.

[38] I. Krikidis, J. S. Thompson, P. M. Grant, and S. McLaughlin, "Power allocation for cooperative-based jamming in wireless networks with secrecy constraints", in *2010 IEEE Globecom Workshops*, 2010, pp. 1177–1181.

[39] M. Z. I. Sarkar and T. Ratnarajah, "Bounds on the secrecy capacity with diversity combining techniques", in *2012 IEEE Wireless Communications and Networking Conference (WCNC)*, 2012, pp. 2847–2851.

[40] P. C. Pinto, J. Barros, and M. Z. Win, "Secure communication in stochastic wireless networks—part ii: Maximum rate and collusion", *IEEE Transactions on Information Forensics and Security*, vol. 7, no. 1, pp. 139–147, 2012.

[41] S. Bayat, R. H. Y. Louie, Z. Han, B. Vucetic, and Y. Li, "Physical-layer security in distributed wireless networks using matching theory", *IEEE Transactions on Information Forensics and Security*, vol. 8, no. 5, pp. 717–732, 2013.

[42] W. Saad, Z. Han, T. Basar, M. Debbah, and A. Hjorungnes, "Physical layer security: Coalitional games for distributed cooperation", in *2009 7th International Symposium on Modeling and Optimization in Mobile, Ad Hoc, and Wireless Networks*, 2009, pp. 1–8.

[43] L. Liu, R. Zhang, and K. Chua, "Multi-antenna wireless powered communication with energy beamforming", *IEEE Transactions on Communications*, vol. 62, no. 12, pp. 4349–4361, 2014.

[44] G. Yang, C. K. Ho, and Y. L. Guan, "Dynamic resource allocation for multiple-antenna wireless power transfer", 14, vol. 62, 2014, pp. 3565–3577.

[45] X. Lu, P. Wang, D. Niyato, and Z. Han, "Resource allocation in wireless networks with rf energy harvesting and transfer", *IEEE Network*, vol. 29, no. 6, pp. 68–75, 2015.

[46] P. Grover and A. Sahai, "Shannon meets tesla: Wireless information and power transfer", in *2010 IEEE International Symposium on Information Theory*, 2010, pp. 2363–2367.

[47] V. N. Q. Bao, N. Linh-Trung, and M. Debbah, "Relay selection schemes for dual-hop networks under security constraints with multiple eavesdroppers", 12, vol. 12, 2013, pp. 6076–6085.

[48] T. D. Hieu, T. T. Duy, and S.-G. Choi, "Secrecy performance of a generalized partial relay selection protocol in underlay cognitive networks", *Int. J. Commun. Syst.*, vol. 31, no. 17, 2018. DOI: 10.1002/dac.3806. [Online]. Available: https://doi.org/10.1002/dac.3806.

[49] D. Ha and N. Yo, "Physical layer secrecy performance with transmitter antenna selection over dissimilar fading channels", in *2014 International Conference on Computer, Communications, and Control Technology (I4CT)*, 2014, pp. 140–144.

[50] B. C. Nguyen, T. M. Hoang, and P. T. Tran, "Performance analysis of full-duplex decode-and-forward relay system with energy harvesting over nakagami-m fading channels", *AEU - International Journal of Electronics and Communications*, vol. 98, pp. 114–122, 2019, ISSN: 1434-8411. DOI: https://doi.org/10.1016/j.aeue.2018.11.002. [Online]. Available: http://www.sciencedirect.com/science/article/pii/S1434841118320090.

[51] T. M. Hoang, B. C. Nguyen, N. N. Thang, M. H. Tran, and P. T. Tran, "Performance and optimal analysis of time-switching energy harvesting protocol for mimo full-duplex decode-and-forward wireless relay networks with various transmitter and receiver diversity techniques", *Journal of the Franklin Institute*, 2020, ISSN: 0016-0032. DOI: https://doi.org/10.1016/j.jfranklin.2020.09.037. [Online]. Available: http://www.sciencedirect.com/science/article/pii/S0016003220306839.

[52] N. B. Cao, T. M. Hoang, X. N. Pham, and P. T. Tran, "Performance analysis of energy harvesting-based full-duplex decode-and-forward vehicle-to-vehicle relay networks with nonorthogonal multiple access", *Wirel. Commun. Mob. Comput.*, vol. 2019, 6097686:1–6097686:11, 2019. DOI: 10.1155/2019/6097686. [Online]. Available: https://doi.org/10.1155/2019/6097686.

[53] H. M. Tran, C. B. Nguyen, P. T. Tran, and D. T. Le, "Outage analysis of rf energy harvesting cooperative communication systems over nakagami-m fading channels with integer and non-integer m", *IEEE Transactions on Vehicular Technology*, pp. 1–1, 2020, ISSN: 1939-9359. DOI: 10.1109/TVT.2020.2964809.

[54] P. H. Tan, "Performance enhancement solutions in wireless communication networks", Dostupnéz: http://hdl.handle.net/10084/138562, Ph.D. dissertation, Vysoká škola báňská - Technická Univerzita Ostrava, Ostrava, 2019-10.

[55] T. T. Phu, "Impact of hardware impairments on secrecy performances of wireless relay systems", Dostupné z: http://hdl.handle.net/10084/137502, Ph.D. dissertation, Vysoká škola báňská - Technická Univerzita Ostrava, Ostrava, 2019-02.

[56] A. Sabharwal, P. Schniter, D. Guo, D. W. Bliss, S. Rangarajan, and R. Wichman, "In-band full-duplex wireless: Challenges and opportunities", *IEEE Journal on Selected Areas in Communications*, vol. 32, no. 9, pp. 1637–1652, 2014.

[57] B. C. Nguyen, T. M. Hoang, P. T. Tran, and T. N. Nguyen, "Outage probability of noma system with wireless power transfer at source and full-duplex relay", *AEU - International Journal of Electronics and Communications*, p. 152 957, 2019, ISSN: 1434-8411. DOI: https://doi.org/10.1016/j.aeue.2019.152957. [Online]. Available: http://www.sciencedirect.com/science/article/pii/S1434841119314141.

[58] A. D. Wyner, "The wire-tap channel", *The Bell System Technical Journal*, vol. 54, no. 8, pp. 1355–1387, 1975-10, ISSN: 0005-8580. DOI: 10.1002/j.1538-7305.1975.tb02040.x.

[59] S. Leung-Yan-Cheong and M. Hellman, "The gaussian wire-tap channel", *IEEE Transactions on Information Theory*, vol. 24, no. 4, pp. 451–456, 1978-07, ISSN: 1557-9654. DOI: 10.1109/TIT.1978.1055917.

[60] I. Csiszar and J. Korner, "Broadcast channels with confidential messages", *IEEE Transactions on Information Theory*, vol. 24, no. 3, pp. 339–348, 1978-05, ISSN: 1557-9654. DOI: 10.1109/TIT.1978.1055892.

[61] A. Mukherjee, S. A. A. Fakoorian, J. Huang, and A. L. Swindlehurst, "Principles of physical layer security in multiuser wireless networks: A survey", *IEEE Communications Surveys Tutorials*, vol. 16, no. 3, pp. 1550–1573, 2014-Third, ISSN: 2373-745X. DOI: 10.1109/SURV.2014.012314.00178.

[62] D. Ha, N. G. Nguyen, D. Tran, and T. Nguyen, "Physical layer security in uwb communication systems with transmit antenna selection", in *2014 International Conference on Computing, Management and Telecommunications (ComManTel)*, 2014, pp. 280–285.

[63] S. Bi, C. K. Ho, and R. Zhang, "Wireless powered communication: Opportunities and challenges", *IEEE Communications Magazine*, vol. 53, no. 4, pp. 117–125, 2015. DOI: 10.1109/MCOM.2015.7081084.

[64] H. Yu, H. Lee, and H. Jeon, "What is 5g? emerging 5g mobile services and network requirements", *Sustainability*, vol. 9, no. 10, p. 1848, 2017.

[65] H. Ju, E. Oh, and D. Hong, "Catching resource-devouring worms in next-generation wireless relay systems: Two-way relay and full-duplex relay", *IEEE Communications Magazine*, vol. 47, no. 9, pp. 58–65, 2009.

[66] T. Riihonen, S. Werner, R. Wichman, and J. Hamalainen, "Outage probabilities in infrastructure-based single-frequency relay links", in *2009 IEEE wireless communications and networking conference*, IEEE, 2009, pp. 1–6.

[67] D. W. K. Ng, E. S. Lo, and R. Schober, "Dynamic resource allocation in mimo-ofdma systems with full-duplex and hybrid relaying", *IEEE Transactions on Communications*, vol. 60, no. 5, pp. 1291–1304, 2012.

[68] I. Krikidis, H. A. Suraweera, P. J. Smith, and C. Yuen, "Full-duplex relay selection for amplify-and-forward cooperative networks", *IEEE Transactions on Wireless Communications*, vol. 11, no. 12, pp. 4381–4393, 2012.

[69] R. H. Louie, Y. Li, and B. Vucetic, "Practical physical layer network coding for two-way relay channels: Performance analysis and comparison", *IEEE Transactions on Wireless Communications*, vol. 9, no. 2, pp. 764–777, 2010.

[70] T. Riihonen, S. Werner, and R. Wichman, "Hybrid full-duplex/half-duplex relaying with transmit power adaptation", *IEEE Transactions on Wireless Communications*, vol. 10, no. 9, pp. 3074–3085, 2011.

[71] H. A. Suraweera, G. K. Karagiannidis, and P. J. Smith, "Performance analysis of the dual-hop asymmetric fading channel", *IEEE Transactions on Wireless Communications*, vol. 8, no. 6, pp. 2783–2788, 2009.

[72] i. I S Gradshteyn; I M Ryzhik; Daniel Zwillinger; Victor Moll; Scripta Technica, *Table of integrals, series, and products*, 8th ed. Academic Press, , Elsevier Inc, 2014, ISBN: 978-0-12-384933-5,9780123849342,0123849349,0123849330. [Online]. Available: `http://gen.lib.rus.ec/book/index.php?md5=61138768dcd8e578e836aa12c0203f7f`.

[73] M. R. Bhatnagar, "On the capacity of decode-and-forward relaying over rician fading channels", *IEEE Communications Letters*, vol. 17, no. 6, pp. 1100–1103, 2013.

[74] T. N. Nguyen, T. H. Q. Minh, P. T. Tran, M. Voznak, T. T. Duy, T.-L. Nguyen, and P. T. Tin, "Performance enhancement for energy harvesting based two-way relay protocols in wireless ad-hoc networks with partial and full relay selection methods", *Ad hoc networks*, vol. 84, pp. 178–187, 2019.

[75] E. K. P. Chong and S. H. Zak, *An Introduction to Optimization*, 4th. Hoboken, New Jersey, USA: John Wiley & Sons, 2013, ISBN: 9781118279014.

[76] T. N. Nguyen, P. T. Tran, and M. Voznak, "Power splitting based energy-harvesting protocol for wireless-powered communication networks with a bidirectional relay", *International Journal of Communication Systems*, vol. 31, no. 13, e3721, 2018, e3721 dac.3721. DOI: `10.1002/dac.3721`. eprint: `https://onlinelibrary.wiley.com/doi/pdf/10.1002/dac.3721`. [Online]. Available: `https://onlinelibrary.wiley.com/doi/abs/10.1002/dac.3721`.

[77] T. N. Nguyen, T. H. Quang Minh, P. T. Tran, and M. Vozňák, "Energy harvesting over rician fading channel: A performance analysis for half-duplex bidirectional sensor networks under hardware impairments", *Sensors*, vol. 18, no. 6, p. 1781, 2018.

[78] T. N. Nguyen, T. H. Q. Minh, P. T. Tran, and M. Voznak, "Adaptive energy harvesting relaying protocol for two-way half-duplex system network over rician fading channels", *Wireless Communications and Mobile Computing*, vol. 2018, 2018-04, ISSN: 1530-8669. DOI: `0.1155/2018/7693016`.

[79] D. Niyato, D. I. Kim, M. Maso, and Z. Han, "Wireless powered communication networks: Research directions and technological approaches", *IEEE Wireless Communications*, vol. 24, no. 6, pp. 88–97, 2017.

[80] S. Salari, I.-M. Kim, D. I. Kim, and F. Chan, "Joint eh time allocation and distributed beamforming in interference-limited two-way networks with eh-based relays", *IEEE Transactions on Wireless Communications*, vol. 16, no. 10, pp. 6395–6408, 2017.

[81] T. D. P. Perera, D. N. K. Jayakody, S. K. Sharma, S. Chatzinotas, and J. Li, "Simultaneous wireless information and power transfer (swipt): Recent advances and future challenges", *IEEE Communications Surveys & Tutorials*, vol. 20, no. 1, pp. 264–302, 2017.

[82] M. R. Bhatnagar, "On the capacity of decode-and-forward relaying over rician fading channels", *IEEE Communications Letters*, vol. 17, no. 6, pp. 1100–1103, 2013.

[83] A. A. Okandeji, M. R. Khandaker, and K.-K. Wong, "Two-way beamforming optimization for full-duplex swipt systems", in *2016 24th European Signal Processing Conference (EUSIPCO)*, IEEE, 2016, pp. 2375–2379.

[84] A. A. Okandeji, M. R. Khandaker, K.-K. Wong, and Z. Zheng, "Joint transmit power and relay two-way beamforming optimization for energy-harvesting full-duplex communications", in *2016 IEEE Globecom Workshops (GC Wkshps)*, IEEE, 2016, pp. 1–6.

[85] Y. Hu, Y. Zhu, and A. Schmeink, "Simultaneous wireless information and power transfer in relay networks with finite blocklength codes", in *2017 23rd Asia-Pacific Conference on Communications (APCC)*, IEEE, 2017, pp. 1–6.

[86] T. N. Nguyen, T. T. Duy, G.-T. Luu, P. T. Tran, and M. Vozňák, "Energy harvesting-based spectrum access with incremental cooperation, relay selection and hardware noises", 2017.

[87] X. Chen, D. W. K. Ng, and H.-H. Chen, "Secrecy wireless information and power transfer: Challenges and opportunities", *IEEE Wireless Communications*, vol. 23, no. 2, pp. 54–61, 2016.

[88] R. Atallah, M. Khabbaz, and C. Assi, "Energy harvesting in vehicular networks: A contemporary survey", *IEEE Wireless Communications*, vol. 23, no. 2, pp. 70–77, 2016. DOI: 10.1109/MWC.2016.7462487.

[89] L. Liu, R. Zhang, and K. Chua, "Wireless information and power transfer: A dynamic power splitting approach", *IEEE Transactions on Communications*, vol. 61, no. 9, pp. 3990–4001, 2013. DOI: 10.1109/TCOMM.2013.071813.130105.

[90] V. Sharma and P. Karmakar, "A novel method of opportunistic wireless energy harvesting in cognitive radio networks", in *2015 7th International Conference on Computational Intelligence, Communication Systems and Networks*, 2015, pp. 59–64. DOI: 10.1109/CICSyN.2015.21.

[91] M. Matthaiou, A. Papadogiannis, E. Bjornson, and M. Debbah, "Two-way relaying under the presence of relay transceiver hardware impairments", *IEEE Communications Letters*, vol. 17, no. 6, pp. 1136–1139, 2013. DOI: 10.1109/LCOMM.2013.042313.130191.

[92] T. Li, P. Fan, and K. B. Letaief, "Outage probability of energy harvesting relay-aided cooperative networks over rayleigh fading channel", *IEEE Transactions on Vehicular Technology*, vol. 65, no. 2, pp. 972–978, 2016. DOI: 10.1109/TVT.2015.2402274.

[93] A. M. Fouladgar and O. Simeone, "On the transfer of information and energy in multi-user systems", *IEEE Communications Letters*, vol. 16, no. 11, pp. 1733–1736, 2012.

[94] J. Park and B. Clerckx, "Joint wireless information and energy transfer in a two-user mimo interference channel", *IEEE Transactions on Wireless Communications*, vol. 12, no. 8, pp. 4210–4221, 2013. DOI: 10.1109/TWC.2013.071913.130084.

[95] T. Q. Duong, T. T. Duy, M. Matthaiou, T. Tsiftsis, and G. K. Karagiannidis, "Cognitive cooperative networks in dual-hop asymmetric fading channels", in *2013 IEEE Global Communications Conference (GLOBECOM)*, IEEE, 2013, pp. 955–961.

[96] T. N. Nguyen, M. Tran, T.-L. Nguyen, D.-H. Ha, and M. Voznak, "Performance analysis of a user selection protocol in cooperative networks with power splitting protocol-based energy harvesting over nakagami-m/rayleigh channels", *Electronics*, vol. 8, no. 4, 2019, ISSN: 2079-9292. DOI: 10.3390/electronics8040448. [Online]. Available: https://www.mdpi.com/2079-9292/8/4/448.

[97] X. Zhou and Q. Li, "Energy efficiency for swipt in mimo two-way amplify-and-forward relay networks", *IEEE Transactions on Vehicular Technology*, vol. 67, no. 6, pp. 4910–4924, 2018. DOI: 10.1109/TVT.2018.2819682.

[98] Z. Masood, S. P. Jung, and Y. Choi, "Energy-efficiency performance analysis and maximization using wireless energy harvesting in wireless sensor networks", *Energies*, vol. 11, no. 11, 2018, ISSN: 1996-1073. DOI: 10.3390/en11112917. [Online]. Available: https://www.mdpi.com/1996-1073/11/11/2917.

[99] D. W. K. Ng, E. S. Lo, and R. Schober, "Wireless information and power transfer: Energy efficiency optimization in ofdma systems", *IEEE Transactions on Wireless Communications*, vol. 12, no. 12, pp. 6352–6370, 2013. DOI: 10.1109/TWC.2013.103113.130470.

[100] Y. Huang, M. Liu, and Y. Liu, "Energy-efficient swipt in iot distributed antenna systems", *IEEE Internet of Things Journal*, vol. 5, no. 4, pp. 2646–2656, 2018. DOI: 10.1109/JIOT.2018.2796124.

[101] X. Chen, X. Wang, and X. Chen, "Energy-efficient optimization for wireless information and power transfer in large-scale mimo systems employing energy beamforming", *IEEE Wireless Communications Letters*, vol. 2, no. 6, pp. 667–670, 2013.

[102] S. Guo, Y. Yang, and H. Yu, "Energy-efficient cooperative transmission for swipt in wireless sensor networks", in *Wireless Power Transfer Algorithms, Technologies and Applications in Ad Hoc Communication Networks*, Springer, 2016, pp. 253–281.

[103] S. Mao, S. Leng, J. Hu, and K. Yang, "Energy-efficient resource allocation for cooperative wireless powered cellular networks", in *2018 IEEE international conference on communications (ICC)*, IEEE, 2018, pp. 1–6.

[104] G. Lu, C. Lei, Y. Ye, L. Shi, and T. Wang, "Energy efficiency optimization for af relaying with ts-swipt", *Energies*, vol. 12, no. 6, 2019, ISSN: 1996-1073. DOI: 10.3390/en12060993. [Online]. Available: https://www.mdpi.com/1996-1073/12/6/993.

[105] X. Chen, Z. Zhang, H. Chen, and H. Zhang, "Enhancing wireless information and power transfer by exploiting multi-antenna techniques", *IEEE Communications Magazine*, vol. 53, no. 4, pp. 133–141, 2015. DOI: 10.1109/MCOM.2015.7081086.

[106] Y. Luo, J. Zhang, and K. B. Letaief, "Relay selection for energy harvesting cooperative communication systems", in *2013 IEEE Global Communications Conference (GLOBECOM)*, 2013, pp. 2514–2519. DOI: 10.1109/GLOCOM.2013.6831452.

[107] A. A. Nasir, X. Zhou, S. Durrani, and R. A. Kennedy, "Block-wise time-switching energy harvesting protocol for wireless-powered af relays", in *2015 IEEE International Conference on Communications (ICC)*, 2015, pp. 80–85. DOI: 10.1109/ICC.2015.7248302.

[108] Y. Liu, "Wireless information and power transfer for multirelay-assisted cooperative communication", *IEEE Communications Letters*, vol. 20, no. 4, pp. 784–787, 2016. DOI: 10.1109/LCOMM.2016.2535114.

[109] V. Singh and H. Ochiai, "An efficient time switching protocol with adaptive power splitting for wireless energy harvesting relay networks", in *2017 IEEE 85th Vehicular Technology Conference (VTC Spring)*, 2017, pp. 1–5. DOI: 10.1109/VTCSpring.2017.8108268.

[110] X. Zhou, R. Zhang, and C. K. Ho, "Wireless information and power transfer: Architecture design and rate-energy tradeoff", *IEEE Transactions on communications*, vol. 61, no. 11, pp. 4754–4767, 2013.

[111] T. T. Duy, G. C. Alexandropoulos, V. T. Tung, V. N. Son, and T. Q. Duong, "Outage performance of cognitive cooperative networks with relay selection over double-rayleigh fading channels", *IET Communications*, vol. 10, no. 1, pp. 57–64, 2016.

[112] T. N. Nguyen, M. Tran, T.-L. Nguyen, D.-H. Ha, and M. Voznak, "Multisource power splitting energy harvesting relaying network in half-duplex system over block rayleigh fading channel: System performance analysis", *Electronics*, vol. 8, no. 1, 2019, ISSN: 2079-9292. DOI: 10.3390/electronics8010067. [Online]. Available: https://www.mdpi.com/2079-9292/8/1/67.

[113] Y. Chenhong, P. Changxing, and G. Jing, "Performance analysis of two-way af cooperative networks with the nth relay selection", *International Journal of Future Generation Communication and Networking*, vol. 9, no. 8, pp. 149–156, 2016.

[114] H. Chen, Y. Li, J. Luiz Rebelatto, B. F. Uchôa-Filho, and B. Vucetic, "Harvest-then-cooperate: Wireless-powered cooperative communications", *IEEE Transactions on Signal Processing*, vol. 63, no. 7, pp. 1700–1711, 2015. DOI: 10.1109/TSP.2015.2396009.

[115] N. B. Halima and H. Boujemaa, "Exact and approximate symbol error probability of cooperative systems with best relay selection and all participating relaying using amplify and forward or decode and forward relaying over nakagami-m fading channels.", *KSII Transactions on Internet & Information Systems*, vol. 12, no. 1, 2018.

[116] S.-M. Tseng and C.-Y. Liao, "Distributed orthogonal and quasi-orthogonal space-time block code with embedded aaf/daf matrix elements in wireless relay networks with four relays", *Wireless personal communications*, vol. 75, no. 2, pp. 1187–1198, 2014.

[117] Y. Deng, L. Wang, M. Elkashlan, K. J. Kim, and T. Q. Duong, "Generalized selection combining for cognitive relay networks over nakagami-$m$ fading", *IEEE Transactions on Signal Processing*, vol. 63, no. 8, pp. 1993–2006, 2015. DOI: 10.1109/TSP.2015.2405497.

[118] A. A. Okandeji, M. R. A. Khandaker, and K. Wong, "Two-way beamforming optimization for full-duplex swipt systems", in *2016 24th European Signal Processing Conference (EUSIPCO)*, 2016, pp. 2375–2379. DOI: 10.1109/EUSIPCO.2016.7760674.

[119] M. Abramowitz and I. A. Stegun, *Handbook of mathematical functions: with formulas, graphs, and mathematical tables*. Courier Corporation, 1964, vol. 55.

[120] A. Mouapi and N. Hakem, "A new approach to design autonomous wireless sensor node based on rf energy harvesting system", *Sensors*, vol. 18, no. 1, 2018, ISSN: 1424-8220. DOI: 10.3390/s18010133. [Online]. Available: https://www.mdpi.com/1424-8220/18/1/133.

[121] B. Zhou, Y.-Z. Lee, M. Gerla, and F. De Rango, "Geo-lanmar: A scalable routing protocol for ad hoc networks with group motion", *Wireless Communications and Mobile Computing*, vol. 6, no. 7, pp. 989–1002, 2006.

[122] P. Fazio, F. De Rango, C. Sottile, and C. Calafate, "A new channel assignment scheme for interference-aware routing in vehicular networks", in *2011 IEEE 73rd vehicular technology conference (VTC Spring)*, IEEE, 2011, pp. 1–5.

[123] Y. Chen, R. Shi, W. Feng, and N. Ge, "Af relaying with energy harvesting source and relay", *IEEE Transactions on Vehicular Technology*, vol. 66, no. 1, pp. 874–879, 2016.

[124] L. Zheng, C. Zhai, and J. Liu, "Alternate energy harvesting and information relaying in cooperative af networks", *Telecommunication Systems*, vol. 68, no. 3, pp. 523–533, 2018.

[125] Z. Zhou, M. Peng, Z. Zhao, and Y. Li, "Joint power splitting and antenna selection in energy harvesting relay channels", *IEEE Signal Processing Letters*, vol. 22, no. 7, pp. 823–827, 2014.

[126] L. Liu, R. Zhang, and K.-C. Chua, "Wireless information and power transfer: A dynamic power splitting approach", *IEEE Transactions on Communications*, vol. 61, no. 9, pp. 3990–4001, 2013.

[127] P. T. Tran, T. N. Nguyen, and M. Voznak, "Performance analysis of general hybrid TSR-PSR energy harvesting protocol for amplify-and-forward half-duplex relaying networks.", *Journal of Advanced Engineering and Computation*, vol. 2, no. 2, pp. 121–130, 2018-06, ISSN: 2588-123X. DOI: 10.25073/jaec.201822.185.

[128] A. A. Nasir, X. Zhou, S. Durrani, and R. A. Kennedy, "Relaying protocols for wireless energy harvesting and information processing", *IEEE Transactions on Wireless Communications*, vol. 12, no. 7, pp. 3622–3636, 2013.

[129] I. F. Akyildiz, W. Su, Y. Sankarasubramaniam, and E. Cayirci, "Wireless sensor networks: A survey", *Computer Networks*, vol. 38, no. 4, pp. 393–422, Mar. 2002.

[130] R. E. Mohamed, A. I. Saleh, M. Abdelrazzak, and A. S. Samra, "Survey on wireless sensor network applications and energy efficient routing protocols", *Wireless Personal Communications*, vol. 101, no. 2, pp. 1019–1055, May. 2018.

[131] P. T. Tin, P. Minh Nam, T. Trung Duy, P. T. Tran, and M. Voznak, "Secrecy performance of tas/sc-based multi-hop harvest-to-transmit cognitive wsns under joint constraint of interference and hardware imperfection", *Sensors*, vol. 19, no. 5, 2019, ISSN: 1424-8220. DOI: 10.3390/s19051160. [Online]. Available: https://www.mdpi.com/1424-8220/19/5/1160.

[132] C. Xu, M. Zheng, W. Liang, H. Yu, and Y. C. Liang, "Outage performance of underlay multihop cognitive relay networks with energy harvesting", *IEEE Commun. Lett.*, vol. 20, no. 6, pp. 1148–1151, Jun. 2016.

[133] S. K. Singh, P. Kumar, and J. P. Singh, "A survey on successors of leach protocol", *IEEE Access*, vol. 5, pp. 4298–4328, Feb. 2017.

[134] D. T. Hung, T. T. Duy, and D. Q. Trinh, "Security-reliability analysis of multi-hop leach protocol with fountain codes and cooperative jamming", *EAI Transactions on Industrial Networks and Intelligent Systems*, vol. 6, no. 18, pp. 1–7, Mar. 2019.

[135] P. T. Tin, P. M. Nam, T. T. Duy, and M. Voznak, "Security-reliability analysis for a cognitive multi-hop protocol in cluster networks with hardware imperfections", *IEIE Transactions on Smart Processing and Computing*, vol. 6, no. 3, pp. 200–209, Jun. 2017.

[136] P. K. Gopala, L. Lai, and H. E. Gamal, "On the secrecy capacity of fading channels", *IEEE Trans. Inf. Theory*, vol. 54, no. 10, pp. 4687–4698, Oct. 2008.

[137] T. D. Hieu, T. T. Duy, and B.-S. Kim, "Performance enhancement for multi-hop harvest-to-transmit wsns with path-selection methods in presence of eavesdroppers and hardware noises", *IEEE Sensors Journal*, vol. 18, no. 12, pp. 5173–5186, Jun. 2018.

[138] Y. Liu, L. Wang, T. T. Duy, M. Elkashlan, and T. Q. Duong, "Relay selection for security enhancement in cognitive relay networks", *IEEE Wireless Commun. Lett.*, vol. 4, no. 1, pp. 46–49, Feb. 2015.

[139] T. M. Hoang, T. Q. Duong, N.-S. Vo, and C. Kundu, "Physical layer security in cooperative energy harvesting networks with a friendly jammer", *IEEE Wireless Commun. Lett.*, vol. 6, no. 2, pp. 174–177, Apr. 2017-02.

[140] P. T. Tin, N. N. Tan, N. Q. Sang, T. T. Duy, T. T. Phuong, and M. Voznak, "Rateless codes based secure communication employing transmit antenna selection and harvest-to-jam under joint effect of interference and hardware impairments", *Entropy*, vol. 21, no. 7, (700), Jul. 2019.

[141] J. Mo, M. Tao, and Y. Liu, "Relay placement for physical layer security: A secure connection perspective", *IEEE Commun. Lett.*, vol. 16, no. 6, pp. 878–881, Jun. 2012.

[142] C. Cai, Y. Cai, W. Yang, and W. Yang, "Secure connectivity using randomize-and-forward strategy in cooperative wireless networks", *IEEE Commun. Lett.*, vol. 17, no. 7, pp. 1340–1343, Jul. 2013.

[143] J. Yao, J. Ye, D. Wang, H. Lei, and G. Pan, "Secure source-relay link based threshold df relaying scheme", *AEU-International Journal of Electronics and Communications*, vol. 85, pp. 144–149, 2018.

[144] T. T. Duy, T. Q. Duong, T. L. Thanh, and V. N. Q. Bao, "Secrecy performance analysis with relay selection methods under impact of co-channel interference", *IET Communications*, vol. 9, no. 11, pp. 1427–1435, 2015, ISSN: 1751-8636. DOI: 10.1049/iet-com.2014.1128.

[145] A. Sun, T. Liang, and B. Li, "Secrecy performance analysis of cognitive sensor radio networks with an eh-based eavesdropper", *Sensors MDPI*, vol. 17, no. 5, 2017.

[146] C. Xu, C. Song, P. Zeng, and H. Yu, "Secure resource allocation for energy harvesting cognitive radio sensor networks without and with cooperative jamming", *Computer Networks*, vol. 141, pp. 189–198, 2018.

[147] Q. Li and S. Zhao, "Secure transmission for multi-antenna wireless powered communication with co-channel interference and self-energy recycling", *Computer Networks*, vol. 134, pp. 202–214, 2018.

[148] H. Jung and I. H. Lee, "Secrecy performance analysis of analog cooperative beamforming in three-dimensional gaussian distributed wireless sensor networks", *IEEE Transactions on Wireless Communications*, vol. 18, no. 3, pp. 1860–1873, 2019.

[149] Y. Zou and G. Wang, "Intercept behavior analysis of industrial wireless sensor networks in the presence of eavesdropping attack", *IEEE Transactions on Industrial Informatics*, vol. 12, no. 2, pp. 780–787, 2016.

[150] J. M. Moualeu, W. Hamouda, and F. Takawira, "Intercept probability analysis of wireless networks in the presence of eavesdropping attack with co-channel interference", *IEEE Access*, vol. 6, pp. 41 490–41 503, 2018.

[151] D. D. Tran, N. N. Vo, T. L. Vo, and D. B. Ha., "Physical layer secrecy performance of multi-hop decode-and-forward relay networks with multiple eavesdroppers", in *In Proc. of WAINA2015*, 2015, pp. 1–6.

[152] P. T. Tin, D. T. Hung, T. T. Duy, and M. Voznak, "Analysis of probability of non-zero secrecy capacity for multi-hop networks in presence of hardware impairments over nakagami-m fading channels", *RadioEngineering*, vol. 25, no. 4, pp. 774–782, 2016.

[153] N. Q. Sang and H. Y. Kong, "Exact outage analysis of the effect of co-channel interference on secured multi-hop relaying networks", *International Journal of Electronics*, vol. 103, no. 11, pp. 1822–1838, 2016.

[154] J. H. Lee, "Optimal power allocation for physical layer security in multi-hop df relay networks", *IEEE Transactions on Wireless Communications*, vol. 15, no. 1, pp. 28–38, 2016.

[155] L. Qing, H. Guangyao, and F. Xiaomei, "Physical layer security in multi-hop af relay network based on compressed sensing", *IEEE Communications Letters*, vol. 22, no. 9, pp. 1882–1885, 2018.

[156] Q. Liu, C. Zhu, H. Xiao, X. Qiu, and L. Yu, "Online scheduling for multi-hops wireless networks with security constraints", *IEEE Access*, vol. 7, pp. 21 409–21 419, 2019.

[157] K. Shim, T. V. Nguyen, and B. An, "Exploiting opportunistic scheduling schemes and wpt-based multi-hop transmissions to improve physical layer security in wireless sensor networks", *Sensors MDPI*, vol. 19, no. 24, 2019.

[158] L. Tang and Q. Li, "Wireless power transfer and cooperative jamming for secrecy throughput maximization", *IEEE Wireless Communications Letters*, vol. 5, no. 5, pp. 556–559, 2016.

[159] H. Xing, K. K. Wong, A. Nallanathan, and R. Zhang, "Wireless powered cooperative jamming for secrecy multi-af relaying networks", *IEEE Transactions on Wireless Communications*, vol. 15, no. 12, pp. 7971–7984, 2016.

[160] M. Liu and Y. Liu, "Power allocation for secure swipt systems with wireless-powered cooperative jamming", *IEEE Communications Letters*, vol. 21, no. 6, pp. 1353–1356, 2017.

[161] J. M. Kang, J. Yang, J. Ha, and I. M. Kim, "Joint design of optimal precoding and cooperative jamming for multiuser secure broadcast systems", *IEEE Transactions on Vehicular Technology*, vol. 66, no. 11, pp. 10 551–10 556, 2017.

[162] K. Cao, K. Cai, Y. Wu, and W. Yang, "Cooperative jamming for secure communication with finite alphabet inputs", *IEEE Communications Letters*, vol. 21, no. 9, pp. 2025–2028, 2017.

[163] T. M. Hoang, T. Q. Duong, N. S. Vo, and C. Kundu, "Physical layer security in cooperative energy harvesting networks with a friendly jammer", *IEEE Wireless Communications Letters*, vol. 6, no. 2, pp. 174–177, 2017.

[164] J. H. Lee, "Full-duplex relay for enhancing physical layer security in multi-hop relaying systems", *IEEE Communications Letters*, vol. 19, no. 4, pp. 525–528, 2015.

[165] E. R. Alotaibi and K. A. Hamdi, "Secure relaying in multihop communication systems", *IEEE Communications Letters*, vol. 20, no. 6, pp. 1120–1123, 2019.

[166] V. N. Vo, S. I. Chakchai, D. D. Tran, and H. Tran, "Optimal system performance in multihop energy harvesting wsns using cooperative noma and friendly jammers", *IEEE Access*, vol. 7, pp. 125 494–125 510, 2019.

[167] S. Mottaghi and M. R. Zahabi, "Optimizing leach clustering algorithm with mobile sink and rendezvous nodes", *AEU-International Journal of Electronics and Communications*, vol. 69, no. 2, pp. 507–514, 2015.

[168] T. M. Behera, U. C. Samal, and S. K. Mohapatra, "Energy-efficient modified leach protocol for iot application", *IET Wireless Sensor Systems*, vol. 8, no. 5, pp. 223–228, 2018.

[169] G. Rezgui, E. V. Belmega, and A. Chorti, "Mitigating jamming attacks using energy harvesting", *IEEE Wireless Communications Letters*, vol. 8, no. 1, pp. 297–300, 2018.

[170] P. Chakraborty and S. Prakriya, "Secrecy outage performance of a cooperative cognitive relay network", *IEEE Communications Letters*, vol. 21, no. 2, pp. 326–329, 2017.

[171] S. Vahidian, S. Hatamnia, and B. Champagne, "On the security analysis of a cooperative incremental relaying protocol in the presence of an active eavesdropper", *IEEE Access*, vol. 7, pp. 181 812–181 828, 2019.

[172] W. Wang, K. C. Teh, and K. H. Li, "Generalized relay selection for improved security in cooperative df relay networks", *IEEE Wireless Communications Letters*, vol. 5, no. 1, pp. 28–31, 2016-02, ISSN: 2162-2345. DOI: 10.1109/LWC.2015.2488660.

[173] A. Pandey and S. Yadav, "Physical-layer security for cellular multiuser two-way relaying networks with single and multiple decode-and-forward relays", *Transactions on Emerging Telecommunications Technologies*, vol. 30, no. 12, e3639, 2019, e3639 ett.3639. DOI: 10.1002/ett.3639. eprint: https://onlinelibrary.wiley.com/doi/pdf/10.1002/ett.3639. [Online]. Available: https://onlinelibrary.wiley.com/doi/abs/10.1002/ett.3639.

[174] M. K. Shukla, A. Pandey, S. Yadav, and N. Purohit, "Secrecy outage analysis of full duplex cellular multiuser two-way af relay networks", in *2019 International Conference on Wireless Communications Signal Processing and Networking (WiSPNET)*, 2019, pp. 458–463.

[175] X. Li, M. Zhao, X. Gao, L. Li, D. Do, K. M. Rabie, and R. Kharel, "Physical layer security of cooperative noma for iot networks under i/q imbalance", *IEEE Access*, vol. 8, pp. 51 189–51 199, 2020.

[176] D. Kapetanovic, G. Zheng, and F. Rusek, "Physical layer security for massive mimo: An overview on passive eavesdropping and active attacks", *IEEE Communications Magazine*, vol. 53, no. 6, pp. 21–27, 2015-06, ISSN: 1558-1896. DOI: 10.1109/MCOM.2015.7120012.

[177] J. Chen, R. Zhang, L. Song, Z. Han, and B. Jiao, "Joint relay and jammer selection for secure two-way relay networks", *IEEE Transactions on Information Forensics and Security*, vol. 7, no. 1, pp. 310–320, 2012.

[178] X. Ding, T. Song, Y. Zou, X. Chen, and L. Hanzo, "Security-reliability tradeoff analysis of artificial noise aided two-way opportunistic relay selection", *IEEE Transactions on Vehicular Technology*, vol. 66, no. 5, pp. 3930–3941, 2017.

[179] L. Lai and H. El Gamal, "The relay–eavesdropper channel: Cooperation for secrecy", *IEEE Transactions on Information Theory*, vol. 54, no. 9, pp. 4005–4019, 2008-09, ISSN: 1557-9654. DOI: 10.1109/TIT.2008.928272.

[180] H. Chiang and J. S. Lehnert, "Optimal jamming with codewords", in *MILCOM 2012 - 2012 IEEE Military Communications Conference*, 2012-10, pp. 1–6. DOI: 10.1109/MILCOM.2012.6415873.

[181] S. Lee and A. Khisti, "The gaussian diamond-wiretap channel with rate-limited relay cooperation", *IEEE Communications Letters*, vol. 21, no. 2, pp. 338–341, 2017-02, ISSN: 2373-7891. DOI: 10.1109/LCOMM.2016.2626278.

[182] A. A. Babayo, M. H. Anisi, and I. Ali, "A review on energy management schemes in energy harvesting wireless sensor networks", *Renewable and Sustainable Energy Reviews*, vol. 76, pp. 1176–1184, 2017, ISSN: 1364-0321. DOI: https://doi.org/10.1016/j.rser.2017.03.124. [Online]. Available: http://www.sciencedirect.com/science/article/pii/S1364032117304598.

[183] I. Ahmed, M. M. Butt, C. Psomas, A. Mohamed, I. Krikidis, and M. Guizani, "Survey on energy harvesting wireless communications: Challenges and opportunities for radio resource allocation", *Computer Networks*, vol. 88, pp. 234–248, 2015, ISSN: 1389-1286. DOI: https://doi.org/10.1016/j.comnet.2015.06.009. [Online]. Available: http://www.sciencedirect.com/science/article/pii/S1389128615002029.

[184] L. D. Nguyen, "Resource allocation for energy efficiency in 5g wireless networks", *EAI Endorsed Trans. Indust. Netw. & Intellig. Syst.*, vol. 5, no. 14, e1, 2018-06. DOI: 10.4108/eai.27-6-2018.154832.

[185] N. Hoang An, M. Tran, T. N. Nguyen, and D.-H. Ha, "Physical layer security in a hybrid tpsr two-way half-duplex relaying network over a rayleigh fading channel: Outage and intercept probability analysis", *Electronics*, vol. 9, no. 3, 2020, ISSN: 2079-9292. DOI: 10.3390/electronics9030428. [Online]. Available: https://www.mdpi.com/2079-9292/9/3/428.

[186] C. Shannon, "Two-way communication channels", in *Proc. of the 4th Berkeley Sym. on Math. Stat. and Prob., Volume 1: Contributions to the Theory of Statistics*, 1961, pp. 611–644.

[187] B. Rankov and A. Wittneben, "Achievable rate regions for the two-way relay channel", in *Proc. of IEEE International Symposium on Information Theory*, 2006, pp. 1668–1672. DOI: 10.1109/ISIT.2006.261638.

[188] S. Katti, H. Rahul, W. Hu, D. Katabi, M. Medard, and J. Crowcroft, "Xors in the air: Practical wireless network coding", *IEEE/ACM Transactions on Networking*, vol. 16, no. 3, pp. 497–510, 2008-06, ISSN: 1558-2566. DOI: 10.1109/TNET.2008.923722.

[189] S. Katti, S. Gollakota, and D. Katabi, "Embracing wireless interference: Analog network coding", *ACM SIGCOMM Computer Communication Review*, vol. 37, no. 4, pp. 397–408, 2007.

[190] K. Tutuncuoglu, B. Varan, and A. Yener, "Throughput maximization for two-way relay channels with energy harvesting nodes: The impact of relaying strategies", *IEEE Transactions on Communications*, vol. 63, no. 6, pp. 2081–2093, 2015. DOI: 10.1109/TCOMM.2015.2427162.

[191] A. Salem and K. A. Hamdi, "Wireless power transfer in multi-pair two-way af relaying networks", *IEEE Transactions on Communications*, vol. 64, no. 11, pp. 4578–4591, 2016-11, ISSN: 1558-0857. DOI: 10.1109/TCOMM.2016.2607751.

[192] T. N. Nguyen, P. T. Tran, and M. Voznak, "Wireless energy harvesting meets receiver diversity: A successful approach for two-way half-duplex relay networks over block rayleigh fading channel", *Computer Networks*, vol. 172, p. 107 176, 2020, ISSN: 1389-1286. DOI: https://doi.org/10.1016/j.comnet.2020.107176. [Online]. Available: http://www.sciencedirect.com/science/article/pii/S1389128619314689.

[193] P. N. Son and H. Y. Kong, "Improvement of the two-way decode-and-forward scheme by energy harvesting and digital network coding relay", *Trans. Emerging Telecommunications Technologies*, vol. 28, 2017.

[194] Y. Ai, M. Cheffena, T. Ohtsuki, and H. Zhuang, "Secrecy performance analysis of wireless sensor networks", *IEEE Sensors Letters*, vol. 3, no. 5, pp. 1–4, 2019.

[195] M. K. Shukla, S. Yadav, and N. Purohit, "Secure transmission in cellular multiuser two-way amplify-and-forward relay networks", *IEEE Transactions on Vehicular Technology*, vol. 67, no. 12, pp. 11 886–11 899, 2018.

[196] S. Fu, T. Zhang, and M. Colef, "Secrecy in two-way relay systems", in *2010 IEEE Global Telecommunications Conference GLOBECOM 2010*, 2010, pp. 1–5.

[197] B. Zhong and Z. Zhang, "Secure full-duplex two-way relaying networks with optimal relay selection", *IEEE Communications Letters*, vol. 21, no. 5, pp. 1123–1126, 2017-05, ISSN: 2373-7891. DOI: 10.1109/LCOMM.2017.2655050.

[198] L. Irio, R. Oliveira, D. B. da Costa, and M. Alouini, "Impact of wireless-powered communications in coexisting mobile networks", *IEEE Wireless Communications Letters*, pp. 1–1, 2020, ISSN: 2162-2345. DOI: 10.1109/LWC.2020.2980524.

[199] B. C. Nguyen, T. Nguyen-Kieu, T. M. Hoang, P. T. Tran, and M. Vozňák, "Analysis of mrt/mrc diversity techniques to enhance the detection performance for mimo signals in full-duplex wireless relay networks with transceiver hardware impairment", *Physical Communication*, vol. 42, p. 101 132, 2020, ISSN: 1874-4907. DOI: https://doi.org/10.1016/j.phycom.2020.101132. [Online]. Available: http://www.sciencedirect.com/science/article/pii/S1874490720302093.

[200] X. Liu, "Average secrecy capacity of the weibull fading channel", in *2016 13th IEEE Annual Consumer Communications Networking Conference (CCNC)*, 2016-01, pp. 841–844. DOI: 10.1109/CCNC.2016.7444897.

[201] F. W. Olver, D. W. Lozier, R. F. Boisvert, and C. W. Clark, *NIST Handbook of Mathematical Functions*, 1st. USA: Cambridge University Press, 2010, ISBN: 0521140633.